UNIVERSITÉ DE MONTRÉAL

THE DEVELOPMENT OF AN INTELLIGENT HEALTH MONITORING SYSTEM FOR MICROMETEOROID AND SPACE DEBRIS PROTECTION SYSTEMS AND SPACECRAFT STRUCTURAL COMPONENTS

LUCIAN EDUARD ILIESCU

DÉPARTEMENT DE GÉNIE MÉCANIQUE

ÉCOLE POLYTECHNIQUE DE MONTRÉAL

THÈSE PRÉSENTÉE EN VUE DE L'OBTENTION

DU DIPLÔME DE PHILOSOPHIAE DOCTOR

(GÉNIE MÉCANIQUE)

DÉCEMBRE 2016

UNIVERSITÉ DE MONTRÉAL

ÉCOLE POLYTECHNIQUE DE MONTRÉAL

Cette thèse intitulée :

THE DEVELOPMENT OF AN INTELLIGENT HEALTH MONITORING SYSTEM FOR MICROMETEOROID AND SPACE DEBRIS PROTECTION SYSTEMS AND SPACECRAFT STRUCTURAL COMPONENTS

présentée par : ILIESCU Lucian Eduard

en vue de l'obtention du diplôme de : Philosophiae Doctor

a été dûment acceptée par le jury d'examen constitué de :

M. BALAZINSKI Marek, Docteur ès sciences, président

M. LAKIS Aouni A., Ph. D., membre et directeur de recherche

M. ACHICHE Sofiane, Ph. D., membre

Mme SKULINOVA Michaela, Ph. D., membre externe

DEDICATION

To my daughter Kristin and to my mom

ACKNOWLEDGEMENTS

I would like to express my gratitude to my doctoral advisor Prof. Aouni A. Lakis for his patience, guidance and invaluable support throughout the realisation of this research.

My sincere appreciation goes to Prof. Marek Balazinski, Prof. Sofiane Achiche, Prof. Tew-Fik Mahdi and Mme. Michaela Skulinova for taking part as my thesis committee.

This project has been made possible by precious support from the collaborative research and development grant of Natural Sciences and Engineering Research Council of Canada (NSERC) and the Fonds de recherche du Québec - Nature et technologies (FRQNT).

Special thanks to my colleague and friend Abdelhak Oulmane, your advices and support guided me all along of this research.

RÉSUMÉ

Le début des activités humaines dans l'espace, en 1957, a marqué aussi le début de la pollution graduelle de cet environnement avec des débris orbitaux (DO). Aujourd'hui, ce problème crée ce qui est appelé «l'impact à de très haute vitesse», un des principaux dangers pouvant se produire (impact a hyper vitesse) entre des débris orbitaux et un véhicule spatial ou satellite en cours de vol atour de l'orbite terrestre.

À la suite de ces collisions plus de débris sont formés en basse orbite (région inférieure à 2000 km d'altitude) et un phénomène dit «collision potentielle en cascade» (également connu sous le nom de «syndrome de Kessler») peut survenir. La collision en cascade est mentionnée par plusieurs études de modélisation de l'environnement spatial effectuées par des agences spatiales comme la NASA ou l'ESA.

Un autre type de danger qui peut conduire au même risque d'impact à une très grande vitesse dans l'espace sont les micrométéorites. Les micrométéorites et les débris spatiaux voyagent en orbite terrestre basse à des vitesses allant de 17 à 20 Km/s et 70 à 80 Km/s respectivement, et leur impact sur les véhicules spatiaux peut varier d'une dégradation des performances jusqu'à la perte totale de l'engin. Actuellement, il y a plus de 22000 morceaux de débris orbitaux qui sont suivis et répertoriés, et cela pour des objets avec des dimensions supérieures à 5 cm, pour lesquels la prévention des collisions est la seule option, et pour lesquelles aussi des dizaines de conjonctions d'avertissements sont émises quotidiennement par les centres d'opérations satellitaires.

En revanche, Il y a plus de 500000 morceaux de débris orbitaux avec des dimensions inférieures à 5 cm représentant aussi un haut risque de collision pour les satellites qui sont en orbite basse. Le cas de l'impact de DO ayant des dimensions allant jusqu'à 5 mm pourrait créer une dégradation des fonctions opérationnelles d'un véhicule spatial. Les DO ayant des dimensions de 0,5 à 1 cm sont la principale menace pour les véhicules spatiaux en orbite basse et pour lesquels les solutions actuelles sont juste représentées par des systèmes de protection.

Le maintien d'une structure sûre et saine de satellites ou de véhicules spatiaux et une meilleure compréhension de l'interaction des MMOD avec les systèmes spatiaux motive en effet la création d'un système de surveillance (Health Monitoring System) intégré afin de surveiller en temps réel ou en temps quasi réel la dégradation de la structure ou du système de protection. Basé sur les résultats du système de surveillance, le fonctionnement de véhicules ou autre engins spatiaux

pourrait être ajusté en conséquence et ce suivi continuel aurait également une influence sur les inspections, les calendriers de réparation et la planification des activités extravéhiculaires ou dans le calibrage des modèles de poussière.

Les solutions présentées dans la littérature sur le sujet combinent une série de détecteurs d'impact incrustées dans le matériau qui fournissent des informations sur la détection de l'impact externe et la profondeur de la pénétration. En revanche aucune une méthode fiable intégrée permettant de quantifier l'impact qui pénètre dans chaque couche de blindage n'a été élaborée.

Le présent travail de recherche représente la base de développement pour un système original de détection et de classification des défauts du système de protection et cela en utilisant l'analyse temps-fréquence (T-F) ainsi que le développement d'une base de données sous forme de dictionnaire regroupant les signaux de chaque état d'un composant de protection (dommages de couche ou pénétration).

La première partie de notre travail élabore une série de tests expérimentaux d'impact à très grande vitesse afin d'obtenir des signaux de vibration de référence. Le choix des matériaux pour les cibles a été basé sur les matériaux les plus utilisés dans la conception de systèmes de protection d'impact et de structure de véhicules spatiaux. En effet, un examen sur les technologies de détection d'impact a également été réalisé afin de sélectionner le meilleur choix pour ce genre de tests. Dans un premier temps, six essais ont été effectués à de très grande vitesse sur des cibles en aluminium et en fibre de carbone. Les accélérations de références ont été obtenues à partir des capteurs montés sur les cibles et à l'extérieur de la chambre d'essai. La session de test a également permis d'acquérir un bon procédé expérimental concernant la préparation de ce type de tests, la réalisation de tests d'impact à très grande vitesse et finalement l'enregistrement des signaux de vibration pour éventuels future tests.

La deuxième partie de cette étude est focalisée sur l'analyse des signaux obtenus à partir des signatures vibratoires des différentes sessions de test. L'analyse vibratoire en Temps-Fréquence a été effectuée en utilisant un logiciel spécifique développé par le groupe de recherche du Prof. A. A. Lakis. Nous avons utilisé le logiciel maison TF-Analysis comme un outil de calcul utilisant différentes transformations en temps-fréquence ou en temps-échelle afin d'analyser le fichier de données.

Pour l'analyse du signal, les méthodes de Choi-Williams et la transformée en ondelettes qui sont habituellement utilisés pour l'analyse des vibrations d'impact à très haute vitesse ont été appliquée. L'analyse nous a permis de distinguer les différentes caractéristiques des deux principaux états de cibles touchées ; perforation et non-perforation.

La simulation d'impact à très grande vitesse et l'analyse des accélérations mesurées pour la corroboration des résultats des tests et valider la performance du système de surveillance en temps réel utilisant un dictionnaire contenant les matériaux des véhicules spatiaux a fait l'objet de la troisième partie de nos travaux de recherche. Dans cette partie, l'identification des matériaux les plus utilisés dans la fabrication des véhicules spatiaux et de les trier en trois groupes principaux (les métaux d'alliages, les composites et les panneaux sandwich) était la phase principale dans l'établissement des matériaux choisis comme cibles pour la simulation numérique.

La simulation numérique de l'impact à très grande vitesse a été élaborée avec le logiciel LS-Dyna et la méthode utilisée pour l'analyse du signal a été la distribution de Choi-Williams du logiciel maison TF-Analysis.

La méthode de Choi-Williams a clairement identifiée les différences dans la forme et la fréquence d’amplitude d’impact, pour un ou deux matériaux identifiés de chaque groupe, pour le cas de pénétration. En effet, les caractéristiques de chaque perforation sur les matériaux considérés sont discutées.

Sur la base de ces résultats, qui sont en bonne concordance avec d'autres analyses et essais expérimentaux, un dictionnaire de référence contenant des matériaux utilisés pour la protection des véhicules spatiaux sera créé, ce qui va grandement aider à l'identification automatique des dommages des débris spatiaux.

ABSTRACT

Human activity in the space environment began in 1957. From this moment forward, these activities have created another phenomena; the gradual pollution of space with orbital debris (OD). Today this accumulated debris is one of the main hazards in the near–Earth space environment. More specifically, hypervelocity impact between OD and every satellite and space vehicle that is launched or is currently orbiting the Earth. As each collision occurs more OD is created and, in the Low Earth Orbit (LEO) zone (the region below 2000 km altitude), a potential ongoing collision cascade effect (also known as the "Kessler Syndrome") can occur. This potential for collision cascade has been identified during space environment modeling studies performed by space agencies such as NASA or ESA. Increased space activity combined with poor standardization of space activity and the limited options for cleaning the space environment will lead to an increased frequency of collisions. Within the next few decades we will not be able to use the LEO for practical purposes. Another type of particle that creates the same primary risk of hypervelocity impact in the space environment is micrometeoroids. Micrometeoroids and space debris travel in low earth orbit at velocities up to 17-20 Km/s (OD) and 70-80 Km/s respectively, and their impact on space assets can vary from degraded performance to catastrophic loss.

More than 22000 pieces of OD are currently tracked. These are objects with dimensions larger than 5 cm for which collision prevention is the only option, and for which tens of conjunction warnings are issued daily by satellite operations centers. In addition, there are more than 500,000 pieces of OD with dimensions less than 5 cm that present a high risk for collisions with satellites that are orbiting in the LEO. Solutions for debris in this dimensional range still have to be developed and include concepts capable of preventing and blocking the huge energy of hypervelocity impact and/or concepts for OD removal. Impact between OD with dimensions up to 5 mm and spacecraft is a special case because it could create a degradation of operational functions. OD in the 0.5 to 1 cm dimensional range, which represents 80 % of debris larger than 0.5 cm, is the main threat to spacecraft in the LEO. The only current solutions are protection systems or shields.

To evaluate the risks associated with spacecraft impact with micrometeoroids and orbital debris (MMOD) we have to analyze factors such as: environment (the fluxes of particles), damage prediction (number of impacts) and damage tolerance (how much damage the structure can stand).

To maintain safe and healthy structures of satellites or crewed spacecraft and to better understand the interaction of MMOD with space systems it is necessary to create an integrated Health Monitoring System (HMS) to monitor in real time or near-real time the condition of the structure or shield degradation. Spacecraft operation can be adjusted based on the monitoring results. Continuing monitoring of shield condition also influences inspection and repair schedules, planning extra-vehicular activities or even the calibration of dust models.

MMOD impact detection systems for spacecraft started to be developed from the first launches in space going back to 1960. These first series of sensors were mainly used to characterize the Lower Earth Orbit (LEO) space environment.

The solutions presented in literature on this subject include a series of impact sensors imbedded in the material which provide information on the frequency of external impacts and the depth of penetration. There is no integrated method that quantifies the penetration of each layer of the shielding.

Our research work provides a basis for the development of an original system for detection and classification of system faults using Time-Frequency (TF) analysis together with a signal database/dictionary for describing the state or condition of each shield component (layer damage or penetration).

The first part of our work is a series of experiments. Hypervelocity impact tests were done in order to obtain valid vibration signals. Materials that are most frequently used for the design of spacecraft structure and impact protection systems were selected for the targets. Also, a review of impact detection technologies was performed in order to select the most appropriate sensors for the tests. The final choice was based on availability, timing and financial restrictions. The resulting protocol included six hypervelocity tests in a low-velocity range on aluminum and carbon fiber targets. Valid acceleration data were obtained from the sensors, which were mounted on the targets and outside the testing chamber. The testing session also provided practice in preparing for this type of test, in performing hypervelocity impact tests and in recording the vibration signals. This experience will be useful to improve efficiency and results in further test sessions.

The second part of the work concentrates on analysis of signals obtained from the testing session. TF analysis was done using specific software developed in-house by Prof. A. A. Lakis' research group; a platform for implementation of research work for different applications of various

vibration methods. We used the TF Analysis software as a tool for calculation of different time-frequency or time-scale transforms during analysis of the impact data.

Signal analysis was completed by applying two methods that are usually used for analyzing hypervelocity impact vibrations, Choi-Williams Distribution (CWD) and Wavelet transforms. The analysis allowed us to distinguish the different characteristics of the two main states of impacted targets; perforation and non-perforation.

The third part of our research work includes simulation of hypervelocity impact and TF analysis of the accelerations. The simulation output was corroborated with test results to validate the method and its potential for development of a real-time monitoring system with a spacecraft material dictionary.

For the simulation, we identified the most-used materials in the manufacture of spacecraft and sorted them into three groups: metals alloys, composites and sandwich panels. This was the corner stone in establishing simulation target materials.

Numerical simulation of hypervelocity impact was carried out using a student version of LS-Dyna software.

During signal analysis, the CWD method clearly identified differences in the HVI form and frequency amplitude for one or two target materials from each of the three groups, and for the case of penetration. Our conclusion includes a discussion on the characteristics of perforation on each of the materials considered.

Based on these results, after corroboration with further analysis and experimental tests, a dictionary of materials that are recommended for spacecraft protection is created. This is essential to enable automatic identification of space debris damage.

CONDENSÉ EN FRANÇAIS

Introduction

Le début de la conquête de l'espace par l'Homme à la fin des années cinquante a aussi marqué le début de la surpopulation de cet environnement par les débris orbitaux (*DO*). En raison de la très grande vitesse de vol des débris orbitaux des micros météorites (*DOMM*), l'énorme énergie due à l'impact de ces objets avec des satellites varie d'une dégradation des performances à la perte totale de ces derniers.

En conséquence de ces collisions accidentelles (en 2007, la destruction prévue d'un satellite dans l'espace par un missile chinois - Jean Etienne, 2007, « Un missile chinois détruit un satellite en orbite », trouvé sur http://www.futura-sciences.com.) le nombre de ces débris orbitaux a augmenté jusqu'à plus de 500000 morceaux avec des dimensions supérieures à 0,5 cm. La solution actuelle pour minimiser le risque d'impact pour les engins spatiaux est principalement l'élimination active des morceaux de *DO* de l'environnement spatial et d'accroître la protection contre un tel impact à une très grande vitesse.

Les effets de l'impact à très grande vitesse dépendent d'une série de paramètres qui sont liés aux caractéristiques du projectile et de la cible ainsi que de la vitesse d'impact. La taille et la vitesse de la particule d'impact jouent un rôle important, mais des facteurs secondaires tels que : l'angle d'impact, la forme et la densité du matériau de l'impacteur ou de la cible (objet impacté) devraient également être pris en considération.

Les résultats de l'impact à très grande vitesse varient d'un simple cratère à une pénétration complète du bouclier de protection ou de la coque. Afin de maintenir l'intégrité d'un satellite ou d'un vaisseau spatial, un système intégré de surveillance d'un tel impact est plus que nécessaire. Les solutions actuelles sont basées sur une combinaison de différents capteurs imbibés dans le matériau de la structure. La présente recherche propose d'une part, un système intégré de surveillance afin de protéger les structures et les boucliers de protection pour développer un système de détection et de classification en temps réel des impacts à l'aide d'analyse vibratoire en utilisant les méthodes temps-fréquence et d'autre part, le développement d'une base de données sous forme de dictionnaire contenant les signaux de chaque état du composant de bouclier (que ce soit les dommages de la première couche de la structure ou la pénétration de cette dernière).

A la suite de ces considérations, la question de recherche, l'hypothèse sur la façon dont nous résolvons les questions de recherche et les objectifs du projet de recherche pour approuver notre hypothèse seront élaborés comme suit :

Question de recherche

Afin de créer un système intelligent de surveillance pour la détection des dommages causés par les débris spatiaux contre le système de protection, le projet de recherche doit répondre à la question suivante : Quand et dans quelle mesure les vaisseaux spatiaux ou plus précisément le système de protection contre les débris spatiaux soit endommagé / affecté par soit les débris orbitaux, soit par l'impact des micrométéorites ?

Hypothèse

Basée sur la question de recherche élaborée ultérieurement, notre hypothèse est comment l'analyse temps - fréquence pourrait être utilisée pour la détection et la classification de ces dommages d'impact à très haute vitesse.

Objectifs

Sur la base de ce qui a été dit jusqu'à présent, l'objectif général de ce projet de recherche est l'élaboration d'une méthode pour la création d'un système intelligent de surveillance et de protection contre les impacts des micrométéorites et les débris spatiaux. Les objectifs spécifiques dérivés sont ainsi comme suit :

- Le développement d'un système original de détection et de classification des défauts du système de protection en utilisant l'analyse temps-fréquence (TF) ;

- Le développement d'une base de données de signaux ainsi qu'un dictionnaire pour chaque état de la composante du blindage (endommagement de la couche ou pénétration) ;

- L'identification de la composante endommagée et du type de dommage ;

- L'amélioration et la validation du système de surveillance de l'état des véhicules spatiaux et la mise en œuvre d'un véritable système de protection des engins spatiaux en temps réel.

Afin d'analyser les dommages d'impact, à très grande vitesse, et afin d'obtenir les accélérations de vibration, d'impact, deux méthodes de simulation des dommages ont été utilisés : une première

méthode basée sur des tests expérimentaux d'impact à très grande vitesse et une autre basée sur des simulations numériques de ces impacts.

Les tests à très grande vitesse ont été effectués pour valider la capacité de protection de certains matériaux ou de systèmes de protection car la majorité des tests d'impacts à très grande vitesse couvre environ 40% de débris orbitaux. Au Canada, la vitesse maximale atteinte pour ce genre de tests est d'environ 8 à 9 Km/s. Pour le reste de la plage de vitesse des DO des simulations analytiques et numériques ont été utilisées.

La première partie de ce travail de recherche donne un aperçu détaillé sur les essais d'impacts à très grande vitesse effectués. Elle couvre entre autre toutes les fonctionnalités du lanceur de projectiles, le choix lors de la séparation du sabot du projectile, la méthode d'acquisition de signaux et de l'équipement. Les résultats de la session de test sont représentés par six signaux enregistrés utilisables et disponibles pour l'analyse.

La deuxième partie se focalise sur l'utilisation du logiciel maison TF-Analysis dans l'interprétation et l'analyse du signal d'accélération obtenu précédemment. La distribution dite Choi-Williams (CWD) et la transformée en ondelettes ont été les deux méthodes principalement employées dans cette étude.

Pour la troisième partie de cette recherche, une simulation numérique d'impacts sur plusieurs matériaux utilisés principalement dans la construction des satellites était nécessaire pour assurer une certaine concordance avec les résultats des tests, pour vérifier la méthode de surveillance en temps réel et finalement, pour la création d'une base de données contenant la plupart des matériaux de satellite fondée sur l'analyse des signaux de vibration.

Première partie - Séance d'essai d'impact à très grande vitesse

Introduction et choix des matériaux

L'objectif du premier volet de notre recherche est de présenter la partie expérimentale et la session de tests, qui ont été réalisés en vue d'acquérir des signaux vibratoires pour les quels seront étudiés dans la deuxième partie et cela en utilisant le logiciel maison TF-Analysis afin de déterminer en temps réel les caractéristiques des dommages d'impact à très grande vitesse.

Les dommages et les débris générés par un impact causé par les débris orbitaux des micrométéorites sont un phénomène complexe qui implique de résoudre des problèmes tels que le choc et le

comportement dynamique des matériaux. Dans le cas d'un alliage d'aluminium utilisé comme matériau cible, la collision crée un cratère ayant une forme hémisphérique dépendant de l'épaisseur utilisée et de la fracturation interne.

Cette première partie du projet de recherche fait une synthèse des connaissances des différents aspects de l'étude ainsi que les expériences acquises à partir des tests d'impact à très grande vitesse. En effet, une série d'essais a été effectuée sur différents matériaux avant la pénétration du projectile et cela en utilisant les équations balistiques. L'objectif principal de cette partie était le regroupement des résultats et des signaux obtenus à partir de différents tests. Cette partie comprend également une brève revue de la littérature des tests d'impact à très grande vitesse existants et réalisés sur différents matériaux utilisés dans la protection des débris orbitaux des micros météorites et un résumé sur les différents types de capteurs utilisés pour la détection des dommages d'impact à très grande vitesse. Cette revue de littérature a montré que différents tests d'impact à très grande vitesse ont été effectué pas juste sur une multitude de matériaux tels que l'aluminium, le titane, le cuivre, l'acier inoxydable, le nickel, le nickel / chrome, réticulé carbone vitreux, de l'argent, la céramique, l'aramide, le verre, la céramique, ou de la fibre de carbone, mais également sur des structures telles que: les plaques monolithiques, la mousse à cellules ouvertes, les tissus souples et les mailles rigides disposées dans différentes configurations de bouclier simple ou multiple qui ont été testés pour évaluer leur efficacité dans des blindages contre les *DOMM* .

Lors de cette partie du projet de recherche il a été démontré que le carbone renforcé de fibres de polymère (CRFP), l'un des matériaux utilisé pour les simulations des derniers essais, peut être considérée comme un choix potentiel pour la fabrication des structures primaires des futurs systèmes spatiaux. En effet, les CFRP ont des mécanismes de dommages très complexes tels que la délamination interne, et une série de tests d'impact à très grande vitesse sont fortement recommandés afin d'analyser toutes les propositions d'utilisation de ce type de matériaux.

Tests d'impact à très grande vitesse et sélection de la méthode de détection

La prochaine section de la première partie de cette recherche débute par la description du lanceur qui est entraîné par un réservoir contenant un gaz à haute pression utilisant un mécanisme à double membrane de propulsion.

Le mécanisme du lanceur à gaz est contrôlé à l'aide d'hélium (He) un gaz à haute pression pour obtenir les pressions de lancement ciblées et de l'azote gazeux pour le décapage dynamique du

sabot. Pour les besoins de notre essai initial, les pressions de 2000 psi à 4000 psi ont été utilisés afin d'obtenir des vitesses allant de 560 m / s à 1670 m / s. Afin d'obtenir une pression de conduite finale de 2000 psi pour le lanceur un mécanisme à double membrane a été utilisé à cet effet, et la différence de pression à travers les membranes est en fait, le moteur du mécanisme. Dans un premier temps, les deux sections à haute et basse pression sont remplies à moitié de la pression totale (1000 psi), ce qui correspond à une différence de pression de 0 psi à travers le premier diaphragme et 1000 psi à travers le second. La section haute pression est alors remplie à la pression d'entraînement finale de 2000 psi, ce qui correspond à une différence de pression de 1 000 psi à travers les deux membranes. Enfin, le réservoir à basse pression a été évacué afin de donner une différence de pression de 2000 psi au premier diaphragme.

Un autre élément essentiel pour le lanceur, outre le mécanisme à double membrane était le sabot qui, avec un aimant de terre rare (utilisé pour déterminer la vitesse) a été utilisé pour lancer le projectile.

Le mécanisme de décapage du sabot nécessitait une attention particulière. Deux méthodes sont généralement utilisées au laboratoire : une méthode dynamique et l'autre mécanique. Pour la session de test, la méthode dynamique a été opté qui consistait à remplir une section avec de l'azote (*N2*), un gaz plus lourd que l'Hélium. Lorsque le sabot avec le projectile entre dans la section contenant le *N2*, une onde de choc est créée ce qui ralentissait sensiblement la vitesse du sabot. Cette diminution soudaine de la vitesse sépare le projectile du sabot.

Pour les essais, le matériau proposé de la cible était l'Aluminium 6061-T6 (0,8129 mm et 3,75 mm d'épaisseur) une tôle rigide en composite de fibre de carbone / Epoxy (épaisseur de 3,155 mm et 6,35 mm) en. Le choix des matériaux a été adopté afin de créer au moins deux types de dommages par impact à très grande vitesse : le cratère et la perforation, dans deux matériaux différents et en tenant compte d'autres facteurs tels que le choix des matériaux, la disponibilité du marché, la disponibilité des installations d'essai et le calendrier.

Pour ajuster les cibles dans la section d'essai, les plaques de matériau ont été coupées en carrés de dimension 11 x 11 mm. Ces plaques ont été serrées entre deux cylindres en bois qui s'adaptent étroitement à l'intérieur de la section d'essai.

Le système d'acquisition de données utilisé pour les signaux préliminaires était le Ni PXI couplé avec trois accéléromètres *PCB* Piezotroniques. Un accéléromètre a été monté sur l'échantillon et les deux autres ont été montés à l'extérieur de la section d'essai.

Un autre choix de solution qui pourrait être envisagée à l'avenir est l'utilisation de capteurs de fibre optique ou de fibre de verre qui présente de nombreux avantages dans la surveillance des impacts a de très grande vitesse, telles que la capacité de surveiller une variété de paramètres, une perte minimale ou la distorsion du signal et finalement la robustesse environnementale. Ces avantages favorisent l'utilisation de cette technologie pour le contrôle et le diagnostic future des structures aérospatiales.

Comme résultats de la session d'essai, six tests satisfaisants enregistrés ont été réalisés sur des échantillons d'aluminium et de fibre de carbone utilisant le lanceur à gaz à différentes pressions de gaz, et donc différentes vitesses de projectile.

Deuxième partie - Analyse du signal d'impact à très grande vitesse

Introduction et réflexion théorique

Cette deuxième partie de ce projet de recherche présente une méthode basée sur l'analyse temps-fréquence réalisée à l'aide du logiciel maison TF-Analysis. Dans cette alternative, quatre cas de tests ont été analysés comme point de départ dans le développement d'une méthode de détection automatique des dommages d'impact à très grande vitesse pour différents types de matériaux.

La théorie de l'impact décrit l'impact en fonction de l'application, du chargement statique ou rapide et du matériau impacté comme ayant un comportement fluide. Notre approche considère les aspects vibratoires de l'impact, en examinant les phénomènes d'onde afin de préciser la déformation transitoire et les contraintes. En théorie, il existe deux approches : la théorie du comportement hydrodynamique des solides et la théorie du flux plastique. La théorie hydrodynamique de la propagation des ondes dans les solides, qui est habituellement employée dans l'étude de d'impact à très grande vitesse, considère les matériaux cibles comme un fluide compressible sans résistance au cisaillement afin de pouvoir dériver l'équation d'état des différents matériaux. Dans notre cas, les parties impliquées dans l'impact sont le projectile et la cible, et pour ce cas, les vibrations du projectile sont négligées.

Pour le cas particulier d'un impact d'un projectile sphérique sur une cible, la force de contact est décrite comme une distribution de pression sur la surface avec une amplitude variable. De plus, la force d'impact conjointement avec des déplacements modaux de la plaque cible donnent lieu à une réponse transitoire forcée matérialisée par une vibration libre. Dans la littérature, le signal dans un régime à faible vitesse est dominé par un grand mode de flexion, l'amplitude globale augmente avec la vitesse, surtout pour les composantes à haute fréquence, en revanche, pour un signal d'impact à très grande vitesse, les composantes du mode extensionnel et celui de flexion ont une amplitude comparable pour les impacts non pénétrants, mais seule une composante d'extension est évidente lorsque la cible est perforée. Dans le cas d'un impact à faible vitesse, le mode extensionnel se propage avec une vitesse plus rapide et une faible dispersion par rapport au mode de flexion qui se déplace à une vitesse plus faible et à une dispersion plus élevée. Le mode de flexion est créé par le plan médian à travers la grande flexion qui est produite parce que les projectiles à faible vitesse n'ont pas perforé la cible.

Pour l'analyse des signaux d'accélération, deux méthodes sont utilisées : la Transformée en ondelettes la Distribution Choi-Williams (*CWD*), qui est une transformation bilinéaire.

La méthode d'analyse dite transformée en ondelettes (*WT*) donne de bons résultats pour les études des phénomènes transitoires. Cette méthode associe des informations de temps avec le contenu de fréquence, chaque onde étant caractérisée par la bande de fréquence et le temps d'arrivée. L'application de la transformée en ondelettes pour caractériser le champ d'onde complexe qui résulte d’un impact a très grande vitesse a déjà été utilisée dans la littérature afin d'expliquer différents phénomènes tels que le dysfonctionnement et la rupture des composantes électroniques sensibles à bord d'un satellite.

La fonction de distribution de Choi-Williams fait partie des distributions de la classe de Cohen qui utilise un noyau exponentiel pour supprimer les termes croisés résultant des composantes qui sont à la fois dans le temps et en fréquence. Cette distribution est principalement utilisée dans l'analyse temps-fréquence des signaux de vibrations et pour le diagnostic de machines tournantes.

Analyse des résultats des tests

Pour les quatre signaux de durée comprise entre 10 secondes et 2 min qui ont été analysés, l'amplitude et la forme ont été comparées pour chaque signal. Des signaux ont été enregistrés à partir des deux capteurs (un sur la cible et l’autre à l'extérieur) afin d'identifier correctement les

dommages (pénétration ou non) sur deux types de matériaux, l'aluminium et la fibre de carbone. En raison des limitations de calcul, les signaux plus étroits (les signaux un, deux et trois) ne pouvaient pas être analysés sur toute la durée et devaient être segmentés en plusieurs signaux plus courts.

En plus du capteur placé sur la cible, le capteur secondaire monté à l'extérieur de la chambre d'essai a enregistré le signal qui montre que l'impact peut être capturé et identifié distinctement sur une structure complexe à une certaine distance de la cible impactée, tels que le dernier bouclier de protection ou la paroi intérieure dans le cas d'un système complexe de protection des débris orbitaux (blindage).

Dommages sur les matériaux et analyse des signaux

Le premier dommage qui est la perforation, correspond au premier essai sur la plaque *CFRP* de 3,175 mm d'épaisseur avec une vitesse d'impact de 1,57 km/s. L'analyse en ondelettes a montré que les grandes amplitudes du signal sont compressées dans un intervalle de 5 ms et que la largeur des pics aux amplitudes maximales n'est que de quelques microns. Pour le même signal, l'analyse avec la distribution de Choi-Williams a montré les trois pics avec 15 Hz comme maximum de l'amplitude de fréquence, pour la cible perforée *CFRP*.

Le deuxième dommage, qui représente un cas de non perforation, correspond au deuxième essai sur la plaque *CFRP* de 3,175 mm, avec une même épaisseur que le premier cas, et une vitesse d'impact de 0,88 km/s. Pour ce test, la forme de l'ondelette est modifiée, et le signal est plus court dans le temps (moins de 5 ms) avec une amplitude maximale des pics supérieur à 1 ms. La distribution de Choi-Williams a montré quant à elle les mêmes trois pics avec un pic plus prononcé et avec 30 Hz comme maximum de l'amplitude de fréquence, pour la cible non perforée *CFRP*. La double valeur de l'amplitude de fréquence est une indication importante de non-pénétration. Le matériau a absorbé la vibration (grands pics, plus petite propagation dans le temps), amplifiant la fréquence maximale.

Le troisième type de dommage, qui représente un autre cas de perforation, correspond à un essai sur une plaque d'aluminium de 0, 8128 mm d'épaisseur, à une vitesse d'impact de 0,57 km/s. La transformé en ondelettes montre deux pics de fréquence accentués avec de multiples pics d'amplitude inférieure avec une forme plus mince, sur un intervalle de 5 ms, et ayant la largeur des pics à une amplitude maximale dans la plage de microns secondes. La forme de l'ondelette est

similaire avec celle de l'ondelette du premier essai, cette forme pourrait être une caractéristique de la pénétration. La distribution de Choi-Williams montre un pic très accentué et quelques pics d'amplitude non significatifs très petits avec une fréquence maximale de 20 Hz pour l'aluminium perforé. Une valeur supérieure à la valeur enregistrée pour le premier essai sur une cible *CFRP* indique une plus grande rigidité de la cible en aluminium.

Le quatrième dommage, représentant un autre cas de non perforation, correspond à l'essai sur une tôle en aluminium de 3,175 mm d'épaisseur, à une vitesse d'impact de 0,54 km/s. Dans ce cas la transformé en ondelettes montre seulement un pic de fréquence défini avec deux pics d'amplitude inférieurs dans un intervalle de 2 ms et ayant la largeur du pic à une amplitude maximale supérieure à 1µs, ce qui est similaire à l'analyse du second test sur *CFRP*. La forme de l'ondelette est semblable a la forme de l'ondelette du deuxième essai, en effet, cette forme pourrait être une caractéristique de non-pénétration. La distribution de Choi-Williams ne montre que les deux fréquences avec une amplitude de fréquence maximale de 40 Hz pour l'aluminium non perforé. Cette constatation s'explique par le fait que le matériau a absorbé la vibration (grands pics, plus petite propagation dans le temps), amplifiant la fréquence maximale.

Discussions

L'analyse des signaux a clairement montré les différences entre les caractéristiques du signal pour le cas d'impact avec pénétration et celui de non-pénétration : forme, profil de pic et plage de la fréquence maximale.

En utilisant les mêmes caractéristiques nous pouvons également différencier la résistance des matériaux ; en effet un matériau plus rigide présente des formes plus minces sur une période plus courte et avec moins de réverbération dans le temps. Le facteur le plus important qui peut être utilisé pour identifier le type d'endommagement (pénétration ou non-pénétration), il semble être l'amplitude de la fréquence maximale. L'analyse a montré que l'amplitude a presque doublait pour le cas de non-pénétration pour les deux matériaux et est inférieure (approximativement cinq points) pour le cas d'un matériau moins rigide.

Troisième partie-Simulation numérique d'impact à très grande vitesse et analyse des signaux

Simulation des matériaux subissant des impacts à très grande vitesse

Sur la base d'un examen approfondi sur des matériaux fréquemment utilisés dans la fabrication des engins spatiaux, la troisième partie de notre recherche débute par une identification des matériaux utilisés pour les simulations numériques d'impacts à très grande vitesse.

Une revue de littérature des matériaux a révélé une variété de solutions de matériaux qui sont actuellement utilisés pour la structure des satellites et la plupart de ces matériaux sont déjà testés avec des impacts à très grande vitesse. Ces matériaux peuvent être regroupés en trois grandes catégories. La première catégorie sont les alliages métalliques tels que : l'aluminium, l'acier, les alliages de titane ou les alliages les plus récents comme le béryllium. La deuxième catégorie regroupe les matériaux composites avec différents types de fibres (fibres de verre, de carbone ou d'aramide) imbriquées dans une matrice habituelle (matrice époxy, céramique ou métallique). La troisième catégorie sont les structures sandwiches avec différents types de matériaux qui sont utilisés comme des feuilles de face (de différents types d'alliages aux composites) et différents types de noyaux (en nid d'abeille en céramique ou en mousse métallique).

Basées sur ces considérations, des simulations numériques d'impacts à très grande vitesse utilisant le logiciel LS-DYNA ont été réalisées sur un ou deux matériaux appartenant aux deux premiers groupes identifiés comme cibles et ayant comme projectile une sphère d'aluminium de type 2017 *T*4 avec un diamètre de 0,3125 cm.

Formulation numérique de l'impact

Utilisées pour générer des impacts à très grande vitesse, des simulations numériques sont utilisés spécifiquement pour les impacts à des vitesses qui sont hors de la gamme des tests. Les résultats des simulations d'impacts à très grande vitesse sont influencés par le degré des détails utilisés, par les matériaux des modèles et finalement par les équations d'état choisies.

En utilisant la modélisation par la méthode des éléments finis deux manières différentes sont utilisées pour décrire le mouvement du matériau dans l'espace : soit la grille lagrangienne (coordonnées adaptées du corps) ou la grille Eulérienne (fixée dans l'espace) soit les méthodes dites « sans maillage » appelées : Lissage Hydrodynamique des Particules (*Smoothed Particle Hydrodynamique* : *SPH*).

La modélisation par la méthode du Lissage Hydrodynamique des Particules est la méthode la plus prometteuse pour simuler l'impact à très grande vitesse mais pour notre cas, nous avons utilisé la méthode des éléments finis lagrangiens discrets, une méthode qui est similaire à celles déjà utilisés dans la littérature pour des impacts à très grande vitesse mais dans une gamme à faible régime.

Le projectile et les cibles sont modélisés à l'aide des éléments solides à 8 nœuds hexaèdre en utilisant un point d'intégration. Pour le projectile, un treillis papillon avec un élément d'une taille similaire à la taille de l'élément cible dans la zone d'impact a été utilisé. Pour modéliser le matériau du métal, nous avons choisi le modèle Johnson Cook, ce dernier inclut le dommage et le modèle de rupture en traction qui prend en considération trois effets différents, l'écrouissage, la viscosité et le ramollissement thermique.

Connaissant le diamètre du projectile, nécessaire dans la détermination des vitesses de pénétration pour la calibration des modèles numériques, nous avons utilisé les équations balistiques tirées tout simplement à partir de la littérature. Pour les simulations numériques, en plus de la vitesse de pénétration, une basse et haute vitesse ont été utilisées afin d'obtenir le signal avant la limite de pénétration et après cette dernière. Pour toutes les simulations, les caractéristiques de projectiles sont les mêmes, toutes les cibles sont des feuilles carrées rigides de 12 x 12 cm fixées autour de tous les 4 bords du carré et l'accélération résultante pour toutes les simulations est mesurée à une distance de 3,5 cm par rapport au d'impact sur la face arrière de la cible.

Pour l'étude du signal d'accélération, nous avons analysé la forme et l'amplitude de la fréquence obtenue par la distribution de de Choi-Williams.

Simulations d'impacts à très grande vitesse et analyse des signaux

À partir de la première catégorie de matériaux, les alliages métalliques, l'aluminium et le titane ont été utilisés comme cible. Pour les simulations d'impact sur les matériaux en alliage d'aluminium et pour une meilleure compréhension des caractéristiques de l'impact, nous avons utilisées l'aluminium Al 6061 -T6 alliage en deux épaisseurs : 0.08128 cm et 0,3175 cm. Pour la plaque d'aluminium Al d'épaisseur 0.08128 cm, les vitesses d'impact étaient de 0,1 km/s, 0,14 km/s et 0,3 km/s. Ce premier cas de simulation a donné un résultat soit disant particulier ne montrant aucune diminution de l'amplitude de la fréquence à la pénétration, ce qui pourrait être expliqué par le fait que de petites variations de vitesses ont conduit à l'augmentation de l'amplitude de la fréquence après la pénétration.

La deuxième plaque d'aluminium Al prise comme cible avait une épaisseur de 0,3175 cm et les vitesses d'impact étaient 0,7 km/s, 0,9 km/s et 1,1 km/s.

L'analyse utilisant la distribution de Choi-Williams pour la plaque d'aluminium épaisse Al a montré une série de pics de fréquence avec une amplitude maximale de 5 x 10^{15} Hz dans une gamme de temps de 5 ms pour les dommages avec non-pénétration. Pour les dommages avec pénétration un pic de fréquence est plus accentué avec une amplitude maximale qui a diminué presque de la moitié de la valeur (approximativement 3 x10^{15}). Ces résultats obtenus à partir des premières simulations sont en bon accord avec les essais expérimentaux effectués auparavant.

Pour la deuxième catégorie de simulations faites sur les alliages de métaux nous avons considéré le matériau Ti-6Al-4V largement utilisé dans l'industrie aérospatiale. Nous avons utilisé une plaque de 0.08128 cm d'épaisseur et les vitesses d'impact étaient 0,4 km/s, 0,5 km/s et 0,7 km/s. L'analyse de la distribution de Choi-Williams a identifié une série de similitudes avec le cas de la cible Al avec pénétration. Dans le cas de non-pénétration, seulement un pic de fréquence plus accentuée est enregistré avec une amplitude située entre 4 et 5 x10^{16}, la spécificité de la cible en titane est la cause probable de l'apparition d'une valeur différente de fréquence, au moment de l'enregistrement du pic. Les cas avec pénétration présentent la même multitude de pics de fréquence enregistrés aux différents moments de l'impact, cela pourraient être expliqué par le fait de la particularité de la plaque en titan Ti prise comme cible. Encore une fois, la même similitude avec les résultats de la session de test a été remarquée, et dans ce cas encore, l'amplitude de la fréquence des pics avec pénétration est à peu près de la moitié de la valeur des cas de non-pénétration qui ont une amplitude maximale de 2,5x 10^{16}.

Pour la simulation d'un matériau provenant du deuxième groupe (le modèle de la plaque *CFRP*), nous avons utilisé un type de fibres de carbone léger à haute résistance, des feuilles rigides carrés de 0,3175 cm d'épaisseur.

Comme modèle, nous avons utilisé un simple modèle *CFRP* bidirectionnelle avec toutes les fibres orientées dans les directions 0^o et 90^o, le résultat donne un modèle *CFRP* avec rigidité longitudinale élevée et une rigidité en torsion inférieure. Les vitesses d'impact sur la plaque CFRP était de 0,6 km/s, 0,8 km/s et 1 km/s. L'analyse la distribution de Choi-Williams pour le cas de non-pénétration a montré deux amplitudes de fréquence très nettes de 4x10^{14} sur une plage de temps de 0,5 ms. Les

deux cas de limite de pénétration et avec pénétration ont montré une diminution de la fréquence d'amplitude entre 1,5 et 2 $x10^{14}$ Hz.

Conclusion

En somme, les trois parties décrites précédemment, représentent les travaux de recherche fondamentale effectuée dans le but de développer un système de surveillance utilisant le logiciel maison TF-Analysis et basé sur un dictionnaire contenant la plupart des matériaux utilisés dans la fabrication de satellites permettant d'identifier en temps réel les dommages créés par l'impact des débris orbitaux.

Pour la session des essais expérimentaux, les tests d'impacts à très grande vitesse ont été réalisées avec succès à une vitesse d'impact soit disant dite faible, atteignant 1,6 km/s. Cette vitesse ne représente pas les vitesses des débris orbitaux des micros météorites mais elle est assez suffisante pour offrir des enregistrements de signaux valides pour une analyse préliminaire avec le logiciel TF-Analysis, la pierre angulaire de nos travaux futurs dans ce domaine. L'essentielle prochaine étape sera de continuer à effectuer ces tests avec le même mécanisme de déclanchement, afin d'obtenir une meilleure précision de la vitesse et de la séparation du sabot, mais plus important sera d'effectuer de nouveaux tests d'impacts à très grande vitesse allant de 4.5 à 5 km/s à 8 km/s, des vitesses relativement proches des vitesses d'impact des débris orbitaux des micros météorites.

Lors de la deuxième partie, l'analyse des signaux enregistrés pour les tests d'impacts à très grande vitesse donne des résultats valides identifiant le matériau le plus rigide des deux matériaux testés, soit le *CFRP* et l'aluminium Al, les amplitudes de fréquence des signaux du matériau Al étaient plus élevées que pour celui du modèle *CFRP*. Pour le même matériau, les amplitudes de fréquence du signal sont extrêmement différentes selon le type de dommage et les amplitudes de la non-pénétration qui étaient presque le double que la pénétration.

L'analyse avec le logiciel TF-Analysis de la simulation numérique d'impacts à très grande vitesse a donné les mêmes résultats que celles obtenues à partir des essais expérimentaux. La même diminution de l'amplitude de la fréquence pour l'impact à très grande vitesse a été constaté pour le cas de la limite de la pénétration, pour les deux alliages d'aluminium Al et le titan Ti pour le modèle *CFRP*.

En dépit des bons résultats obtenus lors de cette étude, ces derniers doivent être validées par un plus grand nombre tests futurs d'impacts à très grande vitesse et analysés pour différents

matériaux. Une fois ces données recueillies, il représentera une base de données importante pour la création d'un processus automatique qui reconnaît automatiquement les dommages pour les différents matériaux qui sont utilisés dans l'espace. En termes générale, l'analyse du logiciel TF-Analysis fournit des caractéristiques claires, et des amplitudes de fréquence très nettes à différentes formes la distribution de Choi-Williams. Ces nouvelles connaissances constituent une base pour la recherche future et constitue un point de départ pour le développement d'un système de surveillance des débris orbitaux des micrométéorites.

TABLE OF CONTENTS

LIST OF TABLES

LIST OF FIGURES

LIST OF SYMBOLS AND ABBREVIATIONS

AE	Acoustic emissions
AFM	Atomic force microscopy
AIAA	American Institute of Aeronautics and Astronautics
AO	Atomic oxygen
AO	Atomic oxygen
ATV	Automated Transfer Vehicle
BLE	Ballistic Limit Equations
BMG	Bulk metallic glass
BS	Bumper shield
CCD	Charge-coupled device
CFOAM	Carbon foam
CFRP	Carbon-fiber-reinforced polymer
CFRP/Al-HC	Carbon fiber reinforced plastic/aluminum honeycomb
CISAS	Center of Studies and Activities for Space
CNT	Carbon nanotube
CWD	Choi-Williams Distribution
DCPD	Dicyclopentadiene
DHC	Double honeycomb
DLC	Diamond-like carbon
DRS	Damage Recording System
EDR	Embedded Damage Recorder
EFM	Electrostatic force microscopy
EFPI	Extrinsic fiber Fabry-Perot interferometer

EMAA	Ethylene-co-methacrylic acid
EMI	Electromagnetic interference
EMI	Ernst Mach Institute
EMLI	Enhanced Multi-layer insulation
EOS	Equation of State
ESA	European Space Agency
ESD	Electrostatic discharge
EWIS	External Wireless Instrumentation System
FBG	Fiber glass
FEM	Finite element method
FFT	Fast Fourier transform
FRQNT	Fonds de recherche du Québec - Nature et technologies
GrEp	Graphite-Epoxy
HAAS	Heavy All Aluminum Shield
HC/SP	Honeycomb sandwich panels
HMS	Health Monitoring System
HRTEM	High-resolution transmission electron microscopy
HVI	Hypervelocity Impact
IADC	Inter-Agency Space Debris Coordination Committee
ICC	Integrated Cargo Carrier
IFPI	Intrinsic fiber Fabry-Perot interferometer
ISS	International Space Station
KFRP	Kevlar-fiber-reinforced polymer
LADEE	Lunar Atmosphere and Dust Environment Explorer

LDFP	Laser driven flayer plate
LEMUR	Legged Excursion Mechanical Utility Rover
LEO	Low Earth Orbit
LEO	Lower Earth Orbit
LGG	Light-gas gun
MLI	Multi-layer insulation
MM	Micrometeoroids
MMOD	Micrometeoroid and orbital debris
MPM3D	Three-dimensional material point method
MTTR	Mean time to repair
NASA	National Aeronautics and Space Administration
NDE	Nondestructive Examination
NSERC	Natural Sciences and Engineering Research Council of Canada
OBSS	Orbiter Boom Sensor System
OD	Orbital debris
OFDR	Optical frequency domain reflectometry
OFS	Optical fiber sensors
PEG	Polyethylene glycol
PZT	Piezoielectric
RBS	Rutherford backscattering
RF	Radio frequency
SAS	Solar array substrates
SBIR	Small Business innovation Research
SEM	Scanning electron microscope

SEM	Scanning electron microscopy
SHC	Single honeycomb
SHM	Structural health monitoring
SiC	Silicon carbide
SMA	Shape-memory alloy
SOLID	Solar panel based space debris impact detector
SOM	Self-organizing map
SPH	Smoothed-particle hydrodynamics
SRL	Schaefer Ryan Lambert
SRS	Shock response spectrum
STF	Shear thickening fluid
STFT	Short-Time Fourier Transform
SWCNT	Single walled carbon nanotube
TEM	Transmission electron microscopy
TF	Time- Frequency
TMLI	Toughened Multi-layer insulation
TPS	Thermal Protection System
UHMWPE	Ultra-high-molecular-weight polyethylene
WDM	Wavelength division multiplexing
WLEIDS	Wing Leading Edge Impact Detection System
WT	Wavelet transform
XMM	X-ray Multi-Mirror Mission
XPS	X-ray photoelectron spectroscopy
YSZ	Yittria stabilized zirconia

LIST OF APPENDICES

CHAPTER 1 INTRODUCTION

1.1 Introduction

The current space environment is becoming increasingly hostile for all types of space vehicles due to the accumulation of orbital debris (OD). Based on recent studies this number continues to increase and the process is irreversible. This phenomenon is called the Kessler effect.

The velocities of OD are up to 17-20 Km/s and micrometeoroid (MM) velocities are up to 70-80 Km/s. The effect of an impact on space assets varies from degraded performance to catastrophic loss.

This research is conducted to respond to the need to provide a safe and healthy structure for satellites or crewed spacecraft that operate in this environment.

The high-energy damage caused by impacts from micrometeoroids and orbital debris (MMOD) could pose risks to the crew, resulting in loss of life or in loss of critical spacecraft subsystems.

The growing need for a better understanding of the interaction of space debris with space systems motivates the creation of an integrated Health Monitoring System (HMS) to monitor shield degradation in real time or near-real time. Based on the monitoring results, the spacecraft operation could be adjusted accordingly.

Continuous monitoring of MMOD protection systems or shields would greatly increase the effectiveness of inspection and repair schedules and planning of extra-vehicular activities.

In addition to benefits for MMOD protection, HMS information could also be used for calibration of dust models.

The critical element in the design of a spacecraft is the mass and the cost to launch and place that mass into orbit. Due to recent developments in sensor technology, low-mass and low power sensors provide new possibilities for detection and location of MMOD impacts. These sensors can provide data for anomalies and failure analysis and can even gather and send signals describing orbital debris fluxes.

Data collected simultaneously from a variety of sensors should be integrated; the fusion of this data becomes useful for effective decision making in spacecraft operations.

The main objective of this research project is to provide a method that leads to the development of an intelligent Health Monitoring System (HMS) for Micrometeoroid and Space Debris (MMOD) protection systems. This comprehensive method could also be applied to other spacecraft structural components.

The HMS for MMOD protection system will have the following capabilities:

- Provide real time or almost real time monitoring of the condition of protective shields;
- Provide information for scheduling maintenance;
- Determine if the shield meets specified performance criteria for no penetration and also, depending on the location or interest, for other types of damage, such as detached spalling;
- Identification of damage at a component level and provide useful information regarding the condition of component such as incipient cracks or cratering;
- Assess the integrity of shields after impact;
- Provide estimation of the lifetime of a structure based on damage and operating parameters of spacecraft;
- Provide information that can be used in the development of new shields or in optimizing the current shielding;
- Increase safety of spacecraft.

To meet these objectives the system has to detect damage at the component level.

1.1.1 Hypervelocity Impact (HVI) Tests

HVI tests are the most important part of developing an HMS for MMOD protection; these tests must be done to validate any MMOD protection design.

MMOD protection or shields are the protection system developed generally for the spacecraft with crew such as the International Space Station or Columbus Orbital Facility.

In this case the shields are mounted on top of the spacecraft shell. The impact sensors should detect the impact on the shields at the component (bumper), on the other side the level of the pressure inside the spacecraft is monitored by the pressure sensors.

HVI tests are also the most direct method of deriving the Ballistic Limit Equations (BLEs). Numerical simulations must be developed and results obtained correlated with test results since the range of test velocities are much lower than the actual impact velocities in LEO space. This validation of numerical simulations using HVI test results is the only means available to analyze impact phenomena for velocities that lie outside the tested velocity range.

Knowledge of impact phenomena at the tested velocities is important to establish the Equations of State (EOS) of shielding materials to extrapolate and model the behavior of shields at higher velocities.

HVI tests results are the reference points for BLEs within the testable range and their verification provides data for hydrocode simulation.

The set-up of a testing session could be either a simple low-cost series of tests or a detailed set of tests depending on the goal in understanding impact phenomena. A testing session requires launching facilities and also a recording methodology.

Facilities used for HVI could be:

- One-stage powder guns;
- Two-stage light-gas guns (LGG) – generally used for HVI tests;
- Three stage LGG – velocities up to 19 km/s;
- Electromagnetic launchers;
- Electrostatic launchers;
- Blast/explosive launchers.

Analysis and simulations are used along with test data to develop BLEs for use in MMOD risk assessment. BLEs should be obtained from a combination of laboratory experiments, analytical models and numerical simulations.

1.1.2 HVI simulations

The HVI simulations or hydrocodes solve all the fundamental conservation equations (mass, momentum and energy) as well as equations describing shock and dynamic material behavior. These equations are highly coupled and non-linear.

The name ‘hydrocode’ refers to the fluid-like behavior of a material when local pressures are experienced during HVI; as the distance from the impact point increases, the strength of the material becomes more important. HVI tests should be used to establish the EOS of the impacted materials, the relationship between pressure, density and internal energy of the materials and provide a complete set of equations governing hydrodynamic behavior.

The standard approach to solve partial differential equations is to discretize the domain through a grid of nodes connected together. There are two general techniques to describe material motion in space: body-fitted coordinates – a Lagrangian grid used for structural dynamics and a grid fixed in space – a Eulerian grid more common for fluid dynamics. There are also some other techniques based on both of these, such as SPH or the particle-element technique.

1.1.3 Time- Frequency (TF) analysis

There are two major approaches to detect and classify hypervelocity impact damage; one based on consideration of the spectral content (time-frequency method) or another aimed at analyzing the behavior of the signal in various scales of observation (time-scale methods).

In this work, Time-Frequency analysis is proposed to identify the damage of an MMOD impact protection system. This TF analysis is based on the study of the frequency domain transformed signal form in the time domain.

The two most popular time-frequency distributions are; Short-Time Fourier Transform (STFT) or spectrogram and the Wigner-Ville distribution.

Cohen reviewed a class of time-frequency distributions which included spectrogram, Wigner-Ville distribution, Choi-Williams and others.

For the present research a spectral analysis is used, which helps in detection of the damage and the signal evolution in time and gives information on type and position.

Based on the TF analysis the development of a signal database/dictionary for the state or condition of the shield component (layer damage or penetration) can be done.

A shield health monitoring system cannot be efficient without identification of the damaged shield component.

In identifying the shield component, measured vibrations are very important elements. In a multi-component shield the recorded vibrations could describe the damage or penetration of one bumper or multiple bumpers and, in case of complete failure, penetration of the rear wall.

Furthermore, depending on the type of bumper the damage could have different forms, from surface degradation to spalling, cracking, delamination and to complete perforation.

Each type of damage and component can be identified by the vibration measured. Unfortunately however, the case of HVI shield damage is a complex phenomenon which involves a combination of components and types of damage.

One solution to this complex problem would be to mount the sensors as close as possible to the damaged area, as is presented in the literature review. This can be done by imbedding the sensors in the component material. This solution is still in development and embedding sensors in material remains a very expensive process.

Also, this approach works only with new protection systems and not with existing systems such as the current International Space Station (ISS) shielding. Inaccessibility to the components of existing spacecraft shielding is the problem.

For existing shielding the only way to measure these vibrations is to mount the sensors on the rear wall (the spacecraft shell) or in the best case on the external surface of the spacecraft, represented by the first bumper of the shield. Consequently, the vibrations measured will represent the vibration of the entire protection system.

The solution proposed in this research provides a method applicable to existing as well as new shielding. Also this research solution is a competitive and accessible alternative.

After mounting the sensors and recording the vibrations, the challenge is to decompose or separate de signal to identify the shield component and the type of damage.

Validation of the developed system will conclude the research and further development of the system.

CHAPTER 2 LITERATURE REVIEW

The literature review for this research concentrated on two main areas: a review of work done on the subject and a review of the methods used to develop solutions that are similar to the present method.

The present chapter will cover the literature review related to work done in HMS of spacecraft structures in general and of protection systems/shields in particular.

There are vast and diverse publications on structure health monitoring, mostly applied in the civil sector. This will not be the object of this review, but was accounted for in the development process of the research.

MMOD impact detection systems for spacecraft started to be developed from the first launches into space in the 1960s. The sensors were mainly used to characterize the Lower Earth Orbit (LEO) environment.

The solutions presented by literature on the subject include various combinations of sensors proposed to detect impacts on the ISS, Shuttle Orbiter and other spacecraft [3], [8], [9].

These combinations of sensors are embedded in the material and provide information on the detection of external impact and depth of the penetration. There is no integrated method that quantifies the impact that penetrates each layer of the shielding.

Most of the proposed solutions include sensing material layers that are intended to be intercalated between the shielding components/bumpers, such as thin aluminized polymer sheets.

Other solutions present acoustic or piezoelectric sensors embedded under the top or inner layers of materials that will sense impact-generated holes.

The only impact monitoring system qualified to be used on manned spacecraft is the Wing Leading Edge Impact Detection System (WLEIDS). For this system, accelerometer sensors are integrated into the leading edge of wing of the shuttle and continuously record data during launch. The data recorded are wirelessly transferred to an internal data acquisition system [3].

The system that monitors impacts on the Thermal Protection System (TPS) requires high power consumption is therefore limited to the launch phase. For the remainder of the mission an optical system is used.

An alternative solution is presented by NASA's recent MMOD Damage Recording System (DRS); a mass and power-efficient wireless impact detection system designed for future incorporation in the Crew Exploration Vehicle shell [24].

Designed wireless nodes record impact data through an Embedded Damage Recorder (EDR) sensor. A variety of EDR sensors were considered based on the damage that will be detected and how the sensors are integrated into the TPS. The EDR sensor is a network of wire traces embedded within a flexible printed circuit board. A continual test is performed on the network to determine the impact damage fracture. The EDR represents a solution that could be used to monitor the impact on the rear wall of the space vehicle underneath the TPS or it could be embedded between composite face sheets in an aluminium honeycomb rear wall.

Other technologies fitted to detect a MMOD hypervelocity impact could use acoustic emission [2] or fiber optic [26] sensors.

The main advantage of Acoustic Emission (AE) sensors, a piezoelectric element, is the fact that a power source is not necessary to generate the signal. The sensor is used as a trigger for data acquisition. The systems are in low power mode in case of no impact.

Other advantages include the potential to determine impact location through triangulation and comparison of signal strength and characterization of damage depth and area.

As disadvantages, there is potential for false data such as recording an impact that does not produce damage and the short-time sensing required to record the event (μs).

A solution that uses fiber optic technology was developed at the University of Toronto Institute for Aerospace Studies. Based on the same approach of embedding sensors, optical fiber sensors are arranged to form an impact detection grid in a "Smart" Kevlar fabric material. In case of damage the light signal that circulates through the fibers is attenuated. This is a major advantage of this sensor type. In case of perforations the fibers are also perforated and the signal is cut in these areas.

MBP Communications Inc investigates an MMOD impact detection system that uses a fast acquisition (2MKz) optical fiber sensor. The developed model is calibrated using standard strain gauges [8].

The main factor in using fiber optic sensors is the development cost associated with miniaturization on a broad production scale.

An inflatable or deployable structure is studied for future space vehicles and as habitats for future surface operations [9-11]. Inflatable structures are considered in this review due to their similarity to Multi-Shock shields and because the entire structure provides an MMOD impact protection function.

There is currently no design in place for such space vehicles or habitats and therefore it is not possible to develop a detailed impact health monitoring system. However, the need to maintain a safe environment exists and some solutions can be identified.

The requirements are similar; time, location of impact, depth of the penetration and extent of the damage. An additional requirement that could be addressed by the HMS is an assessment of the structural strain around material interfaces, flexible and rigid components or to monitor the deployment dynamics to ensure proper inflation.

In the case of inflatable space vehicles the traditional health monitoring solution using strain gages or fiber optic sensors is not appropriate due to the difficulty of integrating these sensors in a flexible structure and the deployment process.

The proposed solutions for such structures involve the use of networks of ultra-low or no power sensors. These sensors and their associated wireless communications systems must be integrated in a thin "blanket" sensor array that covers the critical surfaces. One approach is based on embedded flexible inductors [12] and the other is based on embedded capacitors [10].

In all solutions identified in the present review, largely based on embedding specific kinds of sensor technology, real-time sensing is the essential element of the impact monitoring system. There are a variety of sensors that could be implemented, such as fiber optic sensors, active and passive acoustic sensors, accelerometers, resistor based detectors, capacitive sensors and remote wireless technologies.

There is another type of sensing solutions that does not require embedding in the material. These are non-contact systems such as laser vibrometry [13], shearography [14], laser ultrasound [15], infrared thermography [16] and cameras/optical systems [17].

Using bumper vibrations to monitor the health of a spacecraft shield is one approach that was previously used in impact monitoring of a spacecraft (WLEIDS) and would also be suitable for the proposed research due to the complex vibrations that are generated. Use of accelerometers to

monitor these vibrations is a feasible option [18] based on the ability of these sensors to detect the impact and also the intensity of the damage.

Depending on the mounting locations on the shield, disturbances in the signals due to the impact, such as attenuation, reflection, and superimposition should be considered.

The system must be tailored for this special application so that measurements are taken at multiple points simultaneously. In order to improve accuracy it's important to have spatial-temporal cross correlations between the data obtained by each sensor.

Comparison of the time-frequency [1] and/or wavelet analyses of the signals [13-17] obtained in baseline and impacted conditions can lead to identification of different types of damage [19-20].

Different types of sensors are evaluated [13] from the point of view of working principle, measurement capabilities and ranges, potential application to space, demands on the spacecraft and readiness at the state of the art. Acoustic sensor or accelerometer networks appear to be the most suitable sensors for spacecraft protection systems.

The application of acoustic sensors on real spacecraft structures is challenging task, particularly for use on an existing shielding system [17].

2.1 References

[1] A. A. Lakis, M. H. Toorani, "Application of time-frequency method in fault diagnosis of rotating machinery", 3rd International Conference on Integrity, Reliability and Failure. Porto/Portugal: Mechanical Engineering Dept., École Polytechnique of Montréal, 2009.

[2] Champaigne, K.D., "Low-power Electronics for Distributed Impact Detection and Piezoelectric Sensor Applications", Aerospace Conference, 2007 IEEE. Big Sky, 2007.

[3] Champaigne, K.D., Sumners, J., "Wireless Impact and Leak Detection and Location Systems for the ISS and Shuttle Wing Leading Edge", Aerospace Conference, 2005 IEEE. Conroe, TX, 2005. 1-8.

[4] Christiansen, Eric L., *Handbook for Designing MMOD Protection*. Houston, NASA Johnson Space Center, 2009.

[5] Cohen, L., "Time-frequency distribution - a review". Proceedings of the IEEE, Vol. 77, 1989: 941-981.

[6] Cramer, K. E., Winfree, W. P., “Thermal characterization of defects in aircraft structures via spatially controlled heat application”. Thermosense XVIII. Orlando, 1996.

[7] Deobling, S.W., C.R. Farrar, and M.B. Prime, “Summary Review of Vibration-Based Damage Identification”, *The Shock and Vibration Digest*, Vol. 30, 1998: 91-105.

[8] E. Igenbergs, et al., “Mars Dust Counter”. In Dust in the Solar System and Other Planetary Systems, by I. Williams, T. McDonnell, N. McBride S.F. Green, 176-180. Oxford: Elsevier science Ltd., 2002.

[9] Eckart, Peter, “Parametric Model of a Lunar Base for Mass and Cost Estimates”. Munchen, 1996.

[10] Eric I. Madaras, Robert F. Anastasi, Jeffrey P. Seebo, George Studor, Douglas L. McMakin, Robert Nellums, William P. Winfree, “The potential for imaging in situ damage in inflatable space structures”. AIP Conf. Proc. 975. Golden, 2007. 437-444.

[11] Erik J. Brandon, Max Vozoff, Elizabeth A. Kolawaa, George F. Studor, “Structural health management technologies for inflatable/deployable structures: Integrating sensing and self-healing”. *Acta Astronautica*, Vol 68, Issues 7-8, 2011: 883-903.

[12] F. A. Andrade, I. Esat, M. N. M. Badi, “Gearbox fault detection using statis-tical methods, time-frequency methods (STFT and Wigner-Ville distribution) and harmonic wavelet - A comparative study”. 12th International Congress on Condition Monitoring and Diagnostic Engineering Management (COMADEM'99). 1999. 77-85.

[13] IADC WG3, “Sensor systems to detect impacts on spacecraft”. Inter-Agency Spacel Debris Coordination Committee, 2012.

[14] K, Maji A, “Assessment of Electronic Shearography for Structural Inspection”. *Experimental Mechanics*, Vol. 34, No.2, 1997: 197-204.

[15] Krohn, N., Stoessel, R., Busse, G., “Defect-selective imaging by non-linear scanning vibrometry and by non-linear air-coupled ultrasound inspection”. *Review of Progress in QNDE*, Vol. 20, 2000: 1666-1672.

[16] Max Welling, Markus Weber., “A Constrained EM Algorithm for Independent Component Analysis”. *Neural Computation*, Vol13, No.3, 2001: 677-687.

[17] N. Baydar, A. Ball., "A comparative study of acoustic and vibration signals in detection of gear failures using Wigner-Ville distribution", in *Mechanical Systems and Signal Processing*, Vol 15, by IDEAL (Project), 1091-1107. Academic Press, 2001.

[18] P.Castellini, G.M.Revel., "Damage Detection by Laser Vibration Measurement". 15th World Conference on Nondestructive Testing. Roma, 2000.

[19] Q. Meng, L. Qu., "Rotating machinery fault diagnosis using Wigner distribution" in *Mechanical Systems and Signal*, Vol 5, by IDEAL, 155-166. Academic Press, 1991.

[20] R J Dewhurst, Q Shan., "Optical remote measurement of ultrasound". *Measurement Science and Technology*, Vol. 10, No.11, 1999.

[21] S.E. Woodard, B.D. Taylor, T.W. Jones, Q.A. Shams, F. Lyons, D.A., "A method to have multi-layer thermal insulation provide damage detection". 48th AIAA/ASME/ASCE/AHS Structures, Structural Dynamics, and Materials, AIAA, 2007. 1-23.

[22] Shannon Ryan, Eric L. Christiansen, *Micrometeoroid and Orbital Debris (MMOD) Shield Ballistic Limit Analysis Program*. Houston, NASA Johnson Space Center, 2010.

[23] Sirkis, James S., J. K. Shaw, Timothy A. Berkoff, Alan D. Kersey, E. J. Friebele, and Richard T. Jones, "Development of an impact detection technique using optical fiber sensors and neural networks". Smart Structures and Materials 1994: Smart Sensing, Processing, and Instrumentation. Orlando, 1994.

[24] Swanson, G.T., Cassell, A.M., "Micrometeoroid and Orbital Debris impact Damage Recording System". Aerospace Conference, IEEE. Big Sky, 2011. 1-8.

[25] Tarazaga, Pablo A., Daniel M. Peairs, W. Keats Wilkie, and Daniel J. Inman, "Structural health monitoring of an inflatable boom subjected to simulated micrometeoroid/orbital debris damage". Nondestructive Evaluation and Health Monitoring of Aerospace Materials, Composites, and Civil Infrastructure. San Diego, 2006.

[26] Tennyson, R. C., "Spacecraft damage assessment due to hypervelocity impacts using a micrometeoroid and orbital debris detection system". *Canadian Aeronautics and Space Journal*, 55(2), 2009: 89-95.

[27] Tennyson, RC, Morison, WD., “Design Study of Fiber Optic MOD Impact Detection System for Spacecraft Structures”. *NASA Tech Briefs*, June 2012; 37.

[28] U. Qidwai, A. H. Costa, C. H. Chen., “Detection of Ultrasonic NDE Signals Using Time-Frequency Analysis”. *Insight*, vol. 41, no. 11, 1999: 700-703.

[29] W. J. Wang, P. D. McFadden, “Early detection of gear failure by vibration analysis I. Calculation of the time-frequency distribution” in *Mechanical Systems and Signal Processing*, Vol. 7, by IDEAL (Project), 193-203. Academic Press, 1993.

[30] Welling, Max, Markus Weber, “Independent component analysis of incomplete data". Proc. of the 6th Annual Joint Symposium on Neural Computation. Pasadena, 1999.

[31] IADC WG3, *Protection manual.* 2012.

CHAPTER 3 PROJECT DESCRIPTION

The present thesis describes the work done for the development of a new method of monitoring MMOD impact damage on a spacecraft structure or its protection system. The presented research is the basis for creation of an integrated MMOD health monitoring system.

The effects of HVI vary from cratering to complete penetration of the protective bumper or shell. In order to maintain the integrity of a satellite or crewed spacecraft, an integrated system of monitoring of such impacts is necessary. Current solutions are based on a combination of different sensors embedded in the structure material. This research proposes an integrated health monitoring system for the structure or shield protection system for detection and classification of impacts in real time using Time- Frequency (TF) analysis. To achieve this it is also necessary to develop a signal database/dictionary to accurately describe the state of each shield component (layer damage or penetration).

Vibration acceleration caused by impact is the principal parameter for our analysis of hypervelocity impact damage. Two methods are used to create data describing impact damage; hypervelocity impact tests and numerical simulations.

Hypervelocity tests are performed to validate the protection capability of certain materials or protection systems. However, the range of hypervelocity impact tests only covers about 40% of the actual velocity of orbital debris. In Canada the maximum attained velocity for this kind of tests is approximately 8 to 9 Km/s. To estimate impact damage for the remainder of the OD velocity range, numerical simulations and analysis are applied.

After a short introduction in Chapter 1 and the literature review in Chapter 2, the thesis continues with the essential work that was published in a series of three articles that cover the HVI testing session, the numerical simulations and the TF analysis of the signals recorded.

The rest of this thesis is structured as follows:

Chapter 4 presents the results of an experimental testing session, which was carried out to acquire valid vibration signals. These acquired signals are then studied using in-house signal analysis software to determine the characteristics of HVI damage.

In Chapter 5, a method of detection and classification of HVI damage is developed based on time-frequency analysis using the TF-Analysis software. To reach this goal, four test cases were

analyzed as a starting point. The intention is to develop a method of automatic detection of HVI damage for different types of materials.

Chapter 6 presents the second part of the research; the HVI simulations that were performed on one or two materials from each categorized material group. These categories were identified based on an extensive review of materials that are frequently used in the manufacture of spacecraft. Using the LS- DYNA software and TF analysis of the HVI, the numerical simulation generated the same results as the analysis done on the signals obtained in the experimental test session.

CHAPTER 4 ARTICLE 1: HYPERVELOCITY IMPACT (HVI) TESTS & SIGNAL RECORDINGS

L. E. Iliescu, A. A. Lakis and A. Abou – Antoun

Department of Mechanical Engineering, École Polytechnique de Montréal
C.P. 6079, Succ. Centre-Ville, Montréal
Québec, Canada H3C 3A7

Universal Journal of Aeronautical & Aerospace Sciences 2 (2014), 80-113
www.papersciences.com

4.1 Abstract

Among the other hazards that occur in space environment, due to the increased space activity, especially the intensification of spacecraft lunches but also to the poor standardization of space activity or lack of means in cleaning the space environment from space debris and non-functional satellites, the number of potential micrometeoroid and orbital debris impact continue to grow exponentially, fact that could render the space in-utilizable in the next decades. The aim of this paper, as a part of larger work, is to present the experimental part that was performed in order to acquire valid vibrational signals that afterwards will be studied using an in-house signal analysis software in order to determine in real-time the characteristics of hypervelocity impact damage. Starting from the selection of materials which are used mostly for the impact protection systems but also for the spacecraft structure and from of thoroughly review of impact detection technologies, six hypervelocity tests were performed in low-velocity regime on aluminum and carbon fiber targets. As a result, valid recordings of accelerations were obtained from the sensors mounted on the targets and outside of testing chamber. Moreover, the experimental session permitted to have an insight in preparation of this type of tests, specific to space debris hypervelocity impact, as well as the particularities in performing the test and acquiring useable signal for further analysis.

Key Word and Phrases

Hypervelocity Impact, Orbital Debris, Vibrational Signals, Collision Risk, Damage Tests.

4.2 Introduction

Every satellite or space vehicle launched in space has the potential to create orbital debris. Any hypervelocity impact between two objects of sizeable mass can spall off a debris cloud and secondary eject from the force of collision. Each piece of material resulting from the impact has the potential to cause further damage, creating even more space debris. If the collision is large (i.e. between a space station and a defunct satellite), the amount of cascading debris could be enough to render Low Earth Orbit essentially unusable. Damage due to smaller debris has now grown to become a significant problem in its own right. Chipping of the windows of the space shuttle along with minor damage to its thermal protection (TPS) system tiles became common by the 1990s.

There are currently more than 22,000 pieces of orbital debris that are tracked and their presence around the planet poses a high collision risk to valuable satellites and other spacecraft. Considering that space debris is largely uncharacterized, it is hard to protect against it. Using existing technology, debris with sizes in the 1 to 5 cm range cannot be detected and tracked. Although most debris will burn up in the atmosphere, larger objects can reach the ground intact and present a risk. A lack of test data poses a threat to the detection of space debris. In addition, some research work is classified or only preferentially shared.

Improved definition and characterization of orbital debris (OD) through development of HVI testing capabilities to over 10 km/s and high strain modeling hydro-codes is a major international issue. An additional global challenge is the development of new light materials and new design configurations offering protection against OD in the 1 to 5 cm range.

The damage and debris generated by an MMOD impact is a complex phenomenon that involves resolving problems such as shock and dynamic material behaviour. In the case of an aluminum shield, for example, the collision creates a nearly hemispherical crater and, depending on the thickness used, internal fracturing or attached/detached spallation.

The aim of this document is to provide a synthesis of knowledge and experience on the HVI impact test and damage. Tests were performed at the Shock Wave Physics laboratory of McGill University with respect to spacecraft protection against orbital debris and micro-meteoroids. The primary objective of the paper is to capture results and signal recordings of the tests. This document provides a framework that allows further time- frequency analysis of the signals in order to produce a real-time detection of different types of HVI damage. More specifically, this paper provides a

short literature review of materials used in MMOD protection, a summary of sensor types used to detect HVI impact damage, a description of the impact facility and recorded test data/results. This document is the first part of a larger work that will include; TF analysis of signals, HIV tests at higher speeds (up to 8 km/s) and the use of fiber glass (FBG) sensing technology to enable accurate detection of HVI damage in real time.

4.3 Literature review of micrometeoroids and orbital debris (MMOD) and impact protective materials

4.3.1 General considerations

A short literature review summary is presented to describe the characteristics of materials that are generally used to shield against high velocity impacts. To assess the potential of various types of materials for use as protection against MMOD impact, a significant number of tests should be carried out and the results compared to a baseline material, usually Al6061T6.

E. L. Christiansen [1] performed a series of 66 HVI tests to assess the potential of various materials such as aluminum, titanium, copper, stainless steel, nickel, nickel/chromium, reticulated vitreous carbon, silver, ceramic, aramid, ceramic glass, and carbon fibre. In addition, structures such as monolithic plates, open-cell foam, flexible fabrics and rigid meshes, arranged in various single or multiple bumper configurations were tested to evaluate their effectiveness as MMOD shielding.

The performance of these materials and structures was evaluated through target damage assessment reported to their respective weight. Cour-Palais [2] presents one of the first reviews of HVI on metallic, glass and composite materials. The paper describes in detail the impact damage phenomena on these materials. Schonberg [3] presents the results of several tests performed on different composite materials, taking into consideration the advantages and disadvantages of using composites in MMOD shielding structures. The results show that composite materials perform differently depending upon their location within the shielding structure. The conclusion was drawn that the use of composite materials in combination with metallic materials such as aluminum in a shielding structure can significantly increase MMOD impact protection compared with traditional all-metallic structures of similar weight. K. Fuji [4] performs HVI in a very low-velocity regime (500–1230 m/s) using a steel sphere as a projectile and analyzes the perforation behaviour of targets

of different carbon fibers, interlaminate sequences and configurations (cross-ply, woven cloths, or thickness).

The paper analyzes the damage mechanism from the point of view of absorbed energy using high speed cameras and after-shot observations and concludes that fracture mechanisms occur in different manners depending on the thickness, strength and fracture strain fiber of the sample. A detailed examination was also made of the fracture on the rear and front faces of the sample (corroborated with delamination) depending on the impact energy. Y. Nagao [5], through the measurement of collision fractures, internal damage and residual compression strength, reports a relation between collision energy and damaged area based on the results of HVI and non-destructive tests. Compression tests showed that the residual strength depends on plate thickness when it is not perforated. In the case of a perforation, a plate of different thickness has the same residual strength. Also, a reduction in residual strength is caused by the many cracks that occur inside the laminar.

D.Burger [6] presents a ballistic impact simulation using three constitutive models on an alumina plate and an ultra-high molecular weight polyethylene (Dyneema HB25) composite. The damage results were compared with experimental low velocity tests, which were done at a similar velocity to that recorded during the McGill testing session presented in the next chapters (approx. 550 m/s).

The constitutive models used are:

- JH-2 model; a constitutive model suitable to predict the behaviour of brittle materials subjected to extreme loading (pressure-dependent strength, damage and fracture, significant strength after fracture, bulking and strain rate effects).
- Johnson-Cook model; a phenomenological model commonly used to predict the material response of metals subjected to impact and penetration (reproducing strain hardening, strain-rate effects, and thermal softening).
- Contact logic to predict mixed-mode delamination growth in composites (formulation for the interfacial material behaviour is defined in terms of a linear-polynomial stress-relative displacement constitutive law).

As result, the ceramic model can only accurately predict the energy absorption and does not predict delamination or residual deformation. M. Tanaka [7, 8] describes the development of four kinds of

shields using Vectran (liquid crystal polymer) fibers in different forms; a cloth, sheet or a lump of threads and in different shield configurations. Six HVI test were performed with a 13 mm diameter polycarbonate projectile and results showed that the targets offered the same protection capability as in the case of using Kevlar. This was achieved due to the method of sewing along with the mixture of knitted cloth with the lump of threads, which contributed to the distribution of shock impact energy.

Y. Akahoshi [9] presents an inflatable MMOD impact protection that contains aluminum (Al2024-T3), high strength Vectran fiber and inflatable polyurethane. The HVI tests were performed on configurations containing polyurethane with different areal density and parameters, such as; penetrated areal density, penetrated total thickness or mass distribution of fragments in a debris cloud. The HVI test results showed that the damage is not proportional to, but depends on the areal density of the polyurethane. The best performance of shields was recorded for a 0.525 kg/m2 areal density. Polyurethane and the Vectran fibers are also effective in capturing the debris cloud and might cause a secondary impact. Further configurations that use aluminum foam instead of aluminum or variable space intervals could bring an improvement in the level of MMOD protection.

In Z.G. Wei's review [10], there is an entire paragraph on the use of shape-memory alloys - SMA (dissipate strain energy: four times more effective than high alloy steel and 16 times more than graphite/epoxy composites) to stop the propagation of cracks and for closure of cracks that appear due to HVI. He also studies the hybridization of thermoset matrix composites with SMA in order to increase the impact damage resistance. For low-velocity impacts SMA hybrid composites increase the total energy absorbed, with contact energy absorption being the most effective mechanism. At high velocities more work is needed to have a validated conclusion, but SMA hybrid composites with improved impact resistance could be a valid option for future MMOD impact shields.

In one of the earliest papers written on subject, J.H. Robinson [11] introduces metal matrix components as bumper materials due to an essential property: they can be tailored for such applications. The paper presents a study of seven aluminum matrix composites of two types; containing continuous graphite fibers and silicon carbide particulates. These are compared to a baseline, an aluminum bumper, from the point of view of penetration, damage mechanism and the

effect of fiber characteristics. The results showed, in most cases, that there was no perforation or spallation of the rear wall (behind the aluminum bumper), compared to perforations of the rear wall in the case of the metal matrix bumper. Also, the aluminum bumper was much more successful at breaking up the projectile; although for some tests it seemed that the metal matrix composite performed marginally better (smaller crater or no spallation on rear wall). The tests concluded that particulate composites are more effective than continuous fiber composites, especially for the sample 6061 Al w/25V/o SiC particles with no penetration on the rear wall, but hundreds of craters were formed. Ultrasonic scans revealed internal delamination that extended for distances approximately three times the diameter of the penetration hole. Other general conclusions: projectile ratio increases with bumper thickness, particulate composites perform better than aluminum and fiber content and orientation play a role in the effectiveness of composites as bumpers (zero degree fiber orientation was the better of the three tested).

S Katz [12] investigated the HVI of a laser driven flayer plate (LDFP) at 3 km/s on Kevlar 29/epoxy, Spectra1000/epoxy and Spectra-RF/epoxy thin film micro-composites (thickness of about 100 mm). Based on the composite characteristics (the fiber, the matrix and the fiber/matrix interface properties) the paper looks at how these materials respond in the case of HVI, through visual and microscopic examination of the damage. The fracture mechanism in the microcomposites is deduced using the absorbed HVI energy. For each case, the paper presents a discussion of delamination, matrix cracking, fiber/matrix debonding, fiber pull out, new surface creation, interface failure and fiber fracture. A model is proposed that uses the measured material properties, the measured damaged area, visual post-impact observations and analysis of the different damage modes. In terms of damage, Kevlar 29 based micro-composite showed matrix and fiber damage (strong interfacial strength), Spectra 1000/epoxy showed mainly fiber pulls out (new surface creation) and Spectra-RF/epoxy showed cracks in the matrix, breakage of fiber and fiber pull out (increased interface strength due to fibers etching in oxygen RF).

Two other comprehensive papers cover the area of HVI damage prediction and modeling in composites in two parts, part I [13] and part II [14]. Part I [13] presents the development of an extended orthotropic continuum material model and associated material characterisation experiments necessary for AUTODYN simulations of HVI. The proposed model offers a correct thermodynamic response under shock wave loading and predicts the extent of the damage and the residual strength in fibers.

Part II [14] presents the results of the two HVI tests, one to generate a correct evaluation of damage that was performed on an optimized configuration and the second to reproduce the HVI strain rates and compression in a target. Multiple damage analysis techniques are used such us: visual, ultrasonic or residual strength measurements. The paper also presents simulations using mesh-based hydro-code and SPH formulations.

A recent paper by M. Rudolph [15] investigates the possible use of different flexible materials as first bumpers in a shield configuration. Materials such as ceramic, aramid, carbon fabrics and thin metallic mesh were HVI tested to determine the projectile fragmentation they induce. The results of these tests are compared with results of HVI tests on aluminum targets that have the same areal density.

The paper presents the most important factors that should be considered in a case of HVI on this type of targets:

- Location of impact with respect to the dimensions of fabric texture, compared with the projectile diameter;
- Multi-shock effects due to the standard thickness of the fabric sheets; multiple layers are used to adapt to the necessary thickness;
- Weave-dependent effects, multiple weaving patterns on the market - Directional effects, different number of fabrics on opposed directions.

Impact patterns are an important impact detail analyzed in the paper together with penetration diameter and location. This was done using analysis software developed by the Ernst Mach Institute (EMI). The results show a random impact pattern for some fabrics, whereas others show a symmetric damage pattern around the shot axis (similar to aluminum targets) induced by the shock transfer. The beta-cloth and Multi-layer insulation (MLI) used on top of the target played an important role by providing the ability to induce a projectile fragmentation symmetric shock. The paper indicates that the Reflex 1420 and Kevlar 129 fabric samples are the best materials for fragmenting a spherical aluminum projectile of 5 mm diameter at 6.3 km/s with the reserve that more tests need to be performed in order to confirm this result to a higher degree of certainty.

B. Cheeseman [16] presents a detailed review of the factors that influence ballistic performance of flexible materials targets; the material properties of the yarn, fabric structure, projectile geometry

and velocity, far field boundary conditions, multiple plies and friction. After a vast review of different fabric materials (Spectra, Twaron, UHMWPE, Dyneema or Kevlar), each assessed individually, the paper recognizes that hybrid combinations of these materials could offer increased ballistic performance.

The paper also shows the effect of factors such as ketene dimer surface treatment, which include decreasing friction and influencing ballistic results. R. Destefanis [17] provides a good characterisation of Kevlar material, which is presently used in different material combinations for MMOD protective shields. Also, based on its excellent ballistic properties, compatibility with the space environment and extensive data from HVI tests and simulations, Kevlar represents one of the first choices as a material for future flexible structures to be used in space. The paper evaluates the performance of Kevlar subjected to thermal cycling, flammability, radiation (penetrating), vacuum and outgassing tests that are applied during the selection process performed by Thales Alenia Space-Italia. It also uses past HVI results obtained over a period of 15 years by the Ernst Mach Institute (EMI) and the Center of Studies and Activities for Space (CISAS). Kevlar is not usually used as the first layer and is often protected by multi-layer insulation (MLI), so its behaviour under UV radiation (non-penetrating) and Atomic oxygen (AO) was not evaluated. For manned spacecraft the paper presents configurations that are used for the Columbus module and the ATV Integrated Cargo Carrier (ICC). In these applications the Kevlar is used together with Nextel as internal layers. Future inflatable structures are also discussed; here the Kevlar is used as an energy absorbing component and an internal barrier.

The paper concludes that Kevlar is a key material for use in future MMOD shield designs due to its exceptional ballistic behaviour and its strong performance record in space applications. R. Destefanis [18] also presents an analysis of the use of Kevlar material to reduce the HVI energy and the mass of the debris and target fragment cloud hitting the rear wall in new 3-wall systems, providing an effective MMOD shield. The paper presents HVI tests (normal or oblique) on a few configurations in which certain specific parameters were held constant, such as shell thickness or the stand-off distance. The first configuration uses an intermediate bumper made of aluminum, Kevlar high strength fabric and Nextel ceramic fabric. Another configuration uses flexible blankets of advanced materials such as Kevlar composite with Epoxy resin (stiff plate) or options without resin such as flexible bumper and an all-aluminum configuration named Heavy All Aluminum Shield (HAAS).

As a general conclusion of the article, shield configurations that have intermediate bumper materials such as Kevlar and Nextel provide excellent protection against MMOD impact. Details are noted, including decreasing of debris cloud velocity and fragments for low or high velocity tests. The shield configuration that used a combination of Nextel and Kevlar-Epoxy was effective in normal HVI tests with a 4.5 g projectile at 6.5 Km/s compared with the HAAS configuration, which was only effective for a projectile of 1.1 g. The projectile mass was the key parameter identified when evaluating rear wall damage. E. A. Taylor [19] writes a comprehensive comparison of the results obtained between a plastic face-sheet reinforced with 1.6 mm fibers bonded to 45 mm aluminum honeycomb core (CFRP/Al-HC) target and a classic Whipple shield in terms of damage characteristics.

The paper characterizes the impact damage as a function of projectile density, impact angle and impact energy and concludes that the energy required for perforation increases as the impact angle increases. At small incidence angles (0 to 50^{o}) the honeycomb blast area, for impacts with the same energy, does not change. The debris cone angles for impacts at the same impact angles (rotation of the cone with respect to the line of flight increases with impact angle) also do not change. Spacecraft honeycomb targets at very high speed regimes were also studied by E.A. Taylor [20]. Hydro-code simulations were performed at HVI speeds of 7, 11 and 14 km/s, velocities that cannot be attained with current experimental technologies, to investigate damage characteristics that have already been encountered during previous experimental tests, such as the influence on the honeycomb core (channelling) or the influence of oblique impacts. The simulation was performed using AUTODYN-2D and 3D with Lagrange Shell and Smooth Particle hydrodynamics (SPH) solvers. Results showed good agreement with prediction equations and were able to predict the channelling effect of the debris cloud and the perforation on the rear face sheet that occurred in the same honeycomb cell as on the front face sheet.

A Francesconi [21] introduced the characteristics of vibration induced by MMOD impact on aluminum honeycomb sandwich panels. A series of 30 tests were carried out, launching 0.8–2.3 mm aluminum projectiles in the velocity range 4–5.5 km/s on targets. The signals were recorded using tri-axial accelerometer assemblies mounted on both the front and rear faces of the panel at a nominal distance of 150 mm from the impact point. Using shock response spectrum (SRS), three different types of waves were identified; out-of-plane, in-plane longitudinal and in-plane shear (based on acceleration direction). The influence of projectile mass and velocity on SRS appeared

to vary with frequency (the most significant difference in the range between 103 and 104 Hz). The empirical equation developed based on the test data predicts the near-field vibration environment produced by HVI with MMOD size and velocity at an average uncertainty of +/- 6 dB.

Inter-Agency Space Debris Coordination Committee (IADC) [22] presents a description of failure modes of a honeycomb sandwich panel for the case of HVI, which occurs differently on the top or rear face. Internal damage could range from no penetration to blasting of honeycomb cells. Some methods of increasing the performance of honeycomb sandwich panels are also presented, such as decreasing the diameter of honeycomb cells, use of metal foam, thicker rear face, larger face sheet spacing or honeycomb multi-layer designs.

M. Grujicic [23] investigates the protection properties (extent of damage and probability of failure) of a composite that contains an inner ply made of carbon-based foam. Results show that the extent of the damage for the case of HVI is directly proportional to the normal component of the momentum of projectile just before impact. Based on a microstructural consolidation process of the foam, it was noted that the carbon-foam could offer increased protection since it absorbs a high amount of projectile kinetic energy. The foam used is CFOAM-17 (17 represents the material density, lbs/ft3), a carbon-based foam developed by Touchstone Research Laboratory Ltd. using high sulfur bituminous coal, with thermal, mechanical and physical properties that can be tailored based on the application. CFOAM is available in two principal microstructures; an open-cell reticulated microstructure consisting of a ligament network and a closed-cell (cellular) microstructure consisting of thin-wall spherical cells. The results of the paper were validated using a non-linear dynamics computational analysis of HVI with a velocity range between 5 and 15 km/s.

S. Ryan [24] presents the results of 19 HVI tests on similar ISS structure panels where the honeycomb core was replaced by metallic open-cell foam. The experiments revealed that secondary impacts on individual foam ligaments were found to raise the thermal state of projectile and bumper fragments (inducing break-up and melt) generating a performance increase of 3-15% (the performance decrease with impact velocity increase) for the case of normal HVI. Oblique impacts showed an improvement up to 29%. To prevent the channelling effect from influencing the results the thickness of the honeycomb panels were kept less than twice the diameter of projectile used. Using the foam enhanced the level of MMOD impact protection, keeping other important parameters constant (mechanical, thermal or weight).

S. Ryan [25] also completed a comprehensive study on the results of 86 HVI tests performed on aluminum open cell foam core sandwich panel structures, with varying impact and target parameters (velocity, angle, projectile diameter, face sheet thickness, core thickness, pore density). The same result was concluded; an increase in MMOD impact performance compared with traditional shields using honeycomb cores and even compared with results obtained on scaled Whipple or stuffed Whipple shields at low velocity (under 5 km/s), although at high velocity regimes these types of shields performed better. Based on these results it is concluded that optimization of the MMOD protective shields could be possible using materials such as open cell foam.

In a recent paper, Zhang X. [26] introduced a Node-separation finite element method (FEM) as a model for HVI and a Sierpinski sponge (fractal curve, based on digital image processing and regression analysis) extended from a Sierpinski carpet to model a 3D Al-foam bumper. His numerical results are compared with experimental data and show that the performance of an Alfoam bumper is much better than an aluminum alloy bumper. Jia B. [27] introduced a metal-foam stuffed Whipple shield as a light-weight MMOD shield spacecraft structure. With this goal, numerical simulations were used to evaluate the performance of three base materials of foam Al 7075-T651, Ti and Al ZL102, incorporated as part of a shield configuration. The results indicated that all of these proposed materials performed better at different impact speeds than the classical solution. With all other conditions held the same, the foam Al ZL102 showed the strongest radial dispersion of the secondary debris cloud and provided the best shield performance for the high velocity range of the investigation. E. Christiansen [28] presents an effective shield configuration; a mesh double-bumper shield, which uses an aluminum mesh as the first bumper. The configuration offers a 30% to 50% weight saving compared with classic Whipple shields at the same performance. The weight saving could increase to 75% for a case of oblique impact. The paper also presents use of a fabric bumper (Kevlar) as a third bumper in front of the rear wall.

M. Higashide [29], also investigated the HVI on metallic meshes and, based on radiographs of the fragment cloud generated by HVI, use of a metallic mesh bumper showed a decrease of 35% in the velocity of the center of gravity of the cloud. This reduction is also influenced by the reduction of ratio between the space (between the wires) and the diameter of the wire. The mesh materials used for the HVI test were steel and copper using a polycarbonate projectile. D. Zhu [30] presents a hybrid solution that uses an Al-6Mg alloy matrix composite reinforced with Ti–6Al–4V meshes

that was fabricated using the pressure infiltration method. The HVI tests were performed at 2.5 km/s low velocity and the results were compared with results of the same test on an Al-6Mg alloy target. The internal damage analysis was made using ultrasonic C-scan. The conclusion states that the proposed target is more efficient and has better energy absorption than the target without mesh and eliminates the adiabatic shear bands that occur in the case of an aluminum alloy matrix.

In another recent paper, Q. Guo [31] presents a similar solution; a 5A06Al matrix composite reinforced with Ti-6Al-4V meshes. The HVI test results are compared with those using an aluminum matrix composite target. Analysis and measurements with powerful equipment such as Philips CM-12 transmission electron microscopy (TEM) or Tecnai G2 F30 high-resolution transmission electron microscopy (HRTEM) allows observation of phenomena such as a decrease in the target depth, the existence of the adiabatic shearing fracture, interface separation and shear of fibers and other characteristics of damaged targets. L. Merzhievsky [32] performs simulations using the model of an ideal plastic as a target to analyze crater formation in case of HVI. The paper determines a formula that uses projectile diameter and velocity to estimate the depth of the crater. The results are compared to those of other researcher's results and not validated by tests. The paper is presented to show that, due to the dependence of strength properties of the target material on deformation velocities, there is a difference in the estimation of crater depth. The model shows a proportionality with the impact velocity to power a=2/3.

Other HVI futuristic protective solutions are found in literature, T. Mudric [33] presents results of six HVI tests performed on ethylene-methacrylic acid ionomer plates (self-healing properties) and compares their behaviour to the behaviour of aluminum plates (eight tests) having the same areal density. Ionomer targets were made of Surlyn a thermoplastic ionomer from DuPont. More precisely the polymer used was Surlyn 8940 (5.4 mol% acid groups, 30% neutralized with sodium and with 95 g/cm3 density). An analysis of the target using visual inspection and a Matlab program for automatic recognition was carried out. The visual analysis concluded that the ionomer plate has a smaller hole compared with the aluminum plate. Based on the witness plate craters however, aluminum targets performed better in projectile fragmentation. The results suggest that the ionomer bumper is not fit to be used as a first bumper, rather as an interior bumper due its self-healing properties. In a paper that explores the self-healing properties of materials [34], Kalista S. presents an attempt to identify the self-healing mechanism of poly ethylene-co-methacrylic acid (EMAA). Several ionic concentrations of these materials were ballistic examined in order to develop a model

of healing behavior. The EMMA healing response was automatically and instantaneously measured. Some other innovative solutions propose new shielding configurations that use magnetic fields, electrical grids, chemical reactants or manufacturing procedures (i.e. vault structures) in combination with different materials. These showed some promising results but current applications are limited. Several materials were found fit to be used in different impact shielding situations. In the following paragraphs we report the main ones and their respective properties and performance levels. The following subchapters concentrate on most qualified materials and solutions, their respective properties and performance levels. These are frequently used in current MMOD impact protection configurations.

4.3.2 Kevlar

Materials incorporating Kevlar fibers are effective in absorbing a debris cloud. This result is based on an extensive analysis on material selection in designing new protection systems against micrometeoroid and orbital debris (MMOD) HVI, found in E. L. Christiansen work [35].

Kevlar 29 is currently evaluated as the best ranked material for this application according to the results of a series of HVI tests (Table 4.1).

Table 4.1: Rear Wall Material's Ability to Absorb Mechanical Energy of Impact (rear wall areal density of 7.5 kg/m2) [35]

Rank	**Material**	**Density (g/cm^3)**	**Tensile Strength (MPa)**	**Strength/weight ($MPa\text{-}m^3/kg$)**	**Elastic tensile modulus (MPa)**	**Critical failure load per unit mass rear wall(N/kg)**
1	Kevlar 29	1.44	3620	2.51	82740	105580
2	Spectra 900	0.97	2620	2.70	117215	39045
3	Nextel 312	2.70	1724	0.64	151690	13059
4	Al 7075T6	2.80	524	0.19	71708	2553
5	Al 2219T87	2.85	462	0.16	73087	1947
6	Al 6061T6	2.71	310	0.11	68950	931

As a catcher material (intermediate bumpers), Kevlar cloth proved to be a very weight efficient material, as per Swift [36].

Other new types of Kevlar (according DuPont) that could be HVI tested [37]:

- Kevlar KM2 Plus fiber is the highest grade protective fiber for military use and offers increased process-ability for conversion to woven fabrics and structures for ballistic fabric weavers and body armor manufacturers;
- Kevlar XP technology offers more bullet-stopping power. This patented technology helps provide approximately a 15% reduction in back face deformation and superior ballistic performance in a 100% Kevlar® solution;
- Kevlar AS450X is a new generation multi-threat solution that is specifically engineered to offer a more comfortable ballistic vest.

4.3.3 Nextel

Woven fabric Nextel; up to 50% higher areal density is required to have the same efficiency as Kevlar, as catcher material according to Swift [36]. Nextel 312 is classed in third place (Figure 1) according the same material analysis, based on HVI tests performed by E. L. Christiansen [35]. Nextel 312 fabrics are materials woven using strong continuous Nextel 312 Alumina-Boria-Silica fibers. These fabrics retain strength and flexibility with little shrinkage at continuous temperatures up to 2012°F (1100°C), properties that are recommended for use in orbital debris shield applications [39]. Protective devices for spacecraft and satellites that contain Nextel ceramic fibers offer weight and space advantages over traditional aluminum alternatives. The dispersion of debris has shown to better shock the projectile fragments and is better than aluminum alternatives at slowing debris cloud expansion, according to NASA data [35]. As can be seen from the following Figure 4.1, the types of Nextel 312 used for aerospace applications are in the range of AF10 to AF20 due to the specific characteristic of this field [38]:

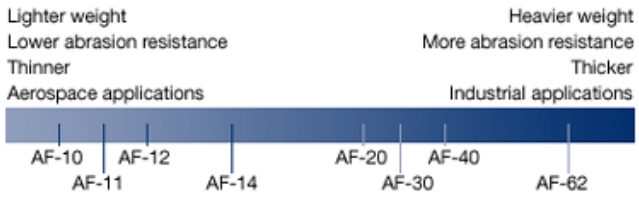

Figure 4.1: General trends for Nextel Woven Fabrics 312 [38]

4.3.4 Kapton

Kapton is mentioned only due to its use in applications such as the solar array and for thermal management. It is not suitable for MMOD HVI shield design. According to the manufacturer (DuPont), Kapton polyimide films have high performance, reliability and durability, offering a unique combination of electrical, thermal, chemical and mechanical properties that withstand extreme temperature, vibration and other demanding environments [40].

4.3.5 Carbon-fiber-reinforced polymer (CFRP)

Plans call for extensive use of CFRP materials in the primary structures of future space systems. These have very complex damage mechanisms however (internal delamination), and a series of HVI tests are required to analyze any proposed CFRP. An extensive study of the performance of CFRP during HVI, which shows the complexity in investigating this issue, is presented by M. Wicklein [41]. Properties of the investigated material (CFRP-Al/HC), which represent the actual satellite wall structures, are shown in Table 4.2.

Table 4.2: Properties of the investigated CFRP- Al/HC by the article [41]

Property	*Value/ description*
Fibre type	Tenax UMS2526
Fibre tensile modulus	395 GPa
Fibre tensile strength	4.56 GPa
Fibre density	1.79 g/cm^3
Fibre volume in CFRP	52%
Single ply	Krempel MUDB 2006
Matrix	Krempel BD System 120^0 C epoxy resin
HC type	Hexcel CRIII-3/16-5056-0.0007
HC thickness	25 mm
Face sheet thickness	1.37 mm
Lay-up	0/45/-45//-45/45/0
Orientation CFRP$\leftrightarrow$ HC	Cell size direction = 90^0

The article tentatively selects the best structure in terms of fiber volume, resins system, lay-up, manufacturing process, cell size and uses 6 mm thick CFRP plates to produce a characterisation of the material. As can be seen from the following table (Table 4.3) the speeds of the debris at impact are similar to those produced by the McGill small launcher that we've used for our tests.

Table 4.3: Planar plate impact tests conducted with CFRP [41]

Test type	*Setup*	*Velocity [m/s]*	*Test no.*
Spallation	2.98 *mm Al* → 6.24 *mm* CFRP	683	2950
	2.96 *mm Al* → 6.26 *mm* CFRP	173	2951
	2.98 *mm Al* → 6.46 *mm* CFRP	418	2961
	2.95 *mm Al* → 6.16 *mm* CFRP	598	2962
	2.98 *mm Al* → 6.42 *mm* CFRP	1073	2963
	3.00 *mm Al* → 6.40 *mm* CFRP	159	2992
	3.00 *mm Al* → 6.40 *mm* CFRP	297	2993
Inverse impact	2.98 *mm Al* + 6.26 *mm* CFRP → 1.94 *mm Cu*	666	2948
	2.96 *mm Al* + 6.50 *mm* CFRP → 1.98 *mm Cu*	1000	2949
	2.98 *mm Al* + 6.26 *mm* CFRP → 2.00 *mm Cu*	231	2952
	2.95 *mm Al* + 6.07 *mm* CFRP → 2.02 *mm Cu*	470	2959
Multi Shock	7.96 *mm Cu* + 1.19 *mm* CFRP → 7.99 *mm Cu*	695	2953
	7.98 *mm Cu* → 1.18 *mm* CFRP + 8.00 *mm Cu*	725	2954
	5.00 *mm Cu* + 1.20 *mm* CFRP → 4.99 *mm Cu*	908	2955
	5.00 *mm Cu* → 1.18 *mm* CFRP + 4.98 *mm Cu*	938	2956
	7.98 *mm Cu* → 1.17 *mm* CFRP + 7.96 *mm Cu*	549	2957
	4.98 *mm Cu* → 1.14 *mm* CFRP + 4.99 *mm Cu*	604	2958

There is a large variety of literature related to HVI on CFRP plates in different configurations. Selecting/proposing the best CFRP material to be future tested (HVI) can only be done after a vast literature review that will cover different disciplines and extensive experimental data.

4.3.5.1 Effects of adding resins

As mentioned earlier, materials used for the first bumpers are usually aluminum 2 series or 6 series, however some particular cases such as the one in Hon Wan's work [42] show that the stacking combination of carbon-fiber-reinforced polymer composite (CFRP) along with aluminum 2024 alloys significantly reduces the peak shock pressure induced by hypervelocity impact. A bumper using this combination resisted a 9 km/s impact without perforation. In addition, and in a similar way to the aluminum/CFRP laminate, aluminum/ Kevlar-fiber-reinforced polymer composites (KFRP) were tested and showed promising results. Moreover, results showed that aluminum/KFRP demonstrates the best shielding effect on resisting HVI.

It is not very common however for Kevlar or Nextel to be used as front bumper materials [42, 43]. These materials are usually used and are more efficient for intermediate bumper shields. For example, in one study [43], Nextel fabric and Kevlar fabric composed with epoxy resin was used

as an intermediate bumper to protect the primary structure. The following figure presents the layout of the Columbus debris shield (Figure 4.2).

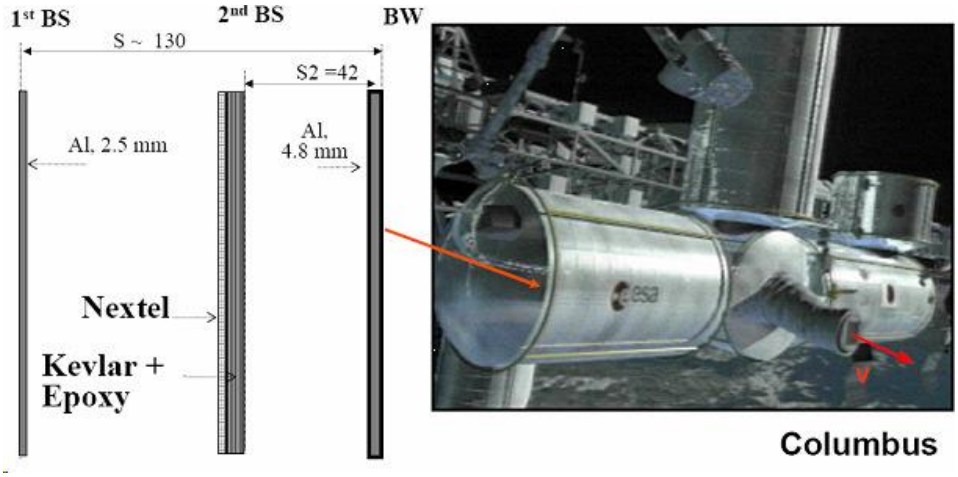

Figure 4.2: Layout of the Columbus debris shield configuration [43]

As we can see from the above figure, the 1st BS is made of aluminum of 2.5 mm thickness, and the 2nd or intermediate BS is made of Nextel and Kevlar/Epoxy. The nature of the material used is shown in Table 4.4. Four layers of Nextel 312 AF-62 were used as fabric; however 18 plies of Kevlar 129 Style 812 were impregnated with Epoxy resin Brochier 914. The Nextel/Kevlar stuffing has shown to be excellent in absorbing the impulsive load of the debris cloud generated by the projectile impact on the external shield.

Table 4.4: Materials data for the Columbus structure

Layer	**Material**
External Bumper (WS)	Al 6061-T6, 2.5 mm
Intermediate Bumper (Stuffing)	Nextel 312 AF-62, 4 layers
	Kevlar 129 Style 812 18 plies + Epoxy resin Brochier 914
Back Wall (BW)	Al 2219-T851, 4.8 mm

4.3.5.2 Effects of adding reinforcers (Carbon Nanotubes, nano particles, self-healing agent, hardening microspheres…)

Some authors have studied the effect of adding nanomaterial reinforcers on the HVI response of these materials [44, 45]. Suman Khatiwada [44] studied the effect of Single walled carbon nanotube (SWCNT) reinforcement in Epoxy/ Ultra-High Molecular Weight Polyethylene (UHMWP) Fiber Composites on the HVI response. The study compares the HVI performance of Nano-composites against that of epoxy/UHMWPE composites without nanotubes (or simply, neat composites) and

aluminum (Al) sheets with an areal density similar to both the composites. Results show that the Nano-composites and the neat composites perform better as rear walls than the Al sheets, but are less effective bumper shields. Comparatively, the two composites perform similarly to one another as rear walls and as bumper shields. For these epoxy/UHMWPE composite samples, reinforcement with 0.5 wt% of SWCNT has no noticeable effect on their HVI response. Similar results were noted for CNT/a-SiC composites studied by Maxim A. Makeev [45].

4.3.5.3 The use of composite as material of MMOD bumpers

Two interesting reviews were done by William P. Schonberg comparing composite bumper materials and pressure wall combinations to aluminum bumper and pressure wall combinations [3, 46]. The review studies the use of composite materials as outer bumpers, inner bumpers and pressure walls, comparing them with their aluminum counterpart while stating the advantages and disadvantages of both materials. In purpose of comparison the study chose aluminum plates thicknesses so that they have the same areal density as the corresponding composite bumper plates.

For the outer bumper, in the composite systems the bumpers were made of Kevlar 49 or Graphite/Epoxy with an aluminum pressure wall. In the aluminum systems the bumpers and pressure walls were made of aluminum. From the result of the HVI tests it appears that the composite dual wall systems do not offer an advantage when used as an outer bumper compared to an all-aluminum dual wall. For the inner bumper, the system was constructed using an aluminum outer bumper and pressure wall while varying the inner bumper by using aluminum, Spectra 900/Epoxy or Kevlar 49/Epoxy. Results show that using composite material as an inner bumper of a multi-wall system gives increased protection against HVI impact. The study extended as far as using composite materials for the pressure wall. Results show that there are three main advantages of using composite material, namely Graphite/Epoxy, as a pressure wall material. First, it eliminates the severe cracking and petaling sustained by aluminum at high speeds. Second, the ballistic performance was superior to the composites. And finally, patching a hole in composite material can easily be done by adhesive bonding.

4.3.5.4 Selection of optimal combination (materials, number of layer, resin or not, reinforcers …)

The information collected above was analyzed taking into consideration cost, preparation time, availability of the materials and the purposes of this study. The most optimal material combination (for the future steps of this research) to achieve a good bumper shield would be to use aluminum 2 series or 6 series for the first bumper shield, followed by a combination of Kevlar 129 or 29 and Nextel fabric with no resin and no reinforcement as an intermediate shield to catch the debris cloud. This combination should prove to be efficient for eventual HVI testing and signal detection in line with the purpose of this study.

4.4 HVI performed at the Shock Wave Physics laboratory of McGill University

4.4.1 Description of test facility

4.4.1.1 The high pressure gas launcher

The launcher shown in Figure 4.3 is driven by a high pressure reservoir of gas using a double diaphragm propulsion mechanism. The gas launcher was operated using high pressure helium gas to obtain the targeted launching pressures and nitrogen gas for dynamic stripping of the sabot. For the purposes of our initial testing, pressures from 2000 Psi to 4000 Psi were used. High pressure reservoirs along with the high pressure regulator are also shown in Figure 4.4.

The use of these pressures resulted in velocities ranging from 560 m/s to 1670 m/s, depending on the pressure, the conditions when performing the shots (into air or vacuum) and unknown events (last two shots). For our future tests, having a precise calculated and sufficient velocity is an essential factor.

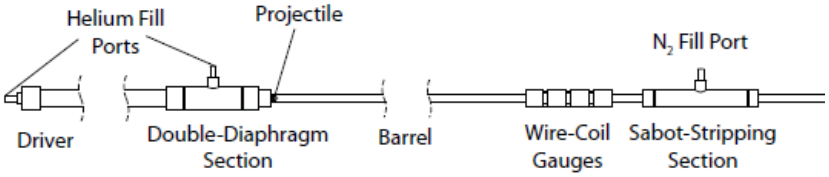

Figure 4.3: Double diaphragm single stage gas driven gun [47]

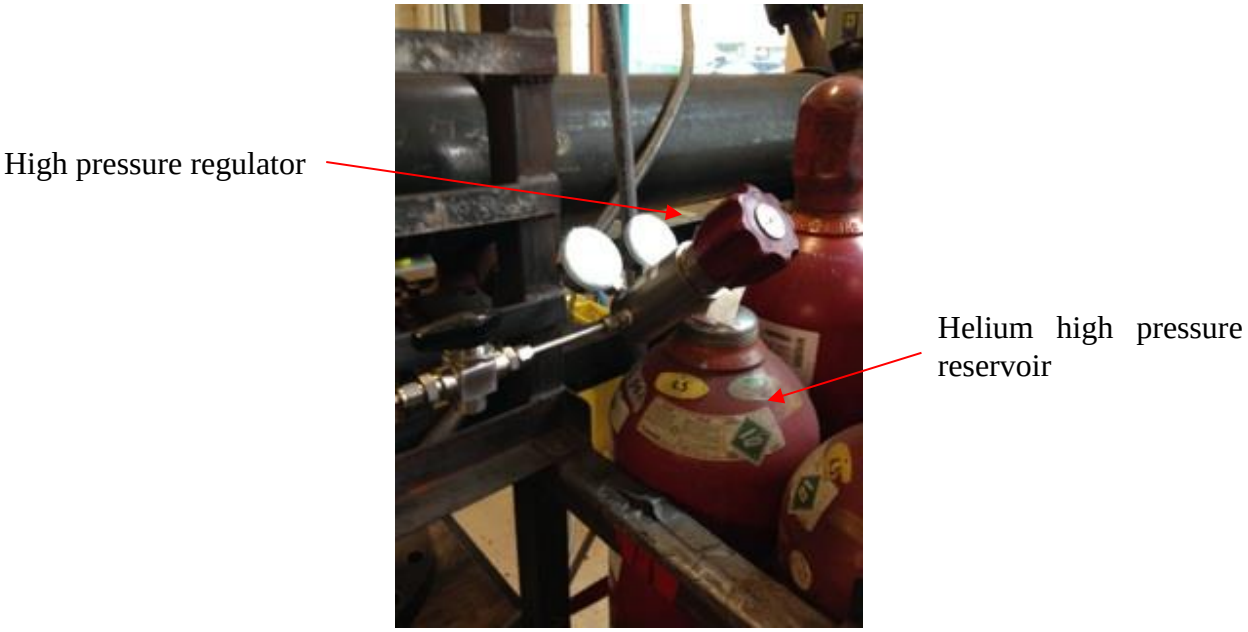

Figure 4.4: High pressure helium reservoirs with high pressure regulator

4.4.1.2 Double diaphragm mechanism

As mentioned earlier a double diaphragm mechanism was used for launching the projectile. This mechanism provides consistency in the results. The diaphragms were circles of 1.9 cm diameter stamped out of Mylar and a brass sheet with a thickness of 0.005 in. The thickness of the diaphragms varies with different pressures.

In order to explain how this mechanism works, we first assume a final driving pressure of 2000 Psi. Although this pressure can change depending on the actual velocity required, the working mechanism remains unchanged. Note that it is not the overall pressure that drives the mechanism; rather it is the pressure difference across the diaphragms. Initially, both the high and low pressure sections are filled to half the total pressure (1000 Psi), corresponding to a pressure difference of 0 Psi across the first diaphragm and 1000 Psi across the second as shown in Figure 4.5 (b). The high pressure section is then filled to the final driving pressure (2000 Psi), corresponding to a pressure difference of 1000 Psi across both diaphragms. Finally, the low pressure reservoir is vented resulting in a pressure difference of 2000 Psi on the first diaphragm. The diaphragm must be able to withstand at least half of the full pressure, therefore its thickness depends on the pressure used; at higher pressures a thicker diaphragm is required.

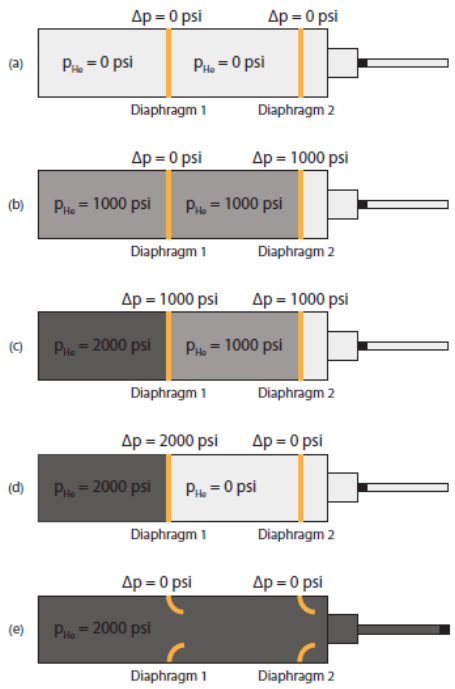

Figure 4.5: Steps for the double diaphragm mechanism [47]

4.4.1.3 Fabrication of the sabot

Using a sabot in firing a small irregularly shaped object is a very common technique. In our tests, the material used for the sabot is polycarbonate. Included with the sabot is a rare earth magnet NdFeB, MAGCRAFT part NSN0591, which is used to determine the velocity of the projectile. The design of the sabot and the projectile is shown in Figure 4.6 and 4.7. The sabot was stamped out of a polycarbonate sheet 4.6 mm thick using a #10 punch (McMaster-Carr part # 3424A22). It was then machined on the lathe to add grooves for the spherical projectile and to create a Bridgman type seal on the back. In addition, a slot for press fit of the rare earth magnet was machined using a mill. Super glue was used to hold the projectile to the sabot so that it is not pulled off during the process of filling the gun with Helium.

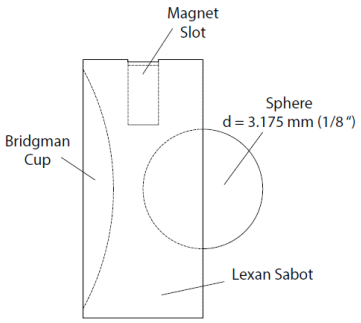

Figure 4.6: Sabot and projectile design

Figure 4.7: Manufactured Sabot

The stripping mechanism of the sabot requires special attention. Two methods are currently used at the McGill testing laboratory: dynamic and mechanical. Due to the time required to perform a series of tests aimed at improving mechanical separation, we opted for the dynamic method. This method has an unwanted effect caused by a secondary impact of the sabot on the target, which adds another peak in our recorded signal. For future tests a combination of the two methods will be used to avoid this secondary impact.

4.4.1.4 Sabot stripping section

In order to avoid the impact of the sabot with our specimen, a separation between the sabot and the projectile was required. The mechanism used was a combination of gas dynamic and mechanical stripping. First, the gas dynamic mechanism consists of filling a section with Nitrogen (N2), which is substantially heavier than the driving gas, He. When the Projectile/Sabot enters the nitrogen section a shock wave is created that substantially slows the speed of the sabot. This sudden decrease in velocity separates the projectile from the sabot as shown in Figure 4.8.

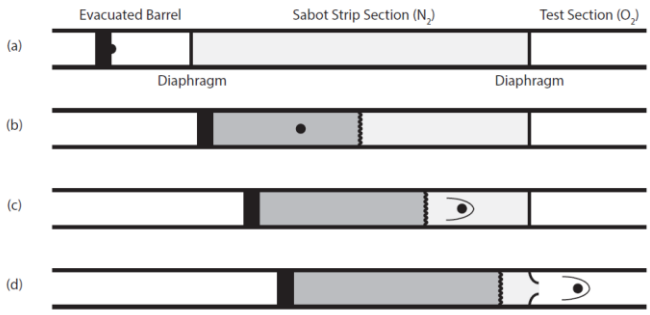

Figure 4.8: Nitrogen stripping section [47]

A second separation mechanism was used to deflect the sabot from its original trajectory to avoid hitting the sample and thus inducing unwanted noise in the signal. The mechanical separator did not give us the desired results and did not efficiently deflect the sabot; further work should be done to resolve this issue.

4.4.2 Target materials

For the initial trial testing (at McGill University on the 1st week of June), the proposed target material was Aluminum 6061-T6 (2 mm and 5 mm in thickness) and Carbon fiber/Epoxy rigid composite sheet (3.175 mm and 6.35 mm in thickness). The material choice was made in order to create at least two types of hypervelocity impact damage: crater and perforation, in two different materials and also considering other factors such as: material review, market availability, test facility availability and the timeframe. To fit the targets into the test section of the McGill setup, the material plates were cut in squares of 11 x 11 cm. These plates were clamped between two wooden cylinders that fit tightly inside the testing section as shown in Figure 4.9.

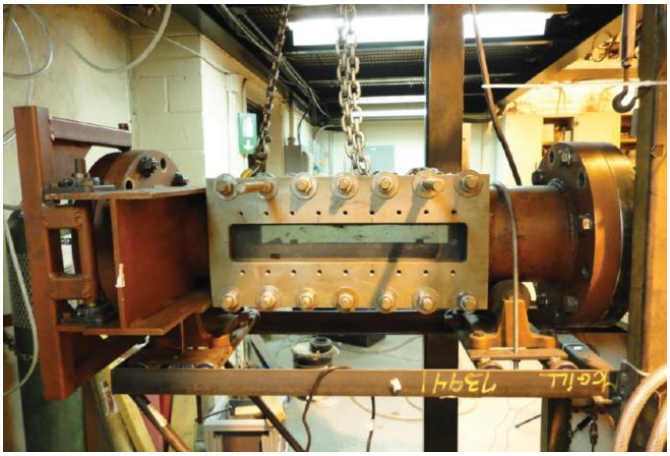

Figure 4.9: Test section in McGill University, Shock Wave Physics laboratory

For our future preliminary tests, the vacuum chamber could be required to generate a hypervelocity impact in a low velocity regime. However, due to the timeframe of this project and the target design requirements we are not planning to use it and, as a consequence, we will not achieve the corresponding decrease in the impact velocity. On the other hand, it was inconvenient for this stage of testing to remove this section and therefore we accommodated it in our initial test session. For future tests, the gun will most likely be fired into air on a test sample held at four points and

mounted using a vibration acquisition system. This more elaborate set up should allow more precise signal analysis.

4.4.3 Data acquisition system

The data acquisition system used for the preliminary signals was the Ni PXI (Figure 4.11) coupled with three accelerometers. The accelerometers were mounted on the testing section as shown in Figure 4.10. One accelerometer was mounted on the sample with crazy glue to hold it in place and the other two were mounted on the outside of the testing section.

Figure 4.10: Accelerometer mounted on sample

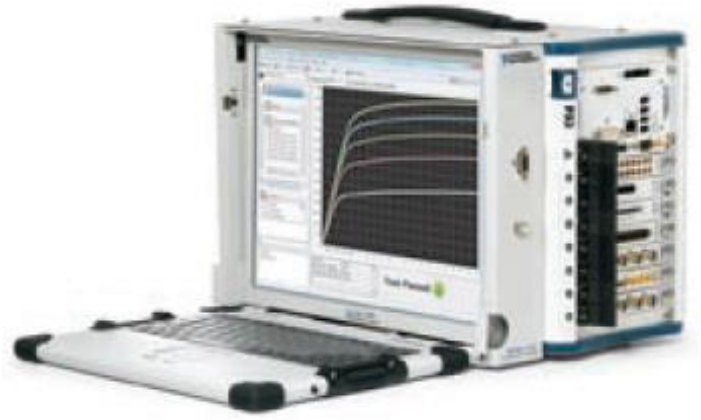

Figure 4.11: NI PXI

4.4.3.1 Acquisition Hardware

NI digitizer (PXIe-1062Q) and LabView software are used to convert the analogue signal to digital and store the signals on a PC. The table below summarizes the main features. The NI PXIe1062Q chassis combines a high-performance 8-slot PXI Express backplane with a high-output power supply and a structural design that has been optimized for maximum usability in a wide range of applications. The chassis' modular design ensures a high level of maintainability, resulting in a very low mean time to repair (MTTR). The NI PXIe-1062Q chassis fully complies with the PXI-5 PXI Express Hardware Specification, offering advanced timing and synchronization features.

The key features of the NI PXIe-1062Q chassis include the following high performance instrumentation requirements:

- Up to 1 GB/s (single direction) per PXI Express slot dedicated bandwidth (x4 PCIe);
- 353.9 W available power for 0 to 55 °C;
- 30 W per slot cooling meets increased PXI Express cooling requirements;
- Low-jitter internal 10 MHz reference clock for PXI slots with ± 25 ppm stability;
- Low-jitter internal 100 MHz reference clock for PXI Express slots with ± 25 ppm stability;
- Quiet operation for 0 to 30 °C at 43.6 dBA.

4.4.3.2 Measurements devices used- accelerometers

As a general definition, sensors are devices that convert the physical phenomena under study (in our case, impact vibration response) into a signal that can be recognized by the data acquisition hardware. Well suited for the McGill testing session, analog sensors produce output signals that are proportional to their inputs and are also continuous in time and magnitude like the observed vibrations. The physical variable measured is the acceleration caused by the impact force generated when a projectile and sabot hit the target.

In general, accelerometers are fixed on the monitored component since the target is usually fixed. In our case, one sensor is fixed directly to the plate surface. The selection procedure was based on a determination of the required sensitivity, bandwidth and resolution needed for the accelerometers to properly collect the vibration responses. The projectile and sabot are moving at a very high speed, i.e. 1670 m/s. If the surface of the plate or structure is contaminated (in the best case with micro-cracks) due to the hyper velocity hit, this means that the system is affected. In our case, we need to have accelerometers with very high sensitivity to detect such micro-cracks. Good candidates for our application are those with sensitivity ranging from 0.1 to 10.2 mv/ (m/s2). Unfortunately, the resolution of accelerometers with high sensitivity is very poor compared to those with low sensitivity. Resolution is defined as the lowest change in amplitude that the accelerometer can detect. As a trade-off in our case, we focused on the sensitivity instead of the resolution.

Figure 4.12 and Table 4.5 present the PCB Piezotronics accelerometers that were considered suited for this type of test.

Figure 4.12: PCB Piezotronics accelerometers, model: 352C33

Table 4.5: PCB Accelerometer specifications

Model	Sensitivity	Measurement Range	Frequency Range (±5%)	Resonant Frequency	Broadband Resolution	Non-Linearity
PCB352C33	10.2 mV/(m/s^2)	± 490 m/s^2	0.5 to 10000Hz	≥50 kHz	0.0015 m/s^2 rms	≤ 5 %

4.5 MMOD impact detection techniques

Next, the paper presents the techniques for impact detection on spacecraft and uses as a guideline the structure described in the document developed by the Inter-Agency Space Debris Coordination Committee (IADC) [48] elaborated in 2013, which presents a comprehensive review of technical options for detecting and characterizing of MMOD impacts. The document [48] includes the schematics of the sensor system, comparative analysis of options based on mass, volume, power, and efforts necessary in order to be integrated on a space vehicle. Information about development status, technology readiness level and the work done in the area is also included.

The necessity of an integrated sensor system in the design of a spacecraft is highly motivated by factors as:

- The MMOD penetration risk that is always present;
- Location and severity of HVI;
- The particularities of an Impact Health Monitoring System for spacecraft;
- The wide area to be monitored;
- The possibility of using of other sensors already integrated

In order to identify a sensor system the document starts from the measurable effects that characterize the HVI: electromagnetic or acoustic emissions, shock-induced accelerations, ejecta, secondary debris or plasma clouds or characteristics and chemical properties of HVI damage.

The effects on micron sized particle HVI are presented by Gerhard Drolshagen [49]. His paper assesses the damage of small particles in the 1–100 μm size range. Particles in this size range have generated damage on the solar cell of Hubble Space Telescope and on Charge Coupled Devices of the XMM-Newton telescope. Also, the degradation of sensors due to a large number of small impacts is analyzed, the case of large sensor is highlighted, along with sensors that are freely exposed to space (Xeus and Gaia space missions).

The IADC document [48] identifies the main requirements of a sensor system:

- Environment (thermal, vibration, shock, radiation, etc);
- Integration in the spacecraft design or the adaptation to the existing spacecraft;
- Calibration;
- Crew systems requirements (for crewed spacecraft);
- Minimization of use of spacecraft resources;
- Detection and report of a specific failure criteria;
- Accuracy of the location of HVI;
- Provide data regarding all critical areas of spacecraft

As a summary, the basic requirements of a sensor system are: capability for location detection of a HVI and detection of damage that is critical, the threshold damage requirement. An option allows the threshold value for the sensor system to be set at a minimum value, corresponding to the point at which penetration of the spacecraft shielding occurs.

Each HVI monitoring technique investigated in the IADC paper [48] is described according to sensor development status and measurement capability, demands on the spacecraft and robustness.

4.5.1 Acoustic Emission

In Acoustic Emission (AE) an elastic wave (ultrasound range: 20 KHz and 1 MHz) is generated by the rapid release of energy from a source within a material. In this case the sensor is a transducer that converts the mechanical wave into an electrical signal in order to identify the characteristics and location of damage.

The choice of the appropriate acoustic emission (AE) sensor, the first part in the measurement chain, is absolutely essential to the success of an application. The AE sensor is selected according to the studied source type, but also according to the attenuation due to propagation in the material. One of the main advantages presented by Dae-Un Sung [50] is the fact that using wavelet transform (WT) allows the AE signal to be decomposed into different waves corresponding to different impact loads that create different types of damage, and these types are identifiable. The paper analyzes the characteristics of the AE signals (for the case of matrix cracks and delamination) in GrEp laminates and quasi-isotropic laminates under tensile loads using WT. Other advantages are related to the fact that the AE techniques can detect the impact of small particles in the micron size range, in real time. This opens up the possibility to analyze the impact of lunar dust on future inflatable modules.

AE methods have already generated useful results in research works done in other industrial applications from the location of leakage in pressure tanks and pipeline monitoring to civil engineering structures monitoring. Vast material has been published on AE applications in composite damage monitoring. The major disadvantage of AE is that the commercial systems only give an approximate solution in detection and location of damage. Also, the amount of noise has to be reduced to have valid results.

J. C. Chen [51] considers the signal processing aspect of a power efficient self-organized and synchronized wireless sensor network for source detection, signal enhancement, localization, and identification. The paper proposes computational algorithms in order to locate the source, estimate propagation velocity and minimize power consumption using an array of passive seismic sensors. Since 1990, the feasibility of AE technique has been demonstrated by tests on full-scale structures in the frame of the ESA Columbus Module, contracts by Norske Veritas [52].

More recently, M. Prokopenko [53] presents a capability for self-organizing diagnosis by a group of autonomous sensors that involves AE resulting from an impact. Diagnostic techniques such as a self-organizing map (SOM) or Kohonen neural networks in combination with Principal Component Analysis are used to characterize the severity of the damage. The experiments performed showed some improvement compared with the standard K-means algorithm in both time and frequency domains. W. Prosser [54] analyzed a large variety of impact conditions using AE technique, from low-velocity to high velocity, from metal to composite targets, with and without

perforation. The paper concluded that the low and high velocity impacts could be easily distinguished using their frequency content and modal analysis. The existence of large flexural modes in the AE signals provides an indication of non- perforation of plates. There are two types of AE sensors; asymmetric sensors, which consist of a single sensing element providing high omnidirectional sensitivity (not affected by the direction from which the waves arrive) and differential sensors, which are capable of common mode rejection of unwanted components of the wave and also offer good protection against electromagnetic interference (EMI). The output of a differential sensor must be directed to a module with at least 24 dB common mode rejection. As an indication of the mass and power resource that a typical AE monitoring system will require on the spacecraft, the IADC document [48] gives the example of the ESA Columbus Module. In this case, the total mass is estimated at 3.2 kg and the power consumption at 20 W. In terms of environmental robustness, vacuum conditions are not a disturbing factor, although the noise level and temperature variations should be taken into consideration during design.

4.5.2 Accelerometers

Accelerometers measure and characterize the mechanical shock that results in an HVI. The shock creates in-plane and out-of plane waves. Furthermore, as Francesconi noted [55], based on Lamb wave theory and using wavelet transform analysis the wave characteristics (wave group velocity, frequency content, time between wave propagation and reflection, amplitude) can be detected, characteristics that could eventually lead to location and identification of impact damage. Due to the large availability of different forms of this type of sensor in engineering, accelerometers represent an appealing solution. A network of such sensors is used by Boeing for the orbiter Discovery to monitor impacts. This same approach is used in the new External Wireless Instrumentation System (EWIS) to monitor and analyze the behavior of a truss structure [56]. Use of accelerometers for impact detection and characterization is a branch of research that has recently been recognized by the NASA Phase 2 Small Business innovation Research (SBIR) program award for development of a miniaturized piezoielectric sensory node that will monitor impacts using an accelerometer, acoustic emission sensor or other PZT element. Details about the circuit design and other potential applications can be found elsewhere [57].

Depending on the distance to impact, point accelerometers can be tailored for near, mid and far fields with a wide range of measurement levels from 0.001 ms-2 to 2x106 ms-2 and bandwidths

200250 kHz (sensor resonance around 1 MHz). In the literature, Endevco, B&K and PCB shock sensors are used to record the shocks generated after a HVI.

Concerning the resources required for a monitoring system using accelerometers, mass and power consumption are not major factors to consider, however data handling could be a major point due to the huge amount of data that needs to be stored and analyzed to enable identification of impact characteristics. From the point of view of environmental robustness, vacuum conditions are well tolerated, but temperature variations could lead to de-calibrations of the sensor, which should not be directly exposed to the space environment.

4.5.3 Thermography/imaging technique

Imaging techniques that can be used to detect HVI include:

- Periodic inspections at very precise time intervals, not suitable for real-time monitoring;
- Continuous sampling, based on the principle that an HVI generates a strong heating effect that can be detected by the appropriate sensors;
- A combination of these 2 methods.

In detecting (measurement) the temperature of a material some general methods are: direct contact with sensitive elements, indirect methods such as extrapolation, and methods of measuring distance.

One method consists in measuring the infrared radiation emitted by the surface which depends also on the state of the surface, its nature and its emissivity factor (which depends on the emission angle). Evaluation of the surface temperature using this method introduces a systematic error that cannot be measured, but it allows a heat map to be drawn without requiring contact.

Microwave thermography is based on detection of electromagnetic waves of thermal origin, radiated by a material. Its disadvantages: not limited to a specified well-delimited area and the electromagnetic waves carrying the information are of very low amplitude. Use of this technique in HVI thermal inspection began in 1992. The results are presented in a NASA technical report [58] in which an NDE approach together with ultrasonic volumetric imaging were used to detect and quantify delamination in a composite. P.A Howell [59] presents an in-space solution for thermal NDE using solar energy as a heat source to overcome constraints due to limited available

resources. He underlined the importance of development of this type of inspection tools for future space missions.

The IADC HVI team proposed a continuous sampling method that uses the detection of thermal emissions that occur due to HVI on CFRP bumpers [48]. One result is that the temperature gradient appears to be impact energy dependent. Unfortunately, the high frame rate necessary to monitor such a short event made it difficult to implement this technique. Other papers suggest a combination with other methods in order to have more valid results. A wide range of thermal detectors have been developed but these sensors are not yet qualified for space. The resources needed are considerable from the point of view of mass, volume, power or data handling. Specialized solutions are needed in order to be operable in a space environment.

4.5.4 Calorimetric impact detection

Calorimetric impact detection is based on the principle that most energy of the impact particle is transferred to the target as heat and a temperature sensor can be used to measure the variance. The monitoring of HVI will be done through a detector that uses the heat conversion efficiency (ratio between measurable calorimetric heat and kinetic energy of the impacting particle). T. Poppe [60] presents a solution for in-space measurement of impacting MMOD. A particularity of the solution is the fact that the detector surface is covered by a conductor network that is severed at the moment of impact.

As a second option for simulating thermal processes during an impact, K.Bunte [61] has another solution that uses calorimetric measurements of the deposed thermal energy, which correlates with the particle's kinetic energy (based on velocity measured by an optical device - laser). Experiments are performed to prove this method. Based on factors such as the properties of the materials used as energy absorbers (metals with high thermal conductivity) and the element size (heat capacitance is proportional to thickness) the calorimetric sensitivity can be adapted to meet the needs of the mission. Research is currently underway on the development of a flight model incorporating this solution. M. Kobush [62] considers a type of sensor that uses a 16x16 array of miniaturized calorimeters to detect the heat generation and as consequence the energy increase caused by the impact of a micron sized iron particle. In the IADC document [48] the calorimetric sensor (AIDA) measurement capability is determined through a series of tests (functional, performance and sensitivity, environmental and HVI) in air or in a vacuum using laser pulse heating and gold

absorbers. Using the calorimetric method, the impact energy can be measured and therefore the location of the impact of a specific design can be estimated. This data, in combination with that gained using other methods could provide information about particle mass, diameter or velocity.

The environmental tests showed that thermal loads can lead to variations in the sensor signals. Radiation and plasma, on the other hand, are not expected to influence to this type of sensor. Other type of factors, such as vibrations or electromagnetic interference, can be addressed through design. Resource demands are; approximately 10 W of power and less than 2 kg of mass.

4.5.5 Optical Fibre Sensors

Fibre optic (glass fibre) sensors as is described by Grattan K. T. [63] are generally composed of:

- A light leading core to transmit the signal, mainly quartz;
- A coating that transmits light at a low refractive index (causes reflection, the light remains in the core), usually quartz;
- A thin film of varnish (2 to 5 μm) for protection;
- A plastic coating for protection against mechanical damage (50 to 500 μm).

Prosser W. H. [64] identify two classes of fiber optic sensors for discrete strains and temperature measurement:

- Cavity based designs, which use an interferometric cavity in the fiber (extrinsic and intrinsic/fiber Fabry-Perot interferometer-EFPI and IFPI or FFPI) and do not allow for multiplexing capability in a single fiber;
- Grating based designs, which use a photo- or heat-induced periodicity in the fiber core refractive index to create a sensor whose reflected or transmitted wavelength is a function of this periodicity and allow multiplexing using gratings of different wavelength (using wavelength division multiplexing –WDM or optical frequency domain reflectometry OFDR principles). Factors limiting the number of sensors in a single fiber include the bandwidth limitations of the source and the range over which the physical parameter of interest is being measured [63, 64, 65]

Chapter 3 of W. Staszewski's book [66] describes load monitoring technologies that use optical fibre sensors (Bragg grating sensors), and discusses various technological aspects that need to be

addressed for effective structural usage monitoring and assessment. These include: specifications and reliability of sensors, fibre coating technology and an optical signal processor, together with a description of the nature of Bragg grating sensors. Prosser [64] considers that fiber optic sensors are leading candidate technology that meets the requirement of minimal weight and also provide a huge advantage in their ability to measure many different structural parameters of interest, offer immunity to electromagnetic interference (EMI), and have the ability to operate over a very large range of temperatures and environments. Wolfgang E. [67] presents an FBG sensor network based on multiplexed Bragg grating technology that was developed for a space application on board the X-38 experimental re-entry vehicle. During launch and re-entry, 12 locally distributed Bragg gratings (eight for strain, and four for temperature measurements) are used to measure the condition of a structural element.

López-Higuera [68] illustrates the potential of optical fiber sensors (OFS) used in structural health monitoring (SHM) applications. A number of cases where OFS for SHM systems have already been demonstrated and checked with real in-field validations are mentioned in applications including renewable energy, transportation, civil engineering, and oil and gas. K. Schroeder [69] presents the design and provides examples of a fibre Bragg grating sensor system that has been installed and successfully operated in a horizontal-axis wind turbine since 2004. Reinhart W. [70] presents systems that are based on potential low-cost components such as draw-tower FBG arrays that use optimized photosensitive fibers with sensor-specific coatings and spectral high-resolution polychromators for sensor interrogation. Performance and reliability of the sensor systems have been demonstrated by tests in the areas such as; electric power generators, aircraft and spacecraft structures, and in geotechnical monitoring applications. Smart Fibers Ltd. [71] demonstrates the measurement capabilities of such sensors and the fact that the FBG allow continuous and autonomous measurements. Single mode fibres, each of which can contain several thousand sensors, have a transmission rate up to 1 Gbit/s.

The measurement range, resolution and sample rate depend on the system itself and can provide for strain measurements ranging up to 80.000 μm/m for a single strain sensor and a temperature measurement range from cryogenic to 300°C. From point of view of possible application of fiber optic sensors for monitoring HVI in space, the problem is the thermally loaded parts of the spacecraft during re-entry (approx. 3% of surface). The fiber optic sensors can withstand a variety of factors as chemicals, radiation and high temperature. Also, they will not react to interference

with electromagnetic fields. MPB in collaboration with McGill University [72] have carried out HVI tests on self-healing CFRP laminates and monitored the effect using fiber sensors, Figure 4.13. The study shows the effectiveness of the fiber sensors in monitoring the debris and their effects after the impact.

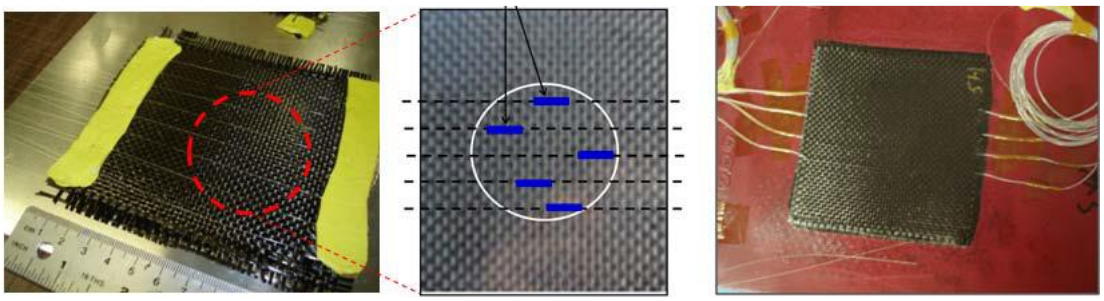

Figure 4.13: MPB Packaging for HVI tests: CFRP, FBG, resin, and self-healing [72]

FBG presents many advantages in monitoring HVI, such as its ability to monitor a variety of parameters, minimal loss or signal distortion, and environmental robustness. These advantages favor use of this technology for future health monitoring of aerospace structures.

4.5.6 Resistor based sensors

The term ‘resistor based sensor’ refers to sensors constructed using a resistance film attached to a pressurized wall to form an area sensor, capable of detecting a perforation resulting from a HVI. The resistance value is measured by a drop in direct current potential caused by the perforation hole. S. Fukushige [73] proposed a system that locates a perforation using this type of sensor. The system is characterized by its simplicity in analysis and measurement. The effectiveness of method is demonstrated by tests using a theoretical equation on an infinite resistance film. A resistivity correction factor is included to account for the shape effect. The method is mainly useful for manned space vehicles because it does not provide accurate information about the size of particle nor the location of the perforation. The method offers a location resolution of approximately 10 cm, which is small enough to provide an evacuation direction for the crew and a repair location for the structure.

In terms of resources, the necessary electric power for simple signal processing is used only after perforation. The environmental robustness of such a system has not yet been tested.

4.5.7 Microwave emission

HVI is a complex phenomenon; at hyper velocities phase transformation of the material occurs. A projectile impact causes evaporation and ionization of the target materials, creating a plasma cloud. A Stanford University [74] study aimed at characterizing hypervelocity impact plasmas provides responses to questions related to the dependence of RF emission power on frequency and the influence of magnetic/electric fields on hypervelocity impact plasmas.

In 1997, a general empirical formula for the charge Q produced during a hypervelocity impact was presented by Ashish Goel [75]. In his paper he presents the results from numerical simulation along with results of experiments with a miniaturized, low-mass, low-cost plasma sensor using circuit boards for detection and measuring of HVI plasma. L. Foschini [76] concludes that impact generated plasma is the major danger for on-board electronics due to electro-magnetic interference produced. He gives the example of the Olympus satellite electrical failure caused by an impact with a Perseid meteoroid. K. Maki [77] shows the results of two types of experiments performed to describe and clarify the mechanism of emission of radio-waves in the microwave frequency range caused by an HVI. The results are afterwards compared with optical imaging methods. Capture of microwave emissions is done using an antenna that operates at a GHz frequency rate together with low-noise amplifiers and fast data recorder (a window of 2 to 22+ GHz and a heterodyne receiver). T. Takano [78] presents a series of HVIs performed in order to detect microwave emissions in waveforms up to 1 ns. The emissions are a random series of pulses that continue for more than 10 μs. He concluded that the timing and duration of the emissions are strongly dependent on the material and thickness of target. Large emission delays were observed in the case of a perforated target. The development of this type of sensor for use as an integrated spacecraft sensor requires a lot of effort due to a limited understanding of the theoretical process and the difficulty in testing and calibrating the sensor.

4.5.8 Surface inspection cameras

Another HVI detection technique currently used on the NASA Space Shuttle is the Orbiter Boom Sensor System (OBSS), used to scan the leading edges of the wings or the nose cap. Surface inspection cameras take a series of digital still images of the spacecraft surface over a period of

time and transmit these images to Earth for analysis (onboard processors could significantly increase the spacecraft resources needed to use this approach).

H. Hirayama [79] presents an onboard surface inspection system that consists of a small high-resolution charge-coupled device (CCD) camera, data handling and communication subsystems that detect impacts on the surface created by micron-sized debris impact. A high resolution image is transmitted to a ground station for further analysis. The paper concluded that the size of the impacting debris can be estimated, but the velocity of the impacting object is difficult to determine. B. Kennedy [80] proposes a small, agile and capable six-legged walking robot that has been built at the Jet Propulsion Laboratory to perform dexterous small-scale assembly, inspection and maintenance. The robot uses an external sensor system composed of a set of black and white cameras. The images taken by these cameras are combined in software to create a 3D model of the world around LEMUR for autonomous operation.

4.5.9 Carbon Nano-tube sensors

W.H Prosser [64] presents this new type of sensor that can be integrated into future onboard spacecraft structural health management SHM systems to detect HVI. Due to the high strength-to-weight ratio of carbon nanotubes combined with quantum transport characteristics, this type of sensor is ideal for future multifunctional structural materials. The Nano-tubes can function as strain sensors (through transfer of the circuit to a flexible substrate) and as magnetic field sensors (through injection of spin-polarized electrons).

4.5.10 Solar panel based space debris impact detector

A solar panel based space debris impact detector (SOLID) is a large-area impact detector presented by W. Bauer [81] that can be used to gather information on MMOD distributions, which is necessary for model validation. The photo-voltaic cells of the solar panels are used as detection surfaces. An insulation layer behind the solar cells is equipped with two layers of copper lines that form a detection grid. Information including damage detection, damage diameter and impacting particle size can be obtained. This method is used exclusively in evaluation of MMOD fluxes and not to monitor HVI on a spacecraft surface.

4.5.11 Smart skin concept

A future approach is presented by BAE Systems [82]. The "smart skin" concept is based on embedding tens of thousands of micro-sensors that can accurately sense wind speed, temperature, physical strain and movement. The presented system will have all the characteristics of a health monitoring system such as real time sensing, increased efficiency and improved safety. The system will use tiny sensors or "motes" and complete computing packets that are smaller than grains of rice or even as small as dust particles at less than 1 square mm (could be applied like spray paint). The smart skin contains its own power source and appropriate data analysis capabilities.

4.5.12 Advantages/disadvantages: accelerometers and fiber optic sensors

Based on this review and as identified in the IADC document, accelerometers represent the currently available first choice as sensors to be used in a hypervelocity impact health monitoring system. Fiber optic sensors, which offer excellent accuracy, coverage, environmental robustness and simplicity, represent one of the top choices for future monitoring systems. Sensor systems that use accelerometers detect and measure vibrations produced by HVI-induced shocks on spacecraft structures. They can assess impact locations and criticality and have the ability to manage signals (high frequency content). However, they use considerable resources of the spacecraft. Integrated impact detection systems that use fiber optic sensors (available and widely used in aerospace structures) are currently under development. The advantages offered make this a promising technology for monitoring HVI in spite of the difficulty in integrating fiber optics into the spacecraft structure.

4.6 Test Results

Six satisfactory recorded tests (5 preliminary signals plus the test "0" signal, which is recorded from outside the vacuum chamber) were performed on our aluminum and carbon fiber samples using the gas launcher at different gas pressures, thus different projectile velocities. The test results are shown in Table 4.6. In addition, a series of tests was done to verify the mechanical stripper proposed by McGill. The data includes cases where similar preparation for the firing was done, but the shots were not performed or were prematurely triggered due to different factors such as coils triggering, diaphragm penetration, mechanical strippers or other unknown factors that will be

analyzed later. Special attention should be given to all these factors in order to be able to perform well-controlled shots.

Table 4.6: Test summary

	Sample	**Projectile**	**Pressure (PSI)**	**Velocity (m/s)**	**Vacuum**	**Others**
Preparatory Test	No sample	Sabot alone	4000	1638	Yes	-
Preparatory Test	CF 1/8''	Full 2 mm sphere	4000	1573	Yes	N_2+Mech. Separator, No penetration No Acquisition
Preparatory Test (test 0)	CF 1/8''	Full 2 mm sphere	4000	1573	No	N2 Separator, No penetration Acquisition (on the vacuum chamber)
Test 1	CF 1/8''	Full 3.2 mm sphere	4000	1570	No	N_2 Separator, Penetration Acquisition
Test 2	CF 1/8''	Full 3.2 mm sphere	2500	880	No	N_2 Separator, No Penetration Acquisition
Test 3	Al 2mm	Full 3.2 mm sphere	4000	570	No	N_2 Separator, Penetration Acquisition
Test 4	Al 5mm	Full 3.2 mm sphere	4000	540	No	N_2 Separator, No Penetration Acquisition

4.6.1 Target damages

The pictures on Figure 4.14 present the two types of damage that were recorded for 2 different Al 6061T6 thicknesses, and one thickness of CFRP.

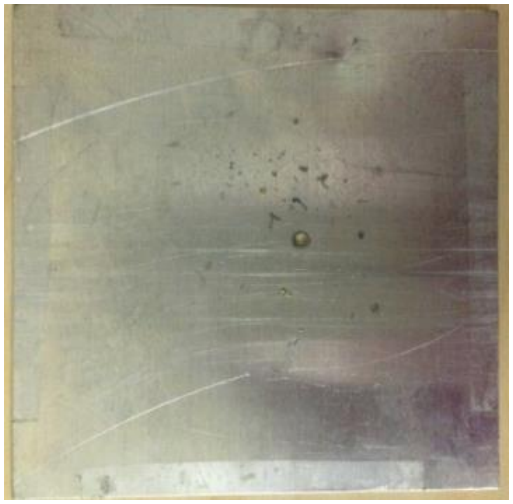

a)

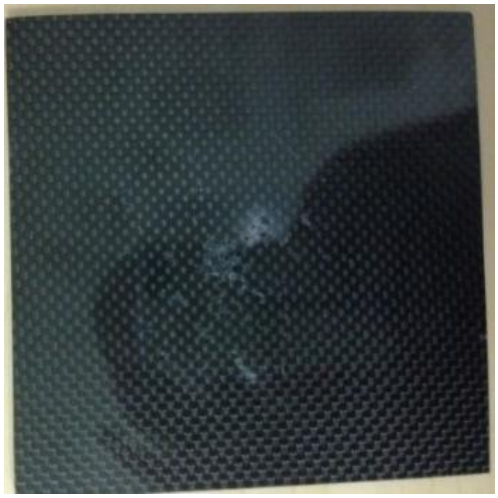

b)

c)

d)

Figure 4.14: Impact on all six targets: a) preparatory test, Al fully perforated, b) test0, CFRP not perforated, c) test1, CFRP, fully perforated, d) test2, CFRP not perforated, e) test3, Al, fully perforated, f) test4, Al not perforated

e)

f)

Figure 4.14 (continued): Impact on all six targets: a) preparatory test, Al fully perforated, b) test0, CFRP not perforated, c) test1, CFRP, fully perforated, d) test2, CFRP not perforated, e) test3, Al, fully perforated, f) test4, Al not perforated

4.6.2 Recordings

In Figure 4.15, we show five signal recording samples acquired during the test session from Shock Wave Physics Laboratory (McGill University); recordings of HVI position and amplitude (with damage characteristics, penetration or not penetration). The time of impact could not be determined.

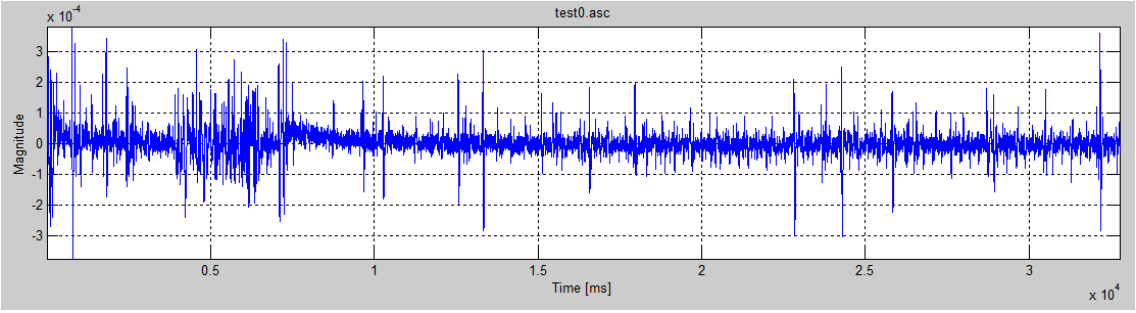

a)

Figure 4.15: The recorded signals for five tests (for the test0 the accelerometer was mounted on the vacuum chamber), y axis represent accelerations (m/s^2)

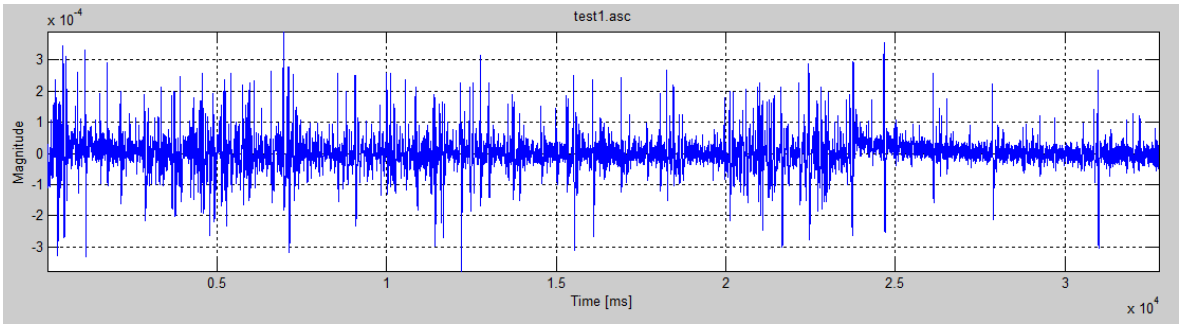

b)

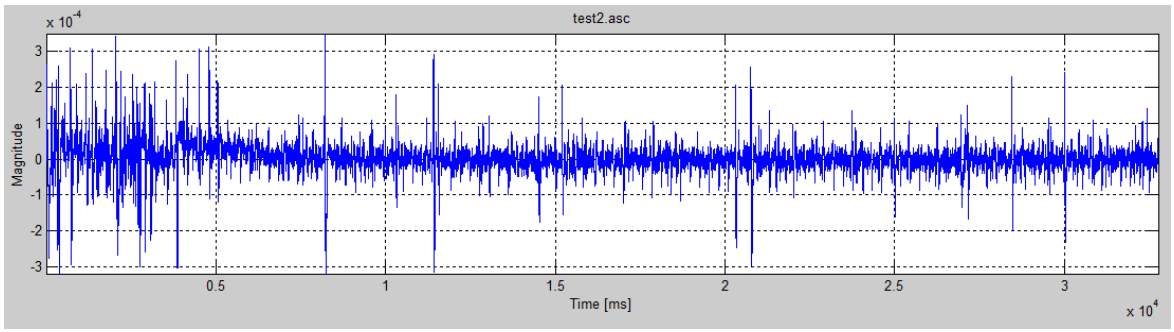

c)

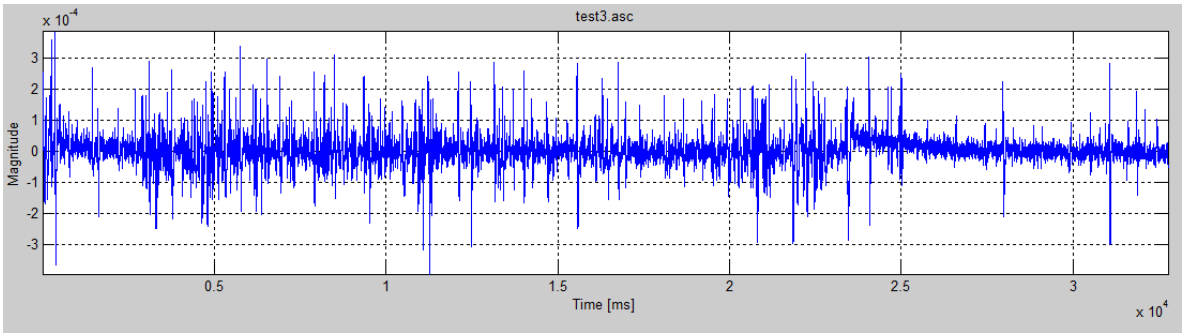

d)

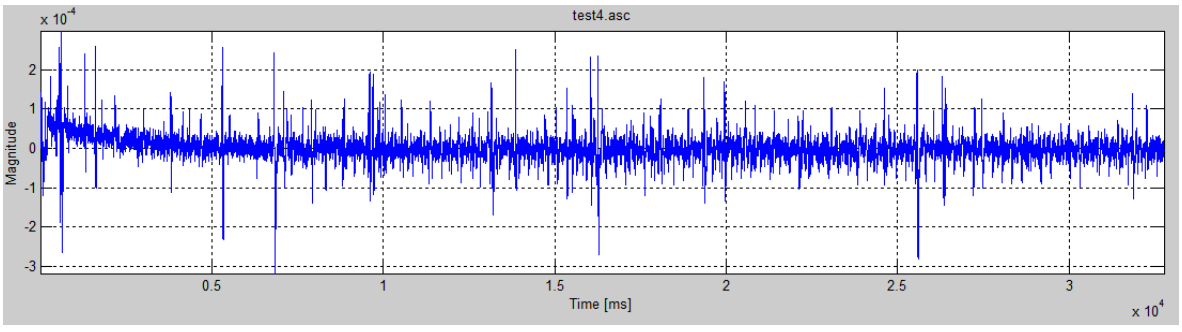

e)

Figure 4.15 (continued): The recorded signals for five tests (for the test0 the accelerometer was mounted on the vacuum chamber), y axis represent accelerations (m/s2)

MPB Communications Inc. [72] previously also performed a series of HVI tests on CFRP modified targets that included self-healing materials and used fiber sensors and fast acquisition (2MHz) to record the impact. The signals were analyzed with the same TF software. The self-healing materials were composed of microcapsules containing combinations of a 5-ethylidene-2norbornene (5E2N) and dicyclopentadiene (DCPD) monomers of 100-300 μm diameter and ruthenium Grubbs' as a catalyst. Using vacuum centrifuge techniques these combinations were blended with a resin epoxy and single-walled carbon nanotubes (SWNTs). The samples also survived thermal shock (20 cycles, -196℃ to +60℃) and were tested for compatibility with a vacuum. HVI tests were performed on 12cm x 12cm x 2 mm thick samples that contained a lay out of resin mixed with microcapsules and a catalyst and a lay out of the fiber sensor. The resin was cured in an autoclave (40℃, 40 psi for 12 hours). Different samples were impacted by projectiles with velocities between 1 to 8 Km/s, the velocities given by standard instruments were validated by measurement of the time between triggering and the effect on FBG. The signal results recorded on a CFRP 828-CHCNT target by the four FBG sensors are shown in Figure 4.16.

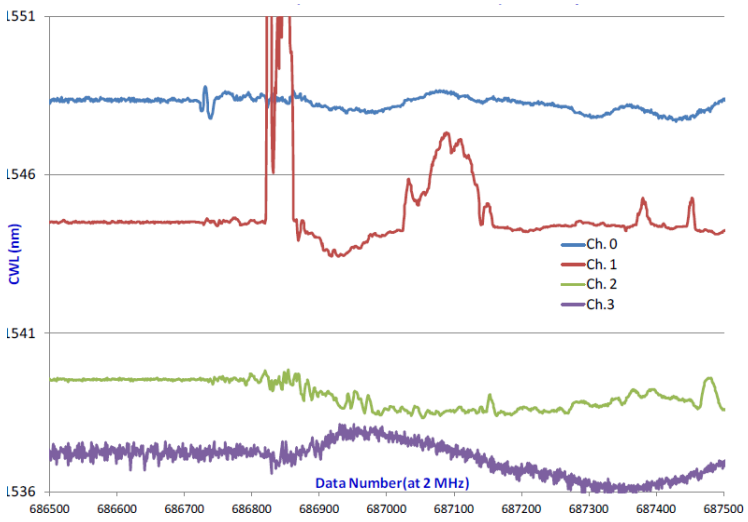

Figure 4.16: The recorded signals for five FBG sensors at 2MHz recording the HVI [72]

The frequency distribution (FFT) of signals, using the FBG sensors, Figure 4.17.

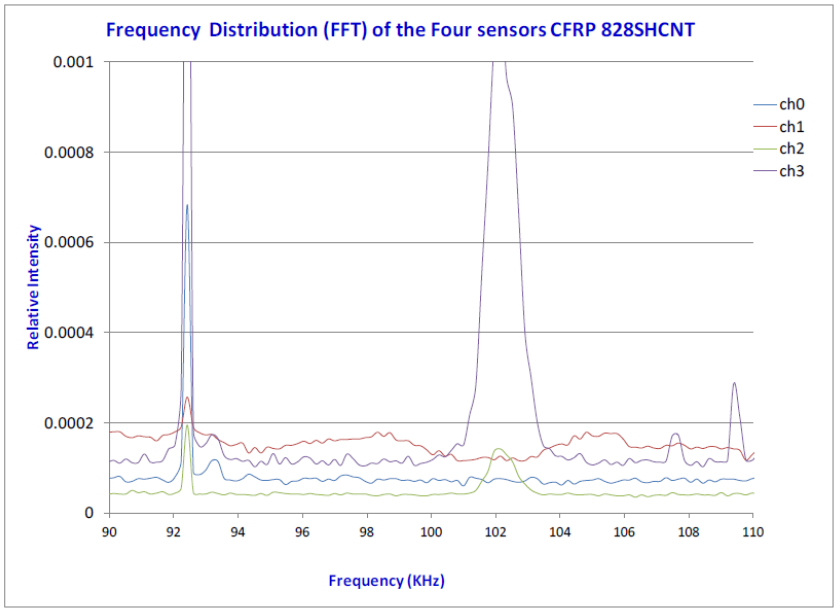

a)

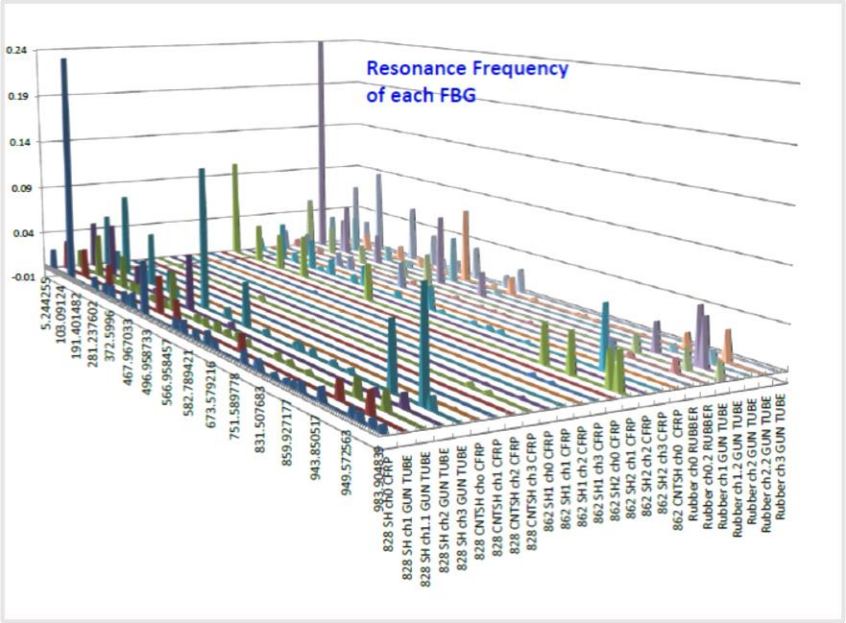

b)

Figure 4.17: FFT analysis: a) CFRP 828-SHCNT sample, b) summary for all samples [72]

4.7 Next steps

Future steps should be taken in essential directions that are closely related, future HVI tests performed and time-frequency analysis (TF) of the signal recordings.

4.7.1 HVI tests

The first essential direction is continuing to perform HVI tests, similar to the primary step using the same gun, with the purpose of obtaining better precision in velocity and sabot separation. Precise velocity control is an important factor in creating the required type of damage. Sabot separation is very important in order to eliminate the secondary impact on the target. For distant future work however, a secondary impact on the target could be a plus in characterizing the response of materials or bringing new information necessary for creation of smart material. An example is a material that uses elements for self-healing.

A further step will be to perform new hypervelocity tests at velocities up to 4.5 to 5 km/s, which are considered intermediate velocities for MMOD impacts, at the same Shock Wave Laboratory at McGill University. These can be done using a new 2-stage light gas gun currently under construction. The use of TF signal analysis for HVI tests performed in the low-velocity regime would generate new information for characterizing impact damage. Note that for this step a phase transformation of the material will occur. A final step in the experimental phase would be to perform HVI tests at speeds relatively close to MMOD impact.

The implosion gun in the same laboratory can perform HVI impact tests at 8 km/s. Preparation of these tests and TF analysis of the data will involve a large amount of work. It is therefore suggested that these types of tests be performed further in the future. At this time the implosion gun is scheduled to fire only two times in a Canadian Space Agency project that involves impact tests on a CFRP material similar to that used in the Canadarm.

4.7.2 TF signal analysis

The other critical direction for future work is in the area of TF signal analysis. This work will involve a considerable amount of time to analyze recorded signals so that the best method can be found that allows identification of the types of damage on different types of materials. A first step in this direction will be to perform a TF analysis [83-85] yielding a compact representation of machine condition which includes important effects associated with non-stationarity. The TF Analysis software developed by the research group is ideally suited for analysis and reduction of multi-sensor spectro-temporal steady and transient data. Signals caused by debris impact are highly

transient and short-lived. Time-frequency analysis methods incorporated in TF-Analysis will be used to efficiently extract the primary features of the impact signals.

Figure 4.18 presents an example of the use of TF analysis software for analysis of one of the tests done at the Shock Wave Physics Laboratory (McGill University).

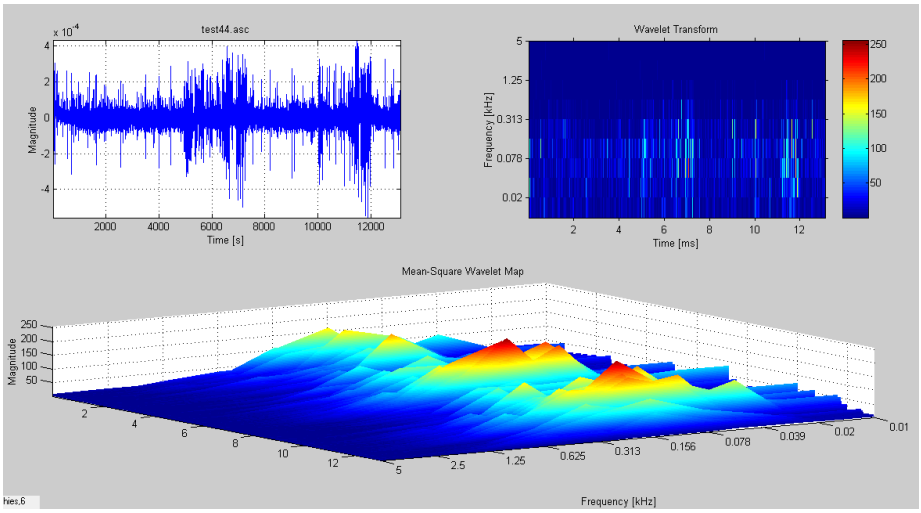

a)

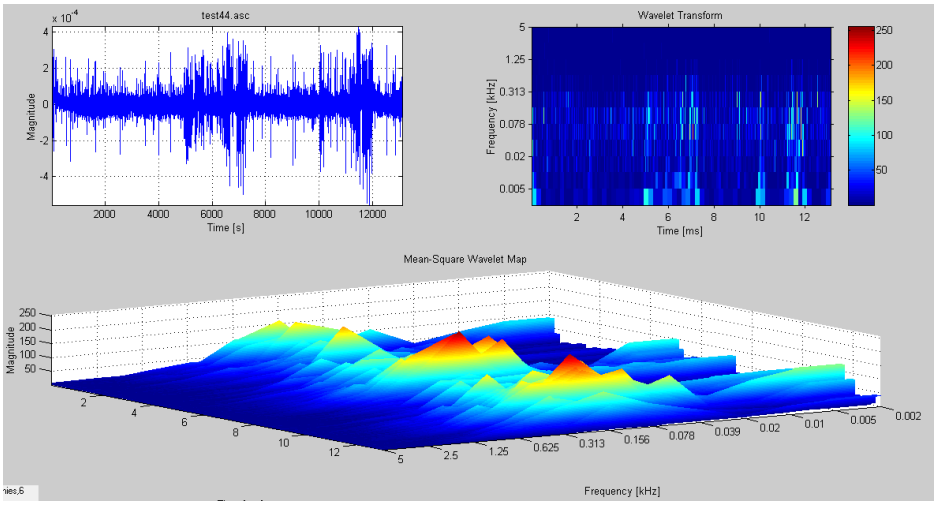

b)

Figure 4.18: An example of the Wavelet transform (WT) signal analysis using our software (decomposition level, 9 and 11)

The above two images present an example of TF analysis performed on the first part of the last signal recorded. It seems that there is a cluster (waves) of frequencies that is constant and is

repeating at some time intervals. This could be a cluster of symmetrical S waves that don't present a dispersive behavior, have un-changed shape and their frequency components travelled at the same speed. The figure could represent the arrival of the first wave group from the impact point and the arrival of the same wave group reflected from the boundary, but this is a very preliminary interpretation and further, deeper analysis must be done. The TF analysis will continue for all sections of signals recorded in order to precisely identify the moment of the signal and also minimize the number of measurement points so that the different in-plane IP or out-of-plane OP accelerations can be recognized. The wavelet transform WT analysis is able to identify both the frequency content and propagation velocity. This information could be important for identifying the type of damage; with or without perforation. The same TF analysis software will be used to analyze the test signal recordings previously obtained by MPB. However, as can be seen in Figure 4.16 above, an initial transformation of signals from deformations to accelerations is needed. This can be done using Matlab software and will be presented in the next work.

As a result of this research work, a new capability for automation of the process and the creation of a library of different types of materials used in space together with damage identification can be achieved.

4.8 Conclusions

The work performed at the Shock Physics laboratory of McGill University, the tests performed and the signal recordings obtained represent an essential first step in applying TF analysis software in a system capable of real-time detection and analysis of the effects of MMOD impacts. The short literature review described the most frequently used materials for these types of applications, the best positions these materials should be mounted in a future shield design based on their characteristics and the difficulties involved in selecting the best material. For the case of composite materials, the choice of the matrix is essential in providing the desired protection. For example, metallic or ceramic matrices presented good results in shattering the projectile.

Kevlar fiber materials, due to their unique characteristics, perform very well in catching the fragments of a debris cloud. Tests were performed at low impact velocity, up to 1.6 km/s. This velocity is not representative of MMOD velocities but is sufficient in offering the signal recordings necessary for further investigation. In addition to the test results, new knowledge was gained relative to manipulating the gun, specific gun capabilities/characteristics and methods for

manufacturing different elements such as the sabot (a very complex and essential element) or the mechanical stripper. We also learned about unexpected problems that could arise in this type of test and the necessary equipment and costs involved in performing further HVI tests, especially at the higher velocities essential for characterizing MMOD damage.

The first preliminary recordings that indicate the presence and effect of an impact on targets are very significant to begin to understand the damage mechanism and the potential to gather more information using further T-F analysis. Presently, observations/interpretation of the signal recordings lead us to important conclusions that can be applied during future HVI tests, such as the potential advantages of a second time-recording element and the necessity of preparation of signals in order to identify the time of the HVI impact.

As a general conclusion, the tests performed were successful, the signal recordings are valid. This section of work can be considered the cornerstone of our future work in this are

4.9 References

[1] Shannon Ryan, Eric L. Christiansen, *Hypervelocity impact testing of advanced materials and structures for micrometeoroid and orbital debris shielding*. NASA Johnson Space Center, US (2012)

[2] Burton G. Cour-Palais, *Hypervelocity impact in metals, glass and composites*., NASA (1987)

[3] W.P. Schonberg, "Protecting spacecraft against orbital debris impact damage using composite materials". *Composites*: Part A, 31 (2000) 869–878

[4] Keisuke Fujii, Motokazu Aoki, Noriyuki Kiuchi, Eiichi Yasuda, Yasuhiro Tanabe, "Impact perforation behavior of CFRPs using high-velocity steel sphere". *International Journal of Impact Engineering* 27 (2002) 497–508

[5] Y. Nagao, S. Kibe, K. Daigo, A. Francesconi, D. Pavarin, "Hypervelocity impact studies simulating debris collisions on composites material". Proceedings of the forth European Conference on Space Debris, Darmstadt, Germany, 18-20 April 2005

[6] Daniel Bürger, Alfredo Rocha de Faria, Sérgio F.M. de Almeida, Francisco C.L. de Melo, Maurício V. Donadon, "Ballistic impact simulation of an armour-piercing projectile on hybrid

ceramic/fiber reinforced composite armours". *International Journal of Impact Engineering* 43 (2012) 63-77

[7] Makoto Tanaka, Yoko Moritaka, Yasuhiro Akahoshi, Ryuta Nakamura Akira Yamori, Susumu Sasaki, "Development of a lightweight space debris shield using high strength fibers". *International Journal of Impact Engineering* 26 (2001) 761-772

[8] M. Tanaka, Y. Moritaka, "Single bumper shields based on Vectran fibers". *Advances in Space Research* 34 (2004) 1076–1079

[9] Yasuhiro Akahoshi, Ryuta Nakamura, Makoto Tanaka, "Development of bumper shield using low density materials". *International Journal of Impact Engineering* 26 (2001) 13-19

[10] Z. G. Wei, R. Sandstrom, S. Miyazaki, "Shape memory materials and hybrid composites for smart systems. Part II, Shape-memory hybrid composites". *Journal of materials science* 33 (1998) 3763 — 3783

[11] J. H. Robinson, A. M. Nolen, "An investigation of metal matrix composites as shields for hypervelocity orbital debris impacts". *Int. J. Impact Eng*. Vol. 17, pp. 685-696, 1995

[12] S. Katz, E. Grossman, I. Gouzman , M. Murat, E. Wiesel, H.D. Wagner, "Response of composite materials to hypervelocity impact". International Journal of Impact Engineering 35 (2008) 1606–1611

[13] R.A. Clegg, D.M. White, W. Riedel, W. Harwick, "Hypervelocity impact damage prediction in composites: Part I—material model and characterisation". *International Journal of Impact Engineering* 33 (2006) 190–200

[14] W. Riedel, H. Nahme, D.M. White, R.A. Clegg, "Hypervelocity impact damage prediction in composites: Part II – experimental investigations and simulations". *International Journal of Impact Engineering* 33 (2006) 670–680

[15] Martin Rudolph, Frank Schafer, Roberto Destefanis, Moreno Faraud, Michel Lambert, "Fragmentation of hypervelocity aluminum projectiles on fabrics". *Acta Astronautica* 76 (2012) 42–50

[16] Bryan A. Cheeseman, Travis A. Bogetti, "Ballistic impact into fabric and compliant composite laminates". *Composite Structures* 61 (2003) 161–173

[17] R. Destefanis, E. Amerio, M. Briccarello, M. Belluco, M. Faraud, E. Tracino, C. Lobascio, "Space environment characterization of Kevlar: good for bullets, debris and radiation too" ISMSE -11, 11th International Symposium on Materials in a Space Environment, 15-18 September 2009, Aix-en-Provence, France

[18] Roberto Destefanis, Moreno Faraud, "Testing of advanced materials for high resistance debris shielding". *Int. J. Impact Engng*, Vol. 20, pp. 209-222, 1997

[19] E. A. Taylor, M. K. Herbert, B. A. M. Vaughanh, J. A. M. Mcdonnell, "Hypervelocity impact on carbon fibre reinforced plastic/aluminium honeycomb: comparison with Whipple bumper shields". *International Journal of Impact Engineering* 23 (1999) 883-893

[20] Emma A. Taylor, Jonathan P. Glanville, Richard A. Clegg, Robert G. Turner, "Hypervelocity impact on spacecraft honeycomb: hydrocode simulation and damage laws". *International Journal of Impact Engineering* 29 (2003) 691–702

[21] A. Francesconi, D. Pavarin, A. Bettella, C. Giacomuzzo, M. Faraud, R. Destefanis, M. Lambert, F. Angrilli, "Generation of transient vibrations on aluminum honeycomb sandwich panels subjected to hypervelocity impacts". *International Journal of Impact Engineering* 35 (2008) 1503–1509

[22] IADC WG3, *Protection manual*. IADC-04-03, Version 4.0, April 12, 2011

[23] M. Grujicic, B. Pandurangan, C.L. Zhao, S.B. Biggers, D.R. Morgan, "Hypervelocity impact resistance of reinforced carbon–carbon/carbon–foam thermal protection systems". *Applied Surface Science* xxx (2005) xxx–xxx

[24] S. Ryan, E.L. Christiansen, *Honeycomb vs. foam: evaluating potential upgrades to ISS module shielding.* IAC-09.A6.3.11

[25] S. Ryan, E. Ordonez, E. L. Christiansen, D. M. Lear, *Hypervelocity impact performance of open cell foam core sandwich panel structures*. NASA (2010)

[26] Zhang Xiaotian, Jia Guanghui, Huang Hai, "Numerical Investigation of aluminum foam shield based on fractal theory and node-separation FEM". *Chinese Journal of Aeronautics* 24 (2011) 734-740

[27] Bin Jia, Feng Li, Hai Peng Gong, Bao Jun Pang, "Performance of different metal-foam stuffed Whipple shield against hypervelocity impact of space debris". 2011, *Key Engineering Materials*, 488-489, 122

[28] Eric L. Christiansen, Justin H. Kerr, "Mesh double-bumper shield: A low-weight alternative for spacecraft meteoroid and orbital debris protection"**.** *International Journal of Impact Engineering*, Volume 14, Issues 1–4, 1993, Pages 169–180

[29] M. Higashide, M. Tanaka, Y. Akahoshia, S. Harada, F. Tohyama, "Hypervelocity impact tests against metallic meshes". *International Journal of Impact Engineering* 33 (2006) 335–342

[30] Dezhi Zhu, Guoqin Chen, Gaohui Wu, Pengchao Kang, Wei Ding, "Hypervelocity impact damage to Ti–6Al–4V meshes reinforced Al–6Mg alloy matrix composites". *Materials Science and Engineering* A 500 (2009) 43–46

[31] Q. Guo, D.L. Sun, X.L. Han, W.S. Yang, L.T. Jiang, G.H. Wu, "Damage behaviour of Al matrix composite reinforced with Ti–6Al–4V meshes under the hypervelocity impact". *Materials Science and Engineering* A 535 (2012) 136– 143

[32] L. Merzhievsky, "Crater formation in a plastic target under hypervelocity impact". *Int. J. Impact Engng*, Vol. 20, pp. 557-568, 1997

[33] T. Mudric, C. Giacomuzzo, U. Galvanetto, A. Francesconi, M. Zaccariotto, A. M. Grande, L. Di Landro, "Impact tests and simulations for multifunctional materials". ECCM15 – 15th European conference on composite materials, Venice, Italy, 24-28 June 2012

[34] Stephen J. Kalista Jr., Thomas C. Ward, "Self-Healing of poly (Ethylene-co-Methacrylic Acid) copolymers following ballistic puncture". Proceedings of the First International Conference on Self-Healing Materials, 218-20 April 2007, Noordwijk aan Zee, The Netherlands

[35] Eric L. Christiansen, *Meteoroid/debris shielding*. TP−2003-210788, NASA (August 2003)

[36] Swift, H. F., *Hypervelocity Impact Mechanics, Impact Dynamics*. John Wiley and Sons (1982)

[37] Du Pont, http://www.dupont.com/products-and-services/fabrics-fibers-nonwovens/fibers/brands/kevlar.html

[38] Du Pont, http://www.dupont.com/products-and-services/fabrics-fibers-nonwovens/fibers/press-releases/next-generation-of-innovations-with-Kevlar.html

[39] 3M Nextel Ceramic Textiles and Composites, http://www.3m.com/market/industrial/ceramics/materials/fabric_312.html

[40] Du Pont USA, http://www2.dupont.com/Kapton/en_US/

[41] M. Wicklein, S. Ryan, D.M. White, R.A. Clegg, "Hypervelocity impact on CFRP: testing, material modelling, and numerical simulation". *International Journal of Impact Engineering* 35 (2008) 1861–1869

[42] Hong Wan, Shuxin Bai, Shun Li, Jianjun Mo, Shicao Zhao, Zhenfei Song, "Shielding performances of the designed hybrid laminates impacted by hypervelocity flyer". *Materials and Design* 52 (2013) 422–428

[43] E.L. Christiansen, J.L. Crews-NASA Johnson, J.E. Williamsen, J.H. Robinson, A.M. Nolen-NASA Marshall, "3M Nextel Ceramic Fabric Offers Space Age Protection". *Intl. Journal of Impact Engineering*, Vol. 17

[44] Suman Khatiwada, Carlos A. Armada and Enrique V. Barrera, "Hypervelocity Impact Experiments on Epoxy/Ultra-High Molecular Weight Polyethylene Fiber Composites Reinforced with Single-Walled Carbon Nanotubes". *Procedia Engineering* 58 (2013) 4 – 10

[45] Maxim A. Makeev, Deepak Srivastava, "Molecular Dynamics Simulations of Hypersonic Velocity Impact Protection Properties of CNT/a-SiC Composites". *Composites Science and Technology* 68 (2008) 2451–2455

[46] William P. Schonberg, "Protecting Earth-orbiting spacecraft against micro-meteoroid/orbital debris impact damage using composite structural systems and materials: An overview". *Advances in Space Research* 45 (2010) 709–720

[47] Anthony Devito, "The combustion of bulk metals in a high-speed oxidizing flow". MSc thesis, McGill University, Montreal, Quebec 2014-4-15

[48] IADC WG3, *Sensor systems to detect impacts on spacecraft*. IADC-08-03, Version 2.1, April 2013

[49] Gerhard Drolshagen, “Impact effects from small size meteoroids and space debris”. *Advances in Space Research* 41 (2008) 1123–1131

[50] Dae-Un Sung, Hun-Gou Kim, and Hang-Sun Hong, “Monitoring of impact damages in composite laminates using wavelet transform”. *Composites* Part B, Vol. 33, p. 35-43, 2002.

[51] J.C. Chen, K. Yao, R.E. Hudson, T.L. Tung, C.W. Reed, D. Chen, “Source localization of a wideband source using a randomly distributed beamforming sensor array”. *International Journal of High Performance Computing Applications* (01/2002)

[52] Norske Veritas, “In-Orbit Non-Destructive Testing –Extension”. ESA / ESTEC Contract No. 8433/89/NL/PP (SC), DNV Report 92-3207 Rev. 2, 1992

[53] Mikhail Prokopenko, Peter Wang, Andrew Scott, Vadim Gerasimov, Nigel Hoschke, Don Price, “On Self-organising Diagnostics in Impact Sensing Networks”. Knowledge-Based Intelligent Information and Engineering Systems Lecture Notes in *Computer Science* Volume 3684, 2005, pp 170-178

[54] William H. Prosser, Michael R. Gorman, Donald H. Humes, “Acoustic emission signals in thin plates produced by impact damage”. *Journal of Acoustic Emission*, Vol. 17(1-2), (June, 1999), pp. 29-36.

[55] A. Bettella, A. Francesconi, D. Pavarin, C. Giacomuzzo, F. Angrilli, “Application of Wavelet Transform to analyze acceleration signals generated by HVI on thin aluminum plates and all-aluminum honeycomb sandwich panels”. *International Journal of Impact Engineering* 35 (2008) 1427–1434

[56] Boeing, http://www.boeingtravel.com/assets/pdf/defense-space/space/spacestation/components/docs/EWIS.pdf)

[57] Kevin D. Champaigne, Jonathan Sumners, “Low-power electronics for distributed impact detection and piezoelectric sensor applications”. Aerospace Conference, 2007 IEEE

[58] Smith B. T, *Rapid detection and quantification of impact damage in composite structures*. NASA-CR-190367, 1992.

[59] Howell, P.A., Winfree, W.P., Cramer, K.E., "Infrared on-orbit inspection of shuttle orbiter reinforced carbon-carbon using solar heating". SPIE Optics and Photonics, 31 Jul-4 Aug 2005, San Diego CA USA

[60] T. Poppe, H. Sdunnus, D. Rex, "AIDA - Advanced impact detector assembly for the on-orbit measurement of small impacting debris particles and meteoroids". Adv. Space Res. Vol. 17, No. 12, pp. (12)133-(12)136, 1996

[61] K. D. Bunte, M. Kobusch, J. Hollandt, J. Illemann, F. Jager, M. Glaser, S. Sarge, "AIDA - An Advanced Impact Detector Assembly". IAC-03-IAA.5.P.02 (2003)

[62] M. Kobush, F. Jager, K. D. Bunte, T. Fichna, E. Kessler, "Calorimetric Energy Detector for Space Debris". IAC-06-B6.3.9

[63] Grattan, K.T.V., et al., *Optical Fiber Sensor Technology*, Vol. 3, 1999.

[64] Prosser, W.H., "Development of structural health management technology for aerospace vehicles". JANNAF 39th Combustion/27th Airbreathing Propulsion/21st Propulsion Systems Harzards/3rd Modeling and Simulation Joint Subcommittee Meeting; 1-5 Sep. 2003

[65] Kashima, S. and Ozaki, T., "Structural health monitoring using FBG sensor in space environment". Proc. SPIE Vol. 4332, p.78-87, 2001.

[66] W.J. Staszewski, C. Boller, G.R. Tomlinson, *Health Monitoring of Aerospace Structures*. John Wiley & Sons Ltd, 2004

[67] Wolfgang Ecke, Ines Latka, Reinhardt Willsch, Arnd Reutlinger, Roland Graue, "Fibre optic sensor network for spacecraft health monitoring". *E. Meas. Sci. Technol*. 12 (2001) 974–980

[68] José Miguel López-Higuera, Luis Rodriguez Cobo, Antonio Quintela Incera, Adolfo Cobo "Fiber optic sensors in structural health monitoring". *Journal of lightwave technology*, Vol. 29, No. 4, February 15, 2011

[69] Kerstin Schroeder, Wolfgang Ecke, Jorg Apitz, Elfrun Lembke, Gerhard Lenschow, "A fibre Bragg grating sensor system monitors operational load in a wind turbine rotor blade". *Meas. Sci. Technol.* 17 (2006) 1167–1172

[70] Reinhardt Willsch, Wofgang Ecke, "Potential low-cost optical fiber Bragg-grating sensor systems for structural health monitoring and examples of their application". SPIE 4920, Advanced Sensor Systems and Applications, (9 September 2002)

[71] Smart Fibres Ltd., UK, https://www.smartfibres.com/

[72] B. Aissa, K. Tagziria, W. Jamroz, E. Haddad, M. Asgar-Khan, S. V. Hoa , J. Loiseau, J. Verreault, A. Higgins, "Monitoring with Fiber sensors and Self-Healing of CFRP Laminates Exposed to Hypervelocity Small Pellets Simulating Space Debris". 12th International Symposium on Materials in the Space Environment (IMSE-12) 24-28 September 2012.

[73] S. Fukushige, Y. Akahoshi, T. Koura, S. Harada, "Development of perforation hole detection system for space debris impact". *International Journal of Impact Engineering* 33 (2006) 273–284

[74] Stanford University, Space Environment and Satellite Systems, http://sess.stanford.edu/hvip

[75] Ashish Goel, Paul M. Tarantino, David S. Lauben, Sigrid Close, "Design and testing of miniaturized plasma sensor for space plasma diagnostics". Spacecraft Charging Technology Conference 2014 - 181 Paper

[76] L. Foschini, "The meteoroid hazard for space navigation". Planetary Science: Second Italian meeting. Eds A. Manara and E. Dotto. Alenia Spazio, Torino (1999), p. 131.

[77] K. Maki, T. Takano, A. Fujiwara, A. Yamori, "Radio-wave emission due to hypervelocity impacts in relation to optical observation and projectile speed". *Advances in Space Research* 34 (2004) 1085–1089

[78] Takano, T., Murotani, Y., Toda, T., Fujiwara, A., Hasegawa, S., Yamori, S., "Microwave emission experiment with hypervelocity impacts and applications of its results". Proceedings of the Third European Conference on Space Debris, 19 - 21 March 2001

[79] H. Hirayama, T. Hanada, T. Yasaka, "In situ debris measurements in MEO/HEO using onboard spacecraft surface inspection system". *Advances in Space Research* 34 (2004) 951–956

[80] Brett Kennedy, Hrand Agazarian, Yang Cheng, Michael Garrett, Gregory Hickey, Terry Huntsberger, Lee Magnone, Colin Mahoney, Amy Meyer, Jennifer Knight, "LEMUR: Legged Excursion Mechanical Utility Rover". *Autonomous Robots* 11, 201–205, 2001

[81] Waldemar Bauer, O. Romberg, C. Wiedemann, G. Drolshagen, P. Vorsmann, "Development of in-situ space debris detector". *Advances in Space Research* xxx (2014) xxx–xxx

[82] BAE Systems, http://www.baesystems.com/_article/BAES_175799/aircraft-set-to-become-more-human-as-engineers-develop-smart-skins-which-can-detect-injury

[83] A. Oulmane, A.A. Lakis and N. Mureithi. 2013, "A Method for Analyzing Rotating Machinery Faults using Time-Frequency Application". *International Journal of Condition Monitoring and Diagnostic Engineering Management* Volume 16 No2, April 2013 pages 21-34.

[84] Safizadeh, M.S., Lakis, A.A., and Thomas, M., "Time-Frequency and Their Application to Machinery Fault Detection", International Journal of Condition Monitoring and Diagnostic Engineering Management, (2000), 4(1), pp 10-27.

[85] Mahvash, A., Lakis A.A., "Independent Component Analysis as Applied to Vibration Source Separation and Fault Diagnosis", *Journal of vibration and control*, online: August 2014, DQI: 10.117/107756314544349.

CHAPTER 5 ARTICLE 2: HYPERVELOCITY IMPACT (HVI) SIGNAL ANALYSIS

Iliescu, L. E., Lakis, A. A. & Oulmane, A.
Mechanical Engineering Department, École Polytechnique of Montréal, Canada
C.P. 6079, Succursale Centre-ville, Montréal, Québec, Canada H3C 3A7

European Journal of Engineering and Technology Vol. 4 No. 1, 2016

ISSN 2056-586

5.1 Abstract

Hypervelocity is a specific characteristic of the movement of space debris and micrometeoroids. Their high speeds in the space environment leads to major impact effects on a spacecraft surface or protection shield. Depending on the particle speed and diameter, the damage that occurs could lead to perforation of the spacecraft shell; a catastrophic failure of the spacecraft. The impact of these particles is a complex phenomenon that includes secondary ejecta, plasma or phase transformation of material. This paper presents the analysis of signals obtained from four hypervelocity impact tests, analysis done using specific software developed in-house by our research group as a bridge between theoretical research and practical applications of various vibration methods in different areas. This professional tool allowed us to calculate different time-frequency or time-scale transforms from the data file time signal. The application of two methods usually used for analyzing this type of signal, Choi-Williams distribution or Wavelet transform, allowed us to distinguish the characteristics of the two fundamental states of impacted targets; perforation and non-perforation. Based on these results, corroborated with further analysis and experimental tests, a dictionary of materials used for spacecraft protection will be created that includes automatic identification of space debris damage.

5.2 Introduction

Micrometeoroids and orbital debris (MMOD) represent the two main categories of space particles that travel at average velocities of 16 km/s and 9 km/s, respectively. Micrometeoroids are common space particles of small dimensions made of rock or metal that travel at velocities up to 20 km/s and pose a high risk for objects that spend long periods of time in space such as satellites. Orbital debris on the other hand, represents non-functional man-made objects that have been populating

space since the first space launch in 1957. Since then, the number of such objects has grown to over 22 000 pieces. Space debris has different sources such as; satellite and rocket break-ups, satellite anomalies and mission related debris.

Impact between space vehicles and MMOD or impact between two such space-objects at the high velocities involved is called a hypervelocity impact (HVI). The intensity of these collisions produces a debris cloud and secondary ejecta with the potential to cause further damage, creating even more space debris. Two examples of such space events are the test on the defunct Fengyun-1C satellite in 2007, and the accidental collision of Iridium-33/Cosmos- 2251 satellites in 2009. These events created approximately 5000 pieces of debris, most of them still in orbit.

Existing ground systems cannot detect or track MMOD at sizes between 1 and 5 cm (diameter).

These particle sizes pose the greatest threat to space vehicles. The development of new HVI protection devices that use new lighter materials could be a solution for mitigation of the impact effects of MMOD in this size range. HVI test data, which at this date is limited, would be very useful to aid research work in this area. Due to the extensive use of composite materials in spacecraft structures, characterization of HVI damage is complex. The phenomenon is controlled by failure thresholds and subsequent impact energy consumption [1, 2]. Improved experimental and technical analysis development is essential to more fully evaluate the damage resulting from HVI impact.

This paper presents a method based on time-frequency analysis completed using in-house software. The approach provides advanced knowledge from HVI impact tests and damage analysis on different materials. Four test cases were analyzed with respect to spacecraft protection against orbital debris and micro-meteoroids [3]. The tests were performed at the Shock Wave Physics laboratory. The objective of the tests/analysis was to determine the essential characteristics of damage for two different materials; a metal (aluminium) and a carbon fiber (CFRP). Two different types of target status were analyzed; perforation and non-perforation.

This paper will represent a basis for further time frequency analysis of the signals in order to develop a method for automatic detection of HVI damage for different types of materials. In detail, the paper provides a time frequency analysis of the signals obtained from two sensors, one placed on the target (the main sensor used for the impact analysis) and the other outside of the testing chamber (an auxiliary sensor for impact confirmation and further analysis).

The two methods used are Wavelet Transform (WT) and Choi-Williams Distribution (CWD); a bilinear transformation. The test set up is shown in Figure 5.1.

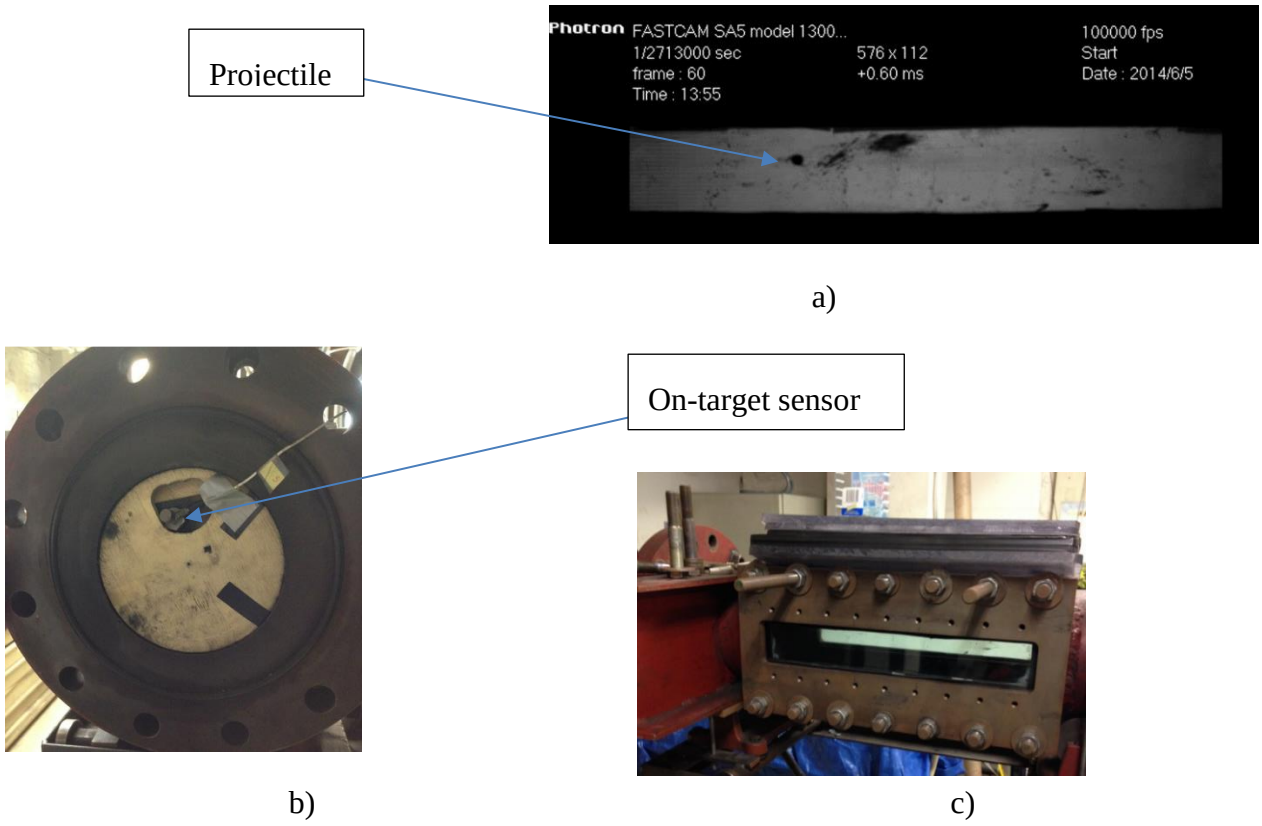

Figure 5.1: HVI testing video recording using FASTCAM a) target and sensor fixed in the testing chamber b) and c) testing chamber

This document is the second part [18] of a larger work that will potentially include (depending on availability of the test facility) further analysis of HVI tests at higher speeds (up to 8 km/s), the use of fiber glass (FBG) sensing technology to enable more accurate detection of HVI damage in real time and the automation of HVI damage detection.

5.3 Theoretical considerations

5.3.1 General considerations

Impact theory and behavior is very well described by W. Goldsmith [19], who presents theoretical vibration aspects and dynamic processes as well as experimental results. The volume presents the impact as a function of the application, static or rapid loading, where the impacted material has a fluid behavior.

Classical impact theory is a starting point; however it is not capable of describing the transient forces or deformations that occur in the case of impact. Our approach considers the vibration aspects of impact, examining the wave phenomena in order to specify the transient deformation and stresses.

Chapter V of the book is of particular interest since it includes a discussion of dynamic processes that lead to permanent deformations. Two approaches are described that could take these large strains and permanent deformations into consideration: the theory of hydrodynamic behavior of solids and the theory of plastic flow. The hydrodynamic theory of wave propagation in solids, which is usually employed in the study of HVI considers the target materials as a compressible fluid without shear resistance to derive the equation of state of different materials.

One element of impact vibration is related to the natural vibration of each of the two parts that are in contact following the transfer of impact energy. In our case the parts involved in the impact are the projectile and the target, and for this case projectile vibrations are neglected. For the particular case of an impact of a spherical projectile on a target, the contact force is described as a pressure distribution on the surface with variable amplitude. Hertz's contact law [23] refers to the localized stresses that occur when two curved surfaces come in contact and, due to the applied loads, deform slightly depending on the modulus of elasticity of the materials. This distribution is usually represented by an elliptical contact surface. Furthermore the impact force together with modal displacements of the target plate give rise to a forced transitory response materialized in a free vibration.

W. H. Prosser [20] analyzed the signals created by impacts on aluminium and graphite/epoxy composite targets in two different impact velocity regimes as both velocity and impact angle were varied. The signal in the low-velocity regime is dominated by a large flexural mode, with the overall amplitude increasing with velocity, mostly for the high-frequency components. Compared with the signal in HVI, both extensional and flexural mode components had comparable amplitude for non-penetrating impacts, but only an extensional component was evident when the target was perforated.

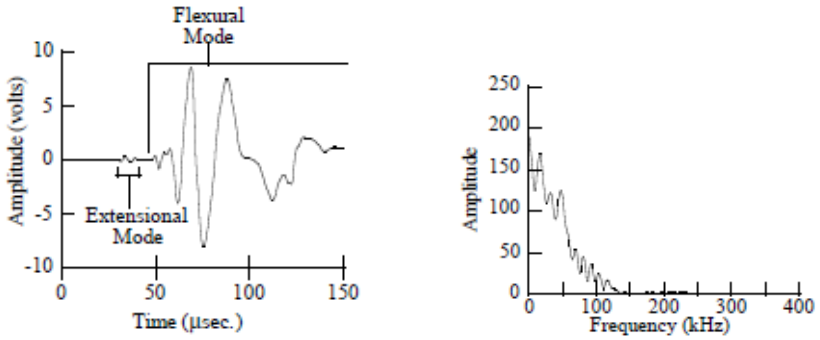

a) b)

Figure 5.2: Low velocity impact on aluminium plates: a) The signal, b) The FFT of (a) [20]

Figure 5.2 presents the signals produced by a low-velocity impact. Extensional and flexural components can be noted, the extensional mode propagating with faster velocity and little dispersion compared with the flexural mode that travels at lower velocity and higher dispersion.

The flexural mode is created by the off-mid plane source through the large bending that occurs because the projectiles at low- velocity did not perforate the target and instead created a larger target.

In his previous work, Prosser [21] studied the signals induced in a thin-walled graphite/epoxy tube (similar to the material at lay-up used by NASA for the struts of the space station) using lead breaks. Measurements of the velocities of the extensional and flexural modes were found to be in agreement with classical plate theory.

Our work, which is described in detail in paragraph 3 below, uses a comprehensive TF analysis tool developed by Prof. A. A. Lakis and his research team [7, 22] in order to better characterize the HVI phenomena. More precisely, analysis of the impact signals obtained after a series of HVI tests led to identification of characteristics that allow us to differentiate the two essential types of target damage or conditions that occur in cases of non-perforation and perforation impacts, the latter of these being critical in the case of a spacecraft impacted by orbital debris or micro-meteoroids. TF analysis was performed on two different materials, aluminium and composite. In further testing campaigns we will consider different types of materials used for spacecraft structure and MMOD protection in order to initiate development of a wide-ranging database of these materials; a dictionary of materials as a function of signal characteristics. Furthermore, the materials dictionary

will be used for development of a fully automatic health monitoring system, capable of identifying in real time the type of damage that occurs in the case of HVI.

5.3.2 Wavelet Transform

The wavelet transform (WT) is a time-frequency analysis method that gives good results in studying transient phenomena. WT associates time information to the frequency content, each wave being characterized by frequency band and arrival time.

In literature there are few papers that present the application of WT to characterize the complex wave field that results in a case of HVI. One important remark is made by A. Bettela [11] in his paper that analyzes HVI waves with different amplitudes, content, velocities and direction of propagation that occur due to superimposition of vibration (original and reflected). More precisely, the paper tries to identify the fundamental constituents of this HVI disturbance field, the shock generation and transient vibration that can cause malfunctioning and breaking of sensitive electronic components on board a satellite.

The study of researcher Bettela present also an alternative method applied to the other analysis tools employed in the similar cases. For example, a Shock Response Spectrum (SRS) is used to evaluate the loads transferred in the case of HVI to the sensitive object through acceleration measurements without requiring characterizing the details of the source. The results are funded by studying the morphology, speeds of propagation, frequency content, superposition, interference and reflection of waves.

The presented method starts from the mathematical form that describes the propagation of elastic waves in plates; the analytical equations are presented starting from 3D equations of waves for an elastic body with solutions which represent the constituent elements of real waves (3D harmonic wave). Full development of these calculations is presented in a book by Graff K.F. [12].

The solutions for the wave equations are represented by symmetrical (S) and anti-symmetrical (A), Lamb waves or guided waves, with different displacement modes.

The WT method was validated through simulation and real HVI tests on Al plates using accelerometer measurements in order to identify, by steps, how the two wave modes (S and A) appear in WT spectrum.

The numerical signals showed that the S waves do not exhibit dispersive behavior, have unchanged shape and their frequency components travel at the same speed. The A waves present dispersive behavior (high frequency components have an earlier arrival time or travel faster and the low frequency ones in shorter time).

Based on the results of experimental signal analysis for tests done on Al plates and honeycomb Al plates at low-speed and at hypervelocity, the paper concludes that two types of wave groups are observed, symmetric S0 and anti-symmetric A0 lamb waves. WT analysis is able to identify both the frequency content and propagation velocity. The experimental results were very effective for identifying the type of damage (with perforation or not) and concluded that, in the case of non-perforation, A0 group waves are predominant and discontinuity (previous hole) is captured.

Lei Wang [13] investigates the existence of multiple higher-order Lamb wave modes in composites using piezoelectric sensors and ultrasonic frequencies. The paper studies the degradation and integrity of composite structures using ultrasonic transient waves for damage detection, localization and assessment of damage.

In this case, due to the composite's multi-layer construction, heterogeneity of components and material anisotropy, the velocity of the wave depends on factors such as; laminate lay-up, direction of wave propagation, frequency and interface conditions.

The paper identifies the different types of Lamb waves that occur due to impact on isotropic plates and multi-layer composites and presents two theoretical approaches used to investigate Lamb waves in composites: exact solutions using 3D elasticity theory (laborious computation of characteristic dispersion-transcendental equations) and approximate solutions using plate theories.

Continued development of our in-house software in the next steps of our work will create an opportunity for validation of our results by comparison with the results presented in the above-mentioned studies that relate the results of Lamb wave theory to impact damage identification.

5.3.3 Choi- Williams distribution function

The Choi–Williams distribution (CWD) function is part of the Cohen's class distribution function that uses an exponential kernel to suppress the cross-terms that result from the components that differ in both time and frequency.

H. Choi and W. J. Williams [14] introduce a time-frequency exponential distribution of L. Cohen's class and examine its properties. After interpretation of the distribution according to a spectral density–estimation point of view, they show how the exponential kernel controls the cross terms and analyze the result on two specific signals. They define the distribution for discrete-time signals and, based on numerical example, conclude that the distribution is very effective in diminishing the effects of cross terms while retaining most of the properties of a time-frequency distribution.

CWD is mostly used in TF analysis of machinery vibration signals and machinery diagnostics. Howard A. Gaberson [15, 16] recognizes evidence of impact in examining the CWD performance on some machinery signals, which provide an impressive level of detail and a significant structure in the TF plane. Analyzing the accelerometer data taken from the intake valve cap on the head of the high-pressure cylinder of a large reciprocating compressor, he noted that the impact events showed a broadband, impact-like wide frequency content in the CWD contour plot and concluded that the CWD displays TF characteristics with the most precision.

In his paper, M. A. Hamstad [17] made a comparison between WT and CWD in order to determine the group velocities for different pairs of acoustic emissions (AE) sensors. Pairs of resonant or non-resonant wide-band AE sensors were used to sense the waves created by breaking pencil leads on an aluminum plate. The recorded signals were analyzed and processed by a WT. The group velocity curves (for the appropriate Lamb modes) were superimposed to clearly identify the modes in the signal. The arrival times at specific signal frequencies were determined (the time of the peak WT magnitude). The experimental group velocity was calculated based on the difference in arrival times and the difference in distance between the locations of the two sensors, and compared with the theoretical group velocity.

In his research, Hamstad used CWD as an alternate TF method following the same procedure and compared the experimental results with a finite element calculation.

The main conclusions of the comparison between the use of WT or CWD to determine wave group velocities for the case of different AE recorded on relatively thin and large plates were:

- Determination of the arrival times of the two fundamental modes is relatively easy using either WT or CWD, independent of the type of sensor used (resonant or wideband);

- The experimental group velocities recorded were close to the theoretical values (less than 6.5 % difference)
- The high intensity regions determined using CWD occurred at a higher frequency compared with the frequency determined by WT (for each intense modal region). WT at higher frequency spreads the intensity from a single frequency.
- The CWD magnitude has sharper peaks as a function of time at lower signal frequency and as a function of frequency at higher signal frequency
- It can be expected that CWD provides more accurate arrival time results than WT for thicker plates (more modes closer in time).

5.3.4 TF analysis software

TF-Analysis software was developed at Polytechnique by Prof. Lakis A, A. and the research team [7, 22]. It offers a wide range of methods in time, frequency, time-frequency analysis and wavelet transforms, see Figure 5.3. It also offers more advanced techniques in the recently-developed domain of automatic classification of rotating machinery using image processing by application of Fourier descriptors and neural networks [22].

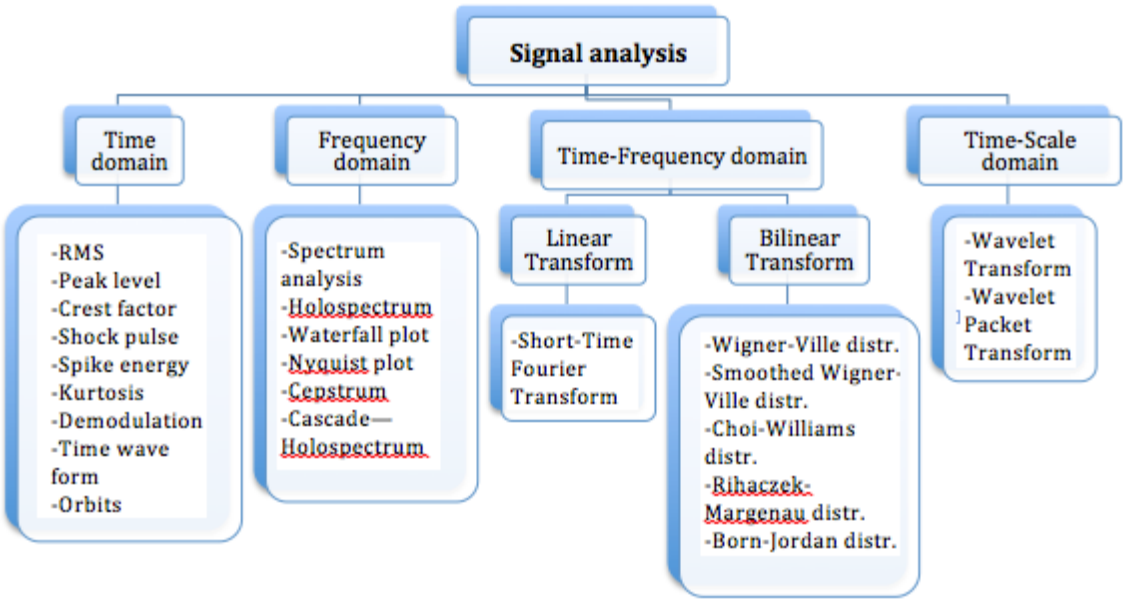

Figure 5.3: Features in TF analysis.

5.4 Work performed and attained objectives

In order to find distinguishable characteristics of HVI impact that will enable classification of different materials used in aerospace our group performed extensive work that covers the following main tasks:

- HVI testing campaign on two different target materials, covering both considered conditions of target, performed using a low-velocity launcher;
- Analysis of signals from sensors mounted on the testing chamber in order to assess the identification of impacts from a signal captured outside the target, the case of perforation of an outside bumper of an MMOD protection system, and a signal captured on the spacecraft shell;
- Assess target damage and analysis of this signal using different TF analysis methods and identifying the methods with the best results;
- Centralize the results in order to observe differences and similarities between analysis outcomes;

The above steps are discussed in detail in the following sections of this paper.

5.4.1 HVI experimental testing

Six signals were recorded during the HVI testing campaign performed at Shock Wave Physics laboratory of McGill University. Projectiles were shot onto aluminum and carbon fiber targets using a gas launcher at different gas pressures (2000 Psi to 4000 Psi). Projectile velocities ranged from 560 to 1670 m/s.

The projectile launcher is driven by high pressure helium gas using a double diaphragm propulsion mechanism and a polycarbonate sabot. A rare earth magnet NdFeB, MAGCRAFT is used to determine the velocity of the projectile. As the stripping mechanism, an essential factor, a dynamic method that utilizes a heavier gas than He, Nitrogen (N2), is used. The method has an unwanted effect; a secondary impact caused by the sabot.

A second separation mechanism could be used in future tests to deflect the sabot from its original trajectory so that it does not hit the sample and thus avoid inducing unwanted noise in the signal.

The materials used as targets were:

- Aluminum 6061-T6, two thicknesses, approx. 1 and 5 mm;

Table 5.1: Aluminum 6061-T6 technical characteristics

Material	**Nominal density (lbs./cu.in.)**	**Tensile strength (psi)**	**Fatigue strength (psi)**	**Shear strength (psi)**
Al 6061-T6	0.0975	45,000	14,000	30,000

- Carbon fiber/Epoxy rigid composite sheet of 3.175 mm thickness

Table 5.2: Carbon fiber/Epoxy rigid composite technical characteristics

Material	**Nominal density (lbs./cu.in.)**	**Tensile strength (psi)**	**Compressive strength (psi)**	**Flexural strength (psi)**
High-strength lightweight rigid carbon fiber	0.05-0.067	120,000-175,000	75,000-128,000	89,000-174,000

The material choice was made in order to create at least two types of hypervelocity impact damage, crater and perforation, in two different materials and also to consider other factors such as material review, market availability, test facility availability and the timeframe.

More precise results of HVI could be achieved by applying a vacuum to the test chamber. This was not done for these experiments due to the timeframe of this project and the target design requirements. This option could be considered for future tests at the later stages. For the next tests it is probable that the targets will be suspended at four points and mounted using a vibration acquisition system. This set up should allow more precise signal analysis.

The data acquisition system used for the preliminary signals was a Ni PXIe-1062Q [4] coupled with three accelerometers, one mounted on the sample and other two mounted on the outside of the testing section. LabView software was used to convert the analog signal to digital and store the signals on a PC.

To convert the impact vibration into a signal for the McGill testing session, analog sensors, accelerometers with very high sensitivity ranging from 0.1 to 10.2 mv/ (m/s2), were used. For

these testing sessions PCB Piezotronics model 352C33 accelerometers were considered suitable [4].

Two sensors were used to record valid impact signals. One was mounted on the target at a fixed position in order to not influence the signal. The distance from impact was variable due to the imprecision of the shots. The images show that the distance is around 30 mm (+/- 5 mm). The second sensor was mounted on the outside of the testing chamber, inside of which the targets were mounted.

During the test a frequency sampling rate of 50 KHz\0A was used. For signal analysis the WT was mainly a linear distribution at different levels of decomposition (level 5 is presented in images) with different time and frequency window lengths and using a Daubechies filter. In order to have a distinct difference in frequency amplitude we used various bi-linear transformations and we selected the Choi-Williams distribution results (a member of Cohen's class distribution that suppress the cross terms) to be presented in this paper.

5.4.2 Introduction of test results analysis; preparatory work

Four tests were analyzed using the TF in-house software [6-8], Table 5.1 summarizes the testing conditions and signal recording durations. Amplitude and shape were compared for each signal. Signals were recorded from the two sensors (on target and outside) in order to correctly identify the damage (penetration or non-penetration) on two types of material, aluminum and carbon fiber.

Table 5.3: Test summary

Test No.	**Sample**	**Thickness (mm)**	**Projectile (sphere, mm)**	**Velocity (m/s)**	**Duration (Min:sec)**	**Damage characteristics**
Test 1	CF	3.175	3.2	1570	2:12	Penetration
Test 2	CF	3.175	3.2	880	1:53	No Penetration
Test 3	Al6061 T6	0.8128	3.2	570	0:45	Penetration
Test 4	Al6061 T6	4.826	3.2	540	0:10	No Penetration

Due to computation limitations the larger signals (one, two and three) couldn't be analyzed over the entire duration. These had to be segmented into multiple signals, each with a maximum duration of 40s, and analyzed separately to determine the moment of impact.

Also, in order to analyze the signal in detail, and more importantly to be able to use all the software functions and cover all TF analysis methods, the signal was segmented into time-intervals of 40ms.

5.4.3 Signal obtained from the sensor mounted on the outside of the test chamber

In addition to the on-target sensor, a secondary sensor mounted on the outside of the test chamber was used, see Figure 5.4. This sensor is necessary to have a precise recording of the impact.

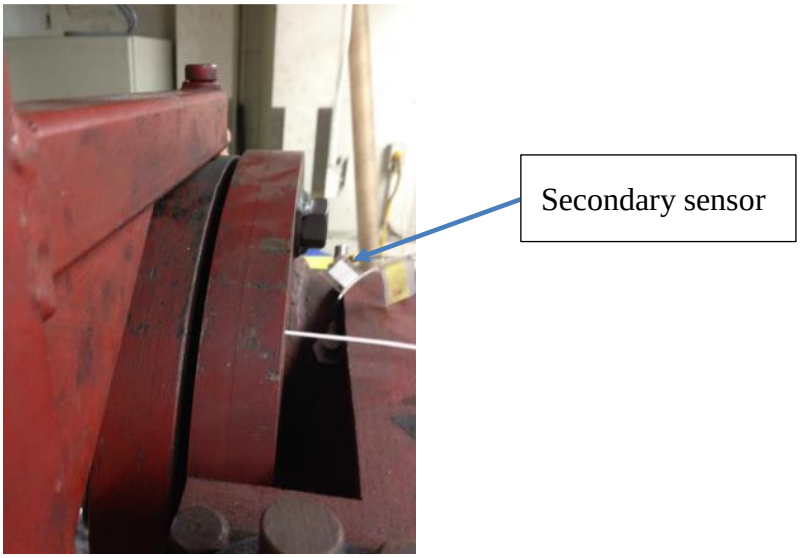

Figure 5.4: Position of the sensor mounted on the outside of the test chamber

The signal recorded from this sensor showed that the impact can be captured and distinctly identified in a signal recorded on a complex structure at a certain distance from the impacted target, such us on the last bumper or interior wall in the case of a complex orbital debris protection system (shield).

One of the recordings of the sensor mounted outside the test chamber (corresponding to Test 1) is presented in the following image, Figure 5.5.

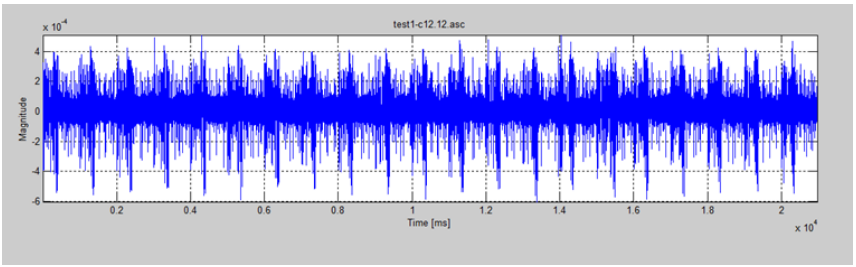

a)

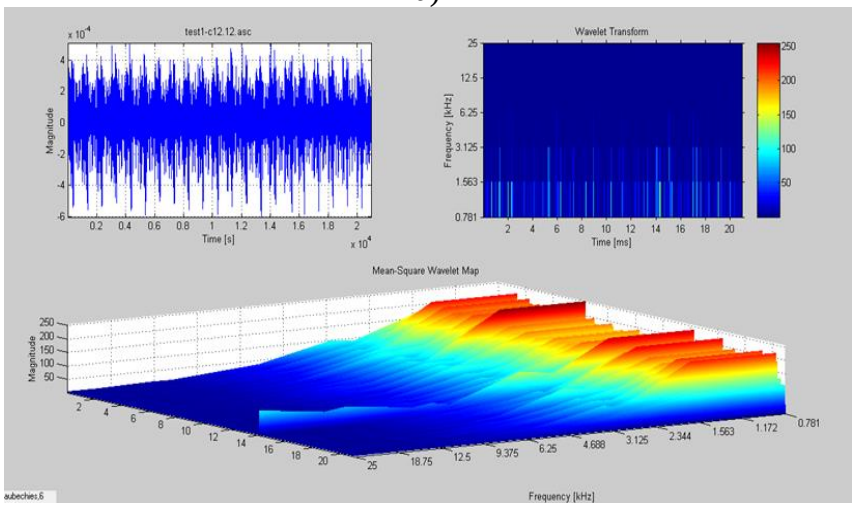

b)

Figure 5.5: a) Signal recordings from Test 1, b) the TF representation of WT

The outside sensor captured all four impacts for the four tests. The above image corresponds to Test 1 performed on CFRP and indicates perforation of the target. This fact is revealed only by the WT (Figure 5.5b). In the first graph, in time dimension (Figure 5.5a), the impact cannot be distinguished.

Also, we notice that for the sensor mounted on the outside of the target the amplitude of all signals in time is of order 10-4. The above analysis represents only a section of Test 1; 20 seconds corresponding to approximately 1 million recording points.

For the second test, Test 2 on CFRP with non-penetration, the moment of impact is again seen on the TF graph of the WT. The same variation in frequency amplitude occurs over the entire time domain. In this case the frequency variation is more attenuated than in Test 1.

The WT signal analysis of Test 3 on aluminum (Al) with perforation as a result, also shows the impact on the TF graph with the same variation in frequency amplitude over the entire time domain, but with a slightly different form and with higher frequency amplitude due to a more rigid Al target.

As in previous tests, the Test 4 impact, on thicker Al plate with non-perforation as a result, was captured by the outside sensor. The TF graph of the WT showed the same variation in frequency amplitude over the entire time domain. This variation was more attenuated than in Tests 1 and 2 with the CFRP target. The shape of the graph was similar to that of Test 3 (on Al).

Due to the short length of the signal, 10 seconds (approximately 500000 points), it could be analyzed entirely and it was not required to use sections.

In conclusion, impacts can be identified using a sensor mounted outside the impacting area on a continuous structure using the TF analysis software. Furthermore, this approach works for different for materials and different types of damage.

5.4.4 Material damage and signal analysis

5.4.4.1 3.4.1.Tests on a CFRP target, penetrated by a projectile

Figure 5.6 represents the target damage corresponding to Test 1, CFRP at 3,175 mm thickness with 1.57 km/s impact velocity.

Visual inspection of the target reveals three types of damage:

- Primary damage: perforation, due to projectile impact;
- Secondary damage: non perforation, from the impacting fragments (18-20 fragments of very small and varied dimensions), dispersed on a 6 cm diameter area;
- Sabot damage: non-perforation, impact of lower intensity.

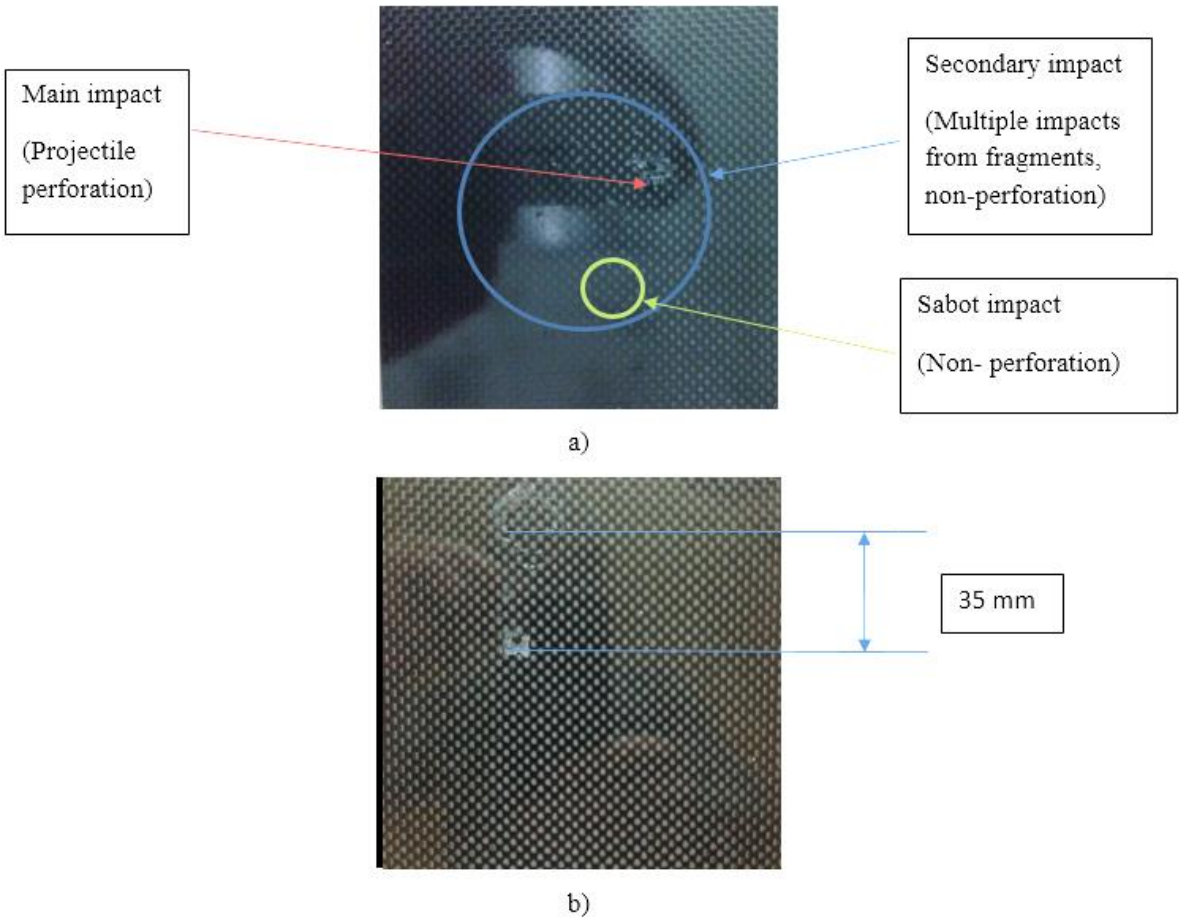

Figure 5.6: Impact damage on test1 CFRP 3.175 mm, fully perforated face a) and back b)

Figure 5.7 represents the recording and WT for the signal captured by the sensor mounted on the CFRP target.

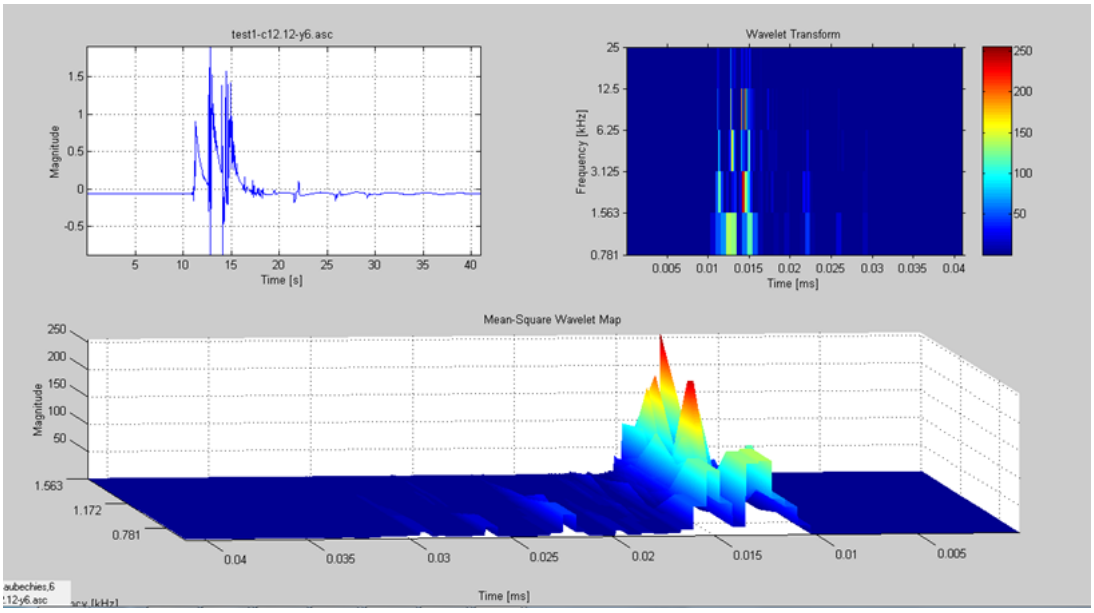

a)

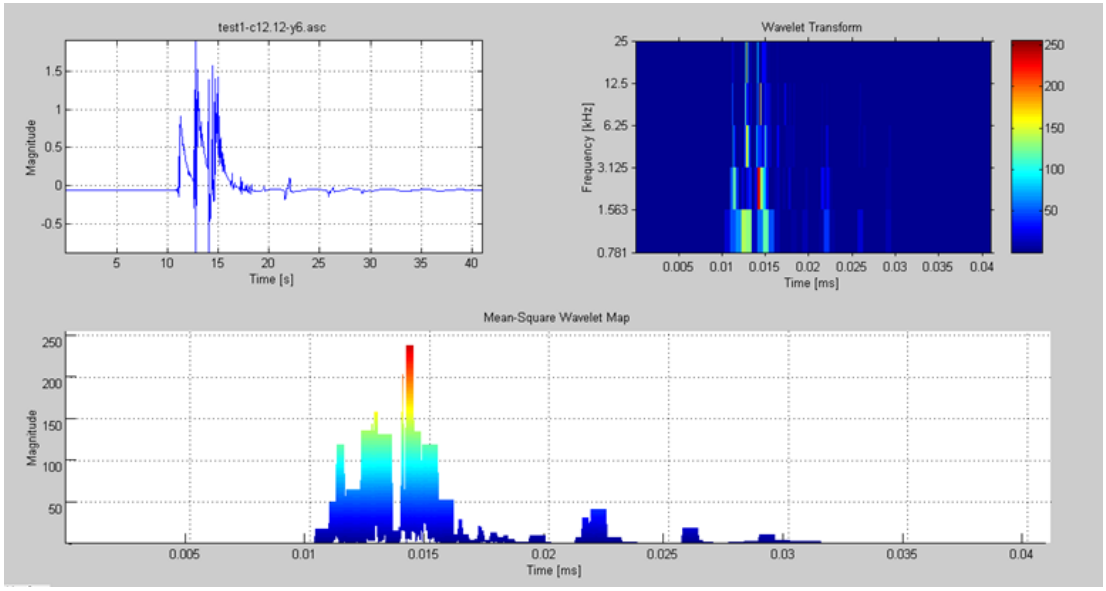

b)

Figure 5.7: On-target mounted sensor, Test 1 signal recording and WT shape a) and profile b)

On the WT graph, three frequency peaks are noted that correspond to the three types of impact, perforation, secondary multiple impact, and sabot impact. The shape of the impact transform is the essential element that should be noted. The large amplitudes are compressed in a 5 ms interval and the width of the peaks at maximum amplitudes is only a few µs.

The Choi- Williams distribution for the Test 1 signal is presented in Figure 5.8.

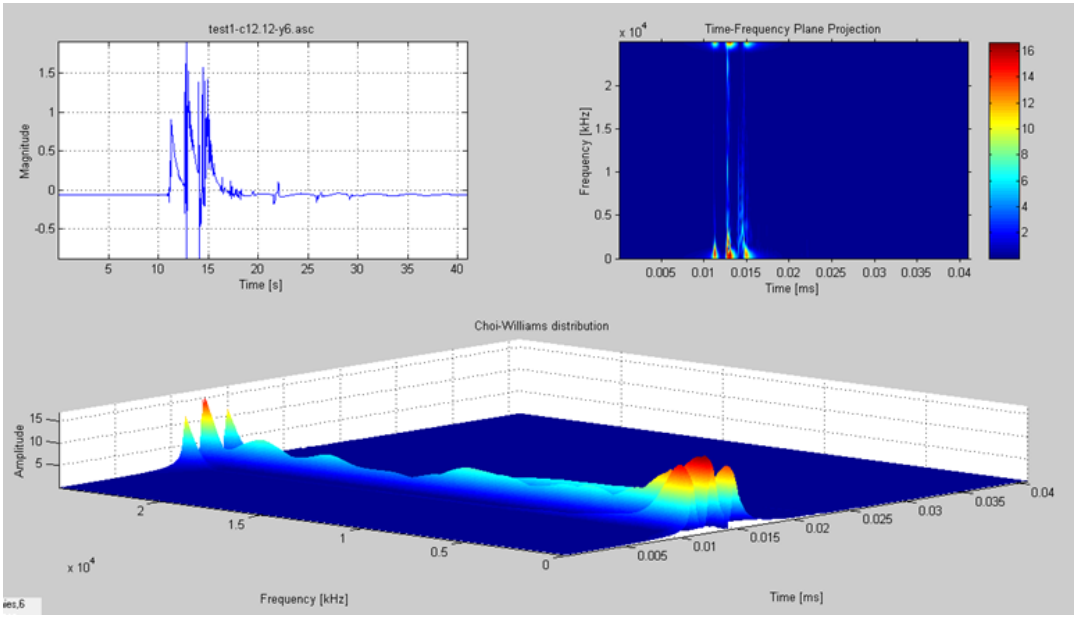

Figure 5.8: CWD corresponding to Test 1 signal

The TF analysis shows the corresponding three peaks, but the most important detail is the frequency amplitude, for a CFRP perforated target the maximum amplitude is 15.

5.4.4.2 Test on CFRP target, not penetrated by a projectile

Figure 5.9 presents the target damage corresponding to Test 2, on CFRP at the same thickness as Test 1 but impacted at lower velocity; 0.88 km/s. In this case the target is non-penetrated.

Visual inspection of the target reveals three types of damage:

- Primary damage: non -perforation, due to the projectile impact
- Secondary damage: non- perforation, fewer impacts from fragments (3-5 fragments), over a 4.5 cm diameter area
- Sabot damage: non-perforation, impact of lower intensity

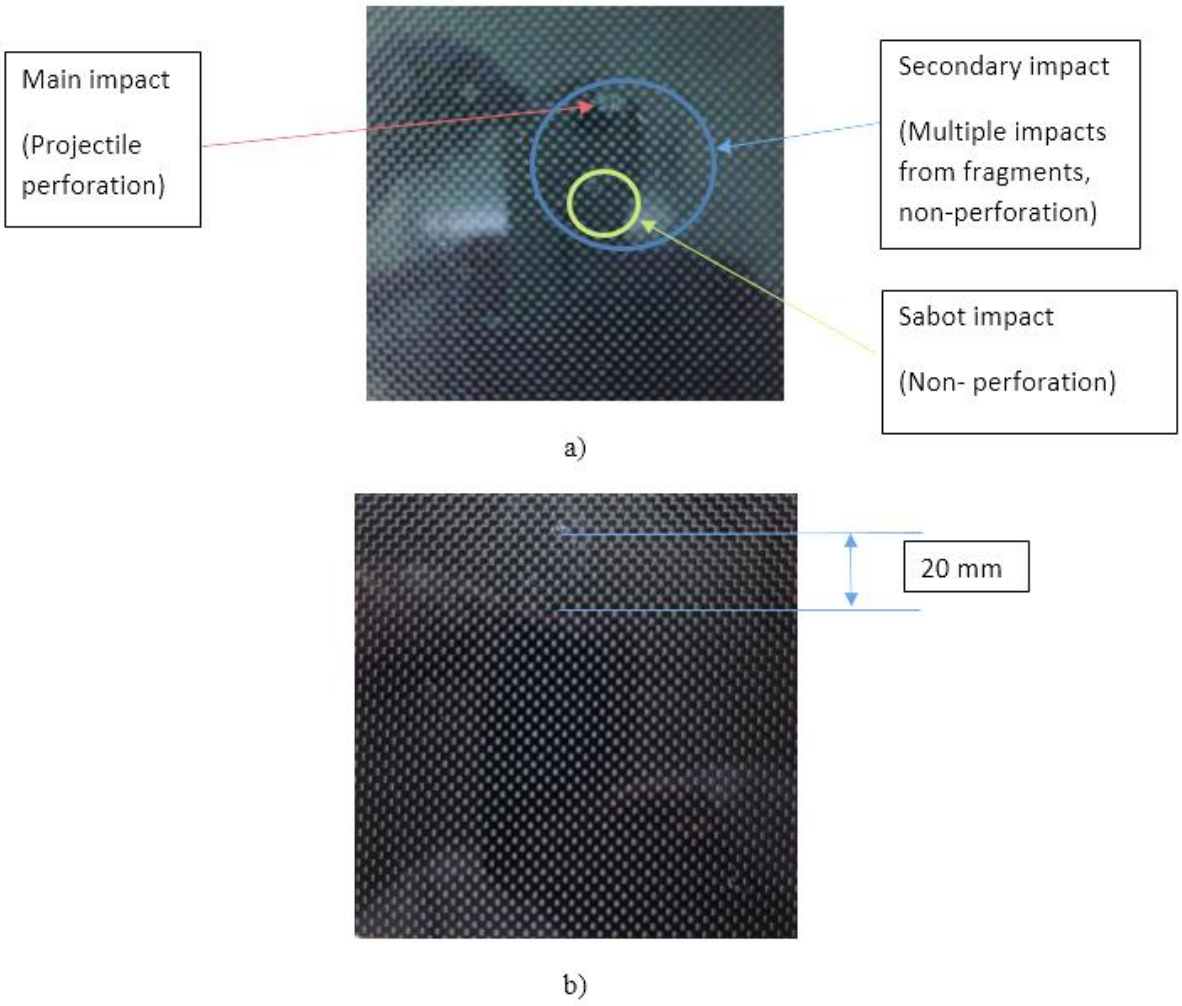

Figure 5.9: Impact damage for Test2, CFRP 3.175 mmm, non-perforated face a) and back b)

The recordings and TF analysis that correspond to Test 2 are shown on the following Figures.

Figure 5.10 presents the recording and WT for the signal captured by the sensor mounted on the target.

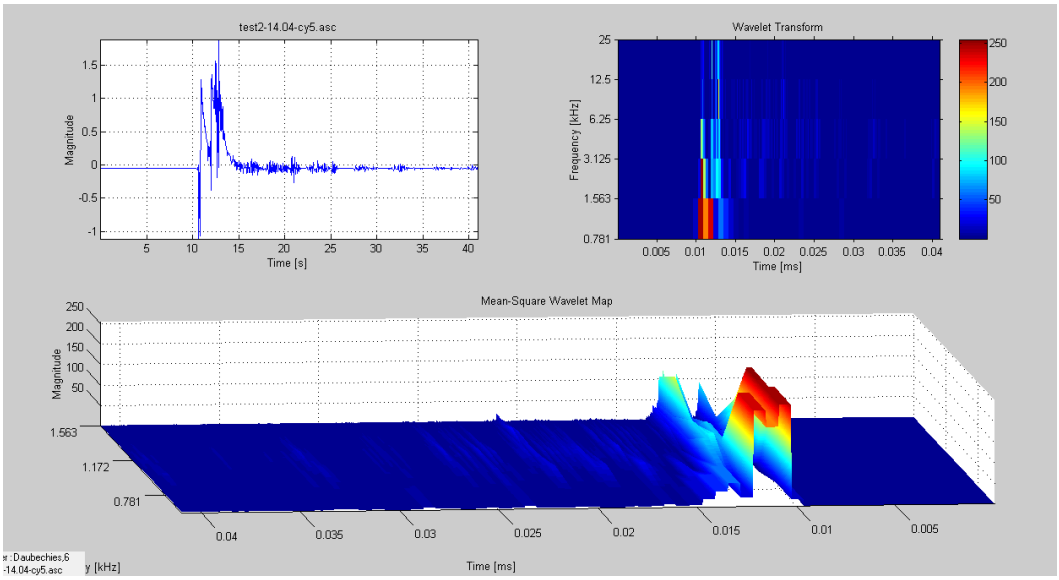

a)

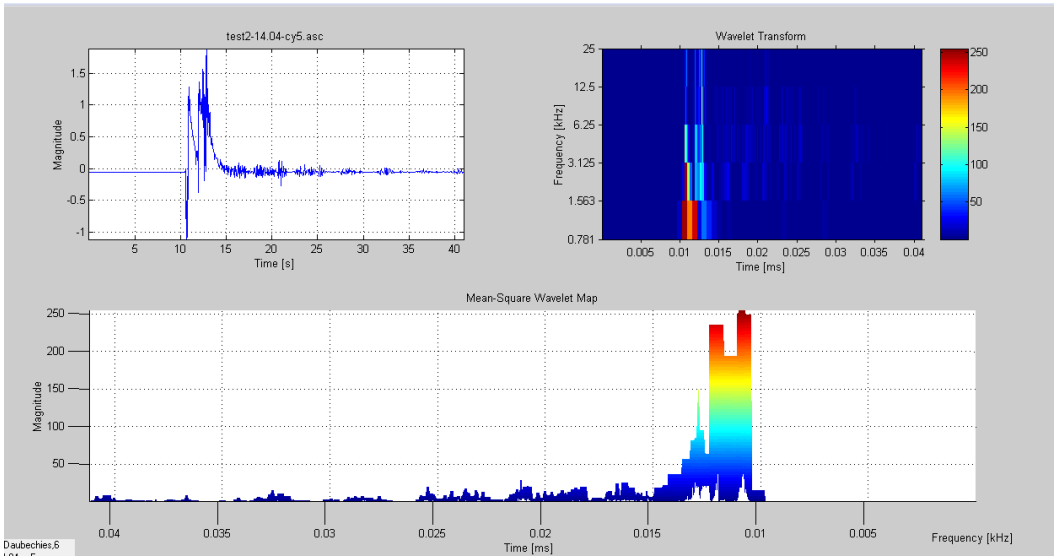

b)

Figure 5.10: On-target sensor, Test 2 signal recording and WT shape a) and profile b)

The TF shows the same three frequency peaks that correspond to the three impacts, projectile, secondary multiple impacts and sabot impact. However this time only two peaks are more emphasized. The shape of the WT has changed, the signal is shorter in time (less than 5 ms), and at maximum amplitude the width of the peaks is more than 1 ms. As can be seen in Figure 5.10a, the first and second frequency peaks are compressed together at almost the same amplitude.

The Choi- Williams distribution for the Test 2 signal is presented in Figure 5.11.

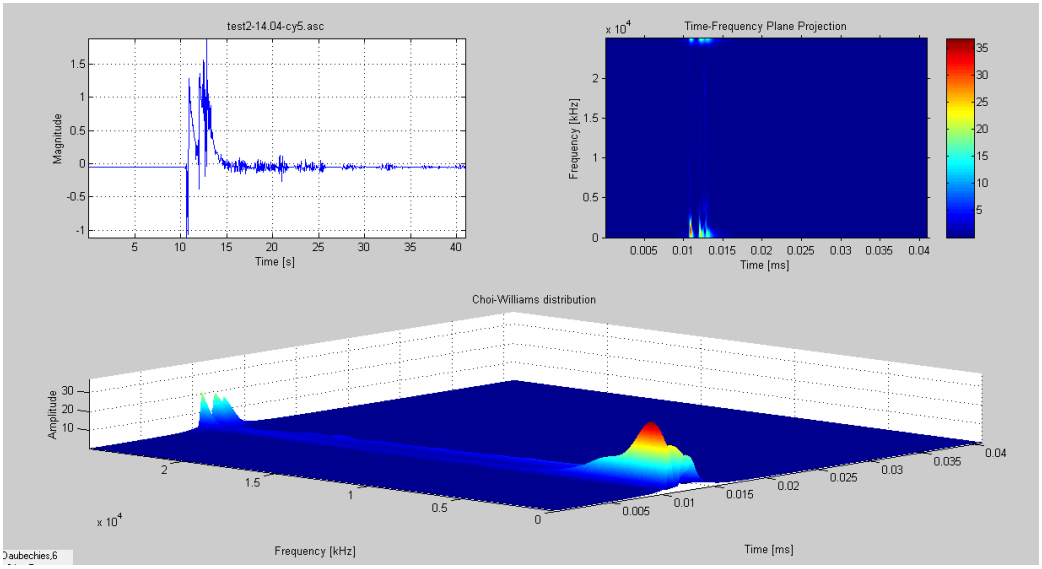

Figure 5.11: CWD corresponding to Test 2 signal

The TF shows the corresponding three peaks with one peak more pronounced, but the most important detail is the frequency amplitude which, for a CFRP non- perforated target, has a maximum around 30. This value, double that shown in Test 1, is an important indication of non-penetration. The material absorbed the vibration (large peaks, smaller propagation in time), amplifying the maximum frequency.

5.4.4.3 Test on an Al target, penetrated by a projectile

Figure 5.12 presents the target damage corresponding to Test 3, an Aluminum target approx. 1 mm thick impacted at a velocity of 0.57 km/s. The target is penetrated by the impact.

Visual inspection of the target again reveals three types of damage:

- Primary damage: perforation due to projectile impact
- Secondary damage: non perforation, fewer impacts from fragments (3 fragments), over a 3.5 cm diameter area and one small perforation (less than 1 mm from one fragment)
- Sabot damage: non-perforation, impact of lower intensity

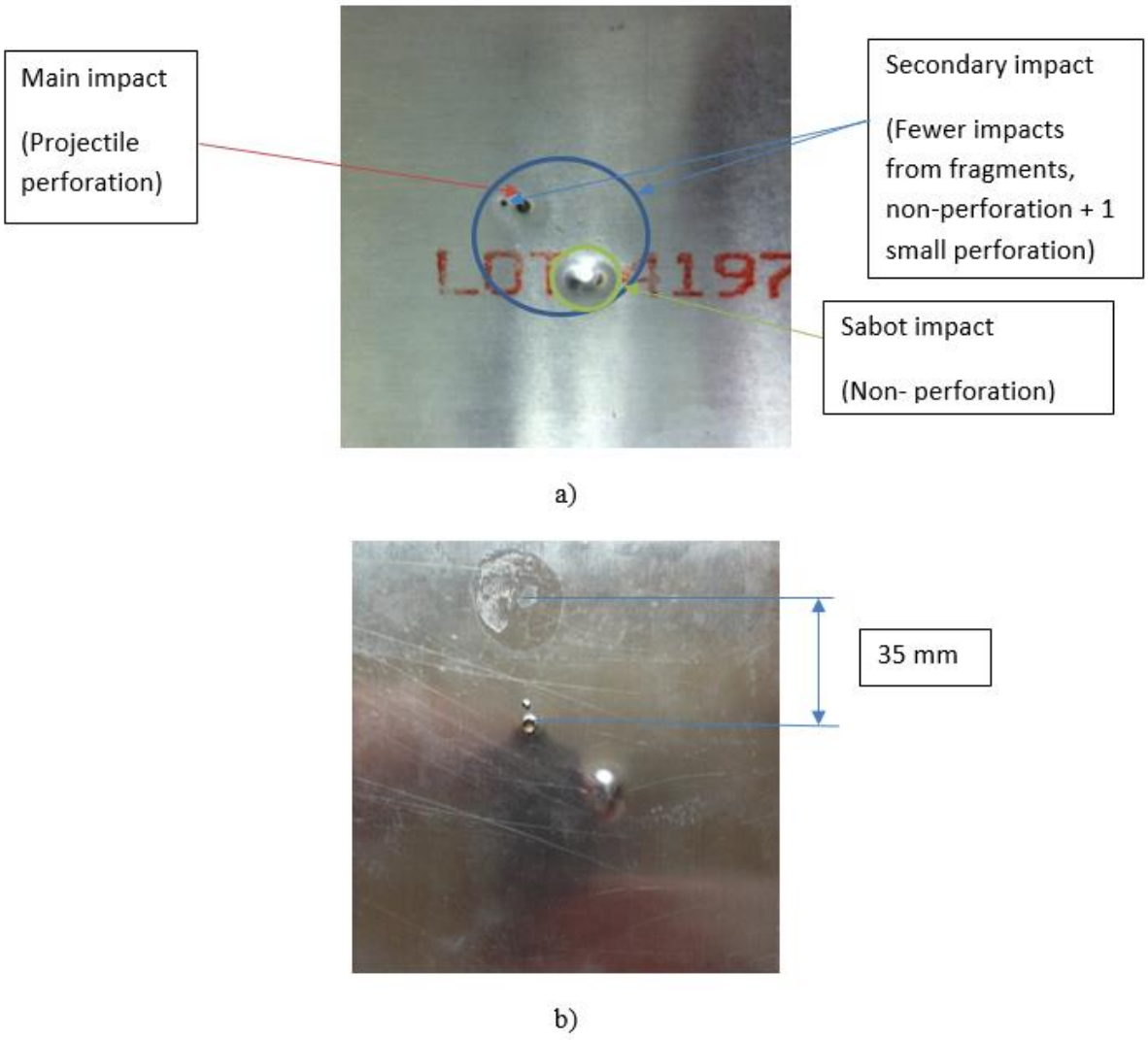

Figure 5.12: Impact damage on Test 3 Al, perforated face a) and back b)

The recordings and TF analysis that correspond to Test 3 are presented on the following figures.

Figure 5.13 presents the recording and WT for the signal captured by the sensor mounted on the target.

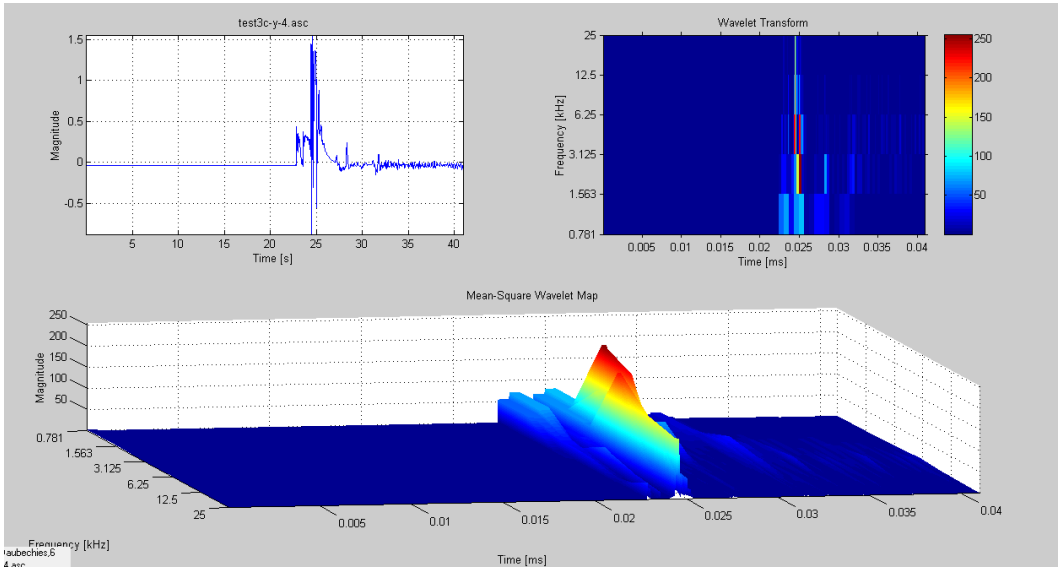

a)

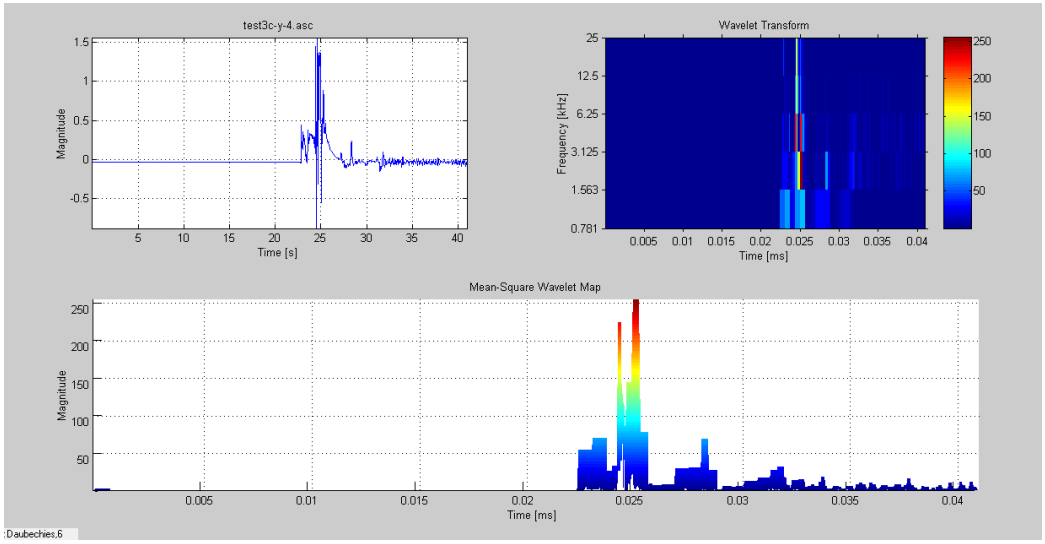

b)

Figure 5.13: On-target sensor, Test 3 signal recording and WT shape a) and profile b)

The WT shows the same two frequency peaks corresponding to the projectile perforation and the fragment secondary non-perforation, along with multiple lower amplitude peaks corresponding to secondary multiple impacts and sabot impact. The form of the impact is cleaner, over an interval of 5 ms, and the width of the peaks at maximum amplitude is in the µs range. Similar to Test 1, the

WT has the same shape, which seems to be characteristic of penetration. As can be seen in Figure 5.13b, the first and second frequency peaks are compressed together and at almost the same amplitude.

The Choi- Williams distribution for the Test 3 signal on aluminum is presented in Figure 5.14.

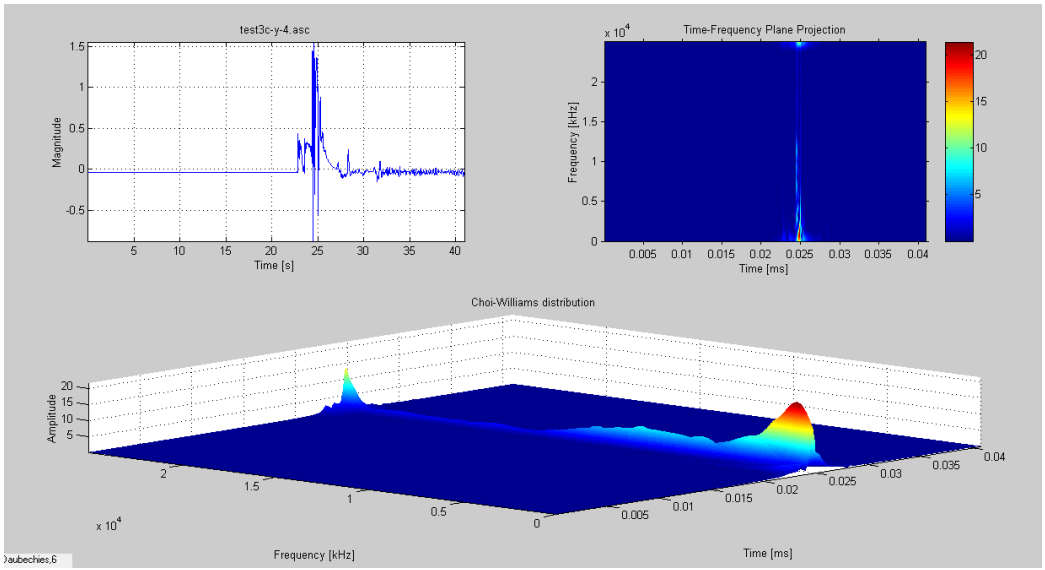

Figure 5.14: CWD corresponding to Test 3 signal

The CWD shows one much accentuated peak and a few non-significant very small amplitude peaks. Again observing the frequency amplitude, the maximum value for an Al perforated target is about 20 which is higher than the value recorded for Test 1 on a CFRP target (amplitude 15).

The material characteristics narrowed on a shorter period of time with large accelerations and, due to the higher rigidity of Al, the CWD shows a higher maximum amplitude of frequency.

5.4.4.4 HVI test on an Al target not-penetrated by a projectile

Figure 5.15 presents the target damage corresponding to Test 4, an Aluminum target at approx. 5 mm thickness impacted at a velocity of 0.54 km/s. No penetration damage occurred. For this case the velocity was kept approximately constant and the thickness of the Al was increased in order to achieve a non-perforation result.

Visual inspection of the target reveals the same three types of damage:

- Primary damage: non-perforation, from the projectile impact.

- Secondary damage: non perforation, fewer impacts from fragments (1-3 fragments), over a 3 cm diameter area.
- Sabot damage: non-perforation, impact of lower intensity

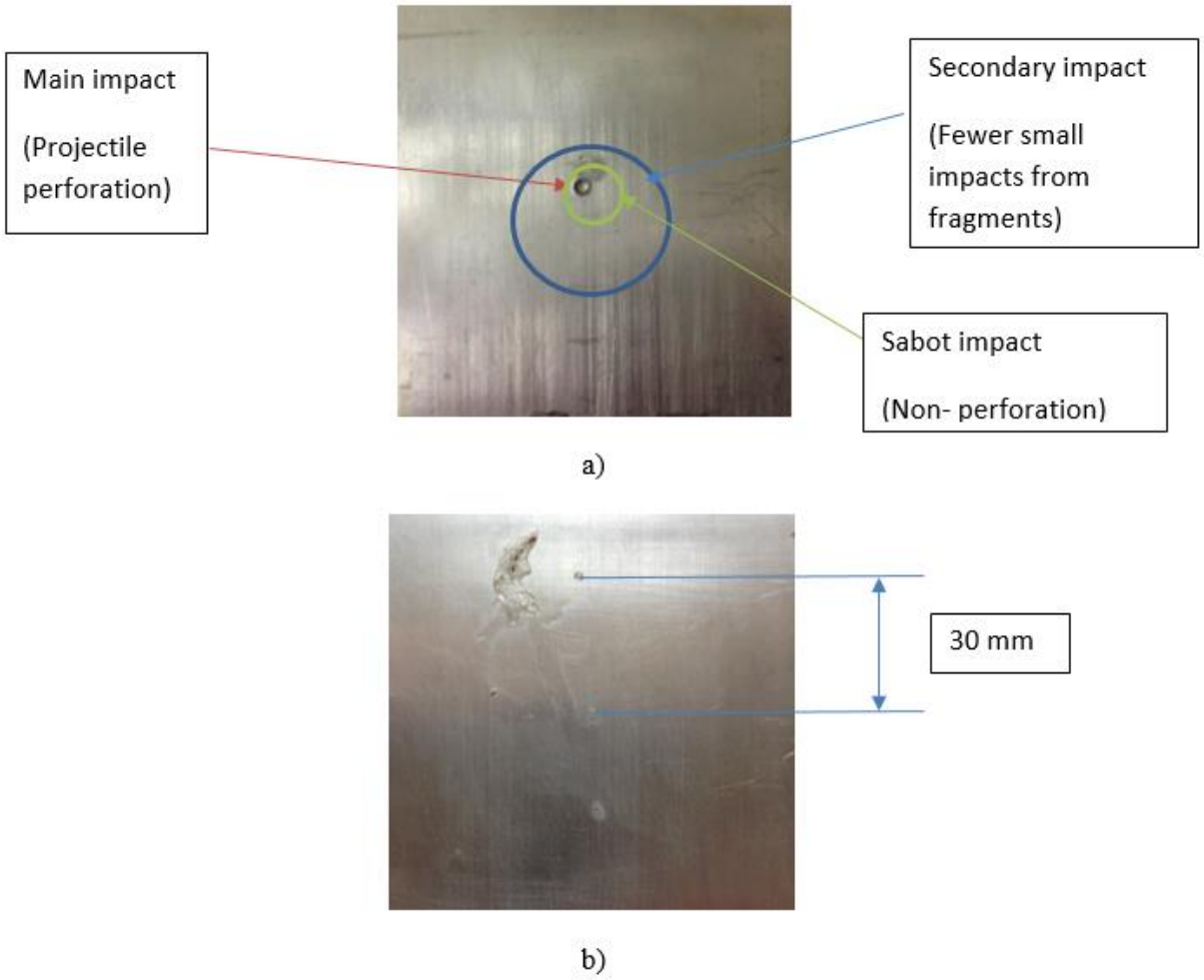

Figure 5.15: Impact damage on Test 4 Al, non-perforated, face a) and back b)

The recordings and analysis that correspond to Test 4 are presented on the following figures.

Figure 5.16 presents the recording and WT for the signal captured by the sensor mounted on the target.

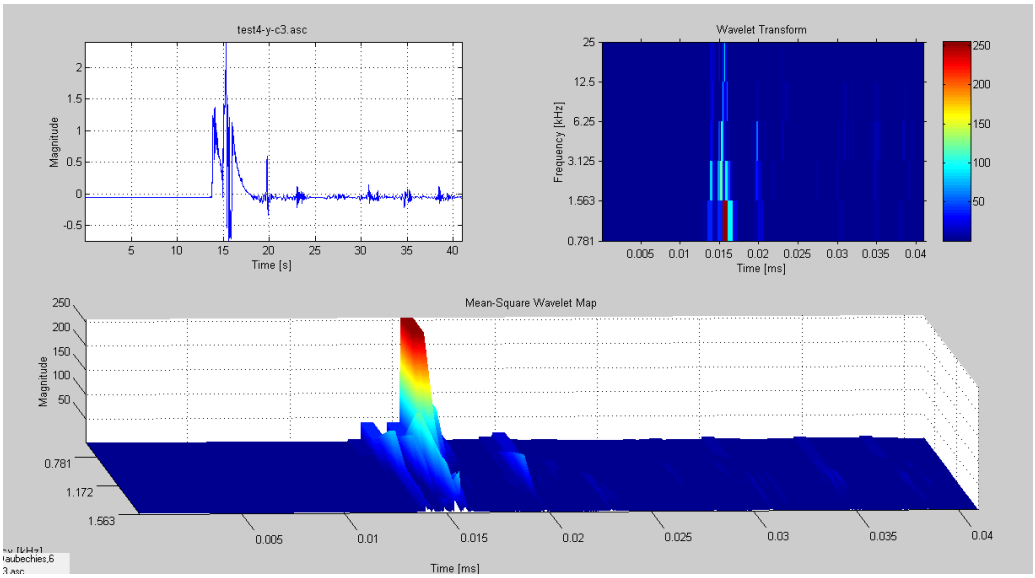

a)

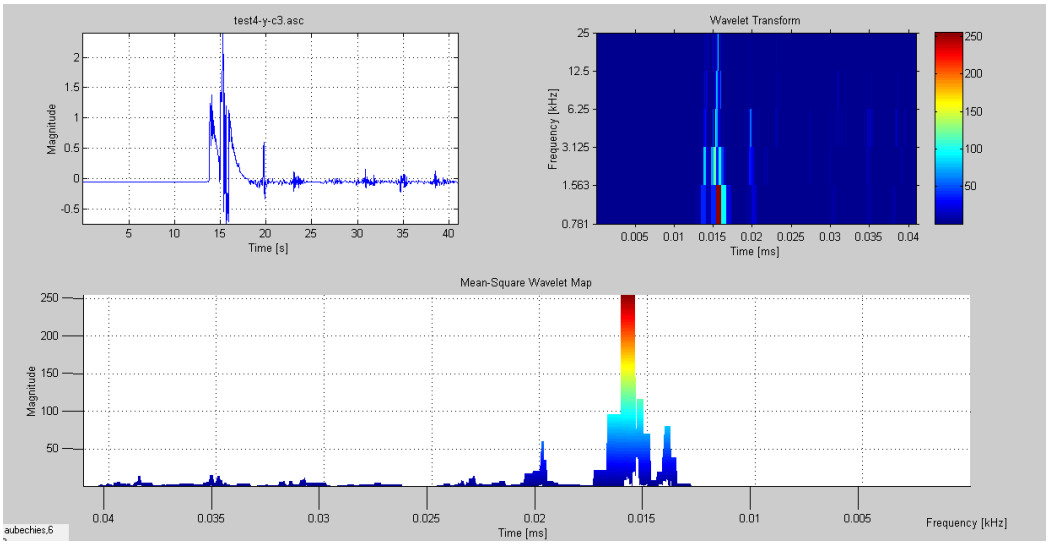

b)

Figure 5.16: On-target sensor, Test 4 signal recording and WT shape a) and profile b)

The TF analysis shows one very well defined frequency peak that corresponds to the projectile impact and two lower peaks corresponding to secondary and sabot impacts. The form of the impact shows two characteristics: the cleanness of the signal (not a multitude of peaks) over a time interval of 2 ms, characteristic to the more rigid material (Al), and the width of the maximum amplitude frequency peak of more than 1 ms. The width of the peak is similar to that of the non- penetrating Test 2 on CFRP. The recorded signal has a compressed form, shown in Figure 5.16a.

The Choi- Williams distribution for the Test 4 signal is presented in Figure 5.17.

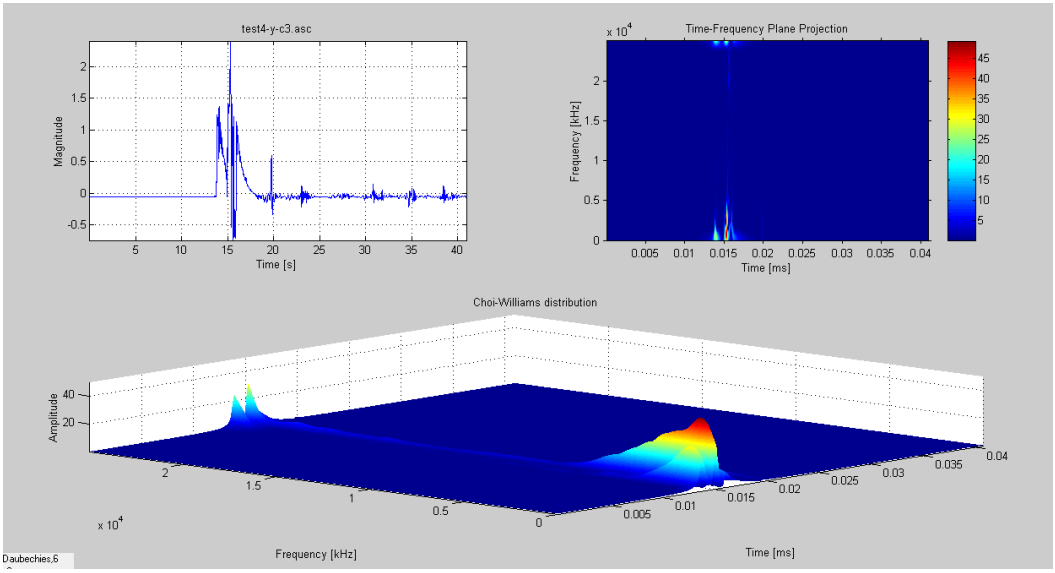

Figure 5.17: CWT corresponding to Test 4 signal

The CWD shows only the two peaks corresponding to the projectile impact and the fragment impact. The factor that really represents the damage is the frequency amplitude. In this case of an Al non- perforated target, the maximum value is about 40. This value is double that of Test 3 and could represent an important indication of non-penetration. The material absorbed the vibration (large peaks, smaller propagation in time), amplifying the maximum frequency.

5.4.5 Summary of the analysis and discussion

A comparative summary of the analysis completed for the four tests is presented in Table 5.4.

Table 5.4: Summary of the analysis

Test No.	**Material, thickness (mm)**	**Damage characte-ristics***	**Shape of the signal**	**Width of signal peaks**	**Frequency amplitude**	**Max. freq. range (kHz)**	**Impact detected by non-target sensor**
Test 1	CF, 3.175	Penetration See *Figure 5.4*	Multiple peaks compacted in more than 5 ms	Thin profile of few µs width	**15**	1.563 to 3.125	yes
Test 2	CF 3.175	No Penetration See *Figure 5.7*	Less peaks compacted in a smaller time interval less than 5 ms	Large profile of peaks of more than 1 ms width	**30**	0.781 to 1.563	yes
Test 3	Al, 0.8128	Penetration See *Figure 5.10*	Clean shape with fewer peaks on an approx. 5ms time interval	Thin profile of few µs width	**20**	1.563 to 3.125	yes
Test 4	Al, 4.826	No Penetration See *Figure 5.13*	Cleaner shape with two peaks on an approx. 2-3ms time interval	Large profile of peaks of more than 1 ms width	**40**	0.781 to 1.563	yes

* 1) No stress or tension measurements were performed on the samples after the tests
2) The test results are only visually analyzed
3) The results represent a basis for a future study on different materials used in aerospace for protection against orbital debris impacts. This future study will allow creation of a functional dictionary of these materials

Table 5.4 clearly shows the differences between the signal characteristics for the cases of penetration and non-penetration impact: shape, peak profile and maximum frequency range. Using the same characteristics we can also differentiate the materials; the more rigid material presents shapes that are cleaner, shorter and with less reverberation in time.

The most important factor that can be used to identify the damage type (penetration or non-penetration) for different types of materials (Al or CFRP) is the frequency amplitude. The

amplitude doubles for the case of non-penetration for both materials and is five points lower for the less rigid material.

It is important to discuss the particularities of our experiments and analysis. The results are based on a small number of tests and should be validated by future tests or virtual simulations. The conditions of the HVI tests changed slightly from one test to another. Although we tried to keep the same projectile velocity, it was not possible because we had to simulate different types of damage. Also, the characteristics of the launcher combined with the timeframe didn't allow better control of the velocity. It is preferred to eliminate secondary impacts from fragments and the sabot to generate a cleaner signal. To achieve this, use of a mechanical stripper is envisaged for future tests. Other factors that could improve the data and the quality of our analysis in future tests include: more precise shots with a constant distance between the location of impact and the location of the sensor, and use of a second recording device to capture signals at the moment of impact.

Even without these improvements, the results of our four tests show clear trends for different types of damage and different types of materials. Nevertheless the execution of future tests and simulations on an extended aerospace material database is a must in order to have the necessary premises for the creation of an automatic material dictionary and real-time monitoring of the health of the protection system.

5.5 Conclusions

Analysis of signals recorded during HVI tests performed at the Shock Wave Laboratory of McGill University provided valid outcomes that can be used as a starting point in the development of a tool capable of real-time detection and analysis of the effects of MMOD impacts.

A review of related theory offers a basis for understanding how different materials will show different behavior in case of hypervelocity impact. Our specific test series aimed at exploring the differences between CFRP and Al from the point of view of recorded signal analysis. For Aluminium, the more rigid of the two materials, the amplitudes of the recorded signals were higher than those recorded for CFRP.

TF-Analysis was carried out for the signals recorded by both (2) sensors; one mounted on the target and the other mounted on the exterior of the test chamber outside the testing area (the chamber was not placed under vacuum for these tests). During the test sessions, different recording durations

were used to see how the impact signal distinguished itself over time. This increased the total duration of the TF-Analysis, and each signal had to be sectioned into time intervals to allow use of our software at full capacity and also to work within the available computation capacity. For example, the number of points for Test 1 (performed on CFRP) was reduced from 7 million points to 3000 points and even lower to 100 points, representing a time decrease from over 2 minutes to microseconds. This reduction allowed deeper analysis of the recorded impact.

For our purposes a TF analysis in the millisecond range was sufficient because it allowed us to use all other linear and bilinear transformations besides WT, such as the presented Choi- Williams distribution which provided clear information related to the amplitude of the signals.

The signal analysis led to the following observations:

- The amplitudes of the test signals are different for different materials, independent of the type of damage. For our tests: 15 and 30 for CFRP versus 20 and 40 for Al;
- For the same material, the amplitudes of the signal are extremely different depending on the type of damage. For our tests, amplitudes for the case of non-penetration were precisely double those observed for penetration damage;
- The shape of the signals is different in 2 ways: non-penetration signals have a different shape than penetration signals, and signal shape is also different in time from one material to the other (less modulations for Al signals);
- The width of signal peaks or the duration of maximum amplitude is different as a function of the type of damage, non-perforation and perforation;

These observation trends were independent of particle velocity or target thickness. In the first two tests, the CFRP targets had the same thicknesses but were tested at different velocities. In the second two tests, the Al targets had different thicknesses and were tested at different velocities.

The observation trends revealed by the TF analysis should be validated by a larger number of future tests on different materials. Once this data is gathered, it will represent a basis for the creation of an automatic process that will recognize the damage in real-time for different materials that are used in space.

In general terms, for the four tests the TF analysis provides clear characteristics, the most important being the frequency amplitude. This new knowledge represents a basis for future investigation and constitutes a starting point for development of a real-time MMOD health monitoring system.

5.6 Future Work

The main direction for future steps is closely related to the necessity to validate these results through further HVI testing, simulations with complementary time-frequency analysis (TF) of the signal and the development of a real-time method of detection and identification of damage.

It is critical to perform further HVI tests, and as a first step we will use the same launcher in a more controlled environment. The results will lead to better observation of the moment of impact, eliminate the impacts of secondary fragments and the sabot, and improve velocity control and sabot separation.

Precise velocity control has an important role in controlling the type of damage. Improved sabot separation will eliminate this secondary impact on the target and provide a clean shot. The presence of multiple secondary impacts however, could be a positive effect since it more closely mimics the effects of impacts in a space environment and the response of materials and structures become closer to reality.

Three series of HVI tests should be planned corresponding to three ranges of velocities; low, medium and high. In the near future low- velocity HVI tests should be conducted at an average speed of 1.5-1.7 km/s. In the more distant future the velocities should be increased; HVI tests at speeds up to 4.5 - 5 km/s (medium velocity range), followed by tests at speeds up to 8 km/s (high velocity range). These series of tests can be done using a new two-stage light gas gun at a Canadian facility in New Brunswick [9] or using the implosion gun at the same Shock Wave Laboratory of McGill University, which allows tests at impact velocities up to 9 km/s [10]. Preparation of these tests and TF analysis of the data will involve a large amount of work over multiple years.

Closely related to the HVI tests is work in the area of TF signal analysis. Considerable resources are required to analyze recorded signals in order to apply a valid method that will lead to real-time identification of the types of damage on different types of materials.

Using TF signal analysis for HVI tests performed in low and high velocity regimes is complex and observation trends may be different than those presented here due to phase transformation of the material which occurs at such large impact speeds.

Further TF analysis will enable continued development of the in-house TF-Analysis software [6-8], ideally suited for analysis and reduction of multi-sensor spectro-temporal steady and transient data. Methods incorporated into the TF-Analysis will be improved to more efficiently extract the primary features of the impact signals and make the results more user friendly and compatible with other TF software solutions.

The results of TF analysis will open other directions of research including automation of damage detection. A software package based on the characteristics presented here could provide real-time information about the status of the target, which could be a space bumper or another element of a space structure

This research work will provide a new efficient tool for automation of damage detection based on a large collection of data on different categories of space materials.

5.7 Acknowledgment

This project has been made possible by precious support from the collaborative research and development grant of Natural Sciences and Engineering Research Council of Canada (NSERC)(No.8482) and the Fonds de recherche du Québec - Nature et technologies (FRQNT).

5.8 References

[1] R.A. Clegg, D.M. White, W. Riedel, W. Harwick, “Hypervelocity impact damage prediction in composites: Part I—material model and characterisation”. *International Journal of Impact Engineering* 33 (2006) 190–200

[2] W. Riedel, H. Nahme, D.M. White, R.A. Clegg, “Hypervelocity impact damage prediction in composites: Part II – experimental investigations and simulations”. *International Journal of Impact Engineering* 33 (2006) 670–680

[3] Anthony Devito, “The combustion of bulk metals in a high-speed oxidizing flow”. MSc thesis, McGill University, Montreal, Quebec 2014-4-15

[4] National instruments, http://sine.ni.com/nips/cds/view/p/lang/fr/nid/202664

[5] PCB Piezotronics, http://www.pcb.com/Products.aspx?m=352C33

[6] A. Oulmane, A.A. Lakis and N. Mureithi. 2013, "A Method for Analyzing Rotating Machinery Faults using Time-Frequency Application". *International Journal of Condition Monitoring and Diagnostic Engineering Management* Volume 16 No2, April 2013 pages 21-34.

[7] Oulmane, A., Lakis, A.A., Mureithi, N., and Safizadeh, M.S., "The Application of Time-Frequency Analysis in Rotating Machinery Fault Diagnosis", 22 nd International Congres and Exhibition on Condition Monitoring and Diagnostic Engineering Management, San Sebatian, Spain, June 2009, pp 597-583.

[8] Mahvash, A., Lakis A.A., "Independent Component Analysis as Applied to Vibration Source Separation and Fault Diagnosis", *Journal of vibration and control*, online: August 2014, DQI: 10.117/107756314544349.

[9] IADC WG3, *IADC Protection manual*. IADC-04-03, Version 4.0, April 12, 2011

[10] B. Aissa, K. Tagziria, W. Jamroz, E. Haddad, M. Asgar-Khan, S. V. Hoa , J. Loiseau, J. Verreault, A. Higgins, "Monitoring with Fiber sensors and Self-Healing of CFRP Laminates Exposed to Hypervelocity Small Pellets Simulating Space Debris", 12th International Symposium on Materials in the Space Environment (IMSE-12) 24-28 September 2012.

[11] A. Bettella, A. Francesconi, D. Pavarin, C. Giacomuzzo, F. Angrilli, "Application of Wavelet Transform to analyze acceleration signals generated by HVI on thin aluminum plates and all-aluminum honeycomb sandwich panels". *International Journal of Impact Engineering* 35 (2008) 1427–1434

[12] Karl F. Graff, *Wave motion in elastic solids*. Courier Corporation, 1975 – Science.

[13] Lei Wang, F.G. Yuan, "Group velocity and characteristic wave curves of Lamb waves in composites: Modeling and experiments". *Composites Science and Technology*, Volume 67, Issues 7-8, June 2007, Pages 1370–1384

[14] H. Choi and W. J. Williams, "Improved time-frequency representation of multicomponent signals using exponential kernels", *IEEE. Trans. Acoustics, Speech, Signal Processing*, vol. 37, no. 6, pp. 862–871, June 1989.

[15] Howard A. Gaberson, "Autocorrelation approaches to time frequency analysis of machinery vibration signals". 20th International Modal Analysis Conference, Los Angeles, CA; February, 2002

[16] Howard A. Gaberson, "Application of Choi-Williams reduced Interference time frequency distribution to machinery diagnostics". *Shock and Vibration*, Vol. 2, No. 6, pp 437-444, 1995.

[17] M. A. Hamstad, "Comparison of Wavelet transform and Choi-Williams distribution to determine group velocities for different acoustic emission sensors". *J. Acoustic Emission*, 26, 2008, 40-59.

[18] L. E. Iliescu, A. A. Lakis, A. Abou – Antoun, "Hypervelocity Impact (HVI) Tests & Signal Recordings". *Universal Journal of Aeronautical & Aerospace Sciences* 2 (2014), 80-113

[19] W. Goldsmith, *Impact. The theory of physical behavior of colliding solids*. Courier Corporation, 2001-11-01 - 379 pages

[20] William H. Prosser, Michael R. Gorman and Donald H. Humes, "Acoustic Emission Signals in Thin Plates Produced by Impact Damage". *Journal of Acoustic Emission*, Vol. 17(1-2), (June, 1999), pp. 29-36.

[21] William H. Prosser, Michael R. Gorman, John Dorighi, "Extensional and Flexural Waves in a Thin-Walled Graphite/Epoxy Tube". *Journal of Composite Materials* Vol. 26(14), 1992, pp. 418-427

[22] A. Oulmane, A.A.Lakis and N. Mureithi, "Application of Fourier Descriptors & Artificial Neural Network to Bearing Vibration Signals for Fault Detection & Classification". *Universal Journal of Aeronautical & Aerospace Sciences* 2 (2014), 37-54.

[23] H. Hertz, *On the contact of rigid elastic solids*. London (1896), p. 156.

CHAPTER 6 ARTICLE 3: SATELLITES/SPACECRAFT MATERIALS AND HYPERVELOCITY IMPACT (HVI) TESTING NUMERICAL SIMULATIONS

Iliescu, L. E., Lakis, A. A. & Oulmane, A.
Mechanical Engineering Department, École Polytechnique of Montréal, Canada
C.P. 6079, Succursale Centre-ville, Montréal, Québec, Canada H3C 3A7

European Journal of Mechanical Engineering Research
Vol.3, Issue 3, pp. 41-77, August 2016
Published by European Centre for Research Training and Development UK
(www.eajournals.org)

6.1 Abstract

Hypervelocity impact damage due to the micrometeoroid and space debris is a common threat of present space environment for any spacecraft orbiting the Earth and for the future launches of new spacecraft. An important issue that is taken in the manufacture of these spacecraft is the choice of structure and protection materials, materials that are considered based on the survivability in the space environment. One of the new hazard that occur in space environment is the micrometeoroid and space debris (MMOD) hypervelocity impact (HVI) and the probability of such impact is determined based on specific impact risk assessment procedure. Starting from the identification of the most used materials for the manufacture of spacecraft and sorting them in three main groups of materials mostly used, metals alloys, composites and sandwich panels, the present work presents the results of the time-frequency analysis of the signal obtained from the numerical simulation of HVI. For the numerical simulation of the HVI a student version of LS-Dyna software was used and the method used for signal analysis was the Choi-Williams Distribution (CWD) using a specific TF-Analysis software in-house developed. Using CWD method clear differences in the HVI form and frequency amplitude, for one or two materials of the each group initially identified in the case of penetration, were identified. In conclusion the characteristics of each perforation on materials considered is discussed and the results obtained are corroborated with the analysis of the signals resulted from a previous HVI test session.

6.2 Materials review

6.2.1 Introduction

W. P. Schonberg [1] presents an overview of the impact tests performed on spacecraft structures generally used, metallic (mostly aluminium) and composites or honeycomb sandwich panels (HC/SP). The paper focused on the hypervelocity impact tests on composites materials, where the impacting material are behaving as fluids, and where such impact create extensive internal damage (e. g. delamination) which extends furthermore than the crater/hole diameter in the case of impact on metallic targets. Also, are presented the advantages of using the composites in the case of a HVI, such as less ejecta or the decrease in total weight compared with metals. Regarding the use of composites in MMOD protection, the dual-wall systems Kevlar and graphite /epoxy (Gr/Ep) as outer bumpers [2] were considered not offering any advantages compared with an Al dual-wall system, other solutions that performed marginally better were CFRP/metal matrix, ceramic materials or porous fillers combined with Al bumpers.

As inner bumpers, Kevlar and Spectra panels were tested to demonstrate that the use of composite offers an increased protection to hypervelocity impacts [3].

Another paper by Frank Schafer [4] investigates the new materials that are used in different configurations in order to increase the spacecraft protection to HVI. The paper also discuss the influence of light layers of materials such as thermal blankets or multi-layer insulation (MLI) in HVI depending of their position in the configuration. The tested configurations were: by-layered aluminium foam bumpers that used AlSi7Mg (10, 20 and 30 ppi- pore per inch) with a density from 7% to 10%, flexible stuffing that used Nextel 312AF62 or Kevlar alone or in combination with polyurethane foam layers, titanium alloys – Ti6Al4V or different hybrid configurations mixing these type of bumpers. As conclusion, the paper mentioned the aluminum foam capability to induce multiple shocks to projectile, the Ti and Al alloys that showed superior capabilities in inducing shock to the projectile and the capability of flexible stuffing in absorbing the debris cloud energy.

6.2.2 Frequently used materials in the manufacture of the spacecraft

6.2.2.1 Aluminium

Aluminium alloys were tested in different configurations, as for example in a recent paper by Wan H [5] the performance of 2024 aluminum alloy panels stacked together with CFRP panels were studied in order to improve the design of the shielding laminate panel. The results showed that this combination could significantly reduce the HVI peak shock pressure and the increase of the layer number will lead to an increased shielding performance.

G. S Guan [6] studied the HVI test capability of an Al bumper that was ceramic coated and the results showed that if the coating is applied on the external, projectile impacted, side of the Al panel, the projectile is better shattered, in smaller particles and with lower kinetic energy.

Gong WW [7] also tries to present the capabilities of the aluminium foam in absorbing the HVI energy using three- dimensional material point model – MPM3D that showed good results comparing with the experimental data. Smoothed Particle Hydrodynamics numerical simulations on aluminum foams with homogeneous open-porosity, cell sizes about 1.6mm and relative densities near 26.9% were also conducted by Ma ZT [8] with the same results showing the effectiveness of Al foam in absorbing the HVI energy.

6.2.2.2 Honeycomb panels

The honeycomb sandwich panels in relation with HVI, one of the most utilised structures for the manufacture of satellites, were also studied by many authors.

In a recent paper, Ping Liu [9] based on HVI simulation on sandwich panels, determined the influence of internal-structure parameters on impact results besides of external parameters such as the oblique impact influence that was studied before by Taylor [10, 11]. The results showed that the impact angle has a marginal influence to perforation limit. The study uses a material point method (MPM) – based internal structure model in order to describe the response of HC/SP to HVI. The basis of a MPM is the use a set of Lagrangian points and an Eulerian background grid, were the Lagrangian points are carrying all the physical variables (the mass, the velocity, the stress and the strain), show the deformation of the material and imply the boundary of the domain and Eulerian background grid solve momentum equations and calculate spatial derivatives. At each

step, the Lagrangian points are bound to the Eulerian grid and they deform together. In order to validate the model, the results were compared with the ballistic limits obtained from previous tests performed by Turner [12] on HC/SP with Al2024-T81 facesheets material and Al5052-H19 honeycomb core, having on the front face-sheet a thin layer of 0.1 mm Teflon. As conclusions of the study, the hole diameter of the front facesheet is influenced much more by the projectile size than the projectile speed. In comparison, the hole diameter on the rear facesheet is influenced by both, the impact velocity and the projectile size. The channeling effect decreases as: the cell size increases, the thickness of the cell wall decreases or the thickness of the whole honeycomb core decreases.

Honeycomb panels represents the most common material used for the satellites primary structure. J.-M. Sibeaud [13] presents HVI test and simulations results done on these satellites representative of structural bodies. The HC/SP used had 150x150 mm or 150x190 mm and consisted in 20 mm aluminum honeycomb cores (0.025 mm thick aluminum sheets) glued with 0.8 mm aluminum face-sheets, and five HVI tests were performed at 5.7 Km/s with a 7 mm diameter projectile. The paper describes the honeycomb channelling effect: the projectile and front face-sheet fragments were absorbed within the honeycomb structure and concentrate on the rear face-sheet, creating holes diameters of more than 10 times the projectile diameters. The HVI simulations done with the Ouranos hydrodynamic software [13], showed the same results, Figure 6.1.

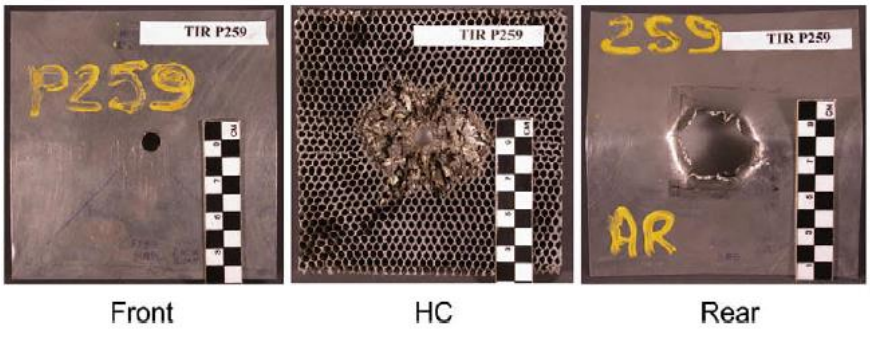

a)

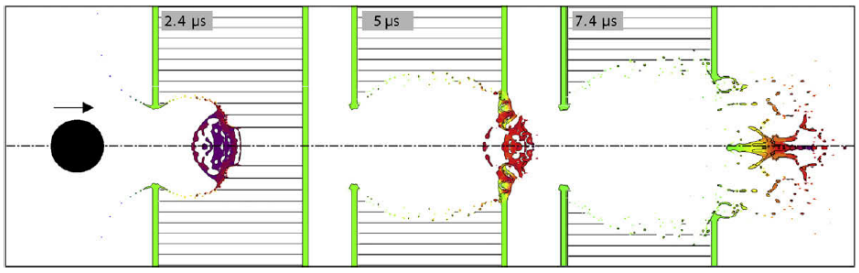

b)

Figure 6.1: Channelling effect created by the HC/SP impacted at 5.7 Km/s; a) test samples, b) simulation [13]

S Ryan [14] studied the HVI test performance of metallic open-cell foams in order to replace the honeycomb sandwich panels (the channelling effect of the honeycomb core) and to obtain the better protection results at the same mechanical and thermal performance and the same weight. For his experiments the author used a target containing two honeycomb sandwich panels spaced at 2 cm with two outer layers of stainless steel mesh as a baseline in order to compare the results with the ones obtained on 12.7 mm thick open-cell Al6101-T6 foam panels (10 ppi – pores per inch as pore density). The conclusion after comparing the results of 19 HVI tests was that the metallic foam configuration performed better in fragmenting and melting the projectile therefore the impact energy on the rear wall have been reduced. However the oblique HVI test results showed a decrease in configuration shielding performance which was attenuated by the presence of outer layers of metallic mesh.

Ceramic foams were used in HVI tests due to the unique combinations of properties such us low densities, high stiffness or very good shock abortion, Silicon oxycarbide (SiOC) microcellular foams were used to enhance the effectiveness of sandwich panels [15].

Also recently, Smoothed particle hydrodynamics (SPH) method was used in modeling the HVI on HC/SP in order to determine the most influential parameter on the channeling effect by Pilseong Kang [16]. The material used for the facesheets is Al 7075-T6 of 0.4 mm thickness, the HC core is Al5056 with an average of 30 mm for core depth, 4.8 mm for cell size and 0.025 mm in for cell wall thickness. The material of the projectile is aluminum alloy with a density of 2.78 g/cm3 of different diameters launched at high speeds up to 7.2 km/s. The simulation results agreed with the tests and showed that the HC core cell size is the most influential parameter on the damage of the rear facesheet due to the channeling effect and the critical projectile diameter decreases due to the presence of HC core and varies with the HC core cell size.

However, a good complete study of HVI on HC/SP is made by W. Schonberg, [17] a study that is based on 400 HVI tests results and leaded to the development of a system of empirical equations that can be used to predict the trajectories and spread of the debris clouds that exit the rear facesheet. The equations results are a good fit to the data, and showed the capability of picking up most of the variations in test conditions, with a correlation coefficient in a range of 60 to 90%. The study predicted the minor and major hole dimensions for the HC/SP facesheets and the trajectory and spread angles for normal and in-line dust & debris clouds for HC/SP with aluminium and composite face-sheets. Based on this development, we can determine what spacecraft components will be impacted by the mass of debris cloud and at what extent, information that furthermore could be introduced in a risk assessment code to calculate the probability of spacecraft failure under a prescribed set of impact conditions.

An improvement to the HC/SP of the satellites (Al and Ca honeycomb or Composite and Al honeycomb) is presented by R. J. Turner (12). Three developments were presented: MLI + front/intermediate material layer or multiple honeycomb layers, the material layer could be Nextel, Kevlar or Al mesh. There were used two types of MLI, the enhanced and toughened MLI. As the enhanced MLI (EMLI) was used a MLI with four layers of betacloth and nine layers of Kevlar 310, as toughened MLI (TMLI) was used MLI and three layers of betacloth. Regarding the honeycomb designs, a double honeycomb (DHC), a single HC with an intermediate 0.4 mm facesheet bonded to the core, and reinforced honeycomb (RSHC) were used. The single HC having an additional 0.2 mm Al bonded to the facesheets. A series of HVI tests were performed at velocities up to 8 km/s, new ballistics limits were developed and tests showed that at 5 km/s the critical diameter of the projectile increased from 1 mm to 1.8 mm for the DHC with TMLI and to 1.93 mm foe SHC and

EMLI. Also the using of a DHC instead of SHC will reduce the number of penetration, to 3.7 times and the use of MLI will reduce the penetration 4.6 times.

Warren J. [18] presents the results of HVI tests performed on foam core sandwich composite specimens infused with a shear thickening fluid (STF). Two 0.064 cm thick aluminum facesheet sandwich composites (1.27 cm thick open cell and 2 pores per cm aluminum foam cores) were filled with a STF consisting of a 0.2 mass fraction of Aerosil 200 fumed silica in 200 molecular weight polyethylene glycol (PEG) and two more identical foam core specimens were filled with only PEG. The HVI tests were performed at velocities of 3.8 Km/s using stainless steel projectile of 1 mm diameter. The results showed that that most of the impact energy was dissipated within the proposed sandwich composites, with almost no damage on rear wall.

Eldon P. [19], in a recent conference paper presenting the Lunar Atmosphere and Dust Environment Explorer (LADEE) project suggests, a "low-cost, reusable, spacecraft bus architecture for future Planetary Science missions". LADEE's uses co-cured structures based on sandwich construction (HC/SP), the skin materials (SP) include carbon fiber and epoxy matrix (resin) glued to the honeycomb core with a film adhesive and the radiator panel skins were aluminum.

6.2.2.3 Composites

Another configuration that is representative for satellite structures (e.g. Radarsat-2), from point of resistance of HVI and presented also by S. Ryan (20) is the CFRP face-sheets bonded to Al honeycomb cores. A series of 55 HVI tests were performed using a 2017-T4 Al projectile of 1.25 mm on different configurations, Table 6.1.

Table 6.1: Different satellites CFRP- Al honeycomb structures HVI tested [20]

Panel	AD (g/cm^2)	Facesheets			Honeycomb	
		t (mm)	Material	Stacking	Configuration	t (mm)
RAD1	0.7017	1.45	FL01 (F)-HMF196/34 T300-1k fabric/ FL02 (P)-HYE 4934C K139 u.d. ply	$(0_F/0_W/+45_W/90_W/-45_P/-45_W/90_W/+45_W/0_P)$	3/16-5056-.001P	50.6
RAD2	0.5847	1.40	FL01(F)-HMF196/34 T300-1k fabric/ FL02(P)-HYE 4934C K139 u.d. ply	$(+45_F/0_W/-45_P/+45_P/90_P)_S$	3/16-5056-.001P	25.3
RAD3	0.4217	1.15	FL01(F)-HMF196/34 T300-1k fabric/ FL02(P)-HYE 4934C K139 u.d. ply	$(0_F/0_F/+9_P/-9_W/+9_W/-9_P/+9_P/-9_W/0_F/0_F)$	3/16-5056-.001P	12.1
GOCE	0.7807	2.30	M18/32%/M55J/145 u.d. ply	$(+45/0_2/-45/0_2/+45/0_2/-45/0_2/+45/0_2/-45)$	3/16-5056-.001P	12.5
SAX	0.4405	0.95	914/34%/137/6K/M40B u.d. ply	$(0/+60/-60)_S$	3/16-5056-.001P	29.7
H/P	0.2300	0.55	M18/G801 u.d. ply	(+45/0/90/−45)	3/16-5056-.0007P	19.9

The results of the tests were furthermore used to determine the ballistic limit equations for this type of configurations.

In an early paper, Timothy C Thompson [21] also presents the development of all- composite spacecraft instead of an all-aluminum spacecraft bus, using the fundamental principles: simplicity, modularity and interchangeability. The use of graphite/epoxy produced a weight saving of 46 pounds with an additional of the solar array substrates (SAS) panels, 0.020" thick (pre-cured panel assemblies of Gr/ET ·50/ERL 1962. [0/45/90/135] with either co-cured 0.2 mil copper on one side or co-cured 2.0 mil Kapton) of 33.9 pounds. The satellite decks are manufactured similarly to the SAS panels (except copper was co-cured on both sides of the deck) and the middle and the lower decks have one inch thick aluminum core. The space frame is made from flat laminates. The skin thickness on all decks is 0.030" with an orientation of [0/60/120]s and the frame subassemblies are made from flat 0.048" thick laminates of T50/ERL 1962 with a [0/45/90/135]s orientation.

Non- metallic spacecraft structure or CFRP is also mentioned by M. Nicoletto [22] as replacement of standard aluminium panels and the electromagnetic interference with high speed digital lines used for data distribution that occur. The CFRP consists of layers of laminates in which several plies are rotated (for the mechanical strength). The plies are made of carbon fiber (25 fibers by 10 μm diameter) impregnated in an epoxy resin matrix. The epoxy/carbon fiber composite generally comprises 57% in volume of carbon fiber with an inter-laminate epoxy layer (M21) to electrically insulate the consecutive carbon fiber layer. The thickness of each carbon fiber layer is around 200 μm while the M21interlayer is approximately 35 μm thick.

In a recent paper, Changqing and Bo [23] analysed three different configurations, specifying the differences between a laminated of aluminum/CFRP layers which performed better than the single aluminum layer or the single CFRP layer, having the same areal density. The multilayer shield made the projectile to rebound multiple times and at high intensities, the projectile has been more fragmented. Consequently, it was proved that the designed multilayer shield is more effective to against the HVI.

One paper presented at the 55th AIAA conference [24] investigates the results performed on two deferent composite laminates. The laminates were made using epoxy-reinforced carbon fiber pre-impregnated unidirectional type: a quasi 3D five-harness satin weave (Q3DO5) and a cross –ply with and without a graphite sheet bonded on the impacted side. The HVI impact tests were performed at velocities of 2.9 to 5.25 Km/s and the results suggested that the targets having graphite sheet bonded had an increased tolerance to HVI.

Modelling of HVI damage in composite is presently covered by a multitude of papers, one recently study by Aleksandr Cherniaev [25] presents an explicit mesa-scale representation of two numerical tests on thermoplastic AS4/PEEK (APC-2) materials with quasi-isotropic layups. To reproduce as close as possible the fracture mechanism that occurs in a HVI, the composite laminate used for the simulations has been represented as a structure consisting in alternating fiber-reinforced and finite-thickness resin-rich layers. Material model was characterized in terms of stress-strain relations, equation of state (EOS), failure initiation criteria and post-failure response. The simulation which employed a combination of SPH and finite element method (FEM) in Lagrangian formulation, to represent the aluminum projectile and the laminate composite, showed a good correlation with the test results in terms of delamination area and external damage and showed that the dynamic fracture toughness has been an essential element for the accuracy of simulation.

Q. Gua [26] investigates the HVI damage in 55% TiB2/2024Al composite as a replacement of 6061 and 2024 aluminum alloys that are presently used on the spacecraft. For this study 2024Al alloy spherical projectiles with the diameter of 1.2 and 1.5 mm were launched from a two-stage light gas gun with the impact velocity of 2.5 km/s. As the results, the TiB2–Al interface formed a new AlxO1−x phase and a crystal parameter of 0.69 nm. The TiB2 particle formed a stacking fault with width of 10–20 nm, the formation of nanograins (about 100 nm) was noticed within Al matrix due to dynamic recrystallization and the lamellar S′ phase was transformed into lenticular or spherical S phase after HVI.

A. H Baluch [27], has studied the HVI on a satellite carbon-epoxy composite wall having a stacking sequence of [(0/±45/90)2]s. The satellite wall, with 16 layers of carbon –epoxy composite that was before exposed to the characteristics of LEO environment, was impacted at an oblique angle by an Al2017 projectile of 5.56 mm diameter. The results which were compared with the data for normal impacts both for Aluminium alloys and composites showed that the oblique angle impacts lead to multi-axial loading on composite wall and shows a more complex behavior than that of normal angle case. Also, the energy absorbed by the non-aged composite laminate is of average 20 Joules more, which shows that the oblique angle impact energy absorption is larger in comparison with the normal impact on composites or on 6061-T6 aluminium alloy plate and that will increase with an increase in velocity. In terms of percentage, 35% more absorption of energy at oblique angle of 45° and for the Aluminium alloy the energy absorption by composite at oblique angles is almost 1.85% higher.

Cheng Wing L [28] presents a new impact model for thick composites based on HVI tests with velocities up to 2 km/s. For the first testing session at 0.6 m/s various woven polymeric composites, with S-2 glass fibers and polyester resins, were used. The thickness of laminates was 4.45 cm. The second series of tests were performed at 1.83 m/s and material tested were Kevlar reinforced plastics, S-2 glass reinforced polyester, rolled homogenous steel, 7039 Aluminum, high hardness laminates, and ceramic (Al2O3) laminate or chemically bonded ceramics.

B. Aissa [29] paper presents a new concept of embedding within a CFRP laminate a self-healing process based on microcapsules filled with 5E2N monomer along with spread catalyst particles (Ruthenium Grubbs). HVI tests were performed using projectiles of 4mm diameters launched at velocities between 1.3 and 1.7km/s. Although the microcapsules would not heal the perforation hole itself, the healing of potential delamination developed around the crater/hole was evident.

Oleg V. Startsev [30] investigate carbon and glass fiber reinforced plastics (CFRP, GFRP), hybrid composites based on epoxy compositions and materials with several variants of surface protection: AZ alloy AMG-Gm, aluminum foil. Lacquer and paint coating LKF 40-1-1 14-87 used on Salyut-type spacecraft that had spent long periods of time in outer space.

Lei Wang [31] in his study uses composite material of T300/ epoxy-resin with high performance that has been widely used in aircraft, spacecraft, watercraft and transportation because of its excellent mechanical characteristics to predict the fatigue life based on fatigue damage accumulation model build on stiffness degradation, according to the damage mechanical theory.

Hoffman [32] describes the use of high-performance composite materials (K1100 graphite fiber/cyanate ester matrix [Gr/CE]) for the structural design of a small satellite. The paper, besides the requirements for the structural performance, detailed design, procurement and test, presents a thoroughly material selection.

6.2.2.4 Bulk metallic glass (BMG)

Starting from the ballistic limit equations, Lee Hamill [33] investigates a new type of material that should have high hardness with the lowest density possible. In addition, a low melting temperature will be a plus, leading to the vaporization of fragments and to an increased toughness in order to carry the launch loads. Based on these properties the author proposes a bulk metallic glass (BMG, amorphous metal) thicker than 1 mm, that have densities similar to other crystalline alloys (e.g.,

titanium) but with hardness typically found in ceramic, also BMGs can have much higher toughness than ceramics. The study presents a series of HVI tests on BMG Vitreloy 1 (Zr41.2Ti13.8Cu12.5Ni10Be22.5) and the BMG matrix composites DH1 (Zr36.6Ti31.4Nb7Cu5.9Be19.1), at velocities of 0.8–2.79km/s using an aluminum spherical projectile of 3.17mm in diameter. The results showed an increased impact resistance of Vit 1, DH1 and DH3 samples and motivates in the use of amorphous materials as spacecraft materials.

Davidson M and all [34] investigated also, the HVI protective qualities of an amorphous metal composite which usually is a multi-component alloy of titanium, zirconium, copper, aluminum, niobium or beryllium that, for the samples thicker of 1 mm, are vitrified and becomes the BMG. Different BMGs thin panels and multi-faced egg box were HVI tested at velocities up to 5.5 km/s. The study demonstrates that the welded panels of BMG composites offer a unique HVI protection solution for future satellites.

Douglas C. Hofmann [35] integrates layers of metallic glasses in order to improve the HVI protective capability of a Whipple shield. The recent study showed that the debris cloud could be significantly diffused by corrugating the bumper shield's surface and that the cellular structures created by the welding of the corrugated panels could prevent penetration of the projectile. The metallic glass used in the study is a commercially available ribbon of Metglas 2605 SA1 with a Vickers hardness of 900, compared to 107 for Al-6061, but has 2.7 times larger density. For the internal stuffing for the Whipple shield, 21cm square sheets of the metallic glass ribbon were cut and then stacked together maintaining the same areal density as the actual spacecraft baseline. The configuration was impacted at an average velocity of 7 m/s using a 2.8mm diameter Al-2014 T4 sphere and showed an improvement of the performance for the configuration that includes the metallic glass. The paper also mentioned some new materials, metallic glass alloys that have a lower density than the alloys that have been used in the current (and previous) studies, low-density metallic glasses developed in Al-based systems (2.8–3.6 g/cm3), Mg-based systems (2.6–4.2 g/cm3), Ca-based systems (1.9–2.6 g/cm3), and Ti based systems (4.5–7.2 g/cm3).

6.2.2.5 Fabrics: Nextel and Kevlar

S Katz [36] studied the response of micro-composites under HVI. In this research the materials used are Kevlar 29/epoxy and Spectra1000/epoxy thin film micro-composites (thickness of about 100 μm). These materials are used extensively in spacecraft structures and satellite components

such as antenna struts, panels and low distortion frames (high specific strength, high stiffness and low coefficient of thermal expansion). The targets used are films based on epoxy resins (Araldite LY564, Ciba-Geigy mixed with hardener HY560). The different type of fibers used were UHMWPE fibers (Ultrahigh molecular weight polyethylene, Spectra 1000 fibers), surface-treated Spectra 1000 fibers (referred to as Spectra-RF), and Kevlar 29 poly (paraphenylene terephthalamide), Table 6.2.

Table 6.2: Material properties used as micro-composites targets [36]

Property	Kevlar 29	Spectra 1000	Spectra-RF	Explanation
σ_f (GPa)	3.1	3.9	1.5	Fiber ultimate strength
E_f (GPa)	65	175	175	Fiber Young's modulus
N	4	None	5	Number of broken fibers
n	7	7	7	Number of embedded fibers
r (μm)	6	13.5	13.5	Fiber radius
ϕ_f	2.64×10^{-3}	0.013	0.013	Fiber volume fraction $\phi_f = n\pi r^2/tw$
τ (MPa)	24.6	5.8	11.8	Interfacial shear strength
t (μm)	100	100	100	Specimen thickness
L_{avr} (mm)	1.4	2	2.5	Fiber debonding length
w (mm)	3	3	3	Specimen width

The targets were impacted with a 1 mm diameter aluminium flyer at velocities up to 3 km/s using a laser driven flyer plate (LDFP) system. The micro-mechanical response of different micro-composite materials to HVI was studied before the tests and the HVI damage characterization of 50 specimens showed permanent damage such as the crater hole, fiber breakage, fiber pull out and fiber debonding. The study concluded, based on the main fracture mechanism of each micro-composite (absorbed energy calculated for the classical absorption mechanisms), that for the Kevlar 29 based composites the damage was to the matrix as well as to the fiber due to the strong interfacial strength and the dominant fracture mechanism was fiber pull out. In the case of Spectra 1000/epoxy, new surface creation was the main damage mechanism. For Spectra –RF, the prior etching in oxygen RF caused fiber surface restructuring and increasing the interface strength, leading to cracks in the matrix and breakage of the fiber as well as fiber pull out, the untreated fiber failed predominantly by fiber/matrix separation.

Nextel and Kevlar as cloth materials (fabric or a flexible woven material consisting of a network of natural or artificial fibres often referred to as thread or yarn), especially used in composition of internal bumper of different shield configurations, are studied by many authors in relation to HVI and the results mainly confirm the same capabilities: for Nextel to shatter the projectile and dissipate the impact energy and for Kevlar in catching the projectile fragments and absorb the impact energy.

Eric P. Fahrenthold [37] presents the results of HVI simulation on a shielding configuration that used Kevlar aramid fiber 129 and Nextel woven cloths that were compared with test results presented in a prior report by Grosch [38]. The simulations were done for two types of projectiles one of inhibited shape and the other of spherical shape at a velocity of 11 km/s. The simulations required 252 hours and underestimate the composite shield performance, the high computational cost being a characteristic of the HVI.

6.2.2.6 Fused silica/windows materials

HVI on spacecraft windows used for navigation or observation, especially fused silica (SiO2) windows was studied by R.R. Burt and E. L. Christiansen [39] for a wide range of projectiles types. The targets consists in fused silica, a high purity synthetic amorphous silicon-dioxide, of 76 mm diameter impacted with a 0.4 mm diameter Al2017-T4 spherical projectile in principal (other projectile materials used were steel, nylon, aluminum –oxide and copper alloy), at velocities up to 7 km/s and at different impact angles. Other HVI tests were made on Chemcor windows which are made of two panels of chemically tempered silica with a laminate silicon interlayer and on Hyzod –AR polycarbonate, a transparent amorphous thermoplastic with a hard coated surface. The paper concluded that Hyzod polycarbonate has an improved penetration performance compared to Fused Silica at the same mass per unit area and the Chemcor glass showed the least HVI performance compared with the other two materials.

A paper, written by Song LiHong [40], analyses the HVI on fused silica, an appropriate optical material used on spacecraft for sensitive surfaces as mirrors or sensors. The experiment uses the same LDF launcher to shot at velocities up to 3.7 Km/s, an aluminium flyer of 16 um thickness in a transparent glass (fused silica glass) of 15 mm thickness and 40 mm diameter coated with a metal or non-metal film. The HVI damage morphology was measured with an optical microscope and a scanning electron microscope (SEM). The damage types noticed were: cratering, ejecta and micro-

cracking. These damage types caused by the non-homogeneity of surface and the optical absorption or scattering and depend of optical constant of the fussed silica and the surface morphology.

6.2.2.7 Other materials solutions

X. Huang [41] proposes also a new material, an amorphous alloy, which could be used in order to improve the performance of a Whipple shield. The amorphous alloy used consists of a Fe-based amorphous alloy coating and an LY12 aluminum alloy substrate and was used as first bumper of the shield configuration. The coating materials are amorphous Fe–Si–B ribbons of 50 μm thickness, with the nominal composition of Fe77Si14B9 and as substrate LY12 aluminum alloy with the thickness of 2.85 mm is used. Four tests were performed at the impact velocities used were 3.5 km/s and 5.5 km/s launching spherical projectiles of solid LY12 aluminum alloy with a 4 mm diameter. Results showed that this type of configuration performed better at the lower speed, at 5.5 km/s the shield performed slightly better than the baseline and concluded that the amorphous alloy reinforced bumper can produce higher shock pressures and induce higher temperature rise in the projectile.

Materion Beryllium & Composites [42] provides materials for satellites such us Beryllium, with the lower cost version Al Beryllium, used for structures and optics, or Supremex as a replacement of Titanium. Materials with attractive qualities to be used in the space environment such us: lightweight (less than aluminum), High specific stiffness and thermal stability, good thermal conductivity, high melting temperature or heat capacity and dimensional stability.

Serhan Avcu [43] discuss the process of structural material selection for spacecraft focusing in special o the atomic oxygen (AO) effect (LEO environment) but also the space environmental effects are considered. As structural materials should have the main properties the lightweight, high stiffness and dimensional stability and commonly used metals are Aluminum, Magnesium Beryllium, Titanium, Molybdenum, Tantalum and Tungsten. Polymers are used for the central body structure of communications satellites and antenna reflectors, temperature resistant parts, electronics, communication and power devices, life support systems, sensors and detector structures and the most used are Kapton, Teflon FEP, Polysulfone, Mylar, Tedlar, PEEK, Halar and Kevlar. As protective coatings (AO): Polycrystalline ceramic films, such as SiOx ($1.9<x<2.0$), SiO2, fluoropolymerfilled SiO2, Al203 and Germanium are proven to be effective in protecting polyimide Kapton.

Although are not used for satellite structures, Kapton films [44], as thermal control blankets were also HVI tested using a laser driven flyer (LDF) systems at velocities up to 2.9 km/s. The damage created was analysed for the low-velocities and high velocities (starting with 1.7 Km/s). The Kapton HN polyimide films used as target had three different thicknesses, 25, 50 and 125 um, in order to reveal the transition from brittle to ductile fracture as the thickness increases, fact explained by the capacity of Kapton film to absorb energy and reduce his strain rate when it became thicker. Moreover, as the velocity increases the fracture morphology is changed indicating a different fracture mechanism that could be explained by high temperature gradient that is created when the flayer hits the polymer target. The paper concluded, that at low velocities a brittle fracture occurs, which become a ductile fracture as the thicknesses increases, and at high velocities is noticed the ductile fracture at the central region of impact and the brittle fracture at the remote areas.

The effect of HVI on polymers is also presented by R. Verker [45], using the same experiments: a laser drive flyer (LDF) to launch projectiles of dimensions ranging from 10 to 100 um at velocities up to 3 Km/s.

Irina Gozaman [46] presents an effective protective solution for coating of Kapton polyamide which is widely used for the external surfaces of spacecraft in low Earth orbit (LEO) and which is exposed to atomic oxygen (AO) and to problems of electrostatic discharge (ESD). The coating, 100-300 nm thick, was deposited on Kapton at near-ambient conditions by LPD using an aqueous solution of a metal-fluoride complex and boric acid. The oxide-coated Kapton was analysed using methods such as; atomic force microscopy (AFM), electrostatic force microscopy (EFM), scanning electron microscopy (SEM), Rutherford backscattering (RBS) and X-ray photoelectron spectroscopy (XPS).

A.A. Voevodin [47] presents a tribological coating concept in order to improve the reliability of satellite systems degraded by the characteristics of the space environment: atomic oxygen, solar radiation, energetic particles, and temperature cycling. The coating is done in order to change the surface chemistry and structure to adapt to the environment. The first coatings were made of WC, WS2, and diamond-like carbon (DLC). The second coatings were made of yittria stabilized zirconia (YSZ) in gold or in Al2O3 matrix, with encapsulated nanosized reservoirs of MoS2 and DLC. The toughness was enhanced using a grain boundary sliding mechanism.

Joo Hyun Han [48] studied multi-walled carbon nanotube (MWNT)/epoxy composites that were fabricated with different nanotube weight percent (wt.%) concentrations exposed to the LEO space environment. The MWNTs (>95% purity), used as filler, were synthesized by CVD, thermal decomposition of hydrocarbon. The diameter and the length of the MWNT used were 10~20 nm and 10~50 um. Epoxy (from HK fiber Co.) used is a copolymer solution composed of acetone, anhydride-type resin and hardener.

An improvement of space debris protection of satellite structures using glassy-rubbery layered block-copolymer nanostructure is presented by Jae-Hwang Lee [49]. The paper presents a microscopic ballistic test using micron-size silica sphere as projectile, shot by an energetic laser pulse and the results showed, depending on the orientation of the layers in the nanocomposite, different responses. But, the compression-dominant response in the perpendicular impact to the layer orientation dissipates the impact energy more efficiently than the impact parallel to the orientation and shows a 30% improvement in penetration depth which was made possible by proper orientation of the layers.

6.2.3 Materials review summary

Our materials review concludes that there is a variety of materials that could be used for the satellites structure and most of these materials are already HVI tested.

These materials depending of the goal that is pursued, design or operational considerations, could be grouped in three large categories:

- Metal alloys such as: aluminum, steel, titanium alloys or newer alloys as beryllium;
- Composites materials, different types of fibers (glass, carbon or aramid fibers) imbedded in a usually matrix (epoxy, ceramic or metallic matrix);
- Honeycomb sandwich panels, with different types of material that are used for facesheets (from different types of alloys to composites) and different cores (honeycomb to ceramic or metallic foam).

A comprehensive review of the materials properties on different groups is made by Francois Cardarelly [50] but information on the satellite material selection are presented by J. Wijker book [51] or C. Annarella [52].

For our HVI test simulations will use LS- DYNA software and we will simulate the impact on one or two materials from each group identified. The simulations targets will be squared 12”x 12” and for all the simulations the projectile used is a sphere of Al 2017 T4 with 0.3125 mm diameter.

The ANNEX attached presents the tables of the most used satellite materials with the main mechanical properties needed in order to perform the HVI test simulations on the materials which characterise each group above mentioned.

6.3 HVI test simulations

6.3.1 Introduction

When we talk about hypervelocity impact of the orbital debris on a spacecraft and about the investigation of the damage performed by such impact, three main approaches are used:

- Tests, generally expensive and are technology limited, the present launchers not covering the entire range of impact velocities reported to the space debris/projectile dimension and form. But having the advantage, for the velocities up to 8-9 km/s, to mimic the real space debris impact;
- Analytical methods, such as ballistic limit equations developed by Cour-Palais [53] and the shield sizing equations developed by Christiansen [54] and Reimerdes [55] or impact damage equations developed by Watts [56]. Generally using assumptions and simplifications and valid for a limited range of situations;
- Numerical/simulation methods derived from experimental data. Could be used for a variety of cases, with special insight for the velocities out of the testing range. The HVI simulations results are influenced by the degree of details used, by the materials models and equation of state. Conventional numerical methods, Eulerian, Lagrangian and Smoothed Particle Hydrodynamics (SPH) or hydrocodes are generally ill suited to address important features of MMOD impact. New methods are proposed by literature, methods that use a parallel hybrid particle –element model, particles will help modeling inertia, contact impact, thermodynamic and compressed states and element modeling the strength effects, tension and elastic-plastic shear. Some of the different models that use the Lagrangian methods

where used by Beneneti [57], Guangyu [58] or Bashurov [59] in order to simulate the impact damage accurately.

Both of the last two methods have to be validated by comparison with the test results.

Using the finite element modeling two different ways are used to describe the material motion in space: Lagrangian grid (body fitted coordinates) or Eulerian grid (fixed in space) and the meshless methods (Lagrangian without grid), also called SPH, Figure 6.2.

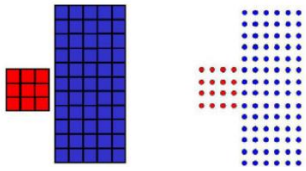

Figure 6.2: Grid based modeling and meshless discretization of a HVI [60]

The following Table 6.3 presents a comparison between the three modeling methods using modeling criteria specific to HVI.

Table 6.3: Lagrangian, Euler and SPH method comparison table

Characteristics/models	**Lagrangian**	**Euler**	**SPH**
History dependent	Yes	No	Yes
Representing high material deformation	No (rezoning, erosion technique)	Yes	Yes
Simulating diffusion and mixing problems	No	Yes	Yes
Accuracy of debris cloud	No	No	Yes
Instability(lack of nodal completeness)	No	No	Yes

SPH modeling is the most promising method in simulating HVI impact but for our simulation, due to various facts as: the impact velocities used (in order to compare with the tests previously performed) that are in the low velocity regime, the limitations of resources (time and computational) and the fact that the criteria related to accuracy are not a priority, we utilise a finite discrete element Lagrangian method similar to the one used by R. Vignjevic [61]. All the simulations were performed using a LS-Dyna student version [62].

6.3.2 Impact numerical formulation

For our simulations we started from the common method used in solving of an engineering problem, the discretization of the impact components through a grid of nodes connected together, and modelling the targets and the projectile using connected grid nodes. In the impact the

connections are broken, the impact propagates and the element remain intact in order to conserve the mass and the momentum.

The Lagrangian finite element grid based method we use is mainly used in structural dynamics and has the following conservation equations:

LAGRANGE

Mass:

$$\dot{\rho} + \rho \frac{\partial u_i}{\partial x_i} = 0$$

Momentum:

$$\dot{u}_i = f_i + \frac{1}{\rho} \frac{\partial \sigma_{ji}}{\partial x_j}$$

Energy:

$$\dot{e} = f_i u_i + p\dot{V} + \frac{1}{\rho} S_{ij} \dot{\varepsilon}_{ij}$$

The projectile and the targets are modeled using 8-node hexahedron solid elements and using one integration point. For the projectile was used a butterfly mesh with an element size similar with target element size in the area of impact.

For the metals material model we chose Johnson Cook model that include a damage and a tensile failure model [63]:

$$\sigma^0 = \left(A + B\left(\varepsilon^p\right)^n\right)\left(1 + C \log\left(\frac{\dot{\varepsilon}^p}{\dot{\varepsilon}_0}\right)\right)\left(1 - \hat{T}^m\right)$$

with

$$\hat{T} = \begin{cases} 0 & for \quad T < T_r \\ \dfrac{T - T_r}{T_m - T_r} & for \quad T_r \le T \le T_m \\ 1 & for \quad T > T_m \end{cases}$$

and ε^p is the equivalent plastic strain.

The model, the most used in finite element modeling, takes in considerations three different effects, strain hardening, viscosity and thermal softening.

The following table, Table 6.4, presents the input materials parameters used for Johnson Cook plasticity model [61, 63].

Table 6.4: Johnson Cook plasticity model parameters for the metals used in simulatio

Material	**Reference density (Kg/m3)**	**Specific heat (J/KgK)**	**Melting temp (K)**	**Room temp (K)**	**A (MPa)**	**B (MPa)**	**n**	**m**	**c**	$\dot{\varepsilon}^0$ (s^{-1})
Al2024-T3	2.77	875	775	300	265	426	0.34	1	0.015	1
Al6061-T6	2.7	885	925	300	324.1	113.8	0.42	1.34	0.002	1
Ti-6Al-4V	4.43	670	1903	300	862	331	0.34	0.8	0.012	1

In order to model the fracture and element deletion we used the Johnson Cook fracture model which compare the effective plastic strain with the failure strain (maximum allowed deformation of an element before is deleted)[64, 65]:

$$\bar{\varepsilon}_f = \left[D_1 + D_2 \cdot exp\left(D_3 \eta\right)\right] \left[1 + D_4 ln\left(\frac{\dot{\bar{\varepsilon}}}{\dot{\varepsilon}_0}\right)\right] \left[1 + D_5\left(\frac{T - T_{room}}{T_m - T_{room}}\right)\right]$$

where Di, i=1 to 5 are input constants (five failure parameters) and η is the stress triaxiality parameter (ratio of the pressure to the effective stress). Determination of the five parameters (Di) involves a series of experimental fracture tests, which would've complicate the simulation procedure and is not within the goal of research. For our work we use values of these parameters already determined, found in literature [57, 66], and we adapted them in order to obtain results in agreement with theoretical penetration limit calculated for each material case.

Knowing the projectile diameter, in determination of the penetration velocities necessary in order to calibrate our models we used the following ballistics equations [67]:

- For Aluminium targets, Cour-Palais semi-infinite plate equations [68] that considers the impact of a spherical projectile into- semi-infinite metallic plate

$$d_c = \left[\frac{t_s}{k} \cdot \frac{HB^{0.25}\left(\rho_s/\rho_p\right)^{0.5}}{5.24\left(V\cos\theta/C\right)^{2/3}}\right]^{18/19} \qquad \text{If } \left(\rho_p/\rho_s\right) < 1.5$$

$$d_c = \left[\frac{t_s}{k} \cdot \frac{HB^{0.25}\left(\rho_s/\rho_p\right)^{3/2}}{5.24\left(V\cos\theta/C\right)^{2/3}}\right]^{18/19} \qquad \text{If } \left(\rho_p/\rho_s\right) \geq 1.5$$

- For Titanium targets, the same equations slightly modified [69]

$$d_c = \frac{t_s}{k} \cdot \frac{HB^{0.25}\left(\rho_s/\rho_p\right)^{0.5}}{5.24\left(V\cos\theta/C\right)^{2/3}}$$

- For carbon fiber reinforced plastic (CFRP), crater formation and shock transmission in multilayer is different to that in metals. We use Schaefer [70] modified equation that uses a single empirically determined material parameter (KCFRP) that summarize the material properties

$$d_c = \frac{t_s\left(\rho_s/\rho_p\right)^{0.5}}{k \cdot K_{CFRP} \cdot \left(V\cos\theta\right)^{2/3}}$$

- For honeycomb panels, we used the Schaefer Ryan Lambert (SRL) triple-wall BLE [71,72] in low velocity range (up to 3 km/s)

$$d_c = \left[\frac{t_w/K_{3S} \cdot \left(\sigma/40\right)^{1/2} + t_b}{0.6\left(\cos\theta\right)^{\delta} \rho_p^{1/2} V^{2/3}}\right]^{18/19}$$

Where:

dc – projectile diameter, for the ballistic limit (cm),

ts - target (shield) thickness (cm),

HB - Brinell hardness (HB),

k - failure coefficient, for perforation is equal with 1.8,

V - projectile velocity (km/s),

ρ - density (g/cm3), p- projectile, s- target,

θ- impact angle measured from target normal to velocity vector (radians),

KCFRP – material constant = 0.62,

K3s - low-velocity coefficient, 1.4 for Al facesheets and 1.1 for CFRP,

t – facesheet thickness (cm), b- bumper, w – rear wall,

σ - Rear wall yield stress (ksi) (Note: 1 ksi = 1,000 lb/in2 = 6.895 MPa),

δ – constant function of impact angle, 4/3 for Al and CFRP at normal impact angle,

C – sound speed.

The following tables summarise the properties and dimensions of materials used in simulation.

Table 6.5: Simulation materials mechanical properties

Material	**Density (g/cm3)**	**Yeld strength (ksi)**	**Sound Speed (km/s)**	**Brinell hardness (HB)**
Al 6061-T6	2,7	40	5,05	95
Al 2024-T4	2,77	47	5,11	120
Ti-15V-3Cr-3Al-3Sn	4,73	181	4,26	257
CFRP	1,38-1,85	59,5		
Ti-6Al-4V	4,43	128		334

Table 6.6: Projectile and target dimensions

Type	**Material**	**Diameter (cm)**	**Thk (cm)**
Projectile	Al2024-T4	0,3175	
Target	Al6061-T6		0,4826
Target	Al6061-T6		0,08128
Target	CFRP		0,3175
Target	Titanium		0,08128
HC/SP facesheets	Al6061-T6		0,08128
HC/SP facesheets	CFRP		0,15875

Using the material characteristics, dimensions and the ballistic equations described above we obtained the following results.

Table 6.7: Calculated velocity for the proposed materials

Material	Thk. (cm)	Projectile diam (cm)	Perforation Vel. (Km/s)
Al6061-T6	0,08128	0,3175	0,13445481
Al6061-T6	0,4826	0,3175	1,945278452
Al6061-T6	0,3175	0,3175	1,03804551
Ti-15V	0,08128	0,3175	0,227968483
Ti- 6Al	0,08128	0,3175	0,401085717
Ti-15V	0,15	0,3175	0,571526214
Ti- 6Al	0,15	0,3175	0,704585179
CFRP	0,3175	0,3175	0,561996833
CFRP	0,15875	0,3175	0,198695886
HC/SP-Al	0,08128	0,3175	0,320567441
HC/SP-CFRP	0,15875	0,3175	0,898928919
HC/SP-CFRP	0,145	0,3175	0,799914848

6.3.3 HVI simulations

6.3.3.1 Introduction

As previously mentioned at the end of Chapter 1, we performed LS-DYNA impact simulations for materials of each of the groups in order to identify distinct characteristics of the impact.

The projectile characteristics are the same for all simulations; Al 2024- T4 is the material and the projectile diameter is 0.3175 cm.

All targets are square rigid sheets, 12 cm x 12 cm fixed around all four edges.

The resultant acceleration is captured at a distance of 3.5 cm from the impact.

6.3.3.2 Aluminium

In order to have a better understanding of impact characteristics, two target thicknesses were used; 0.08128 and 0.3175 cm. Target material was Al 6061–T6 alloy

For the 0.08128 cm thickness, impact velocities were 0.1 km/s, 0.14 km/s and 0.3 km/s. Screen shots of the impacts are presented in Figure 6.3.

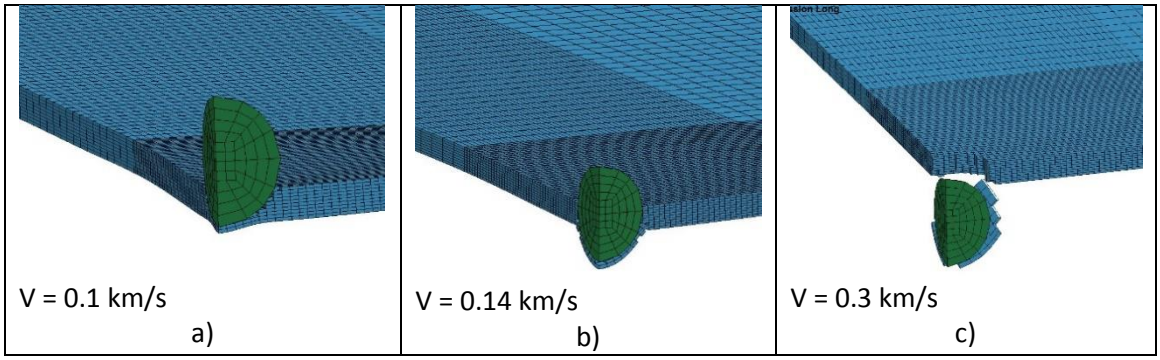

Figure 6.3: Impact simulation on an Al plate of 0.08128 cm thickness: a) non-penetration; b) penetration occur/penetration limit; c) full penetration

The time-frequency analysis Choi–Williams distribution (CWD) shows the following results for the three different velocities. Three types of damage can be identified: a back-face bump, occurrence of cracks/penetration limit and perforation, Figure 6.4.

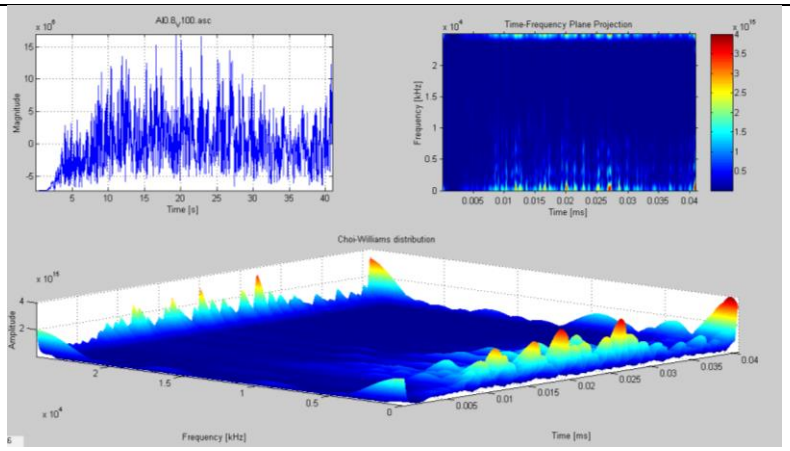

a)

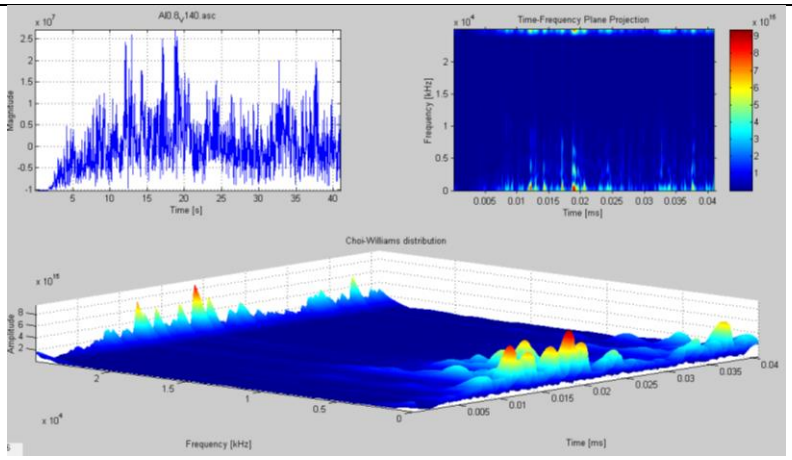

b)

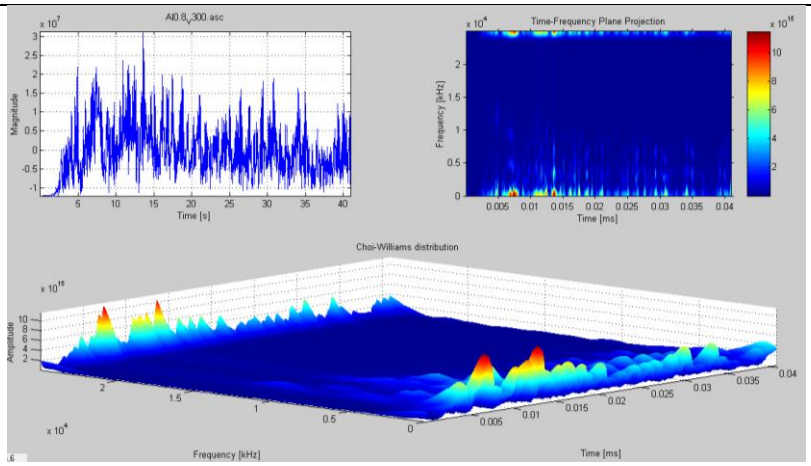

c)

Figure 6.4: CWD for impact on Al6061-T6 of 0.08128 cm thickness: a) non-penetration; b) penetration limit; c) full penetration

The CWD shows that, in the case of a thinner Al target (0.8128 cm thk.) in the non-penetration state (a) a series of frequency peaks occur with amplitudes between 2 to 4 x 1015 in a time range of 0.01 to 0.03 ms. The sensor recorded the first impact wave group, which was followed by different waves reflected back from the lateral edges.

At the penetration limit (b) the frequency amplitude is higher and more compact on a 0.01 ms time interval. This interval is even smaller in the case of full penetration (c) and two individual frequency peaks of 10 x 10^{15} become apparent. These could represent the different impact waves that were captured by the sensor at the moment of impact on the front and back face. In the same moment a series of smaller accentuated frequency peaks are present at the limit of penetration (b)

Identification of the origin of the frequency peaks is not the object of our work. The study of impact wave behavior is a complex process. Some work in this area has been done by Betella [73].

In order to confirm a specific form of the penetration on Al plates a second simulation was made on a thicker target using the same projectile characteristics.

The second target is a 0.3175 cm Al plate. Impact velocities were 0.7 km/s, 0.9 km/s and 1.1 km/s. Screen shots of the impact can be seen in Figure 6.5.

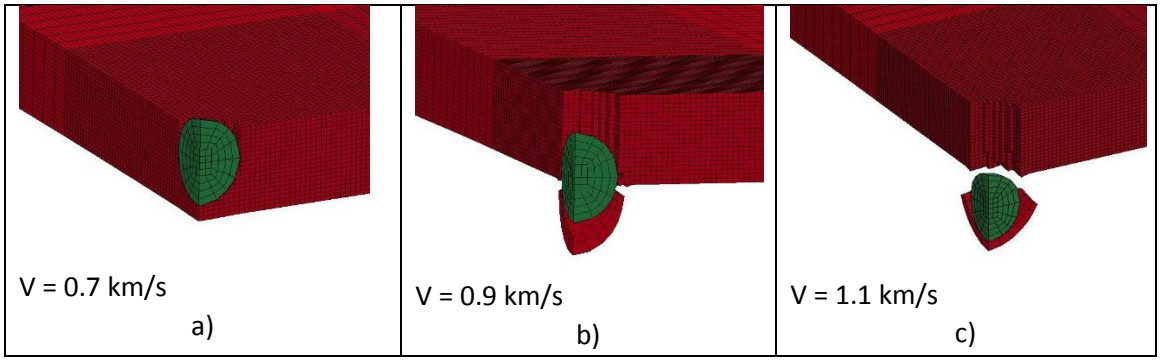

Figure 6.5: Impact simulation on an Al plate of 0.3175 cm thickness: a) non-penetration; b) penetration occur/penetration limit; c) full penetration

The CWD with the corresponding three types of damage are presented in the following figure, Figure 6.6.

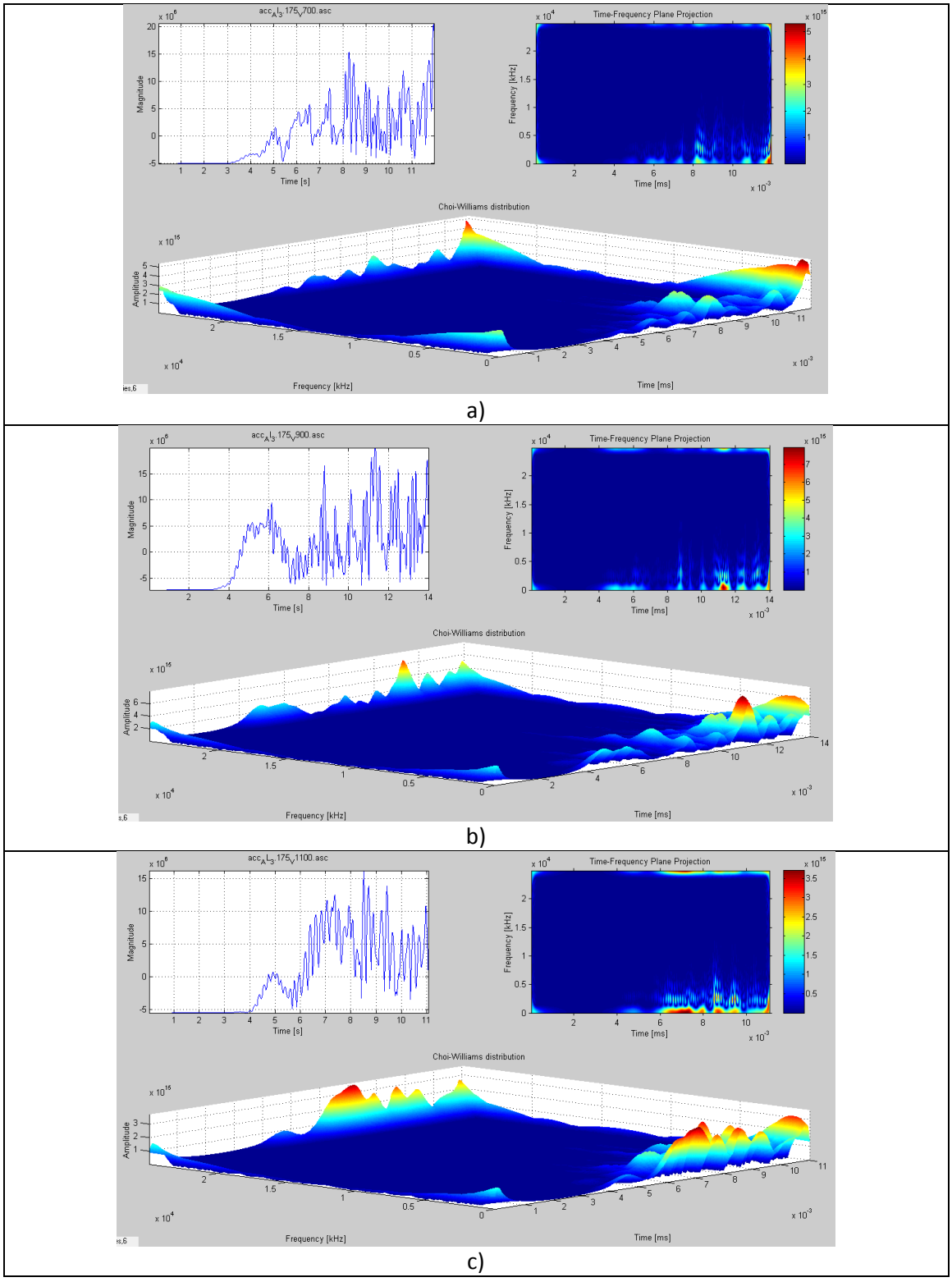

Figure 6.6: CWD for impact on Al6061-T6 of 0.3175 cm thickness: a) non-penetration; b) penetration limit; c) full penetration

For this plate the same non- penetration characteristics are shown on the CWD (a), a series of frequency peaks occur. The peaks have amplitudes from 1.5 to $5x10^{15}$ in a time interval of 5 μs. Both peaks exhibit a slight contour.

The following two states show the corresponding two peaks that define penetration. In the case of full penetration (c), the first peak is more accentuated and reaches a higher frequency amplitude, around 3 - 4 $x10^{15}$.

These simulation results are in good agreement with previously mentioned experimental tests [74]. The large frequency peaks profile recorded for the non-penetration case in the experimental session correspond to the series of frequency peaks obtained in our simulation. Another good correlation between the simulation and testing session was noticed at the level of frequency amplitude for the case of non-penetration on the thicker plate. This amplitude is almost half that obtained for the case of penetration of the thinner target.

The sensor used for the experimental session was not specifically designed for hypervelocity impact; since wave velocities are high the frequency modification and traveling time of the impact wave is very small (μs).

6.3.3.3 Titanium

Titanium is the second metal from the first group of materials used in manufacture of spacecraft. Simulations were carried out using the characteristics of this material in order to have a better analysis of impact and to understand the characteristics of the three types of damage. For our impact model we used Ti-6Al-4V, which is widely used in the aerospace industry and already implemented in LS-Dyna.

We used a 0.08128 cm thickness Ti plate. Impact velocities were 0.4 km/s, 0.5 km/s and 0.7 km/s. A capture of the impact is presented in Figure 6.7.

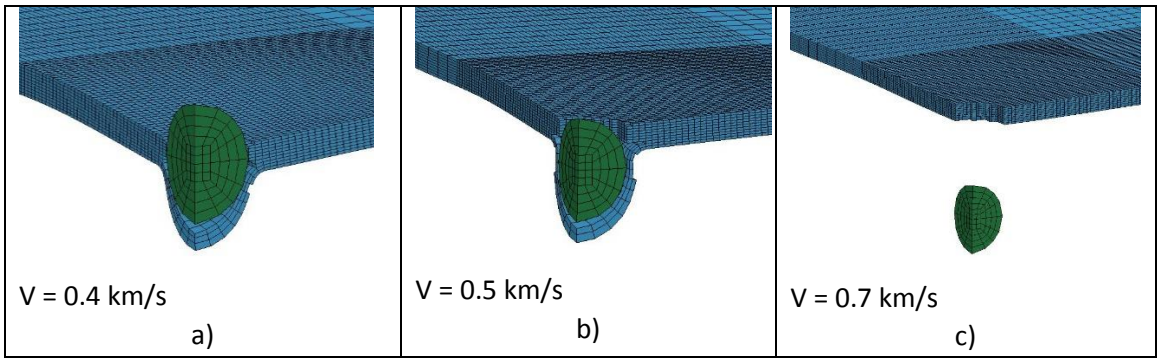

Figure 6.7: Impact simulation on Ti plate of 0.08128 cm thickness: a) non-penetration; b) penetration occur/penetration limit; c) full penetration

The following figure, Figure 6.8, shows the CWD for the three types of damage that occurred on the titanium target.

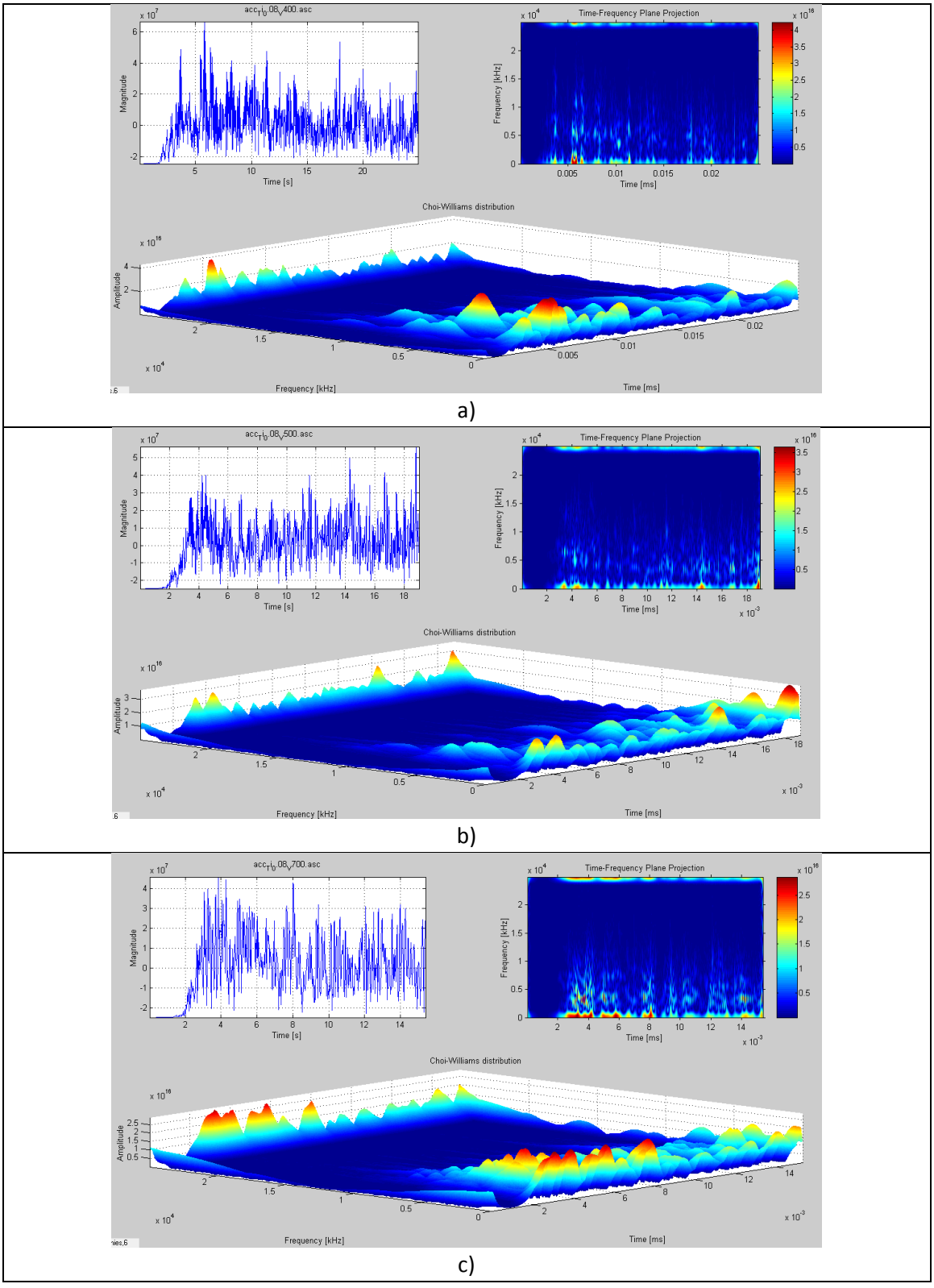

Figure 6.8: CWD for impact on a Ti-6Al-4V target of 0.08128 cm thickness: a) non-penetration; b) penetration limit; c) full penetration

The simulations of impact on titanium plate exhibit a series of similarities with the aluminium simulations. For example the same multitude of frequency peaks occur for the case of penetration (c).

In the no-penetration case (a), a more accentuated frequency peak is recorded with an amplitude of 4 to 5 $x10^{16}$. One particularity for the titanium target is the occurrence of a different frequency value at the recorded peak. Also, for this case we notice a second peak that occurs at the moment of initial impact after 5 μs.

The next two cases, penetration limit (b) and full penetration (c), exhibit the same multitude of frequency peaks at different moments of impact. This appears to be characteristic of Ti targets.

At the moment of full penetration (c) the series of multiple frequency peaks are more accentuated and the peaks seem to group around two or three time moments. A similarity is again noticed with the testing session results; the frequency amplitude of the peaks in the case of penetration is almost half the value recorded for the non-penetration case (a), at a maximum amplitude value of 2.5x 10^{16}.

6.3.3.4 CFRP

For the CFRP target model we used high-strength lightweight carbon fiber, square rigid sheets of 0.3175 cm thickness.

As a mode, a simple bi-directional CFRP was used with all the fibers oriented in the 0o and 90o directions. The result is a CFRP panel with high longitudinal stiffness and lower torsional stiffness, Figure 6.9.

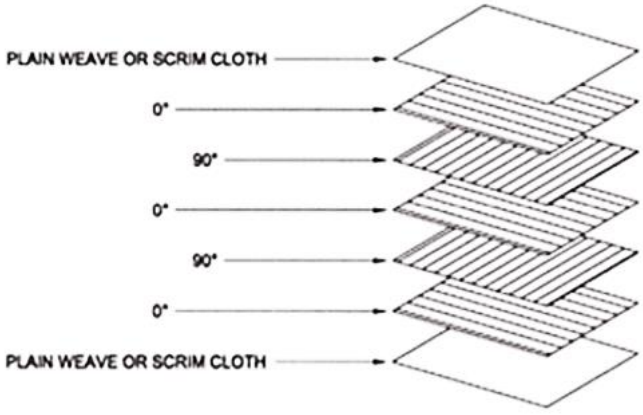

Figure 6.9: Schematics of the fiber layers for one half of the bi-directional CFRP model [42]

The impact velocities on CFRP were 0.6 km/s, 0.8 km/s and 1 km/s. A capture of the impact is presented in Figure 6.10.

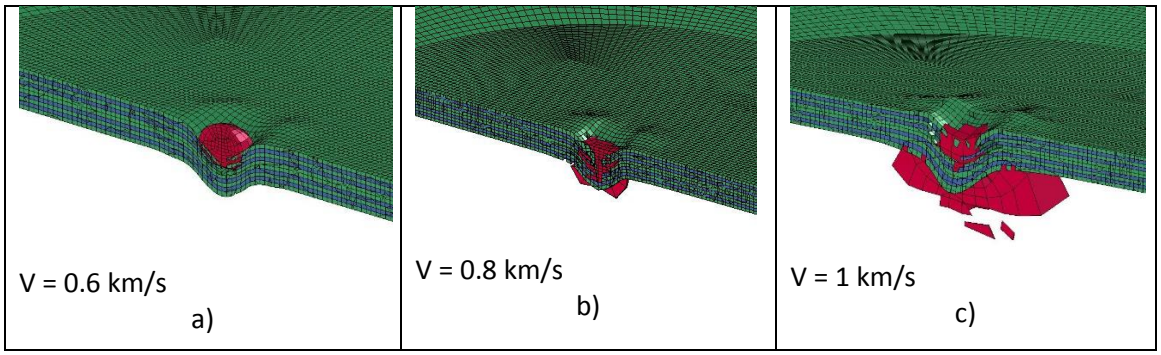

Figure 6.10: Impact simulation on a CFRP plate of 0.3175 cm thickness: a) non-penetration; b) penetration occur/penetration limit; c) full penetration

The following figure, Figure 6.11, shows the CWD for the three types of damage that occurred on the CFRP target.

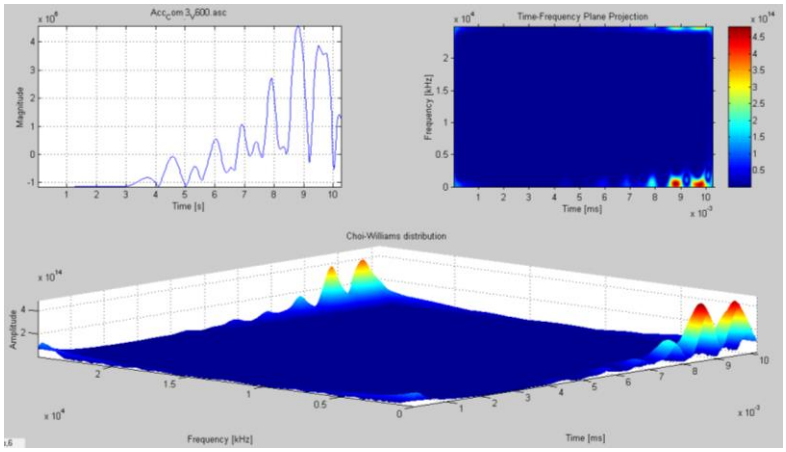

a)

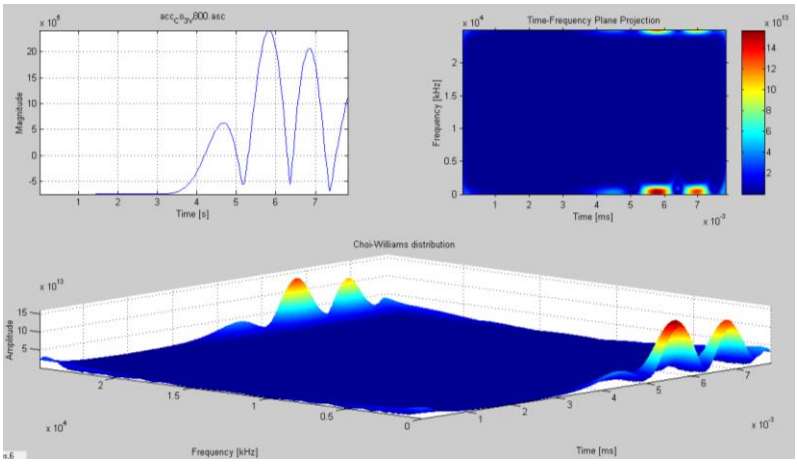

b)

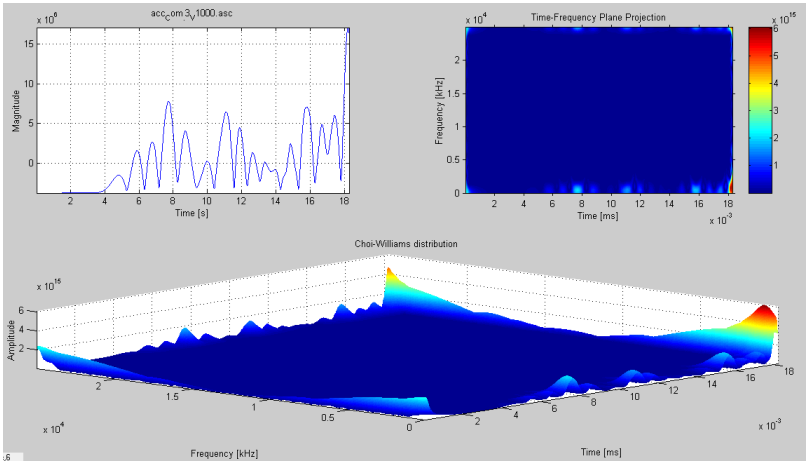

c)

Figure 6.11: CWD for impact on a CFRP plate of 0.3175 cm thickness: a) non-penetration; b) penetration limit; c) full penetration

Due to the characteristics of the material, very little variation in the acceleration was recorded during impact simulation on the CFRP target.

The CWD for the first case of non-penetration (a) shows two very clean frequency peaks at amplitude $4x10^{14}$, each of them with their maximum value in the range of 0.5 μs. A few very small frequency peaks (increasing in amplitude) occur prior to this moment.

The penetration limit (b) signal analysis shows the same two main frequency peaks but the interval on the maximum values is much larger, up to 1 μs. The same characteristics common to penetration damage can be seen. A decrease in frequency amplitude for the second case (b) is seen, the value of this amplitude is $1.5\ x10^{14}$.

The penetration case (c) shows three frequency peaks of maximum amplitude value $2x\ 10^{15}$. These are not well represented, probably because the final period of the simulation shows the impact of a fragment cloud on the target. This fact is not representative of the characteristics of impacts occurring after penetration is complete.

6.3.3.5 Honeycomb panels

Honeycomb panels with Al or CFRP facesheets and Al honeycomb as a material structure are often used for satellites. They are included in this work as an example of the third group of spacecraft materials.

In order to simulate and analyze the impact the HC/SP can be characterized as a dual or triple wall shield structure. In this manner, we use signal analysis of AL or CFRP or analyze the acceleration obtained and considering this material as a spacecraft “material” category.

Due to the increased complexity in modeling the HC/SP, and particularly in modeling the interaction between facesheet and honeycomb material, signal analysis of impacts on HC panels will be the object of future work.

6.4 Analysis summary and discussions

The following table, Table 6.8, presents a summary of HVI simulations made in the low-velocity range on aluminium, titanium and CFRP, all of which are frequently-used materials for satellite structures.

Table 6.8: Summary of CWD analysis on type of damage

Material, thickness (cm)	**Damage type a)Non-penetration b)Penetration limit c) Full penetration**	**Frequency amplitude**	**Shape of the signal, frequency in time and amplitude variation**
Al 6061 –T6 0.08128 See Fig. 4-3	a	$4x10^{15}$	Few dispersed peaks concentrated around 2 – 3 max frequencies
	b	$8x10^{15}$	More grouped peaks
	c	$10x10^{15}$	Fewer peaks concentrated
Al 6061 –T6 0.3175 See Fig. 4-5	a	$5x10^{15}$	Few frequency peaks
	b	$6x10^{15}$	Increase in the no. of peaks
	c	$3x10^{15}$	Multiple peaks, max frequency larger in time
Ti-6Al-4V 0.08128 See Fig.4-7	a	$4x10^{16}$	Few peaks, variation in frequency
	b	$3x10^{16}$	Increase in the no of peaks
	c	$2.5x10^{16}$	Multiple peaks, variation in time and frequency
CFRP 0.3175 See Fig 4-10	a	$4x10^{14}$	Three main peaks
	b	$1.5x10^{14}$	Three main peaks + max frequency on a larger time range
	c	$2x10^{15}$	Three main peaks +Multiple peaks

The summary table provides a clear indication of the two factors that are related to penetration; the shape/form of the recorded signal and the variation of frequency amplitude.

The frequency amplitude decreases for the case of penetration or at penetration limit. As impact velocity increases this amplitude will increase again for aluminium (thick plate), titanium and CFRP. Also, it seems that the value of the decrease in frequency amplitude is half the value of the non-penetration amplitude. But again, the frequency amplitude is related to the impact velocity. A particular case is represented by the thinner aluminium plate, which shows no decrease in amplitude. This behaviour can be attributed to the small variations in velocities that tend to increase the frequency amplitude.

The second indication of penetration is the form of the signal. For all cases of penetration an increase in the number of frequency peaks is noted. Titanium, the strongest material, presents the largest number of peaks in time and also in the frequency range.

The LS-Dyna simulation model we used is limited due to software and time constraints and could be improved to be better suited for modeling hypervelocity impacts, not only in the lower velocity regime but also in higher velocity regimes where phase transformations of materials occur.

Calibration of the model was based only on theoretical calculations of the penetration velocities. Further calibration of models should include a series of experimental testing.

The simulation results clearly showed that, based on accelerations obtained during a series of impact simulations, different distinct penetration characteristics can be identified for each of the materials studied. The in-house TF-Analysis software was adequate to reveal this distinction. All of the materials studied are frequently used in current satellite structures.

This research definitely provides the premise that could lead to automation of the process and the creation of a viable real-time impact health monitoring system for satellites that is capable of identifying penetration due to high velocity impact of micrometeoroids and space debris for an extensive database of materials.

6.5 Conclusions and future work

This work presents the HVI simulation portion of an overall research project which has been undertaken to achieve a specific goal: development of a real-time detection tool capable of quantifying the damage created by micrometeoroid and orbital debris impacts on a spacecraft. The impact simulations were made using a student version of LS-Dyna software, a general-purpose finite element program capable of simulating transient dynamics problems, which are typically encountered when simulating hypervelocity impacts.

In order to select the materials for our simulations, an extensive review was made of the types of materials that are used in the manufacture of spacecraft. This review led to the identification of three main material groups. Representatives of these groups were studied during our simulations. Due to time constraints and complexity of the model, simulations on a material from the third group, sandwich panel materials, were not made. This will be studied in a future work.

Hypervelocity impact simulations were performed on targets made of aluminum (two different thicknesses; 0.08128 and 0. 3175 cm), titanium (0.08128 cm) and CFRP (0.3175 cm). The resulting accelerations were captured using a virtual sensor mounted 3.5 cm from the point of impact on the back face of the target. All targets were square rigid plates 12cm x 12cm fixed around all four edges.

The resulting acceleration signals were further analyzed using TF-Analysis software developed in-house. This software offers a wide range of analysis methods. This Time-Frequency analysis of

signals was carried out using the Choi –Williams distribution method, a method that has been previously used in literature to analyze impact vibrations [75, 76].

Time-Frequency analysis clearly shows that, for aluminium, titanium and CFRP materials, amplitude of the frequency signal decreases upon occurrence of perforation. At the same time the form of the CWD is different for each type of material. For aluminium, a decrease in amplitude from 5-6x1015 to 3x1015 is seen in the case of perforation. For titanium the amplitude drops from 4x1016 to 2-2.5x1016, and for CFRP it decreases from 3-4x1014 to 1.5x1014. These values are also an indication of the rigidity of these materials. Titanium, the most rigid material simulated, exhibits a frequency amplitude (in the case of penetration) 100 times higher than CFRP. The value of frequency amplitude obtained using the time-frequency analysis also indicates the most resistant material to impact (in correlation with the perforation velocities).

The second particular characteristic for each material is the form of the CWD in the case of penetration. Although all materials showed a multiplication of the frequency amplitude peaks upon perforation, each capture exhibits different forms. The penetration of aluminium showed multiple peaks grouped together on a shorter time interval. The maximum intensity of the frequency is largest, up to 2 μs. For the penetration of titanium the time interval of the frequency peaks is largest with the most obvious frequency variations. The perforation of CFRP shows the smallest number of frequency peaks (approximately three frequency peaks).

The simulation results are in good agreement with measurements previously made during HVI tests [74, 77]. Using a sensor, not necessarily fit for HVI, these experimental test results showed the same decrease in frequency amplitude for the case of penetration, up to half of the maximum amplitude. The highest frequency amplitude recorded was higher for the most rigid material, and had a unique, particular shape of CWD for each material tested.

These two results obtained independently, from numerical simulation and physical tests are clearly an indication that a material database can be established for each of materials from the groups identified at the end of the Chapter 1. However, a larger number of HVI tests are necessary together with the refinement of the simulation model.

Further investigation in this direction is needed, but this proposed work represents only a starting point towards automatic classification of different types of impact damage (especially perforation) on different materials. This can be done by processing images using Fourier descriptors and neural

networks, with the end goal of creating a real-time micrometeoroid and space debris health monitoring system.

Completion of future work requires a larger number of simulations and HVI tests. For HVI tests, an increase in velocity of testing is needed to cover medium and high impact velocity ranges. The choice of the test facility will influence the quality of results. Ideally, we need to eliminate the second impact from the sabot, improve the acquisition system, and improve the sensoring method. These improvements will lead to better results that will also help in calibrating the simulation model.

For HVI simulation in the higher velocity regime the use of SPH is highly recommended in order to capture the phase transformation of the material from solid to liquid and vapor and to obtain a signal that closely mimics the reality of HVI.

Further development of the TF-Analysis software [78, 79] will also be needed for more efficient extraction of the features of the HVI signals and to create results that are more user-friendly and compatible with other specific software.

The most important result of this work is that the use of Time-Frequency analysis in identifying HVI damage for different types of materials opens the door for other research, ultimately leading to the automation of HVI damage detection on spacecraft.

6.6 Acknowledgment

This research work has been made possible by precious support of a collaborative research and development grant from the Natural Sciences and Engineering Research Council of Canada (NSERC)(No.8482) and the Fonds de recherche du Québec - Nature et technologies (FRQNT).

6.7 Bibliography

[1] William P. Schonberg, “Protecting earth-orbiting spacecraft against micro-meteoroid/orbital debris impact damage using composite structural systems and materials: An overview”. *Advances in Space Research* 45 (2010) 709–720

[2] Schonberg, W.P, “Hypervelocity impact response of spaced composite material structures”. *Int. J. Impact Eng.* 10, 509–, 1990.

[3] Schonberg, W.P., Walker, E.J., “Use of composite materials in multi-wall structures to prevent perforation by hypervelocity projectiles”. *Compos. Struct.*19, 15–, 1991.

[4] Roberto Destefanis, Frank Schäfer, Michel Lambert, Moreno Faraud, Eberhard Schneider, “Enhanced space debris shields for manned spacecraft”. *International Journal of Impact Engineering*, Volume 29, Issues 1–10, December 2003, Pages 215–226

[5] Wan, H; Bai, SX; Li, S; Mo, JJ; Zhao, SC; Song, ZF, “Shielding performances of the designed hybrid laminates impacted by hypervelocity flyer”. *MATERIALS & DESIGN*, 12/2013, Volume 52

[6] G. S. Guan, Q. Bi, Y. Zhang, “Research of Performance about Ceramic Coating on Aluminum Bumper to Resist Hypervelocity Impact”. *Key Engineering Materials*, Vols 577-578, pp. 629-632, Sep. 2013

[7] Gong, WW; Liu, Y; Zhang, X; Ma, HL, “Numerical Investigation on Dynamical Response of Aluminum Foam Subject to Hypervelocity Impact With Material Point Method”. *CMES-computer modeling in engineering & sciences*, 02/2012, Volume 83, No. 5

[8] Ma, ZT; Bin, J; Pang, BJ, “Behavior of aluminum foams under hypervelocity impact: Validation of numerical simulation”. *Advanced engineering materials*, 10/2007, Volume 9, Numéro 10

[9] Ping Liu, Yan Liu, Xiong Zhang, “Internal-structure-model based simulation research of shielding properties of honeycomb sandwich panel subjected to high-velocity impact”. *International Journal of Impact Engineering*, Volume 77, March 2015, Pages 120–133

[10] E.A. Taylor, M.K. Herbert, B.A.M. Vaughan, J.A.M. McDonnell, “Hypervelocity impact on carbon fibre reinforced plastic/aluminium honeycomb: comparison with Whipple bumper shields”. *Int. J. Impact Eng.*, 23 (1) (1999), pp. 883–893

[11] E.A. Taylor, J.P. Glanville, R.A. Clegg, R.G. Turner, “Hypervelocity impact on spacecraft honeycomb: hydrocode simulation and damage laws”. *Int. J. Impact Eng.*, 29 (1–10) (2003), pp. 691–702

[12] R.J. Turner, E.A. Taylor, J.A.M. McDonnell, H. Stokes, P. Marriott, J. Wilkinson, et al., “Cost effective honeycomb and multi-layer insulation debris shields for unmanned spacecraft”, *Int. J. Impact Eng.*, 26 (1–10) (2001), pp. 785–796

[13] J.-M. Sibeaud, L. Thamie, C. Puillet, “Hypervelocity impact on honeycomb target structures: Experiments and modeling”. *International Journal of Impact Engineering* 35 (2008) 1799–1807

[14] S. Ryan, T. Hedman, E.L. Christiansen, “Honeycomb vs. foam: Evaluating potential upgrades to ISS module shielding”. *Acta Astronautica* Volume 67, Issues 7–8, October–November 2010, Pages 818–825

[15] Colombo, P., Arcaro, A., Francesconi, A., Pavarin, D., Rondini, D., Debei, S., “Effect of hypervelocity impact on microcellular ceramic foams from a preceramic polymer”. *Adv. Eng. Mater*. 5(11), 802–805, 2003.

[16] Pilseong Kang, Sung-Kie Youn, Jae Hyuk Lim, “Modification of the critical projectile diameter of honeycomb sandwich panel considering the channeling effect in hypervelocity impact”. *Aerospace Science and Technology*, Volume 29, Issue 1, August 2013, Pages 413–425

[17] William Schonberg, Frank Schäfer, Robin Putzar, “Hypervelocity impact response of honeycomb sandwich panels”. *Acta Astronautica*, Volume 66, Issues 3–4, February–March 2010, Pages 455–466

[18] J. Warren, M. Cole, et al., “Hypervelocity impact of honeycomb core sandwich panels filled with shear thickening fluid”. 28th Technical Conference of the American Society for Composites, State College, 2013

[19] Eldon P. Kasl, “Lessons Learned in Modular Bus Structure Development for the LADEE Mission”. Reinventing Space Conference October 14-17, 2013, Los Angeles, CA

[20] S. Ryan, F.K. Schaefer, R. Destefanis, M. Lambert, “A ballistic limit equation for hypervelocity impacts on CFRP/Al HC satellite structures”. *Advances in Space Research*, 41 (2008), pp. 1152–1166

[21] Thompson, T. C., Grastataro, C., Smith, B. G., Krumweide, G. and Tremblay, G., “Development of an all-composite spacecraft bus for small satellite programs”. In Proceedings from The Eighth Annual AIAA/USU Conference on Small Satellites, Logan, UT, 1994

[22] M. Nicoletto, D. Boschetti, P. Savi, "High Speed Digital Lines routed on non-metallic Spacecraft structures". Proc. of the 2014 International Symposium on Electromagnetic Compatibility (EMC Europe 2014), Gothenburg, Sweden, September 1-4, 2014

[23] Changqing, Miao; Bo, Liu, "Experimental Study on the Behavior of a New Multilayer Shield against Hypervelocity Debris Impact". *Polymers & Polymer Composites* 22.2 (2014): 99-103.

[24] Offenberger, Sean; Warren, Justin; Lacy, Thomas E.; Ostaz, Ahmed Al; Toghiani, Hossein; Kundu, Santanu; Pittman Jr., Charles U.; Li, Xiaobing; Mansrah, Al-Harith, "Novel composite shielding concepts for hypervelocity orbital debris impact mitigation". 55th AIAA/ASMe/ASCE/AHS/SC Structures, Structural Dynamics, and Materials Conference

[25] Aleksandr Cherniaev, Igor Telichev, "Meso-scale modeling of hypervelocity impact damage in composite laminates". *Composites Part B: Engineering*, Vol. 74, 1 June 2015, Pages 95–103

[26] Q. Guo, D.L. Sun, L.T. Jiang, X.L. Han, G.Q. Chen, G.H. Wu, "Residual microstructure associated with impact craters in TiB2/2024Al composite". *Micron* Volume 43, Issues 2–3, February 2012, Pages 344–348

[27] A.H.Baluch, C.G.Kim, J.B.Moon, and G. Lim, "Behavior of carbon-epoxy composite for hypervelocity impacts at oblique angle on spacecraft in low earth orbit environment". 18th International Conference on Compsite Materials. August 21-26, 2011: Jeju- Korea

[28] Cheng, Wing L; Langlie, Scott; Itoh, Shigeru, "High velocity impact of thick composites". *International Journal of Impact Engineering*, 2003, Volume 29, Number 1

[29] B. Aïssa ; E. Haddad ; K. Tagziria ; W. Jamroz ; M. Asgar-Khan ; S. V. Hoa ; J. Verreault ; A. Higgins ; D. Therriault, "Exploring self-healing of CFRP laminates exposed to hypervelocity small pellets simulating space debris". 26th Annual Technical Conference of the American Society for Composites 2011 and the 2nd Joint US-Canada Conference on Composites

[30] OLEG V. STARTSEV and V. V. ISUPOV, "The Gradient of Mechanical Characteristics across the Thickness of Composite Laminates After Exposure to a Low Earth Orbit Environment". *Polymer Composites*, Volume 19, Issue 1, pages 65–70, February 1998

[31] Lei Wang, T. Sui, W. Lin, “Fatigue damage accumulation model and fatigue life predication of composite laminate TT300/ epoxy-resin”. Conference: 2011 International Conference on Advanced Materials and Computer Science, ICAMCS 2011

[32] Hoffman, C.N.; Snyder, B.A.; Dean, M.W., “Development of a composite (K1100/CE) satellite bus structure”. Conference: 41. International symposium of the Society for the Advancement of Material and Process Engineering and exhibition: materials and processes challenges - aging systems, affordability, alternative applications, Anaheim, CA (United States), 25-28 Mar 1996

[33] Lee Hamill, Scott Roberts, Marc Davidson, William L. Johnson, Steven Nutt and Douglas C. Hofmann, “Hypervelocity Impact Phenomenon in Bulk Metallic Glasses and Composites”. *Advanced engineering materials* 2014, 16, No. 1

[34] Marc Davidson, Scott Roberts, Gerhard Castro, Robert Peter Dillon, Allison Kunz, Henry Kozachkov, Marios D. Demetriou, William L. Johnson, Steve Nutt and Douglas C. Hofmann, “Investigating Amorphous Metal Composite Architectures as Spacecraft Shielding”. *Advanced engineering materials* 2013, 15, No. 1—2

[35] Douglas C. Hofmann,Lee Hamill, Eric Christiansen and Steve Nutt, “Hypervelocity Impact Testing of a Metallic Glass-Stuffed Whipple Shield”. *Advanced engineering materials*, Feb.2015

[36] S. Katz, E. Grossman, I. Gouzman, M. Murat, E. Wiesel, H.D. Wagner, “Response of composite materials to hypervelocity impact”. *International Journal of Impact Engineering*, Volume 35, Issue 12, December 2008, Pages 1606–1611

[37] Eric P. Fahrenthold, Young-Keun Park, “Simulation of hypervelocity impact on aluminum-Nextel-Kevlar orbital debris shields”. *International Journal of Impact Engineering*, Volume 29, Issues 1–10, December 2003, Pages 227–235

[38] Grosch, Donald J, “Inhibited Shaped Charge Launcher Testing of Spacecraft Shield Designs”. Apr 24, 1997, Southwest Research Inst.; Materials and Structures Div.; San Antonio, TX, US

[39] Richard R. Burt, Eric L. Christiansen, “Hypervelocity impact testing of transparent spacecraft materials”. *International Journal of Impact Engineering*, Volume 29, Issues 1–10, December 2003, Pages 153–166

[40] SONG LiHong, WEI Qiang, BAI Yu & GAO Cheng, "Impact effects on fused quartz glass by ground simulating hypervelocity space debris". Science China, Technological Sciences, Science China, March 2013 Vol.56 No.3: 724–731

[41] X. Huang, Z. Lina, Z.D. Liu, H.S. Zhang, L.H. Dai, "Amorphous alloy reinforced Whipple shield structure". *International Journal of Impact Engineering*, Vol. 42, April 2012, Pages 1–10

[42] Materion, http://materion.com/Markets/DefenseandScience/SpaceScienceandAstronomy/SpaceStructuresandSatellites.aspx

[43] Serhan Avcu, Bilgin Celd, "Structural Material Selection and Processing for Low Earth Orbit Spacecraft Regarding Atomic Oxygen Effects". Conference: Recent Advances in Space Technologies, 2003. RAST '03

[44] Grossman, E; Eliaz, N; Gouzman, I, "Ground simulation of hypervelocity space debris impacts on polymers, protection of materials and structures from the space environment", *Protection of Materials and Structures from Space Environment*, 153-165, 2006

[45] R. Verker, N. Eliaz, I. Gouzman, S. Eliezer, M. Fraenkel, S. Maman, F. Beckmann, K. Pranzas, E. Grossman, "The effect of simulated hypervelocity space debris on polymers". *Acta Materialia*, Volume 52, Issue 19, 8 November 2004, Pages 5539–5549

[46] Irina Gouzman, Olga Girshevitz, Eitan Grossman, Noam Eliaz and Chaim N. Sukenik, "Thin Film Oxide Barrier Layers: Protection of Kapton from Space Environment by Liquid Phase Deposition of Titanium Oxide". *Applied materials and interfaces*, VOL. 2, NO. 7, 1835–1843, 2010

[47] A.A. Voevodin, J.S. Zabinski, "Nanocomposite and nanostructured tribological materials for space applications". *Composites Science and Technology*, Volume 65, Issue 5, April 2005, Pages 741–748

[48] Joo Hyun Han, Sang Eui Lee, Won Jun Lee, and Chun Gon Kim, "Space environment characteristics of MWNT/epoxy composites". Conference: 49th International SAMPE Symposium and Exhibition: Materials and Processing Technology - 60 Years of SAMPE Progress, SAMPE 2004

[49] Jae-Hwang Lee, David Veysset, Jonathan P. Singer, Markus Retsch, Gagan Saini, Thomas Pezeril, Keith A. Nelson, Edwin L. Thomas, "High strain rate deformation of layered nanocomposites". *Nature Communications*, Vol3 (Oct 2012)

[50] Francois Cardarelli, *Materials Handbook, A Concise Desktop Reference*, Springer-Verlag London, 2008

[51] J. Wijker, *Spacecraft Structures*. Springer-Verlag Berlin Heidelberg, 2008

[52] Annarella, C., 9 *Spacecraft Structures*, 1991

[53] Cour-Palais, B.G., "Hypervelocity impacts in metals". *International Journal of Impact Engineering* 5:221–238, 1986

[54] Christiansen, E.L., R. Bernhard, J. Hyde, J. Kerr, K. Edelstein, J. Ortega, and J. Crews. 1993, "Assessment of high velocity impacts on exposed shuttle surfaces". Pp. 447–452 in Proceedings of the First European Conference on Space Debris, Darmstadt, Germany, 5–7 April 1993. Darmstadt: European Space Operations Center.

[55] Reimerdes, H.-G., K.-H. Stecher, and M. Lambert, "Ballistic Limit Equations for the Columbus-Double Bumper Shield Concept". ESA SD-01, Proceedings of the First European Conference on Space Debris, Darmstadt, Germany, 1993.

[56] Watts, A., D. Atkinson, and S. Rieco, "Dimensional Scaling for Impact Cratering and Perforation". NASA NCR-188259. March 16, 1993, Houston, Texas: National Aeronautics and Space Administration Johnson Space Center.

[57] Bennetti, A., "Numerical and experimental investigation of high velocity impacts for spacecraft protection". MSc Thesis, Cranfield University, 2002.

[58] Guangyu, S. Junyan, G and Chun, L., "Efficient modeling of panel-like targets in perforation simulation", Third European LS-Dyna User Conference, Paris, 2001.

[59] Bashurov, V. V. et al., "Experimental modelling and numerical simulation of high- and hypervelocity space debris impact to spacecraft shield protection". *International Journal of Impact Engineering*, Vol. 20, pp. 69-78, 1977

[60] WG3, IADC-04-03, *Protection manual*, Version 7.0, September 19, 2014.

[61] Rade Vignjevic, James Campbell, Séverine Lepage, “Numerical Simulation of High Velocity Impacts on Thin Metallic Targets I”. Crashworthiness, Impact and Structural Mechanics (CISM) Cranfield University, UK, Conference paper, 2004

[62] LS-DYNA, *Keyword user's manual*. VOLUME I. May 2007. Version 971. LIVERMORE SOFTWARE TECHNOLOGY CORPORATION (LSTC)

[63] Yancheng Zhang, J.C. Outeiro, Tarek Mabrouki, “On the Selection of Johnson-cook Constitutive Model Parameters for Ti-6Al-4 V Using Three Types of Numerical Models of Orthogonal Cutting”. Procedia CIRP, Volume 31, 2015, Pages 112–117, 15th CIRP Conference on Modelling of Machining Operations (15th CMMO)

[64] Hallquist, J. O., *LS-DYNA Theoretical Manual*, Livermore Software Technology Corporation, 1998.

[65] Johnson GR, Cook WH, “A constitutive model and data for metals subjected to large strains, high strain rates and high temperatures”. In: Proc. 7th Int. Symp. On Ballistics, Hague, Netherlands, April 1983; 541–547.

[66] Vignjevic, R., Hughes, K. and Taylor E.A., “Finite element modelling of failure of a multi-material target due to high velocity space debris impacts”. *Space Debris*, Vol. 2, pp. 41-50, 2002.

[67] Shannon Ryan, Eric L. Christiansen, “Micrometeoroid and Orbital Debris (MMOD) Shield Ballistic Limit Analysis Program”. NASA/TM–2009–214789.

[68] B.G. Cour-Palais, “Hypervelocity Impact Investigations and Meteoroid Shielding Experience Related to Apollo and Skylab”. Orbital Debris Workshop, NASA CP-2360 (pp.247-275), Houston, August 27–29, 1982.

[69] E.L. Christiansen, E Cykowski, J Ortega, “Highly Oblique Impacts into Thick and Thin Targets”. Int. J. Impact Eng., 14: 157-168, 1993.

[70] F. Schaefer, E. Schneider, M. Lambert, “Review of Ballistic Limit Equations for CFRP Structure Walls of Satellites”. 5th International Symposium on Environmental Testing for Space Programmes, ESA SP-558, Noordwijk, June 15–17, 2004.

[71] S. Ryan, F. Schaefer, R. Destefanis, M. Lambert, "A Ballistic Limit Equation for Hypervelocity Impacts on Composite Honeycomb Sandwich Panels Satellite Structures". *Adv. Space Res*., 41(7):1152–1166, 2008.

[72] F. Schaefer, S. Ryan, M. Lambert, R. Putzar, "Ballistic Limit Equation for Equipment Placed Behind Satellite Structure Walls". Hypervelocity Impact Symposium, Williamsburg, Va., September 23–27, 2007.

[73] A. Bettella, A. Francesconi, D. Pavarin, C. Giacomuzzo, F. Angrilli, "Application of Wavelet Transform to analyze acceleration signals generated by HVI on thin aluminum plates and all-aluminum honeycomb sandwich panels". *International Journal of Impact Engineering* 35 (2008) 1427–1434.

[74] Iliescu, L. E., Lakis, A. A. & Oulmane, A., "Hypervelocity impact (HVI) signal analysis", *European Journal of Engineering and Technology,* Vol. 4 No. 1, 2016, ISSN 2056-5860

[75] M. A. Hamstad, "Comparison of Wavelet transform and Choi-Williams distribution to determine group velocities for different acoustic emission sensors". *J. Acoustic Emission*, 26, 2008, 40-59.

[76] Howard A. Gaberson, "Application of Choi-Williams reduced Interference time frequency distribution to machinery diagnostics". *Shock and Vibration*, Vol. 2, No. 6, pp 437-444, 1995.

[77] L. E. Iliescu, A. A. Lakis, A. Abou – Antoun, "Hypervelocity Impact (HVI) Tests & Signal Recordings", *Universal Journal of Aeronautical & Aerospace Sciences* 2 (2014), 80-113.

[78] Mahvash, A., Lakis A.A., 2014, "Independent Component Analysis as Applied to Vibration Source Separation and Fault Diagnosis". Journal of vibration and control, online: August 2014, DQI: 10.117/107756314544349

[79] Oulmane, A.A. Lakis and N. Mureithi. 2013, "A Method for Analyzing Rotating Machinery Faults using Time-Frequency Application". *International Journal of Condition Monitoring and Diagnostic Engineering Managemen*t Volume 16 No2, April 2013 pages 21-34.

CHAPTER 7 GENERAL DISCUSSION

These final three chapters present the fundamental research work done to develop a health monitoring system for spacecraft structures/shields. By combining TF analysis and information from a dictionary of materials used in the manufacture of satellites the system should identify, in real time, the damage created by an MMOD impact.

During the experimental session HVI tests were performed successfully at low impact velocity, up to 1.6 km/s. Although this velocity range is not very representative of MMOD velocities, it was sufficient to obtain valid signal recordings for a preliminary TF analysis, a cornerstone of our future work in this area. In order to create a fully functional system, essential next steps will include further high velocity tests with the same gun, obtaining better precision in velocity and sabot separation and, most importantly, new HVI tests at velocities ranging from 4.5- 5 km/s to 8 Km/s, velocities relatively close to those of actual MMOD impact.

TF analysis of the signals recorded during the HVI tests provided valid information such as identifying the more rigid of the two materials tested; CFRP and Al. This can be recognized because the frequency amplitudes of the Al signals were higher than those obtained for CFRP. In addition, for the same material, the frequency amplitudes of the signal are extremely different depending on the type of damage. The signal amplitudes for non-penetration were almost double those obtained for the case of penetration.

TF analysis of the HVI numerical simulation revealed the same results as the analysis done on the signals obtained in the experimental session. The same decrease in frequency amplitude was observed for the HVI done at the limit of penetration, for two metal alloys Al and Ti and also for CFRP.

In future work, results from this research should be validated by a larger number of HVI tests and TF analysis for different spacecraft materials identified. Once this data is gathered, it will constitute a basis for the creation of an automatic process that will automatically recognize the damage for different materials used in space.

In general terms, TF analysis provides clear characteristics, the frequency amplitude and different shapes of CWD to distinctly identify HVI damage.

This new knowledge serves as a basis for future investigation and constitutes a starting point for development of a real-time MMOD health monitoring system.

CHAPTER 8 CONCLUSION AND RECOMMENDATIONS

Originality of this research is derived from the development of an integrated system that will monitor in real time or near-real time the degradation of spacecraft shields or structure.

This constitutes advancement in this area of research because previous development focused only on impact detectors or sensors using different principles that were proposed and developed for specific types of space missions.

Future research will establish and directly implement TF distributions and statistical methods to identify damage in complex protection systems through all phases of the process from diagnostics and classification to decision making.

The final design guideline will be to have a sufficient amount of spacecraft/shied material tested in order to create a comprehensive material dictionary. The material dictionary that not only will lead to the automatic detection of damage but also will be a reference in creation of new protection systems with better shielding capacity.

The developed system will make use of a series of software algorithms that can be further developed and adapted to other different types of protection systems.

The adaptive characteristic of the proposed structural health monitoring system will also make it suitable for off-board utilization. Impact data could be recorded during flight and collected when the aircraft is on the ground. In an off-board system, only the sensors will be permanently installed on board the aircraft; the hardware and software will be on the ground and connected to the aircraft during inspection.

The development of an integrated intelligent health monitoring system is a crucial activity for the design and survival of space missions, especially where human safety is concerned.

The proposed system is a crucial part of the development of the space sector, applied to the area of space debris impact protection. It could also benefit other space activities such as calibration of dust models and planning of spacecraft maintenance.

Inspection, repair schedules and planning of extravehicular activities are directly influenced by information gathered during real time monitoring of impact degradation of the shielding.

The proposed system for detection, prediction, and mitigation of the effects of impacts will save lengthy and unnecessary downtime for repair and maintenance.

Further benefits will be gained in diverse sectors of the economy. These will increase Canadian global competiveness, improve national security and quality of life, and will boost the development and operation of civil and military aerospace systems.

The proposed HMS can be used in modified versions across a diverse range of industries from aerospace, civil (e.g. monitoring an aging infrastructure), energy (e.g. wind turbine components), automobile (e.g. hidden damage) to defence applications (e.g. protective vehicle armour).

BIBLIOGRAPHY

AÏSSA, B. et al, *Exploring self-healing of CFRP laminates exposed to hypervelocity small pellets simulating space debris*. 26th Annual Technical Conference of the American Society for Composites 2011 and the 2nd Joint US-Canada Conference on Composites

AÏSSA, B. et al. *Monitoring with Fiber sensors and Self-Healing of CFRP Laminates Exposed to Hypervelocity Small Pellets Simulating Space Debris*, 12th International Symposium on Materials in the Space Environment (IMSE-12) 24-28 September 2012.

AKAHOSHI, Y. et al, *Development of bumper shield using low density materials*. International Journal of Impact Engineering 26 (2001) 13-19

ANDRADE, F. A. et al, *Gearbox fault detection using statis-tical methods, time-frequency methods (STFT and Wigner-Ville distribution) and harmonic wavelet - A comparative study*. 12th International Congress on Condition Monitoring and Diagnostic Engineering Management (COMADEM'99). 1999. 77-85.

Annarella, C., 9 Spacecraft Structures, 1991

AVCU, S., CELD, B., *Structural Material Selection and Processing for Low Earth Orbit Spacecraft Regarding Atomic Oxygen Effects*. Conference: Recent Advances in Space Technologies, 2003. RAST '03

BAE Systems, http://www.baesystems.com/article/BAES_175799/aircraft-set-to-become-more-human-as-engineers-develop-smart-skins-which-can-detect-injury

BALUCH, A.H. et al, *Behavior of carbon-epoxy composite for hypervelocity impacts at oblique angle on spacecraft in low earth orbit environment*. 18th International Conference on Composite Materials. August 21-26, 2011: Jeju- Korea

BASHUROV, V. V. et al, *Experimental modelling and numerical simulation of high- and hypervelocity space debris impact to spacecraft shield protection*. International Journal of Impact Engineering, Vol. 20, pp. 69-78, 1977

BAUER, W. et al, *Development of in-situ space debris detector*. Advances in Space Research xxx (2014) xxx–xxx

BAYDAR, N., BAYDAR, A., *A comparative study of acoustic and vibration signals in detection of gear failures using Wigner-Ville distribution*. In Mechanical Systems and Signal Processing, Vol 15, by IDEAL (Project), 1091-1107. Academic Press, 2001.

BENNETTI, A., *Numerical and experimental investigation of high velocity impacts for spacecraft protection*. MSc Thesis, Cranfield University, 2002.

BETTELLA, A. A. et al, *Application of Wavelet Transform to analyze acceleration signals generated by HVI on thin aluminum plates and all-aluminum honeycomb sandwich panels*. International Journal of Impact Engineering 35 (2008) 1427–1434

BIN, J. et al, *Performance of different metal-foam stuffed Whipple shield against hypervelocity impact of space debris*. 2011, Key Engineering Materials, 488-489, 122

BOEING, http://www.boeingtravel.com/assets/pdf/defense-space/space/spacestation/components/docs/EWIS.pdf)

Brandon, E. J. et al, *Structural health management technologies for inflatable/deployable structures: Integrating sensing and self-healing*. Acta Astronautica, Vol 68, Issues 7-8, 2011: 883-903.

BUNTE, K. D. et al, *AIDA - An Advanced Impact Detector Assembly*. IAC-03-IAA.5.P.02 (2003)

BÜRGER, D. et al, *Ballistic impact simulation of an armour-piercing projectile on hybrid ceramic/fiber reinforced composite armours*. International Journal of Impact Engineering 43 (2012) 63-77

BURT, R. R., CHRISTIANSEN, E. L., *Hypervelocity impact testing of transparent spacecraft materials*. International Journal of Impact Engineering, Volume 29, Issues 1–10, December 2003, Pages 153–166

CARDARELLI, F., *Materials Handbook, A Concise Desktop Reference*. Springer-Verlag London, 2008

CASTELLINI, P., REVEL, G. M., *Damage Detection by Laser Vibration Measurement*. 15th World Conference on Nondestructive Testing. Roma, 2000.

CHAMPAIGNE, K. D., SUMNERS, J., *Low-power electronics for distributed impact detection and piezoelectric sensor applications*. Aerospace Conference, 2007 IEEE

CHAMPAIGNE, K.D. *Low-power Electronics for Distributed Impact Detection and Piezoelectric Sensor Applications.* Aerospace Conference, 2007 IEEE. Big Sky, 2007.

CHAMPAIGNE, K.D., SUMNERS, J., *Wireless Impact and Leak Detection and Location Systems for the ISS and Shuttle Wing Leading Edge*. Aerospace Conference, 2005 IEEE. Conroe, TX, 2005. 1-8.

CHANGQING, Miao; BO, Liu, *Experimental Study on the Behavior of a New Multilayer Shield against Hypervelocity Debris Impact*. Polymers & Polymer Composites22.2 (2014): 99-103.

CHEESEMAN, B. A, BOGETTI, T. A., *Ballistic impact into fabric and compliant composite laminates*. Composite Structures 61 (2003) 161–173

CHEN, J.C. et al, *Source localization of a wideband source using a randomly distributed beamforming sensor array*. International Journal of High Performance Computing Applications (01/2002)

CHENG, W. L et al, *High velocity impact of thick composites*. International Journal of Impact Engineering, 2003, Volume 29, Number 1

CHERNIAEV, A., TELICHEV, I., *Meso-scale modeling of hypervelocity impact damage in composite laminates.* Composites Part B: Engineering, Volume 74, 1 June 2015, Pages 95–103

CHOI, H., WILLIAMS, W. J., *Improved time-frequency representation of multicomponent signals using exponential kernels.* IEEE. Trans. Acoustics, Speech, Signal Processing, vol. 37, no. 6, pp. 862–871, June 1989.

CHRISTIANSEN, E. L et al, *Mesh double-bumper shield: A low-weight alternative for spacecraft meteoroid and orbital debris protection*. International Journal of Impact Engineering Volume 14, Issues 1–4, 1993, Pages 169–180

CHRISTIANSEN, E. L, *Handbook for Designing MMOD Protection*. Houston: NASA Johnson Space Center, 2009.

CHRISTIANSEN, E. L, *TP−2003-210788. Meteoroid/debris shielding*, NASA (August 2003)

CHRISTIANSEN, E. L., *3M Nextel Ceramic Fabric Offers Space Age Protection.* Intl. Journal of Impact Engineering, Vol. 17

CHRISTIANSEN, E. L., et al, *Highly Oblique Impacts into Thick and Thin Targets*. Int. J. Impact Eng., 14: 157-168, 1993.

CHRISTIANSEN, E.L. et al, Assessment *of high velocity impacts on exposed shuttle surfaces*. Pp. 447–452 in Proceedings of the First European Conference on Space Debris, Darmstadt, Germany, 5–7 April 1993. Darmstadt: European Space Operations Center.

CLEGG, R.A. et al, *Hypervelocity impact damage prediction in composites: Part I—material model and characterisation*. International Journal of Impact Engineering 33 (2006) 190–200

COHEN, L., *Time-frequency distribution - a review*. Proceedings of the IEEE, Vol. 77, 1989: 941-981.

COLOMBO, P. et al, *Effect of hypervelocity impact on microcellular ceramic foams from a preceramic polymer* .Adv. Eng. Mater. 5(11), 802–805, 2003.

COUR-PALAIS, B. G., *Hypervelocity impact in metals, glass and composites*. NASA (1987)

COUR-PALAIS, B.G. *Hypervelocity Impact Investigations and Meteoroid Shielding Experience Related to Apollo and Skylab.* Orbital Debris Workshop, NASA CP-2360 (pp.247-275), Houston, August 27–29, 1982.

COUR-PALAIS, B.G., *Hypervelocity impacts in metals*. International Journal of Impact Engineering 5:221–238, 1986

CRAMER, K. E., WINFREE, W. P. *Thermal characterization of defects in aircraft structures via spatially controlled heat application.* Thermosense XVIII. Orlando, 1996.

DAE-UN, S. et al, *Monitoring of impact damages in composite laminates using wavelet transform*. Composites Pats B, Vol. 33, p. 35-43, 2002.

DAVIDSON, M. et al, *Investigating Amorphous Metal Composite Architectures as Spacecraft Shielding*. Advanced engineering materials 2013, 15, No. 1—2

DEOBLING, S.W. et al, *Summary Review of Vibration-Based Damage Identification*. The Shock and Vibration Digest, Vol. 30, 1998: 91-105.

DESTEFANIS, R. et al, *Enhanced space debris shields for manned spacecraft*. International Journal of Impact Engineering, Volume 29, Issues 1–10, December 2003, Pages 215–226

DESTEFANIS, R. et al, *Space environment characterization of Kevlar: good for bullets, debris and radiation too*. ISMSE -11, 11th International Symposium on Materials in a Space Environment, 15-18 September 2009, Aix-en-Provence, France

DESTEFANIS, R. et al, *Testing of advanced materials for high resistance debris shielding*. Int. J. Impact Engng, Vol. 20, pp. 209-222, 1997

DEVITO, A., *The combustion of bulk metals in a high-speed oxidizing flow.* MSc thesis, McGill University Montreal, Quebec 2014-4-15

DEWHURST, R. J., SHAN Q., *Optical remote measurement of ultrasound*. Measurement Science and Technology, Vol. 10, No.11, 1999.

DEZHI, Zhu et al, *Hypervelocity impact damage to Ti–6Al–4V meshes reinforced Al–6Mg alloy matrix composites* Materials Science and Engineering A 500 (2009) 43–46

DROLSHAGEN, G., *Impact effects from small size meteoroids and space debris*. Advances in Space Research 41 (2008) 1123–1131

DU PONT, http://www.dupont.com/products-and-services/fabrics-fibers-nonwovens/fibers/brands/kevlar.html

DU PONT, http://www.dupont.com/products-and-services/fabrics-fibers-nonwovens/fibers/press-releases/next-generation-of-innovations-with-Kevlar.html

DU PONT, USA, http://www2.dupont.com/Kapton/en_US/

ECKART, P., *Parametric Model of a Lunar Base for Mass and Cost Estimates*. Munchen, 1996.

ELDON, P. K., *Lessons Learned in Modular Bus Structure Development for the LADEE Mission*. Reinventing Space Conference October 14-17, 2013, Los Angeles, CA

FAHRENTHOLD E. P., PARK Y.K., *Simulation of hypervelocity impact on aluminum-Nextel-Kevlar orbital debris shields*. International Journal of Impact Engineering, Volume 29, Issues 1–10, December 2003, Pages 227–235

FOSCHINI, L., *The meteoroid hazard for space navigation*. Planetary Science: Second Italian meeting. Eds A. Manara and E. Dotto. Alenia Spazio, Torino (1999), p. 131.

FRANCESCONI, A., et al, *Generation of transient vibrations on aluminum honeycomb sandwich panels subjected to hypervelocity impacts*. International Journal of Impact Engineering 35 (2008) 1503–1509

FUKUSHIGE, S. et al, *Development of perforation hole detection system for space debris impact*. International Journal of Impact Engineering 33 (2006) 273–284

GABERSON, H. A, *Autocorrelation approaches to time frequency analysis of machinery vibration signals" 20th International Modal Analysis Conference*, Los Angeles, CA; February, 2002

GABERSON, H. A., *Application of Choi-Williams reduced Interference time frequency distribution to machinery diagnostics*. Shock and Vibration, Vol. 2, No. 6, pp 437-444, 1995

GOEL, A. et al, *Design and testing of miniaturized plasma sensor for space plasma diagnostics*. Spacecraft Charging Technology Conference 2014 - 181 Paper

GOLDSMITH, W., *Impact. The theory of physical behavior of colliding solids*. Courier Corporation, 2001-11-01 - 379 pages

GONG, W.W. at al, *Numerical Investigation on Dynamical Response of Aluminum Foam Subject to Hypervelocity Impact With Material Point Method*. CMES-COMPUTER MODELING IN ENGINEERING & SCIENCES, 02/2012, Volume 83, Number 5

GOUZMAN, I. et al, *Thin Film Oxide Barrier Layers: Protection of Kapton from Space Environment by Liquid Phase Deposition of Titanium Oxide.* Applied Materials and Interfaces, VOL. 2, NO. 7, 1835–1843, 2010

GRAFF, K. F., *Wave motion in elastic solids.* Courier Corporation, 1975 – Science.

GRATTAN, K.T.V., et al., Optical Fiber Sensor Technology, Vol. 3, 1999.

GROSCH, D. J., *Inhibited Shaped Charge Launcher Testing of Spacecraft Shield Designs*. Apr 24, 1997, Southwest Research Inst.; Materials and Structures Div.; San Antonio, TX United States

GROSSMAN, E. et al, *Ground simulation of hypervelocity space debris impacts on polymers, protection of materials and structures from the space environment*. Protection of Materials and Structures from Space Environment, 153-165, 2006

GRUJICIC, M. et al, *Hypervelocity impact resistance of reinforced carbon–carbon/carbon–foam thermal protection systems*. Applied Surface Science xxx (2005) xxx–xxx

GUAN, G. S., ZHANG, Q. B., *Research of Performance about Ceramic Coating on Aluminum Bumper to Resist Hypervelocity Impact*, Key Engineering Materials, Vols 577-578, pp. 629-632, Sep. 2013

GUANGYU, S. et al, *Efficient modeling of panel-like targets in perforation simulation*. Third European LS-Dyna User Conference, Paris, 2001.

GUO, Q. et al, *Damage behaviour of Al matrix composite reinforced with Ti–6Al–4V meshes under the hypervelocity impact*. Materials Science and Engineering A 535 (2012) 136– 143

GUO, Q. et al, *Residual microstructure associated with impact craters in TiB2/2024Al composite*. Micron Volume 43, Issues 2–3, February 2012, Pages 344–348

HALLQUIST, J. O., *LS-DYNA Theoretical Manual*. Livermore Software Technology Corporation, 1998.

HAMILL, L. et al, *Hypervelocity Impact Phenomenon in Bulk Metallic Glasses and Composites*. Advanced engineering materials 2014, 16, No. 1

HAMSTAD, M. A., *Comparison of Wavelet transform and Choi-Williams distribution to determine group velocities for different acoustic emission sensors*. J. Acoustic Emission, 26, 2008, 40-59.

HAN, J. H. et al, *Space environment characteristics of MWNT/epoxy composites*. Conference: 49th International SAMPE Symposium and Exhibition: Materials and Processing Technology - 60 Years of SAMPE Progress, SAMPE 2004

HERTZ, H., *On the contact of rigid elastic solids*, London (1896), p. 156.

HIGASHIDE, M. et al, *Hypervelocity impact tests against metallic meshes*. International Journal of Impact Engineering 33 (2006) 335–342

HIRAYAMA, H. et al, *In situ debris measurements in MEO/HEO using onboard spacecraft surface inspection system.* Advances in Space Research 34 (2004) 951–956

HOFFMAN, C.N. et al, *Development of a composite (K1100/CE) satellite bus structure*. Conference: 41. International symposium of the Society for the Advancement of Material and Process Engineering and exhibition: materials and processes challenges - aging systems, affordability, alternative applications, Anaheim, CA (United States), 25-28 Mar 1996

HOFMANN, D. C. et al, *Hypervelocity Impact Testing of a Metallic Glass-Stuffed Whipple Shield*. ADVANCED ENGINEERING MATERIALS, Feb.2015

HONG, W. et al, *Shielding performances of the designed hybrid laminates impacted by hypervelocity flyer*. Materials and Design 52 (2013) 422–428

HOWELL, P.A. et al, *Infrared on-orbit inspection of shuttle orbiter reinforced carbon-carbon using solar heating*. SPIE Optics and Photonics, 31 Jul-4 Aug 2005, San Diego CA USA

HUANG, X. et al, *Amorphous alloy reinforced Whipple shield structure*. International Journal of Impact Engineering, Volume 42, April 2012, Pages 1–10

IADC WG3, *IADC-04-03, Protection manual*. Version 7.0, September 19, 2014.

IADC WG3, *Protection manual IADC-04-03*.Version 4.0, April 12, 2011

IADC WG3, *Sensor systems to detect impacts on spacecraft, IADC-08-03*. Version 2.1, April 2013

IGENBERGS, E., et al, *Mars Dust Counter. In Dust in the Solar System and Other Planetary Systems*, 176-180. Oxford: Elsevier science Ltd., 2002.

ILIESCU, L. E., LAKIS, A. A. & OULMANE, A., *Hypervelocity impact (HVI) signal analysis*. European Journal of Engineering and Technology, Vol. 4 No. 1, 2016, ISSN 2056-5860

ILIESCU, L. E., LAKIS, A. A., *Hypervelocity Impact (HVI) Tests & Signal Recordings*, Universal Journal of Aeronautical & Aerospace Sciences 2 (2014), 80-113

JOHNSON, G. R, COOK, WH., *A constitutive model and data for metals subjected to large strains, high strain rates and high temperatures*. In: Proc. 7th Int. Symp. On Ballistics, Hague, Netherlands, April 1983; 541–547.

KALISTA, S. J. Jr., WARD, T. C., *Self-Healing of poly (Ethylene-co-Methacrylic Acid) copolymers following ballistic puncture*. Proceedings of the First International Conference on Self-Healing Materials, 218-20 April 2007, Noordwijk aan Zee, The Netherlands

KANG, P. et al, *Modification of the critical projectile diameter of honeycomb sandwich panel considering the channeling effect in hypervelocity impact*. Aerospace Science and Technology, Volume 29, Issue 1, August 2013, Pages 413–425

KASHIMA, S., and OZAKI, T., *Structural health monitoring using FBG sensor in space environment*. Proc. SPIE Vol. 4332, p.78-87, 2001.

KATZ, S. et al, *Response of composite materials to hypervelocity impact.* International Journal of Impact Engineering, Volume 35, Issue 12, December 2008, Pages 1606–1611

KEISUKE, F. et al, *Impact perforation behavior of CFRPs using high-velocity steel sphere*. International Journal of Impact Engineering 27 (2002) 497–508

KENNEDY, B. et al, *LEMUR: Legged Excursion Mechanical Utility Rover*. Autonomous Robots 11, 201–205, 2001

KHATIWADA, S. et al, *Hypervelocity Impact Experiments on Epoxy/Ultra-High Molecular Weight Polyethylene Fiber Composites Reinforced with Single-Walled Carbon Nanotubes*. Procedia Engineering 58 (2013) 4 – 10

KOBUSH, M. et al, *Calorimetric Energy Detector for Space Debris*. IAC-06-B6.3.9

KROHN, N. et al, *Defect-selective imaging by non-linear scanning vibrometry and by non-linear air-coupled ultrasound inspection*. Review of Progress in QNDE, Vol. 20, 2000: 1666-1672.

LAKIS, A. A., TOORANI M. H., *Application of time-frequency method in fault diagonsis of rotating machinery*. 3rd International Conference on Integrity, Reliability and Failure. Porto/Portugal: Mechanical Engineering Dept., École Polytechnique of Montréal, 2009.

LEE, J-H. et al, *High strain rate deformation of layered nanocomposites*. Nature Communications vol3 (Oct 2012)

LIU, P., *Internal-structure-model based simulation research of shielding properties of honeycomb sandwich panel subjected to high-velocity impact*. International Journal of Impact Engineering, Volume 77, March 2015, Pages 120–133

LÓPEZ-HIGUERA, J. M. et al, *Fiber optic sensors in structural health monitoring*. Journal of lightwave technology, Vol. 29, No. 4, February 15, 2011

LS-DYNA, *Keyword user's manual*. Volume I. May 2007. Version 971. Livermore Software Technology Corporation (LSTC)

MA, Z. et al, *Behavior of aluminum foams under hypervelocity impact: Validation of numerical simulation*. Advanced engineering materials, 10/2007, Volume 9, No.10

MADARAS, E. I. et al, *The potential for imaging in situ damage in inflatable space structures*. AIP Conf. Proc. 975. Golden, 2007. 437-444.

MAHVASH, A., LAKIS, A.A., 2014, *Independent Component Analysis as Applied to Vibration Source Separation and Fault Diagnosis*. Journal of vibration and control, online: August 2014, DQI: 10.117/107756314544349.

MAJI, A., *Assessment of Electronic Shearography for Structural Inspection*. Experimental Mechanics, Vol. 34, No.2, 1997: 197-204.

MAKEEV, M. A., SRIVASTAVA, D., *Molecular dynamics simulations of hypersonic velocity impact protection properties of CNT/a-SiC composites*. Composites Science and Technology 68 (2008) 2451–2455

MAKI, K. et al, *Radio-wave emission due to hypervelocity impacts in relation to optical observation and projectile speed*. Advances in Space Research 34 (2004) 1085–1089

MATERION, http://materion.com/Markets/DefenseandScience/SpaceScienceandAstronomy/SpaceStructuresandSatellites.aspx

MENG, Q., QU L., *Rotating machinery fault diagnosis using Wigner distribution*. In Mechanical Systems and Signal, Vol 5, by IDEAL, 155-166. Academic Press, 1991.

MERZHIEVSKY, L., *Crater formation in a plastic target under hypervelocity impact*. Int. J. Impact Engng, Vol. 20, pp. 557-568, 1997

MUDRIC, T. et al, *Impact tests and simulations for multifunctional materials*. ECCM15 – 15th European conference on composite materials, Venice, Italy, 24-28 June 2012

NAGAO, Y. et al, *Hypervelocity impact studies simulating debris collisions on composites material*. Proceedings of the forth European Conference on Space Debris, Darmstadt, Germany, 18-20 April 2005

NATIONAL INSTRUMENTS, http://sine.ni.com/nips/cds/view/p/lang/fr/nid/202664

NICOLETTO, M. et al, *High Speed Digital Lines routed on non-metallic Spacecraft structures*. Proc. of the 2014 International Symposium on Electromagnetic Compatibility (EMC Europe 2014), Gothenburg, Sweden, September 1-4, 2014

NORSKE VERITAS, *In-Orbit Non-Destructive Testing –Extension*. ESA / ESTEC Contract No. 8433/89/NL/PP (SC), DNV Report 92-3207 Rev. 2, 1992

OFFENBERGER, S. et al, *Novel composite shielding concepts for hypervelocity orbital debris impact mitigation*. 55th AIAA/ASMe/ASCE/AHS/SC Structures, Structural Dynamics, and Materials Conference

OULMANE, A., LAKIS, A.A. and MUREITHI, N., *A Method for Analyzing Rotating Machinery Faults using Time-Frequency Application*. International Journal of Condition Monitoring and Diagnostic Engineering Management Volume 16 No2, April 2013 pages 21-34.

OULMANE, A., LAKIS, A.A. and MUREITHI, N., *A Method for Analyzing Rotating Machinery Faults using Time-Frequency Application*. International Journal of Condition Monitoring and Diagnostic Engineering Management Volume 16 No2, April 2013 pages 21-34.

OULMANE, A., LAKIS, A.A. and MUREITHI, N., *Application of Fourier Descriptors & Artificial Neural Network to Bearing Vibration Signals for Fault Detection & Classification*. Universal Journal of Aeronautical & Aerospace Sciences 2 (2014), 37-54.

OULMANE, A., LAKIS, A.A., MUREITHI, N., and SAFIZADEH, M.S., *The Application of Time-Frequency Analysis in Rotating Machinery Fault Diagnosis*. 22-nd International Congres and Exhibition on Condition Monitoring and Diagnostic Engineering Mnagement, San Sebatian, Spain, pp 597-583, June 2009.

PCB Piezotronics, http://www.pcb.com/Products.aspx?m=352C33

POPPE, T. et al, *AIDA - Advanced impact detector assembly for the on-orbit measurement of small impacting debris particles and meteoroids*. Adv. Space Res. Vol. 17, No. 12, pp. (12)133-(12)136, 1996

PROKOPENKO, M. et al, *On Self-organising Diagnostics in Impact Sensing Networks*. Knowledge-Based Intelligent Information and Engineering Systems Lecture Notes in Computer Science Volume 3684, 2005, pp 170-178

PROSSER, W. H. et al, *Acoustic Emission Signals in Thin Plates Produced by Impact Damage*. Journal of Acoustic Emission, Vol. 17(1-2), (June, 1999), pp. 29-36.

PROSSER, W. H. et al, *Extensional and Flexural Waves in a Thin-Walled Graphite/Epoxy Tube*. Journal of Composite Materials Vol. 26(14), 1992, pp. 418-427

PROSSER, W.H., *Development of structural health management technology for aerospace vehicles*. JANNAF 39th Combustion/27th Airbreathing Propulsion/21st Propulsion Systems Harzards/3rd Modeling and Simulation Joint Subcommittee Meeting; 1-5 Sep. 2003

QIDWAI, U. et al, *Detection of Ultrasonic NDE Signals Using Time-Frequency Analysis.* Insight, vol. 41, no. 11, 1999: 700-703.

REIMERDES, H.-G. et al, *Ballistic Limit Equations for the Columbus-Double Bumper Shield Concept*. ESA SD-01, Proceedings of the First European Conference on Space Debris, Darmstadt, Germany, 1993.

REINHARDT, W., WOFGANG, E., *Potential low-cost optical fiber Bragg-grating sensor systems for structural health monitoring and examples of their application*. SPIE 4920, Advanced Sensor Systems and Applications, (9 September 2002)

RIEDEL, W. et al, *Hypervelocity impact damage prediction in composites: Part II – experimental investigations and simulations*. International Journal of Impact Engineering 33 (2006) 670–680

ROBINSON, J. H., NOLEN, A. M., *An investigation of metal matrix composites as shields for hypervelocity orbital debris impacts*. Int. J. Impact Eng. Vol. 17, pp. 685-696, 1995

RUDOLPH, M., *Fragmentation of hypervelocity aluminum projectiles on fabrics*. Acta Astronautica 76 (2012) 42–50

RYAN, S. et al, *A ballistic limit equation for hypervelocity impacts on CFRP/Al HC satellite structures.* Advances in Space Research, 41 (2008), pp. 1152–1166

RYAN, S. et al, *Honeycomb vs. foam: Evaluating potential upgrades to ISS module shielding.* Acta Astronautica Volume 67, Issues 7–8, October–November 2010, Pages 818–825

RYAN, S. et al, *Hypervelocity impact performance of open cell foam core sandwich panel structures*. NASA (2010)

RYAN, S., CHRISTIANSEN, E. L., *Hypervelocity impact testing of advanced materials and structures for micrometeoroid and orbital debris shielding*. NASA Johnson Space Center, US (2012)

RYAN, S., CHRISTIANSEN, E. L., *Micrometeoroid and Orbital Debris (MMOD) Shield Ballistic Limit Analysis Program*. NASA/TM–2009–214789.

RYAN, S., CHRISTIANSEN, E.L., *Honeycomb vs. foam: evaluating potential upgrades to ISS module shielding*. IAC-09.A6.3.11

SAFIZADEH, M.S., LAKIS, A.A., and THOMAS, M., *Time-Frequency and Their Application to Machinery Fault Detection.* International Journal of Condition Monitoring and Diagnostic Engineering Management, 4(1), pp 10-27, (2000).

SCHAEFER, F. et al, *Ballistic Limit Equation for Equipment Placed Behind Satellite Structure Walls.* Hypervelocity Impact Symposium, Williamsburg, Va., September 23–27, 2007.

SCHAEFER, F. et al, *Review of Ballistic Limit Equations for CFRP Structure Walls of Satellites.* 5th International Symposium on Environmental Testing for Space Programmes, ESA SP-558, Noordwijk, June 15–17, 2004.

SCHONBERG, W. P. et al, *Hypervelocity impact response of honeycomb sandwich panels*. Acta Astronautica, Volume 66, Issues 3–4, February–March 2010, Pages 455–466

SCHONBERG, W. P., *Protecting Earth-orbiting spacecraft against micro-meteoroid/orbital debris impact damage using composite structural systems and materials: An overview*. Advances in Space Research 45 (2010) 709–720

SCHONBERG, W.P, *Hypervelocity impact response of spaced composite material structures*. Int. J. Impact Eng. 10, 509-, 1990.

SCHONBERG, W.P., *Protecting spacecraft against orbital debris impact damage using composite materials*. Composites: Part A, 31 (2000) 869–878

SCHONBERG, W.P., WALKER,E.J., *Use of composite materials in multi-wall structures to prevent perforation by hypervelocity projectiles*. Compos. Struct.19, 15–, 1991.

SCHROEDER, K. et al, A fibre Bragg grating sensor system monitors operational load in a wind turbine rotor blade. Meas. Sci. Technol. 17 (2006) 1167–1172

SIBEAUD, J.-M. et al, *Hypervelocity impact on honeycomb target structures: Experiments and modeling*, International Journal of Impact Engineering 35 (2008) 1799–1807

SIRKIS, J. S. et al, *Development of an impact detection technique using optical fiber sensors and neural networks*. Smart Structures and Materials 1994: Smart Sensing, Processing, and Instrumentation. Orlando, 1994.

SMART FIBRES LTD., UK, http://www.smartfibres.com

SMITH, B. T, *Rapid detection and quantification of impact damage in composite structures*. NASA-CR-190367, 1992.

SONG, L. et al, *Impact effects on fused quartz glass by ground simulating hypervelocity space debris*. Technological Sciences, SCIENCE CHINA, March 2013 Vol.56 No.3: 724–731

STANFORD UNIVERSITY, Space Environment and Satellite Systems, http://sess.stanford.edu/hvip

STARTSEV, O. V., ISUPOV, V. V., *The Gradient of Mechanical Characteristics Across the Thickness of Composite Laminates After Exposure to a Low Earth Orbit Environment*. Polymer Composites, Volume 19, Issue 1, pages 65–70, February 1998

STASZEWSKI, W.J. et al, *Health Monitoring of Aerospace Structures*. John Wiley & Sons Ltd, 2004

SWANSON, G.T., CASSELL, A.M. *Micrometeoroid and Orbital Debris impact Damage Recording System.*" Aerospace Conference, IEEE. Big Sky, 2011. 1-8.

SWIFT, H. F., *Hypervelocity Impact Mechanics, Impact Dynamics*. John Wiley and Sons (1982)

TAKANO, T. et al, *Microwave emission experiment with hypervelocity impacts and applications of its results*. Proceedings of the Third European Conference on Space Debris, 19 - 21 March 2001

TANAKA, M. et al, *Development of a lightweight space debris shield using high strength fibers*. International Journal of Impact Engineering 26 (2001) 761-772

TANAKA, M., MORITAKA, Y., *Single bumper shields based on Vectran fibers*. Advances in Space Research 34 (2004) 1076–1079

TARAZAGA, P. A. et al, *Structural health monitoring of an inflatable boom subjected to simulated micrometeoroid/orbital debris damage*. Nondestructive Evaluation and Health Monitoring of Aerospace Materials, Composites, and Civil Infrastructure. San Diego, 2006.

TAYLOR, E. A. et al, *Hypervelocity impact on carbon fibre reinforced plastic/aluminium honeycomb: comparison with Whipple bumper shields*. Taylor International Journal of Impact Engineering 23 (1999) 883-893

TAYLOR, E. A. et al, *Hypervelocity impact on carbon fibre reinforced plastic/aluminium honeycomb: comparison with Whipple bumper shields.* Int J Impact Eng, 23 (1) (1999), pp. 883–893

TAYLOR, E. A. et al, *Hypervelocity impact on spacecraft honeycomb: hydrocode simulation and damage laws.* Int J Impact Eng, 29 (1–10) (2003), pp. 691–702

TAYLOR, E. A. et al, *Hypervelocity impact on spacecraft honeycomb: hydrocode simulation and damage laws*. International Journal of Impact Engineering 29 (2003) 691–702

TENNYSON, R. C. et al, *Design Study of Fiber Optic MOD Impact Detection System for Spacecraft Structures*. University of Toronto, Institute for Aerospace Studies.

TENNYSON, R. C., *Spacecraft damage assessment due to hypervelocity impacts using a micrometeoroid and orbital debris detection system*. Canadian Aeronautics and Space Journal. 55(2), 2009: 89-95.

THOMPSON, T. C. et al, *Development of an all-composite spacecraft bus for small satellite programs*. In Proceedings from the eighth annual AIAA/USU Conference on Small Satellites, Logan, UT, 1994

TURNER, R.J. et al, *Cost effective honeycomb and multi-layer insulation debris shields for unmanned spacecraft*. Int J Impact Eng, 26 (1–10) (2001), pp. 785–796

VERKER, R. et al, *The effect of simulated hypervelocity space debris on polymers*. Acta Materialia, Volume 52, Issue 19, 8 November 2004, Pages 5539–5549

VIGNJEVIC, R. et al, *Finite element modelling of failure of a multi-material target due to high velocity space debris impacts.* Space Debris, Vol. 2, pp. 41-50, 2002.

VIGNJEVIC, R. et al, *Numerical Simulation of High Velocity Impacts on Thin Metallic Targets I*. Crashworthiness, Impact and Structural Mechanics (CISM) Cranfield University, UK, Conference paper, 2004

VOEVODIN, A.A., ZABINSKI, J.S., *Nanocomposite and nanostructured tribological materials for space applications, Composites Science and Technology*, Vol. 65, Issue 5, April 2005, Pages 741–748

WAN, H et al, *Shielding performances of the designed hybrid laminates impacted by hypervelocity flyer*. MATERIALS & DESIGN, 12/2013, Volume 52

WANG, L. et al, *Fatigue damage accumulation model and fatigue life predication of composite laminate TT300/ epoxy-resin*. Conference: 2011 International Conference on Advanced Materials and Computer Science, ICAMCS 2011

WANG, L., YUAN, F.G., *Group velocity and characteristic wave curves of Lamb waves in composites: Modeling and experiments.* Composites Science and Technology, Volume 67, Issues 7-8, June 2007, Pages 1370–1384

WANG, W. J., MCFADDEN, P. D., *Early detection of gear failure by vibration analysis I. Calculation of the time-frequency distribution*. In Mechanical Systems and Signal Processing,Vol. 7, by IDEAL (Project), 193-203. Academic Press, 1993.

WARREN, J., COLE, M., et al., *Hypervelocity impact of honeycomb core sandwich panels filled with shear thickening fluid*, 28th Technical Conference of the American Society for Composites, State College, 2013

WATTS, A. et al, *Dimensional Scaling for Impact Cratering and Perforation*. NASA NCR-188259. March 16, 1993, Houston, Texas: NASA Johnson Space Center.

WEI, Z. G. et al, *Shape memory materials and hybrid composites for smart systems. Part II, Shape-memory hybrid composites*. Journal of materials science 33 (1998) 3763 — 3783

WELLING, M, WEBER M., *Independent component analysis of incomplete data*. Proc. of the 6th Annual Joint Symposium on Neural Computation. Psadena, 1999.

WELLING, M., WEBER, M., *A Constrained EM Algorithm for Independent Component Analysis*. Neural Computation, Vol13, No.3, 2001: 677-687.

WICKLEIN, M. et al, *Hypervelocity impact on CFRP: testing, material modelling, and numerical simulation*. International Journal of Impact Engineering 35 (2008) 1861–1869

WIJKER, J., *Spacecraft Structures*. Springer-Verlag Berlin Heidelberg, 2008

WOLFGANG, E. et al, *Fibre optic sensor network for spacecraft health monitoring*. E. Meas. Sci. Technol. 12 (2001) 974–980

WOODARD, S.E. et al, *A method to have multi-layer thermal insulation provide damage detection*. 48th AIAA/ASME/ASCE/AHS Structures, Structural Dynamics, and Materials.AIAA, 2007. 1-23.

XIAOTIAN, Zhang et al, *Numerical Investigation of aluminum foam shield based on fractal theory and node-separation FEM*. Chinese Journal of Aeronautics 24 (2011) 734-740

ZHANG, Y. et al, *On the Selection of Johnson-cook Constitutive Model Parameters for Ti-6Al-4 V Using Three Types of Numerical Models of Orthogonal Cutting.* Procedia CIRP, Volume 31, 2015, Pages 112–117, 15th CIRP Conference on Modelling of Machining Operations (15th CMMO)

3M Nextel Ceramic Textiles and Composites, http://www.3m.com/market/industrial/ceramics/materials/fabric_312.html

APPENDIX A- HVI TEST PREPARATION AND SAFETY MEASURES

The test requires a lot of preparation, safety measures and the purchase of many components.

Necessary (not an exhaustive list, a detailed list will be presented later on):

- High pressure Helium gas Tanks (6000 PSI) and Nitrogen gas
- High pressure Gas regulator
- Polycarbonate sheets for the Sabot
- Mylar and Brass sheets for the diaphragms together with the sealing gaskets
- Rare earth magnet
- Target materials and projectile spheres
- Tooling for the required manufacturing processes
- Additional materials for the target support
- Special materials needed in order to measure and record the speed as: oscilloscope and high speed camera with stroboscope (if considered necessary)
- Miscellaneous

Preparations:

- Placement of the gun and additional equipment in the laboratory (MPB or École Poly)
- Manufacturing of the Sabot and eventually design of the mechanical stripper
- Design and manufacturing of the targets and sample support

Safety measures:

- Safety glasses
- Ear protections
- People cannot be in the room while firing
- Ventilation systems
- Gloves

APPENDIX B- MATERIALS MECHANICAL PROPERTIES

The following tables [51] present the various mechanical properties (at room temperature, usually dependent on the environmental temperature) for:

- metal alloys

Table 8.1: Metal alloys mechanical properties

Material	Density ρ (kg/m^3)	σ_u (MPa)	σ_y (MPa)	E (GPa)
Aluminium				
2014-T6	2.80	441	386	72
2024-T36	2.77	482	413	72
6061-T6	2.71	289	241	67
7075-T6	2.80	523	448	71
Magnesium				
AZ31B	1.77	221	110	44
AZ31B-H24	1.77	269	199	44
Titanium				
Ti6Al-4V	4.43	1103	999	110
Steel				
RH1050	7.60	1310	1170	200
D6AC	7.80	1600	1200	200
AMS-6434	7.88	2100	1400	200
Beryllium				
Lockalloy	2.10	426	310	203

- composite fibers

Table 8.2: Composite fibers mechanical properties

Material	Young's modulus E (GPa)	Ultimate strength σ (MPa)	Density ρ kg/m^3
E-Glass fiber*	72.3	3170	2550
S-Glass fibre*	82.7	4130	2500
E-Glass in epoxy	51.7	1380	1940
S-Glass in epoxy	51.7	2070	1940
Aramid fibre*	137.8	3445	1690
Arimid fibre in epoxy	82.7	1930	1400
HM graphite fibre*	379	2070	1900
HT graphite fibre*	241	2410	1770
AS or T-300 fibre*	207	2760	1850
HM graphite in epoxy	207	930	1610
HT graphite in epoxy	152	1410	1500
AS or T-300 in epoxy	117	1580	1550
Boron filaments*	143	2760	2630
Boron in epoxy	214	1520	2080

- Al-alloy 5056 honeycomb cores

Table 8.3: Al-alloy 5056 honeycomb cores mechanical properties

	d_c cell	ρ	Compr. strength E_c	Shear modulus (MPa)		Shear strength (MPa)	
Type of Honey-comb core	(mm)	(kg/m^3)	(MPa)	G_L	G_T	τ_L	τ_T
1/4-5056-.002p	6.4	69	3.21	462	186	2.24	1.31
3/8-5056-.0007p	9.6	16	0.24	103	62	0.31	0.17
1/4-5056-.0015p	6.4	54	2.17	345	152	1.59	0.90
1/4-5056-.0007p	6.4	26	0.55	138	83	0.54	0.26
3/16-5056-.002p	4.8	91	5.07	648	248	3.31	1.93